Investigating the role of cardiomyocyte senescence in delayed-onset doxorubicin cardiotoxicity

Laura K. Booth

Thesis submitted in accordance with the requirement for the degree of

Doctor of Philosophy

Translational and Clinical Research Institute

Faculty of Medical Sciences

September 2024

Abstract

Although cancer survival rates are continually improving, the delayed onset of cardiotoxicity as a result of chemotherapeutic treatment, particularly the anthracycline class of drug, places an increasing burden on healthcare systems: yesterday's cancer survivors are fast becoming today's heart failure patients. Cellular senescence (a cell fate defined by irreversible cell cycle exit, phenotypic alterations including mitochondrial dysfunction, and the expression of the pro-inflammatory senescence-associated secretory phenotype) has gained significant attention as a contributor to this pathology. Studies have shown that pharmacological elimination of senescence prevents maladaptive remodelling and myocardial dysfunction in preclinical models of anthracycline-induced (specifically doxorubicin-induced) cardiotoxicity, but the interplay of senescence and cardiotoxicity remains poorly characterised at a cellular and molecular level. In this thesis, using clinically representative *in vitro* models of cardiac cells, it was demonstrated that classical senescence is initiated in these cells following exposure to doxorubicin, and these phenotypic hallmarks persist following removal of the drug. Furthermore, these cells exhibit far-reaching changes in their transcriptome. The cardiomyocytes also produce a classical senescence-associated secretome, which in isolation modulates the cardiac fibroblast phenotype and cellular response. Overall, these studies establish an *in vitro* model of doxorubicin-induced cardiomyocyte senescence, the secretome of which can influence other cardiac cell lineages – this may contribute to more global maladaptive myocardial remodelling (e.g. fibrosis) and long-term cardiotoxicity. Building on this work, targeting aspects of the senescent cardiomyocyte phenotype may prove a therapeutic strategy to prevent or treat anthracycline-induced cardiac dysfunction in the future.

Acknowledgments

Firstly, I extend my thanks to the Medical Research Council for funding this Integrative Toxicology Training Partnership project, and other organisations who have supported my research and professional development these past years, including the Gordon Research Conferences, the British Toxicology Society, and several institutions within Newcastle University.

Thanks also to my supervisory team, Dr Jason Gill, Prof Marion MacFarlane and Prof Gavin Richardson. Jason, thank you for always supporting my extracurricular escapades, reminding me to keep my “toxicology hat” on, and being patient with me through the lockdown. Marion, thank you for supporting my placement at the MRC Toxicology Unit. Gavin, thank you so much for taking a chance on me in 2022 – I’m so pleased that our 3-month placement evolved (mutated?!) into what my PhD project became. The belief, time, trust and funding that you invested in me has been transformative for my professional development, and I genuinely look forward to building on this research with you in the next few years. In addition, thank you to my panel members Prof Matt Wright and Dr Helen Phillips, for keeping me on track and asking the difficult questions!

I have been fortunate to know many excellent colleagues throughout this project, who have been such a supportive community to me. From the POG/NUCancer: Ray, Hande, Rachel H, Robyn, Danny, and the prostate cancer groups. From the CfL: Millie, Rachel S, Rach R, Maria CE, Maria B and Simon TC. Thank you all for making me feel welcome, teaching me lab skills, lending emergency reagents, and listening to me vent!

Back in Autumn 2020, I don’t think I’d have stuck with this PhD if it wasn’t for my dear friends, near and far - thank you to Cero for the wonderfully long voice notes, you’re my soul sister and I am so proud of what we have both achieved these last years! I cannot believe how lucky I was in the housemate lottery when I first moved to Newcastle - thank you to The Remainers for welcoming me into the gang, and extra special thanks to the Cardigan Crew Ruby, Daisy, Sam and Tiri, for making the house share so much better than *normal*.

To my wonderful boyfriend Ell, thank you for loving and supporting me in the highs and lows of this project, my life has been considerably brighter since you walked into the back room of the Cumberland Arms that night in February 2023.

Thanks to my family: Dad, Ali, Chris, Alex, Nana, Grandad, Jo, Michael and Inga – I am so lucky to have you all in my corner for whatever life throws at me! I promise I'm done with school now. I am also thankful to the family who shaped me, and who I know would be so proud of me at this time: Mum, Grandpa (the first Dr Booth!), Grandma and GG, I miss you every day. To my siblings, Lucy, Freddy, Amy, Josh and Jacob, I hope you are as proud of me as I am of every one of you.

"Since all models are wrong, the scientist must be alert to what is importantly wrong. It is inappropriate to be concerned about mice when there are tigers abroad."

- George E.P. Box, Science and Statistics 1976

Table of Contents

List of Abbreviations

ACEi = Angiotensin-Converting Enzyme Inhibitor

AIC = Anthracycline-Induced Cardiotoxicity

AICAR = 5-aminoimidazole-4-carboxamide

Ang = Angiotensin

(aq) = Aqueous

ARB = Angiotensin Receptor Blockers

AT_1R = Angiotensin Type 1 Receptor

AT_2R = Angiotensin Type 2 Receptor

ATP = Adenosine Triphosphate

ATP5B = ATP Synthase Subunit Beta (Complex V)

Bcl-(2) = B-cell Lymphoma (2)

Beta-blocker = Beta-adrenergic Blockers

BNP = B-Type Natriuretic Peptide

BrdU = 5-bromo-2'-deoxyuridine

BSA = Bovine Serum Albumin

BTHS = Barth Syndrome

CARE = High-Sensitivity Cardiac Troponin I–Guided Combination Angiotensin Receptor Blockade and Beta Blocker Therapy to Prevent Cardiac Toxicity in Cancer Patients Receiving Anthracycline Chemotherapy

CCSS = Childhood Cancer Survivor Study

CDK(i) = Cyclin-Dependent Kinase (Inhibitor)

cDNA = Complementary DNA

cGAS-STING = Cyclic GMP–AMP Synthase (CGAS)–Stimulator Of Interferon Genes (STING)

CHF = Congestive Heart Failure

c-kitPOS = C-kit Positive

CM = Cardiomyocyte

C_{max} = Maximum Systemic Pharmacokinetic Exposure

cmed = Conditioned Media

COVID-19 = Severe Acute Respiratory Syndrome Coronavirus 2 (SARS-Cov-2)

CPC = Cardiac Progenitor Cell

CSC = Cardiac Stem Cell

cTnC = Cardiac Troponin C

cTnI = Cardiac Troponin I

cTnT = Cardiac Troponin T

CVD = Cardiovascular Disease

D&Q = Dasatinib & Quecertin

DAPI = 4′,6-diamidino-2-phenylindole

DMEM = Dulbecco’s Modified Eagle Medium

DMSO = Dimethyl Sulfoxide

DOX = Doxorubicin

DOXol = Doxorubicinol

(D)PBS = (Dulbecco’s) Phosphate Buffered Saline

ECM = Extracellular Matrix

EDTA = Ethylenediamine Tetraacetic Acid

EdU = 5-ethynyl-2’-deoxyuridine

EMT = Epithelial to Mesenchymal Transition

ER = Oestrogen Receptor

ESMO = European Society for Medical Oncology

ETC = Electron Transport Chain

EV = Extracellular Vesicle

Ex/Em = Excitation/Emission Wavelengths of Light

FAO = Fatty Acid Oxidation

FBS = Foetal Bovine Serum

FOV = Field of View

GDF15 = Growth Differentiation Factor 15

GDSC = Genomics of Drug Sensitivity in Cancer

GI_{50} = Concentration of A Drug Inhibiting Growth of a Cell Type by 50%

GO = Gene Ontology

GSEA = Gene Set Enrichment Analysis

(H)CF = (Human) Cardiac Fibroblast

HF = Heart Failure

HFpEF = Heart Failure with Preserved Ejection Fraction

HFrEF = Heart Failure with Reduced Ejection Fraction

IC_{50} = Concentration of a Drug Required to Reduce the Cellular Activity or Number by 50%

IF = Immunofluorescence

iPSC-CM = Induced Pluripotent Stem Cell-Derived Cardiomyocyte

IQ = Intelligence Quotient

IRI = Ischaemia-Reperfusion Injury

JAK = Janus Kinase

KEGG = Kyoto Encyclopaedia of Genes and Genomes

LC_{50} = Concentration of Drug Inducing Cytotoxicity in 50% of the Population

LCMS = Liquid Chromatography Mass Spectrometry

lncRNA = Long Non-Coding RNA

LV = Left Ventricle

LVEF = Left Ventricular Ejection Fraction

MI = Myocardial Infarction

MiNA = Mitochondrial Network Analysis

MLHFQ = Minnesota Living with Heart Failure Questionnaire

MMP = Matrix Metalloproteinase

MRI = Magnetic Resonance Imaging

MSigDB = Molecular Signatures Database

mtDNA = Mitochondrial DNA

MTS = 3-(4,5-dimethylthiazol-2-yl)-5-(3-carboxymethoxyphenyl)-2-(4-sulfophenyl)-2H-tetrazolium

MTT = 3-(4,5-dimethylthiazol-2-yl)-2,5-diphenyltetrazolium

NAD(P)H = Nicotinamide Adenine Dinucleotide (Phosphate)

NCI-60 = National Cancer Institute 60 Human Tumour Cell Lines Screen

(N)ES = (Normalised) Enrichment Score

NICE = National Institute for Health and Care Excellence

OXPHOS = Oxidative Phosphorylation

PBST = PBS with Tween-20

PCA = Principle Component Analysis

PFA = Paraformaldehyde

PMS = Phenazine Methosulfate

PRADA = Prevention of Cardiac Dysfunction During Adjuvant Breast Cancer Therapy

PROACT = Preventing cardiac damage in patients treated for breast cancer and lymphoma: a phase 3 Randomised, Open label, blinded endpoint, superiority trial of enalapril to prevent Anthracycline-induced CardioToxicity

QC = Quality Control

RAAS = Renin-Angiotensin-Aldosterone System

RNA-Seq = Bulk RNA Sequencing

(RT)-qPCR = (Reverse Transcriptase) Quantitative Polymerase Chain Reaction

ROS = Reactive Oxygen Species

rRNA = Ribosomal RNA

SASP = Senescence-Associated Secretory Phenotype

SA-β-Gal = Senescence-Associated Beta-Galactosidase

SD = Standard Deviation

SEM = Standard Error of The Mean

SIRT1 = Sirtuin 1

SRB = Sulphorhodamine B

STAT = Signal Transducer and Activator of Transcription

T/E = Trypsin/EDTA

TEMRA = Terminally Differentiated Effector Memory T Cells

TFAM = Mitochondrial Transcription Factor A

TopII = Topoisomerase II

List of Tables

List of Figures

Chapter 1. Introduction

1.1 Cancer survivorship and the emergence of anthracycline-induced cardiotoxicity

1.1.1 The long-term wellbeing of cancer survivors is a growing concern – chronic morbidities are associated with anticancer treatments

Cancer is a group of diseases which continues to place a heavy burden on healthcare systems around the world. In line with the ageing and growing population of Britain,[1] it is now estimated that the lifetime risk of cancer for British people born after 1960 is greater than 50%, notably larger than the same estimate for those born in the year 1930 (15% increase for men, 10.8% increase for women).[2] Happily, a striking decrease in the projected overall cancer mortality age-standardised rate has also been predicted, with a fall of 15.3% predicted between the years 2014 and 2035. Due to ever-improving cancer care and decreased cancer mortality, the cancer survivor population will therefore likely see a sizeable increase in the next decades, bringing with it a new set of challenges for clinicians and healthcare systems more broadly. Therefore, it is increasingly important that, alongside aiming to cure the malignancy itself, the medical community better understands how to promote good quality of life (better survivorship)[3] for cancer survivors – i.e. considering "healthspan" alongside lifespan.

Cancer survivors have a specific set of needs, which are often different from non-survivors. Alongside additional financial, informational and psychological needs, cancer survivors may present with physical healthcare needs, which may be due to their disease history (e.g. risk of cancer recurrence) or their treatment history.[4] This was demonstrated by Mandelblatt and colleagues' study of older breast cancer patients (> 60 years old), which found that chemotherapy treatment history was associated with poorer neuropsychological capability (attention, processing speed, and executive function), and hormonal therapy was associated with poorer learning and memory performance, in the same cohort.[5]

The pioneering Childhood Cancer Survivor Study (CCSS) clearly showed how adult survivors of childhood cancer display increased incidence of many chronic health conditions compared to sibling-matched controls.[6] Recent data suggest that in adult survivors of childhood cancer, frailty prevalence increased from 6.2% to 13.6% at 5 years following study entry, with risk factors for increased frailty including chest

radiation > 20 Gy and lack of strength training.[7] Strikingly, the strongest risk factor for death during follow-up in this study was prior frailty, emphasising that mitigating frailty in the survivorship period could impact mortality. Similarly, survivors of childhood medulloblastoma (the most common malignant paediatric brain tumour), have a high prevalence of adverse outcomes manifesting as IQ point loss,[8] impaired global intellectual functioning and other morbidities,[9] which is thought to be at least in part due to treatment with high-dose craniospinal irradiation.

Alongside the aforementioned morbidities, cardiovascular disease (CVD) is particularly common in cancer survivors. For instance, patients in the CCSS cohort were 8.2 times more likely to die from cardiac-related events relative to the United States population,[10] and survivors from a large (n = 4,122) French-British cohort were 5.0-fold more likely to die as a result of cardiovascular diseases than the general population in the longer-term (average follow-up = 27 years).[11] The same phenomenon is observed in patients who received anticancer treatment as adults: cardiovascular disease is an emerging concern in breast cancer survivors,[12] where exposure to common breast cancer therapies is associated with ischemic heart disease and heart failure (HF) and/or cardiomyopathy.[13,14] In lymphoma survivors, one large multi-centre cohort study recently showed that CVD was, strikingly, the leading cause of mortality, ahead of classic Hodgkin's lymphoma, at 5- and 10-year survival follow-ups.[15] In some populations, mortality from cardiovascular disease now presents a greater risk than mortality from cancer recurrence. The field of "cardio-oncology" has emerged in recent years to address this phenomenon, promoting closer relationships between cardiologists and oncologists in a patient's care team and cross-disciplinary research.

In 2022, the European Society for Medical Oncology (ESMO) identified five main components of survivorship care, with the first being the "physical long-term and late effects of cancer and cancer treatment and chronic medical conditions". ESMO stated that despite progress made over the years, a need remains for high-quality care, education and research in the field of cancer survivorship,[16] which will surely increase in importance with the growing cancer survivor population.

1.1.2 Effective chemotherapies like anthracyclines have contributed to the rising cancer survival rate but are cardiotoxic

Improvements in cancer survival can be attributed to many factors, one being the availability of various effective chemotherapy treatments. The anthracycline class of

drugs encompasses some of the most well-established and widely used anticancer chemotherapies in use today. These drugs started life as prospective novel antibiotics, being initially isolated from Streptomyces bacteria in the 1950s.[17] In the early 1960s, the antineoplastic anthracycline daunorubicin was independently discovered in the laboratories of both Farmitalia (coined "daunomycin")[18] and Rhône-Poulenc (coined "rubidomycin").[19] *In vitro*, daunomycin was shown to have striking cytotoxic effects in both normal and neoplastic cells and hence, attention shifted from the antibiotic properties to the broad-spectrum anti-cancer potential of anthracycline drugs.[20]

Anthracyclines have a typical structure which contains a tetracyclic system, in which three of the four rings are planar (**Figure 1.1**),[21] and they disrupt the cell cycle to target cancer cells through several mechanisms. Anthracyclines can interact with cellular DNA through intercalation, alkylation and cross-linking, and furthermore can prevent DNA unwinding by disrupting helicase activity; all of which disrupt the cell cycle. They also inhibit the enzyme topoisomerase IIα (TopIIα), which is overexpressed in fast-replicating cells,[22] leading to DNA damage and apoptosis. Another long-posited mechanism of action involves anthracyclines contributing to the generation of intracellular free radicals and reactive oxygen species (ROS), which induces cellular stress and consequent apoptosis. These mechanisms can be adjusted by modifying the variable groups of the generic anthracycline structure, for instance. Such modifications give rise to four common anthracyclines in use today (**Table 1.1**)

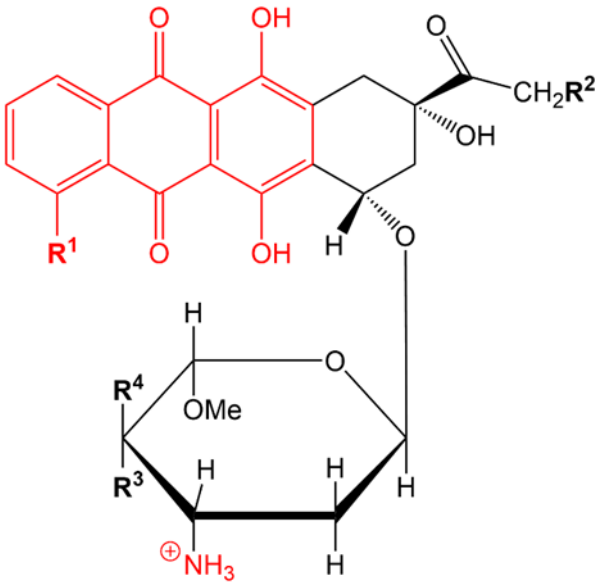

Figure 1.1 Generic chemical structure of an anthracycline. Planar components of the structure are shown in red. Variable chemical groups are denoted R^x.

In the modern era, the anthracycline family are hailed as one of the most important discoveries in oncology therapeutics, with doxorubicin (DOX) notably being named on the World Health Organisation's model list of essential medicines for its use in treating multiple cancers,[23] such as acute lymphoblastic leukaemia, acute myeloblastic leukaemia, Hodgkin and non-Hodgkin lymphoma, alongside metastatic forms of breast cancer, Wilms' tumour, neuroblastoma, soft tissue & bone sarcomas, ovarian carcinoma, thyroid carcinoma, gastric carcinoma, and bronchogenic carcinoma, and in certain settings, primary breast cancer, ovarian cancer, AIDS-Related Kaposi's Sarcoma and multiple myeloma.[24,25] Like many other cancer chemotherapies, anthracyclines exert unwanted acute side effects upon patients, including immune suppression, nausea, vomiting, and fatigue.[26] These side effects are weighed up against the drugs' anticancer effects in risk-benefit analysis, and overall, side effects are usually clinically manageable. But with ever more emphasis being placed on cancer survivorship rather than plain cancer survival, the long-term, off-target effects of chemotherapies including anthracyclines are being more keenly felt by patients than ever, and this is raising new questions in drug safety and toxicology spheres. Perhaps the most notorious of these is anthracycline-induced cardiotoxicity (AIC), which has been recognised as an adverse effect of anthracyclines since the late 1960s.[27]

Table 1.1 Variable chemical groups in four major anthracycline drugs

Anthracycline	R^1	R^2	R^3	R^4
Doxorubicin	OMe	OH	OH	H
Epirubicin	OMe	OH	H	OH
Daunorubicin	OMe	H	OH	H
Idarubicin	H	H	OH	H

1.1.3 The history of anthracycline cardiotoxicity – first documented acute cases to long-term survivors today

Daunomycin was the first anthracycline to be discovered, and its cardiotoxicity quickly became evident in Phase I clinical trials, but this did not preclude its further use in the clinic due to its favourable risk-to-benefit ratio in patients with advanced cancer, and the drive in the field to discover effective antineoplastic drugs.[28] Extensive clinical trials investigating AIC took place in the 1970s and the cardiotoxicity of daunomycin's

derivative DOX has now become well-characterised, and often predominates other anthracyclines in the literature today. In 1973, LeFrak and colleagues showed that out of 399 DOX-treated cancer patients (who had no previous history of cardiac complaints), 11 developed sudden onset severe congestive HF (CHF). This proved fatal for eight out of the 11 patients, who died within three weeks of cardiac symptoms being recorded.[29] Concurrently, a phase II trial was conducted by O'Bryan and colleagues, in which 472 cancer patients were treated with DOX and observed. In this instance, 43 patients displayed acute electrocardiographic changes soon after DOX therapy: three of these patients died suddenly and a further two developed irreversible CHF.[30]

These historic studies of acute AIC paved the way for the first established line of defence against the pathology: reducing the lifetime cumulative dose of anthracycline a patient receives. This simple but effective control measure is still used today and here, the clinician must carefully balance the anti-cancer effects of the therapy and its cardiotoxicity. Various cardiac risk factors must be evaluated when establishing a maximum safe dosage of anthracycline therapy for an individual, but in the case of DOX, a lifetime cumulative dose of < 550 mg per m^2 of body surface area (mg/m^2) was historically generally used as an upper limit to minimise cardiac phenomena.[31] Today however, the National Institute for Healthcare Excellence (NICE) guidelines recommend the limit of 450 mg/m^2, based on more recent studies.[32,33]

In addition to this acute cardiotoxicity, cancer survivors can also present a late-onset, chronic cardiotoxic following anthracycline therapy, in which symptomatic cardiac abnormalities (e.g. cardiomyopathy resulting in diminished cardiovascular performance) do not manifest for months or years after treatment conclusion. This is now considered the most insidious and poorly understood form of AIC. It is now thought that there are "no safe doses" of anthracyclines when considering lifetime effects, particularly in childhood cancer survivors,[34] where late toxic effects become especially noticeable. Steven E. Lipshultz is a prominent researcher in this field, and one of his seminal publications showed how chronic, progressive cardiac abnormalities were strikingly common in survivors of childhood acute lymphoblastic leukaemia many years after therapy conclusion.[35] A large (n = 4122) study in 2010 emphasised these findings by showing that in the long term (average follow-up time = 27 years), survivors of anthracycline-treated childhood cancer had a 4.4-fold higher risk of death from cardiovascular disease than the general population.[11]

1.2 Anthracycline-induced cardiotoxicity in the clinic

1.2.1 Evolving classifications of cardiotoxicity – anthracycline-induced cardiotoxicity

Within AIC, three categorisations of disease presentation have historically been used, well-described by Giantris et al. in their 1998 report.[36] Firstly, acute AIC: “a reversible depression of myocardial function after the initial infusion of anthracycline, [where] discontinuation of the anthracycline usually results in significant improvement”. Secondly, early-onset chronic AIC, which “presents within 1 year after the completion of anthracycline treatment, has known risk factors and will persist or progress even after the discontinuation of anthracycline therapy”. And lastly, late-onset chronic: “cardiomyopathy that manifests itself after a latency period of 1 or more years following completion of anthracycline therapy… there is a period during which no left ventricular dysfunction or arrhythmia is detected, cardiac function appears normal, and the patient is asymptomatic. After this latent period, there is often progressive and rarely fatal deterioration in cardiac function”. However, marrying these manifestations with molecular mechanisms of disease (particularly distinguishing the latter two) is conceptually challenging, and more recently it has been proposed that these manifestations may be based solely on diagnosis timing & methodology, rather than true onset of cardiotoxicity at a biochemical level: it might indeed be the case that AIC is one continuous, progressive disease simply captured at different times by different diagnostic tools (e.g. serum biomarkers vs echocardiographic abnormalities vs HF symptom presentation).[37] Cardinale and colleagues demonstrated that 98% of the time, cardiotoxicity occurred less than one year following completion of anthracycline chemotherapy. The authors monitored patients closely for cardiotoxicity, and promptly began treatment with HF medication upon detection, resulting in full or partial improvement in left ventricular systolic function in 82% of cases. They therefore concluded that AIC is not irreversible and is likely one continuous phenomenon, challenging the historic acute/early-onset/late-onset chronic framework used to categorise clinical presentations of disease.

1.2.2 Risk factors and incidence of anthracycline-induced cardiotoxicity

Risk factors for development of CVD later in life after anthracycline treatment include classical cardiovascular risk factors, for instance modifiable factors like hypertension and dyslipidaemia, which might be measured then evaluated together by a clinician

using an algorithm such as the Framingham Risk Score.[38] The prevalence of such modifiable risk factors was shown to be similar in adults exposed to cardiotoxic cancer therapies in their childhood compared to the general population but interestingly, cancer survivors were nearly twice as likely to be undertreated for these conditions, which could potentiate the late effects of cardiotoxic chemotherapies.[39] Furthermore, patients with pre-existing CVD conditions/a family history of CVD,[40] patients who have received concomitant or sequential thoracic irradiation,[41] and patients who are very young or very old are at higher risk of developing AIC.[42] Interestingly, female sex is significantly associated with a greater incidence and severity of cardiovascular events later in life after receiving anthracycline therapy for a childhood cancer, though precisely why this is remains unclear.[43] Lastly, as was alluded to previously, AIC risk is highly dose-dependent, with higher lifetime cumulative doses correlating strongly with cardiotoxicity risk across patient cohorts – this has been noted historically and was starkly demonstrated by Swain and colleagues in their 2003 retrospective analysis of three clinical trials investigating CHF after DOX exposure (**Figure 1.2**).

Taking into account all these risk factors and the diversity of indications treated with anthracyclines, it is difficult to accurately estimate the overall incidence of AIC in the clinic, and the field acknowledges this uncertainty as a challenge.[44] One robust study of breast cancer and lymphoma patients recently found that the incidence of CHF to be 7.4% over a 15-year period, in anthracycline-exposed patients compared to community controls.[45] This study is considered particularly reliable as the authors robustly defined CHF (using the modified Framingham criteria) and performed manual record reviews to confirm CHF diagnosis.[44]

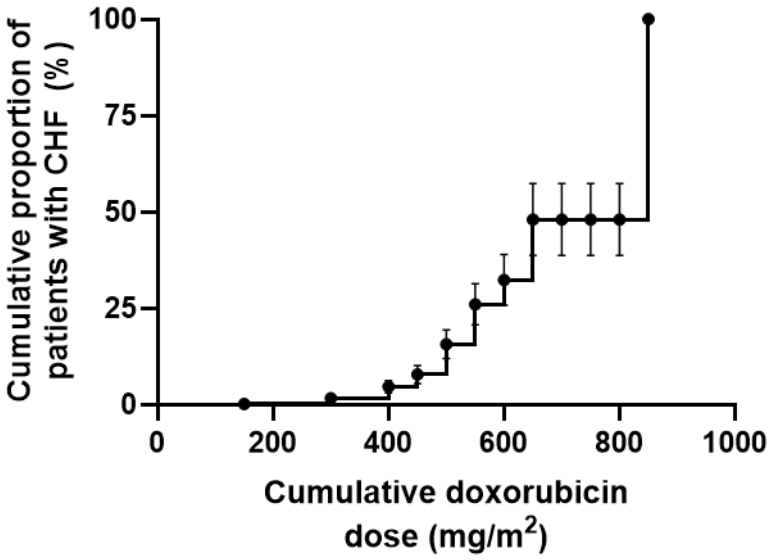

Figure 1.2 Cumulative percentage of patients having experienced congestive heart failure (CHF) increases with higher cumulative DOX dose. Adapted from Swain et al. 2003. Data are expressed as cumulative percentage +/- standard error. n = 630 patients, 32 CHF events.

1.2.3 Anatomical classification of anthracycline-induced cardiotoxicity

Considering the anatomical classifications of AIC, several detectable cardiomyopathies have been reported.[36] Firstly, dilated cardiomyopathy, in which the left ventricle (LV) chamber becomes enlarged, leading to incomplete ejection of blood from the chamber – this is the most typical anatomical presentation of AIC in patients who received anthracycline therapy as adults. Secondly, hypertrophic cardiomyopathy, in which the LV walls themselves become thickened, encroaching on the chamber volume and impairing contraction. Thirdly, restrictive cardiomyopathy, in which the LV wall becomes rigid but not thickened, impairing contraction through loss of elasticity – this has been observed more specifically in patients who received anthracycline therapy as children and survived to adulthood.[46] Another novel clinical presentation of AIC in paediatric populations was coined by Lipshultz and colleagues in 2014; “Grinch syndrome”. Here, it was noted that patients treated with anthracyclines for acute lymphoblastic leukaemia in childhood developed hearts which were too small for their body size.[47] These disparate anatomical presentations of AIC dependent on patient age at point of treatment indicate that anthracyclines may affect myocardial growth (which studies suggest is primarily driven by hypertrophy rather than hyperplasia in the

cardiomyocyte (CM) population, which is the opposite of what is thought to occur in cardiac endothelial and fibroblast populations).[48]

1.2.4 Histopathology of anthracycline-induced cardiotoxicity

Despite the long history of AIC research, there is still relatively little information regarding the histopathology of this chronic disease in its late stages. Historical reports note myofibrillar loss, sarcoplasmic reticulum swelling and “myocyte damage” in endomyocardial biopsies from anthracycline-treated patients.[49,50] In a more recent study using a small cohort of hearts (n = 10) from AIC patients (at autopsy or explanted from cardiac transplant), necrosis and myelocytolysis was not observed, but fibrosis was noted in many forms: Interstitial (10/10), multifocal (6/10), diffuse (3/10), and focal (1/10). Replacement fibrosis was seen in multifocal (2/10) and focal (4/10) formats.[51] At a macro level, it is not thought that concentric remodelling of the myocardium is associated with anthracycline exposure (as assessed by prospective echocardiography),[52] but at a the microenvironmental and cellular level, remodelling processes such as CM hypertrophy, increased collagen deposition and extracellular matrix (ECM) modulation have been demonstrated in preclinical models of AIC.[53-55]

1.2.5 Assessing cardiovascular health: applications for anthracycline-induced cardiotoxicity

Cardiac health can be measured in several ways, including serum biomarkers, imaging techniques, patient questionnaires and exercise tests. To make a diagnosis of cardiac abnormalities, e.g. HF in AIC, a careful combination of approaches provides a comprehensive assessment.

B-Type Natriuretic Peptide (BNP) and the troponin family of proteins constitute the main circulating biomarkers used to assess cardiac health in the clinic. Mature BNP protein is produced in a stepwise manner: firstly, the *NPPB* gene encodes for the preproBNP protein, which is secreted by CMs and other cardiac-resident cells into circulation.[56] In the presence of stress, preproBNP is cleaved via the serine protease corin into NT-proBNP (inactive fragment) and BNP (active hormone).[57] Both NT-proBNP and BNP can be detected in plasma, and are considered useful (often gold-standard) markers of acute myocardial infarction (MI) and end-stage HF in the clinic,[58,59] which are also robust prognostic indicators of morbidity and mortality.[60,61]

Troponins are elements of the calcium-binding troponin complex, which regulates muscle contraction through structural changes of the actin-tropomyosin filaments and

activation of myosin ATPase activity.[62] Three main forms of troponin are expressed by CMs: troponin C (cTnC), troponin I (cTnI), and troponin T (cTnT). cTnI and cTnT are released by necrotic CMs and used as a circulating clinical biomarker of myocardial injury, including AIC. Troponin assays have traditionally been considered as primarily reflective of acute myocardial necrosis, but many studies now suggest that this marker is upregulated in chronic disease also, which was recently reviewed.[63] Interestingly, the 2024 PROACT clinical trial found that breast cancer patients with a history of high-dose anthracycline treatment showed different incidences of myocardial injury dependent on which troponin assay was used as a biomarker of myocardial injury at 1 month post-treatment. When cTnT criteria were used, 89% of patients were deemed to have myocardial injury, whereas when cTnI criteria were used, only 51% of patients were deemed to have myocardial injury,[64] raising questions about how to choose an assay in the clinic and what each assay's clinically relevant thresholds might be.

Cardiac function can also be assessed by imaging techniques, for instance to evaluate how much blood the left ventricle pumps out with each contraction, termed the left ventricular ejection fraction (LVEF). HF can present with preserved or reduced ejection fraction (HFpEF or HFrEF, respectively). This is commonly measured using echocardiography, where reduced ejection fraction is usually defined as < 40%, and preserved ejection fraction ≥ 50%, with a "grey area" between these thresholds termed "mid-range".[65] AIC is typically diagnosed in a HFrEF paradigm (systolic dysfunction) but some studies have suggested that AIC onset could be predicted by diastolic dysfunction (manifesting as HFpEF, perhaps before progressing to HFrEF), and that there may be value in incorporating non-strain parameters as predictors also.[66-68] A powerful imaging method for diagnosis of cardiac dysfunction in AIC is cardiac magnetic resonance imaging (MRI), a comprehensive technique with novel prospective applications.[69] However, its widespread use is hindered by higher costs and invasiveness (intravenous injection of gadolinium dye is required).[70] Lastly, traditional questionnaires like the Minnesota Living with Heart Failure Questionnaire (MLHFQ) are commonly used to assess patient quality of life and the patient's perception of the impact of medical interventions:[71] though it is nearly 35 years old, the MLHFQ remains a robust instrument to assess patient quality of life.[72] These questionnaires are not fully capable of capturing cardiopulmonary functionality however, so exercise tolerance tests are useful in defining a patient's maximum exercise capacity, which is characteristically diminished in HF.[73]

Each screening method carries with it a set of strengths and drawbacks, and a multi-pronged approach should be used to assess cardiac health after anthracycline exposure: several comprehensive reviews and guidelines relevant to paediatric and adult patient populations have been published covering these topics, which emphasise the need for harmonisation of monitoring/screening approaches both domestically and globally.[74-76] The cost-effectiveness and ethics of the routine cardiac screening of anthracycline-treated patients is actively debated by clinicians in the field, especially in healthcare systems in which the patient is liable to pay for their treatment at point of care. Better understanding molecular mechanisms of which may give rise to anatomical abnormalities is a priority in AIC research, given that early detection and intervention can significantly improve cardiac outcomes and lessen the restriction of these efficacious oncology therapies.

Whilst traditional cardiovascular risk factors and cumulative anthracycline dose predominate as risk factors for AIC development, it can remain challenging to predict which patients will develop AIC even after controlling for these factors. Better prediction and earlier diagnosis of AIC allows for more fruitful clinical interventions. Circulating biomarkers BNP and cTnT have been suggested as predictive clinical biomarkers of AIC, in addition to their established diagnostic use, but the evidence base for this is mixed.[77,78] Several molecular mechanisms have been suggested to underpin AIC (which will be discussed later in this thesis) and circulating markers from these mechanisms have consequently been proposed as predictive biomarkers of disease, but none have yet translated to the clinic successfully.

1.2.6 Anthracycline-induced cardiotoxicity has limited targeted treatments available

AIC can in some cases be prevented by co-administering the metal-chelating drug dexrazoxane alongside anthracycline therapy. In the 1970s, researchers facilitated by Imperial Cancer Research Fund developed a class of bisdioxopiperazine-based compounds for use in an oncology setting based on their metal-chelating properties.[79] Being intolerably toxic, the compounds were not successful as antineoplastic agents, but Eugene H. Herman and colleagues discovered that one compound in particular, ICRF-187, was in fact protective against AIC, showing cardioprotective effects in DOX- and daunorubicin-treated dogs, rabbits, and pigs.[80-82] This compound would later be named dexrazoxane, which is now stands alone as the only recognised, preventative, cardioprotective agent against DOX or epirubicin cardiotoxicity.[83]

The Food and Drug Administration first approved the use of dexrazoxane for patients with metastatic breast cancer who had received a DOX cumulative dose of > 300 mg/m^2 and who would continue to receive DOX in their chemotherapy regimen.[83] The European Medicines Authority also now allows for the use of dexrazoxane in cancer patients under 18 years of age who would receive > 300 mg/m^2 of anthracycline therapy.[84] Though this drug is a go-to for many cardio-oncologists, particularly in the paediatric sphere, there is some debate remaining concerning its safety, efficacy and molecular function.

One impactful study from 2007 found that paediatric Hodgkin lymphoma patients pre-treated with dexrazoxane before anthracycline exposure showed a higher incidence of developing secondary malignancies than patients treated with anthracyclines alone.[85] This study understandably received a great deal of attention in the field and remains well-cited: the authors speculated that the only cardioprotective drug available in AIC dampened the antineoplastic effects of anthracyclines. However, this was a very small study: out of 278 patients in both arms of the study, just 10 patients developed secondary malignancies. Using this subgroup, it was calculated that the standardized incidence rate for all second malignant neoplasms was significantly increased at 41.86 with dexrazoxane versus 10.08 without dexrazoxane.[85] Subsequent studies (mostly in studies focused on adult survivors of childhood cancer) have failed to reproduce this phenomenon, and the concept that dexrazoxane treatment increases the risk of secondary neoplasms has largely been disproven.[86] More recent studies point to the long-term cardioprotective effects of dexrazoxane, in long-term follow-up.[87,88] Interestingly however, dexrazoxane has been shown to exert more cardioprotective benefit in young female patients compared to young male patients, and the reason for this is unknown.[86] Furthermore, debate still continues on the molecular mechanisms behind dexrazoxane's cardioprotective effects,[89] which will be discussed later in this thesis.

1.2.7 The utility of standard-of-care heart failure interventions in treating anthracycline-induced cardiotoxicity

Once AIC-associated HF has been diagnosed, standard-of-care treatments which generically aim to manage HF are employed, typically including angiotensin-converting enzyme inhibitors (ACEi), angiotensin receptor blockers (ARBs) and beta-adrenergic blockers (beta-blockers). However, the evidence base for the benefit of these medications in AIC specifically, is mixed.

The renin-angiotensin-aldosterone system (RAAS) is a key regulator of the cardiovascular, renal and vascular systems, and thus is an important pharmacological target in blood pressure management and CVD more broadly.[90] The angiotensin (Ang) hormones and their receptors form a key part of this system. Ang I is cleaved from the circulating prohormone angiotensinogen (produced by the liver) by the enzyme renin. Angiotensin-converting enzyme then cleaves Ang II from Ang I, and Ang II enters into circulation. Two major subtypes of angiotensin receptor are AT_1R and AT_2R, which allow the RAAS system to modulate humoral and haemodynamic effects. Therefore, several components of this system are targeted in the treatment of CVD. Both ACEi and ARB therapies (which aim to attenuate the conversion of Ang II to Ang I, and dampen the signalling of circulating Ang II via competitively inhibiting the AT_1R, respectively) can beneficially alter haemodynamics in patients with CVD,[91-93] which has greatly impacted the management of HF. Beta-blockers are slightly different from ACEi and ARB therapies in that they aim to modulate the effects of the RAAS on the sympathetic nervous system. This system becomes persistently activated in HFrEF, leading to chronic activation of myocardial β-receptors, which regulate heart rate and contractility (via the agonistic action of e.g. adrenaline and noradrenaline hormones). Pharmacologically blocking chronic β-receptor activation can upregulate myocardial β-receptor number and restore their function, thus improving the contractile reserve of the heart, re-balancing the RAAS, improving coronary flow and overall improving the structure and function of the left ventricle.[94]

In the specific context of AIC-HF, however, the benefit of ACEi, ARB and beta-blocker prescription is more contentious. In adult survivors of childhood cancer treated with DOX who were experiencing LV dysfunction, the ACEi enalapril transiently induced improvement in LV structure and function but long-term, the LV wall continued to thin and deteriorate.[95] The short-term benefits of enalapril were therefore attributed to the lowering of diastolic blood pressure. This was mirrored in an adult cohort in the recent PROACT trial, focusing on breast cancer and lymphoma patients who had been treated with high-dose anthracycline, which showed that treating with enalapril alongside chemotherapy regimen did not prevent cardiotoxicity.[64] The PRADA trial showed that treatment with the ARB candesartan and beta-blocker metoprolol during anthracycline therapy for breast cancer did not prevent LVEF decline at two years follow-up. They did however find that candesartan modestly improved LV end-diastolic volume (the amount of blood remaining in the LV prior to contraction) and attenuated a decline in

global longitudinal strain (an echocardiographic measurement of LV shortening from base to apex). Overall, results suggested that most patients with early breast cancer would not benefit from a broadly administered cardioprotective approach such as this.[96] A meta-analysis of 17 trials testing the benefit of prophylactic beta-blocker administration for AIC prevention concluded that beta-blockers could prevent dilation of the LV, development of diastolic dysfunction and LVEF reduction but even so, these effects did not attenuate cardiotoxicity incidence, prevention of hospitalisation for HF, or cardiac death.[97] Lastly, the Cardiac CARE trial recently demonstrated a combination therapy of ACEi candesartan and beta-blocker carvedilol had no demonstrable cardioprotective impact on patients with high-risk cTnI concentrations undergoing anthracycline-based chemotherapy, at 6 months-post treatment.[98] Similar declines were observed in LVEF between treatment groups, and additionally, the usefulness of monitoring cTnI for AIC development was called into question, given that similar declines in LVEF occurred regardless of changes in cardiac troponin concentration during chemotherapy.

In summary, the only AIC-specific treatment used in the clinic today remains dexrazoxane, which has demonstrable cardioprotective effects – however, these effects have a larger evidence base in paediatric populations, and as will be discussed later in this thesis, the molecular mechanisms of this drug are still actively debated. Standard-of-care HF interventions such as ACEis, ARBs and beta-blockers are used in patients but their clinical benefit, as investigated in several recent clinical trials, is questionable. In late-stage AIC-HF refractory to these therapies, the only remaining intervention is transplant. Though outcomes are reportedly equally as positive for AIC patients compared to non-AIC patients requiring heart transplant (e.g. similar rates of organ rejection, transplant-associated malignancy, graft survival), the co-morbidities which anthracycline-treated patients may live with (e.g. active neoplasms, ongoing therapy, frailty) may hinder or exclude their access to transplant.[99] Alongside this, AIC patients typically wait longer for a transplant heart than other patients,[100] against a background of an insufficient donor pool to serve those requiring heart transplant (**Figure 1.3**).[101] Better therapies and interventions are therefore needed for AIC patients, who represent a growing population with specific healthcare needs, and understanding the molecular mechanisms of AIC is key to this objective.

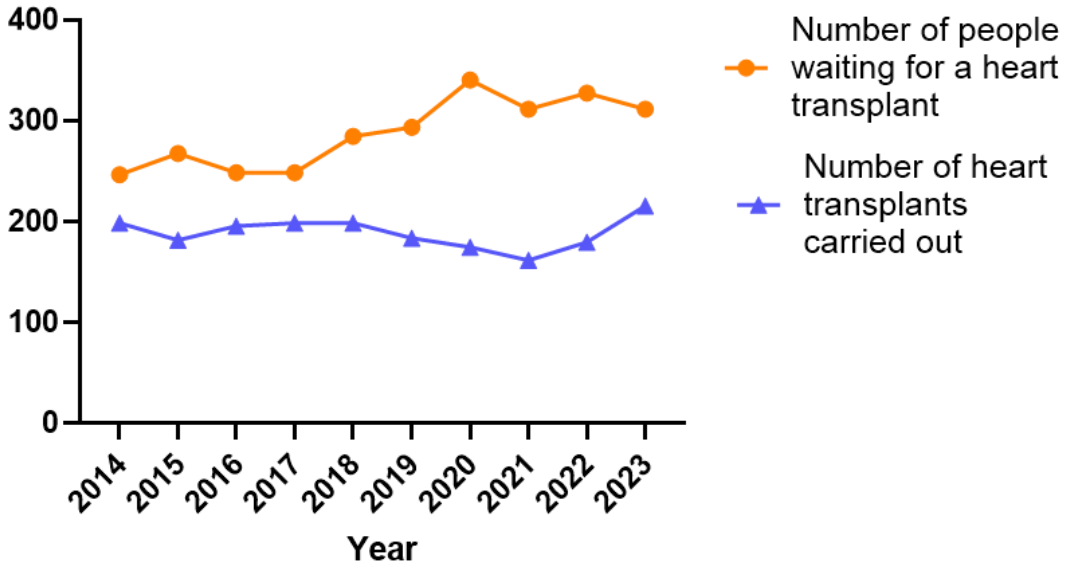

Figure 1.3 The number of people waiting for a heart transplant in the UK and the number of heart transplants carried out in the UK between 2014 and 2023. Data from NHS Blood and Transplant 2023 report.

1.3 Reported molecular mechanisms of anthracycline cardiotoxicity

Although the cardiotoxicity of anthracyclines has been noted in the clinic for over 50 years, the molecular mechanisms underpinning this cardiotoxicity are still not well understood, though a number have been proposed.

1.3.1 Oxidative stress and topoisomerase poisoning as mechanisms of anthracycline-induced cardiotoxicity

Cellular oxidative stress has received longstanding attention in the evaluation of both the anti-cancer and cardiotoxic effects of anthracyclines. Anthracyclines contain a quinone moiety which can undergo reductive activation via several intracellular oxidoreductive enzymes. In the process of conversion from quinone to semiquinone moiety, free radicals are generated, which interact with intracellular oxygen to yield ROS (**Figure 1.4**), causing stress to the cell.

On the other hand, being sufficiently chemically complex, anthracyclines have a wide range of possible metabolic cascades. In the intracellular CM context, further metabolic pathways excluding quinone moieties are possible and may contribute to more chronic forms of AIC, one example being the reductive deglycosidation of DOX. These alternative metabolic pathways may actually be more pathophysiologically relevant, since they are more commonly seen at physiological O_2 partial pressures and are feasible at 10-20 times lower DOX concentrations.[102-104] Minotti and colleagues have proposed that as cardiotoxicity moves from acute to chronic phases, anthracycline redox cycling becomes less relevant.[105]

Iron has been named as a key mediator of anthracycline-induced oxidative stress, but mechanistic studies have historically been mixed. Seminal biochemical studies by Myers et al., amongst others, highlighted the crucial role iron plays as a mediator in anthracycline redox cycling reactions.[106,107] It is believed that anthracyclines stimulate the accumulation of iron and, in particular, low molecular weight iron (the “labile iron pool”) within CMs.[108] Some studies have pointed to this cellular accumulation of iron being a driver of AIC, and more recent investigations have revealed that iron preferentially accumulates in the CM mitochondria.[109] It has also been shown that cardiac cell lysate mitochondrial DNA (mtDNA) alterations are caused by ROS generated by DOX treatment, and that these alterations feed back into further mtDNA damage and respiratory chain defects.[110] This was later posited to deplete the bioenergetic capacity of the organelles,[111] effectively impairing them in the long term.

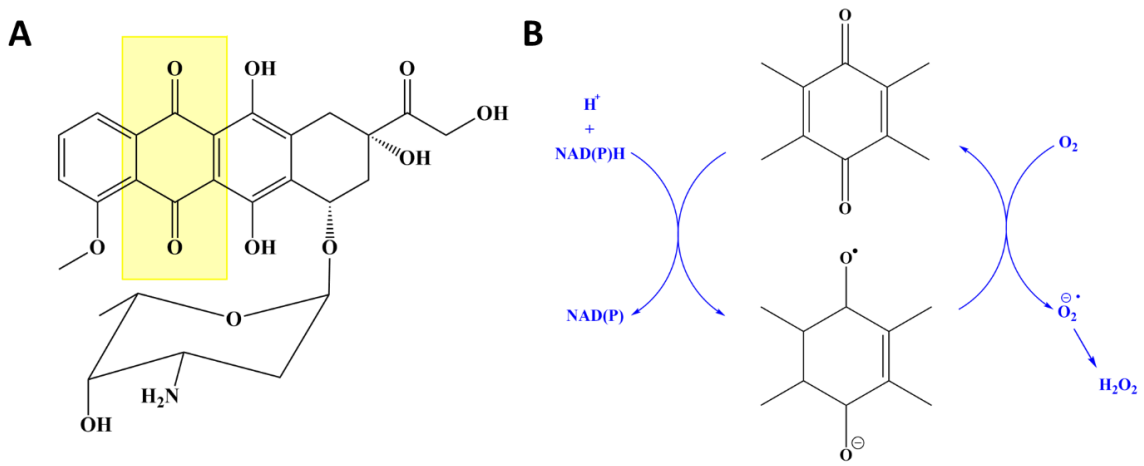

Figure 1.4 Schematic of the reductive activation of the quinone moiety in DOX, a classical anthracycline. A) The structure of DOX, with the mechanistically relevant quinone moiety highlighted in yellow. **B)** NAD(P)H-dependent one-electron reduction of the quinone moiety as proposed by Minotti et al. (2005). An unstable semiquinone forms as a result, which readily regenerates its parent species by reducing oxygen to eventually yield reactive oxygen species like H_2O_2.

On the other hand, the fact that iron-chelating dexrazoxane is clinically cardioprotective in AIC, but its sister compound desferasirox (also an iron chelator) does not provide CMs with protection from DOX-induced toxicity *in vitro*,[112] threw into question the cardioprotective mechanism of action of dexrazoxane and consequently the role of intracellular iron accumulation in AIC. The TopIIα-poisoning property of anthracyclines canonically targets fast-replicating cell types: this underpins their potency as antineoplastic agents. However, CMs show very little TopIIα expression.[113] Instead, they predominantly express the TopIIβ isoform, which studies have shown can be poisoned by DOX, and may contribute to cardiotoxicity.[114] In 2007, Lyu et al. showed that in CMs, dexrazoxane interacts with TopIIβ, rather than acting solely as an iron chelator: dexrazoxane thusly prevents TopIIβ poisoning by anthracyclines and attenuates DNA damage and cellular stress.[89] Building upon this, Martin and colleagues subsequently showed that the TopIIβ-inactive iron chelator ICRF-161 was not protective against the cardiotoxic effect of DOX in an *in vivo* model of chronic anthracycline-induced cardiomyopathy.[115]

These findings highlight the complexity of the intracellular signalling cascades at play, which historically may have been oversimplified. Indeed, the variation in dexrazoxane's cardioprotective effects between young female and male patients, and how these change with age,[116] is a stark indicator that the molecular mechanisms of cardioprotective therapies are not as simple as they first appear.

Finally, it must be noted that ROS generation in cardiac cells has commonly been observed in studies using a supratherapeutic dose of anthracycline. Though historical studies have shown that DOX concentrates significantly in the mitochondria and nuclei of the myelogenous leukaemia cell line K562,[117] this may not be necessarily true of CMs and other cardiac cell types.[118] Much of the historic research in this area has focused on CMs only, giving a restricted view of the molecular processes of the heart more globally, which comprises several cell types, all important for proper function. Finally, in a more general sense, oxidative species such as H_2O_2 are implicated in myriad regular cellular processes and are essential for proper cell signalling, physiologically speaking. Therefore, in this context it can be difficult to fully unpick whether oxidative species release is a primary response to acute damage, or a secondary response further down a signalling cascade. Indeed, generation of ROS within CMs could viably represent both a cause and effect of acute cellular damage from anthracycline exposure. In summary, though mechanisms involving ROS generation and intracellular iron accumulation have garnered a good deal of attention in cardiotoxicity research overall, other mechanisms may also be at play in chronic AIC.[119]

1.3.2 Mitochondrial dysfunction in the pathophysiology of anthracycline-induced cardiotoxicity

Due to their constant mechanical workload, CMs are extremely energetically demanding. Their mitochondria are therefore especially crucial to their function, which rely on a delicate balance of bioenergetics, mitophagy, mitochondrial biogenesis and fission/fusion. Independent of the mechanisms above involving ROS generation, anthracycline-induced mitochondrial dysfunction may have detrimental effects. For instance, the TopIIβ-mediated cytotoxicity of DOX has repeatedly been linked to mitochondrial disturbances including attenuated mitochondrial regulation and biogenesis.[109,114]

Cardiolipin has emerged as a potential target in chronic AIC: cardiolipin is a phospholipid housed in the inner membrane of mitochondria and is crucial to stabilising enzymes and their complexes to facilitate effective energy metabolism.[120] In many tissues, cardiolipin has been implicated in pathologies such as ischemia, ageing and HF.[121] Reduced concentration of cardiolipin, or variation in its composition, is found within Barth syndrome (BTHS), an X-linked recessive disease: these cardiolipin alterations stem from a mutation within the tafazzin gene, which is key to the

biogenesis of cardiolipin.[122] The symptoms of BTHS are heterogeneous, but a key hallmark of the disease is cardiomyopathy. These findings prompt the question of how much influence the cardiac lipidome holds on heart disease in a more general sense, and this has recently been explored in the context of late-onset AIC.

In 2015, Moulin and colleagues found that in a chronic *in vivo* model of DOX-induced cardiotoxicity, DOX had a sex-specific impact on the cardiac phospholipidome, especially on cardiolipin.[123] This supports Lipshultz et al.'s earlier findings that an independent risk factor for cardiac abnormalities after treatment with DOX for childhood cancer was female sex.[43] Loss of cardiolipin and cytochrome c was recently linked to depressed mitochondrial respiration in a chronic DOX-induced cardiotoxicity *in vivo* mouse model, making the heart vulnerable to accelerated ageing and inhibiting its ability to respond to stress.[124] Additionally, Xu et al. found that cardiolipin was degraded too quickly in lymphoblasts taken from patients with BTHS, and that resveratrol protected cardiolipin's degradation into other fatty acid compounds.[125] The group found that resveratrol stabilised existing cardiolipin, rather than stimulating cardiolipin biogenesis, and furthermore their data suggested this stabilisation occurred through the sequestration of cardiolipin into large protein complexes. Resveratrol is an established cardioprotective agent, but its therapeutic benefit was first attributed to its influence in ROS/iron accumulation-type mechanisms,[126] whereas in Xu et al's study, its beneficial effects were attributed to its ability to promote the stabilisation of supercomplexes of phospholipids and proteins.

1.3.3 Anthracyclines can diminish the already limited regenerative capacity of the heart

The regenerative capacity of the heart and its cellular source is much debated. Historically, the dogma has long been that CMs in the human heart are essentially post-mitotic.[127,128] In the early 2000s, studies reported that the adult myocardium did in fact possess some regenerative capacity,[129,130] but unfortunately the reliability of the data in these papers and the wider scientific conduct of selected authors has since been questioned.[131] However, in 2009, an impactful study by Bergmann and colleagues demonstrated that CMs could indeed be regenerated postnatally – albeit much more modestly than was suggested in the aforementioned studies. They elegantly showed this by assessing the integration of carbon-14 into DNA to measure CM age, and although the reported CM turnover was low (< 50% of CMs being exchanged within a human lifetime), this represented compelling evidence that human CMs are not

completely post-mitotic.[132] This sparked a flurry of affirming studies, and discussion in the field.[133-135]

Within this new paradigm, many questions remain concerning why CMs are still relatively limited in their regenerative potential, and what cellular source of this limited regeneration may be. A recent review suggested that the polyploidic nature of CMs may be an obstacle in their continuing the cell cycle and highlighted this as a particularly perplexing part of their physiology.[136] Senyo and colleagues showed in 2014 that turnover of CMs in the absence of injury is underpinned by low-level (0.76% per year) CM proliferation rather than cardiac progenitor involvement.[137] Several nuances such as those explored by Senyo et al. have not yet been fully elucidated. In summary, stimulating any innate proliferative capacity of the CM would represent an exciting opportunity for treating the many CVDs where CMs are lost to apoptosis, which preclinical models indicate does occur in the acute stages of AIC.[138,139]

The concept of a cardiac stem cell (CSC) or cardiac progenitor cell (CPC) came to prominence in the early 2000s. Several stem cell populations, precursor populations, and markers thereof have been proposed, such as endogenous c-kitPOS, Sca-1+, and Side Population cells.[140-143] Some studies have suggested CSCs or CPCs may be drivers of cardiomyogenesis. Separate to CM proliferation, these populations represent alternative sources of new, postnatal cardiac cells, which could renew, replace or expand CM populations. CSCs and CPCs could be a key pathophysiological target for anthracyclines: indeed, DOX has been shown to deplete CPCs, and permanently impair their function.[144] The histone deacetylase SIRT1 has been reported as a protective agent for stem cell populations, including CPCs. By treating with resveratrol, a SIRT1 activator, De Angelis et al. showed that cardiac function could be partly repaired in an *in vivo* DOX-induced cardiotoxicity context.[145] If anthracyclines do damage these populations underpinning cardiac cell generation, various cardiac cell populations may diminish over time, giving rise to a myocardium that may be vulnerable to even mild stresses.

In summary, anthracyclines have been reported to effect many changes in the cells of the myocardium (**Figure 1.5**). Their toxicity to non-myocyte cell populations is acknowledged but not generally as widely studied. Due to the multiple cytotoxic mechanisms that anthracyclines can enact (which makes them such effective antineoplastic drugs), the molecular mechanisms that could underpin cardiotoxicity are myriad, and studies in the literature are disparate. Another mechanism which has

garnered considerable interest in the mechanisms of AIC is the induction of cellular senescence in the myocardium, a cellular fate which draws together many of the above mechanisms into a single comprehensive phenotype.

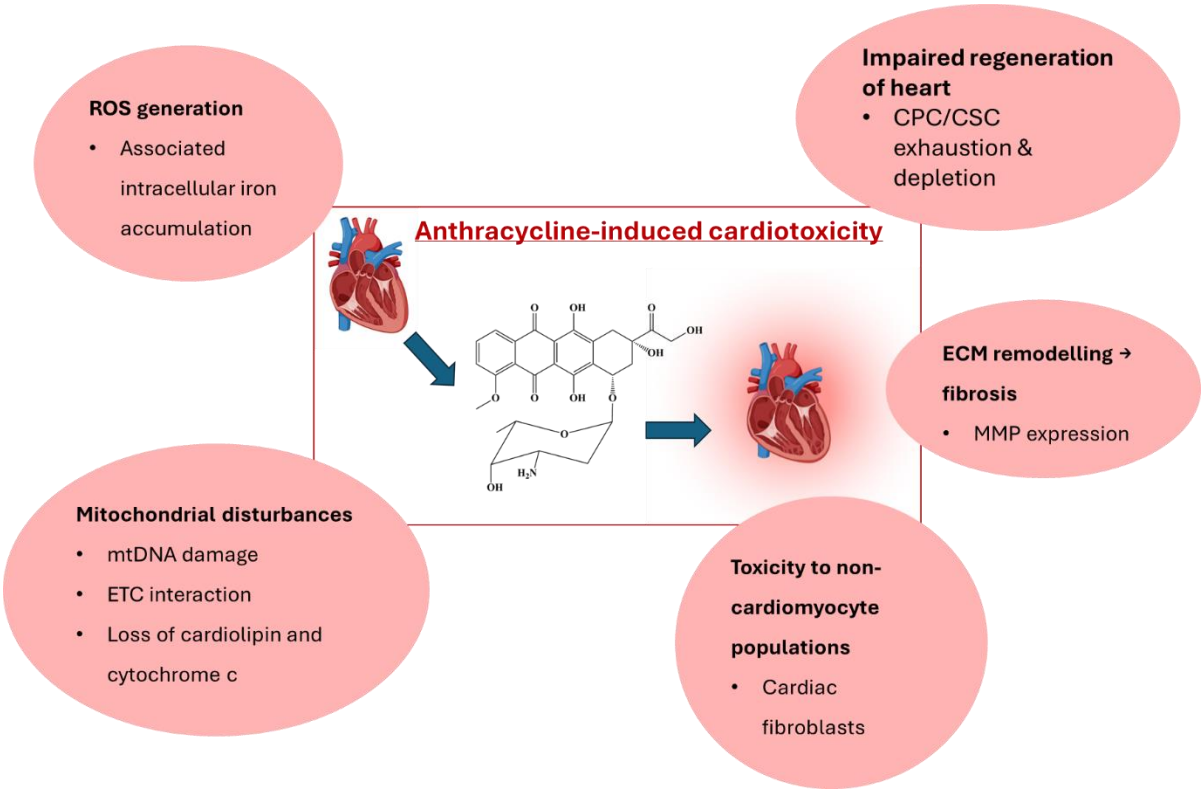

Figure 1.5 Summary of selected molecular mechanisms of anthracycline-induced cardiotoxicity highlighted in the literature. Anthracyclines have been shown to promote ROS generation and disrupt the intracellular concentration of iron, which can mediate these processes. They also are known to deplete the regenerative reserves of the myocardium. Anthracycline exposure is associated with remodelling of the extracellular matrix (ECM) via matrix metalloproteinases (MMPs) and onset of myocardial fibrosis. Anthracyclines are known to be toxic to non-myocyte populations, including cardiac fibroblasts. Mitochondrial disturbances can be caused by anthracycline exposure, including via direct damage to mitochondrial DNA (mtDNA) and interactions with the electron transport chain (ETC). Made using Biorender.com.

1.4 Anthracyclines and cardiac senescence

1.4.1 Senescence – initial definition, canonical markers, and novel approaches for identification

In 1961, Hayflick and Moorhead observed that primary human fibroblasts were only capable of a finite number of population doublings in culture, termed the Hayflick limit, before succumbing to replicative exhaustion.[146] They termed this cell fate "senescence" (derived from the Latin word "sen", meaning old, aged, or old man), which was characterised by irreversible exit from the cell cycle. Since then, senescent cells have traditionally been identified by several additional characteristics. Firstly, senescent cells express upregulated cyclin dependent kinase inhibitor 1A (*CDKN1A*), which encodes for the $p16^{Ink4a}$ (p16) protein,[147] and upregulated cyclin dependent kinase inhibitor 2A (*CDKN2A*), which encodes for the p21 protein.[148] p16 and p21 are key nodes in the $p16^{INK4A}$/pRB and p53/$p21^{WAF1/CIP1}$ tumour suppressor pathways, respectively. Secondly, as demonstrated by Judith Campisi and colleagues, senescent cells also express elevated levels of beta-galactosidase activity (termed senescence-associated beta-galactosidase, SA-β-Gal).[149] Thirdly, senescent cells also exude a cocktail of pro-inflammatory cytokines, termed the senescence-associated secretory phenotype (SASP), which has a broad range of paracrine and autocrine functions. The composition of the SASP is variable, but typically contains factors such as IL-6, IL-8, CXCL1, CCL2, CCL5, and matrix metalloproteinases.[150,151] Hence, p16/p21 activation, SA-β-Gal and SASP expression have traditionally represented the "gold-standard" identifiers of senescent cells.

More recently, senescent cells have also been shown to upregulate pro-survival pathways, including Bcl-2 family members, thus protecting themselves from a hostile microenvironment which may otherwise promote apoptosis.[152,153] Additionally, the senescent cell phenotype is now acknowledged to be heterogeneous, with studies showing variation in phenotype according to senescence-inducing stimulus, cell type, disease state and tissue residence. Several recent studies have therefore aimed to harmonise the criteria for senescent cell identification across the research community.[154] Some common characteristics are generally observed as "hallmarks of senescence", including: activated DNA damage response, activation of CDK inhibitors and cell cycle arrest, a secretory phenotype (SASP), apoptosis resistance, altered metabolism, and endoplasmic reticulum stress.[155] A transcriptomic signature has also been established aiming to identify senescent cells across both human and murine

species, and across different cell types, coined the SenMayo gene panel,[156] with other investigations proposing various individual markers which reportedly identify senescent cells more reliably than the classical p16 and p21 markers.[157]

1.4.2 The function of senescence in physiology and age-related pathologies

Regarding the function of senescence, it is now known that as a cellular fate, senescence embodies antagonistic pleiotropism – that is, at some stages of life it is beneficial towards an organism, whereas at others it is detrimental (**Figure 1.6**).[158] In development, programmed, transient senescence plays a crucial role in tissue patterning to determine correct morphogenesis.[159] In early life, senescence is a built-in defence against tumourigenesis, which can activate cell cycle arrest upon detection of oncogene activation.[160] Indeed, the evasion of senescence is crucial for tumour progression. Senescence also is important for proper wound healing: its induction limits fibrosis during wound healing by temporarily inducing cell cycle arrest in myofibroblasts.[161]

However, in other contexts, senescence can promote pathology. The persistent accumulation of senescent cells can be induced as a result of replication-associated telomere shortening, which is associated with age – this has been reported as a causal mechanism in many age-related pathologies across a variety of organ systems.[162-164] For instance, in the context of osteoporosis, murine *p16Ink4a* transcript expression was significantly higher in chronologically aged mice (6 months old vs 24 months old) in B cells, T cells, myeloid cells, osteoblast progenitors, osteoblasts, and osteocytes, the senescent phenotype of which is thought to contribute to increased osteoclastogenesis.[165,166]

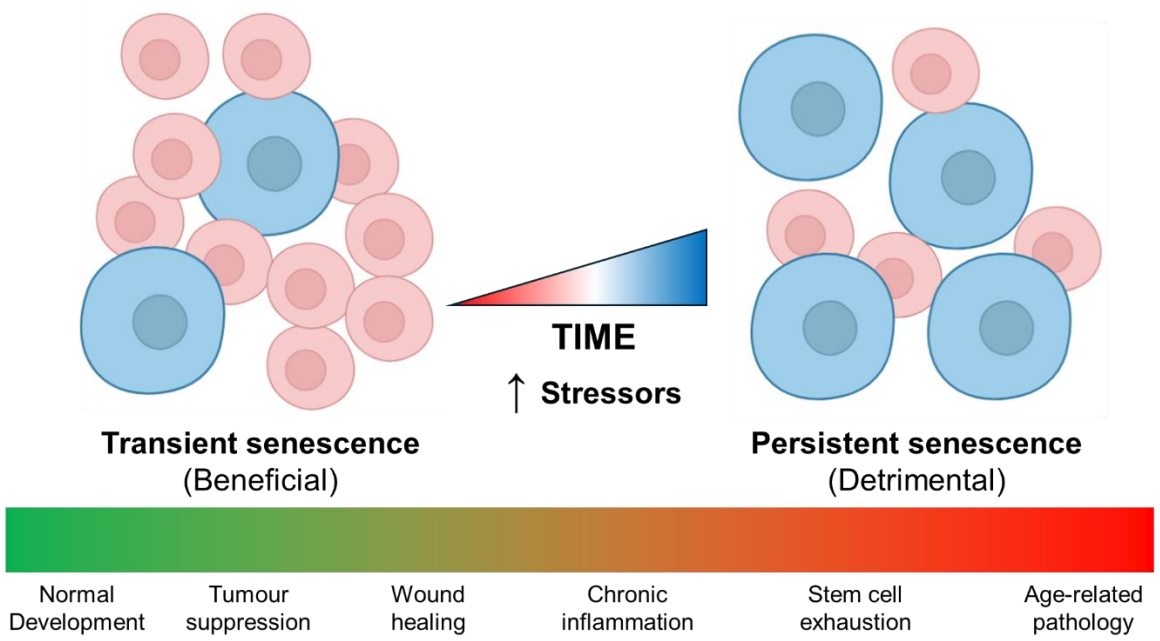

Figure 1.6 Senescence displays antagonistic pleiotropism. Transient senescence is beneficial, particularly in early life where it is essential for tissue patterning in early development, oncogene activation-induced tumour suppression and efficient wound healing. Later in life, senescent cells are not cleared effectively, so accumulate and persistently promote chronic inflammation, exhaust stem cell populations and promote age-related pathology. Adopted from Paramos et al. 2021. Made using Biorender.com.

1.4.3 Eliminating senescence using transgenic and pharmacological approaches

Given the established causal role of senescent cells in age-related disease, interventions to eliminate senescent cells have been developed, either to explore mechanisms of disease using proof-of-principle studies, or with the goal of alleviating disease associated with senescence. $p16^{Ink4a}$-positive cells can be eliminated in transgenic mouse models using an otherwise benign drug, in models such the INK-ATTAC line.[167] Using this line, seminal studies by Baker and colleagues showed how systemic clearance of $p16^{Ink4a}$-positive cells delayed the onset of age-associated pathologies in the adipose tissue, skeletal muscle and eye of old mice, implicating senescence as a causal player in pathology.[167] The p16-3MR line was more recently developed, which also allows for tracking of p16-positive cells via non-invasive whole-body luminescent imaging.[162] In addition, various drugs have been developed which target the upregulated pro-survival pathways of senescent cells – pharmacologically inhibiting these pathways causes selective apoptosis in senescent cells.[152] The small molecules navitoclax and venetoclax, which target the Bcl-2 family of pro-survival

proteins (e.g. BCL-2, BCL-XL, BCL-W and others), have been taken into the clinic for oncology applications and show good safety profiles.[168,169]

1.4.4 Senescence can occur in non-mitotic populations, and be induced by stressors independently of ageing

It was historically thought that senescence, traditionally defined by irreversible exit from the cell cycle, could not conceptually occur in post-mitotic cell types. However, it has since been shown that senescence indeed occurs in, and associates with diseases of, post-mitotic cell populations like neurons, rather than solely mitotic cell types. For instance, in postmortem human brain tissue with age-associated tauopathy (common to several neurodegenerative diseases), *CDKN2A* transcript was upregulated compared to age-matched healthy adult controls, and furthermore, *CDKN2A* transcript showed a positive correlation with neurofibrillary tangle deposition (the accumulation of which is the closest correlate with cognitive decline and cell loss).[170] Furthermore, it is now known that senescence can also be induced by a variety of stressors, not just progressive shortening of telomeres with age, such as oxidative and genotoxic stress, nutrient deprivation, mitochondrial dysfunction, inflammation, irradiation, or chemotherapeutic agents.[171] The accumulation of senescent cells can therefore be thought of as both a driver and product of “biological age”, which may also accumulate with “chronological age”.[172]

Hence, the complex senescent phenotype has come under investigation in many cell types (irrespective of their participation in the cell cycle), and in many pathologies (irrespective of their association with ageing), which led to its investigation in the context of post-mitotic CMs and a variety of cardiovascular pathologies. Subsequently, it was found that senescence can indeed be induced in post-mitotic, mature CMs, which occurs in a telomere-independent manner.[173]

1.4.5 Senescent cells, including cardiomyocytes, contribute to cardiovascular remodelling and pathology

Associations have now been made between cellular senescence and cardiovascular disease more broadly. Indicating that senescent cells contribute to impaired cardiovascular function, in 24-month old (aged) mice, LVEF and fractional shortening were shown to improve upon administration of the combination senolytic therapy of dasatinib & quecertin (D&Q).[152] Suggesting that senescent cells might promote maladaptive myocardial remodelling, the use of navitoclax to eliminate senescent cells

in mice post-MI was shown to attenuate CM hypertrophy and myocardial profibrotic TGFβ2 expression, and these results were bolstered by similar findings in an ischaemia-reperfusion injury (IRI) setting, where navitoclax treatment was associated with reduced infarct scar size, increased angiogenesis, and reduced SASP expression.[174,175] The CM SASP is thought to be quite particular, comprising factors such as GDF15, Endothelin-3 and TGFβ2: these factors in isolation were able to induce α-smooth muscle actin production in fibroblasts *in vitro* (a marker of myofibroblast activation), indicating the CM SASP was functional and may promote fibrosis in a paracrine manner.[173]

In patients > 70 years of age, over half of CPCs have been shown to be senescent, and unable to fulfil their regenerative, reparative role in an infarcted heart. Furthermore, the SASP of these CPCs was able to induce senescence in non-senescent CPC populations *in vitro*, but addition of D&Q abrogated these effects.[176] Clinically, there is extensive evidence of the association between vessel wall senescence accumulation and atherosclerosis: histological analysis of post-mortem tissues has identified that atherosclerotic vessels contain more senescent endothelial and vascular smooth muscle cells than aged-matched healthy arteries.[177] Moreover, expression of p16 in diseased human coronary arteries positively correlates with plaque instability.[178] In summary, these studies support the notion that senescent myocardial cells, including CMs, contribute to remodelling and the promotion of disease in several cardiovascular pathologies.

1.4.6 Myocardial senescence occurs in anthracycline-induced cardiotoxicity

Directly implicating senescence in AIC, seminal studies in 2017 showed how the adverse effects of anthracycline therapy, including cardiovascular phenomena, may be linked to the induction of systemic senescence.[179] Demaria and colleagues demonstrated that DOX promoted a global induction of the senescent cellular phenotype in mice, which persisted and contributed to local and systemic inflammation. Senescence transcript markers *p16^{INK4a}* and *p21* were induced in a variety of cardiac cells upon DOX treatment, though interestingly, not CMs. DOX treatment was associated with a decline in several functional cardiac parameters (which only became significantly detectable 4 weeks after DOX treatment) but elimination of p16^{Ink4a}-positive cells almost completely prevented these declines, as well as reducing several other chemotherapy-related morbidities. The ability of DOX to induce senescence markers in the myocardium *in vivo* has since been validated by other groups, also

using sublethal, clinically relevant doses.[180] Furthermore, systemic, pharmacological elimination of senescent cells using navitoclax has been shown by yet other groups to improve cardiac function in preclinical models of AIC.[181] Importantly, the delayed onset nature of cardiotoxicity in Demaria et al.'s study mirrored the clinical manifestation of AIC faithfully, and the persistence of senescent cells in the myocardium tallies well with the chronic nature of this toxicity. The same group have since shown that senescence-related markers were significantly upregulated in the left ventricles of seven patients who suffered severe AIC (DOX-induced), demonstrating the translation of this mechanism to humans.[182]

1.4.7 How might senescent cardiac cells contribute to anthracycline-induced cardiotoxicity? Lessons from the senescent cellular phenotype in other cardiovascular pathologies

The complex senescent cellular phenotype may contribute to AIC pathology in many ways, which are not yet well-understood, but may be similar to the molecular mechanisms in other CVDs where senescence plays a causal, detrimental role.

Firstly, senescence can be induced by DNA damage, genotoxic and oxidative stress, and mitochondrial dysfunction - all of which can be effected by DOX at a cellular level. For instance, suggesting that increased oxidative stress and mitochondrial dysfunction are indeed key inducers of senescence in CVD including AIC, are studies demonstrating that mitochondrially-targeted overexpression of catalase increases longevity and reduces age-related cardiac pathologies,[183] and heart-specific overexpression of catalase increases resistance to DOX-induced cardiotoxicity.[184]

Though functional studies are lacking, senescent CMs show several changes in their mitochondria which may impact bioenergetics and cellular performance. Senescent CMs isolated from aged mice show decreased nuclear expression of mitochondrial transcripts,[173] and both the mitochondrial inner membrane structure and mitochondrial fusion dynamics display alterations in senescent CMs (induced by DOX).[185] Furthermore, in the hearts of mice post-IRI (where myocardial senescence was observed), proteomic and gene ontology (GO) analyses of heart tissue showed that mitochondrial function and cellular respiration GO terms were significantly de-enriched, and rescued by systemic navitoclax treatment which successfully cleared senescent cells.[175] Mitochondrial disturbances are an acknowledged hallmark of ageing generally,[186] and indeed mitochondria are thought to be required for how cellular

senescence promotes ageing phenotypes.[187] These changes may contribute to the mitochondrial disturbances detailed earlier (see **1.3.2**), but further studies are required to establish a direct link between anthracycline exposure, mitochondrial dysfunction, and the contribution of this dysfunction to pathology in AIC.

From other CVD contexts still, it can be concluded that senescent cardiac cells also display characteristics that may promote myocardial remodelling (see **1.4.5**). For instance, in the context of MI, the p53-mediated induction of senescence in cardiac fibroblasts was associated with attenuated deposition of reparative collagen, which is required for maintaining the integrity of myocardial tissue acutely post-MI, suggesting that senescent cells can modulate wound healing responses in acute CVD.[188] In the senescent myocardium post-IRI, inflammation-associated processes such as “secretion by cell”, “immune response” and “response to cytokine” were seen to be upregulated using proteomic and GO analyses.[175] In the same study, after systemic clearance of senescent cells, proteins involved in biological processes related to “supramolecular fibre organisation” and “cytoskeleton organisation” were downregulated, suggesting attenuated propensity for myocardial remodelling. These molecular processes may contribute to the previously introduced fibrotic histopathology which is noted in late-stage AIC patients, and eventual organ-level changes which result in cardiomyopathy.

Lastly, senescent CMs have been shown to be hypertrophic and express a functional SASP, including pro-inflammatory and pro-fibrotic factors such as IL6, IL8 and TGFβ.[173,174] The ongoing production of SASP would allow CMs induced to senescence by short-term anthracycline exposure to persistently effect change in the myocardium long after the anthracycline has been excreted, which marries well with the delayed-onset nature of toxicity. Overall, several aspects of the senescent CM and cardiac environment align with the pathologies noted in AIC, and senescence presents an attractive lens through which to explore molecular mechanisms of chronic toxicity (**Figure 1.7**).

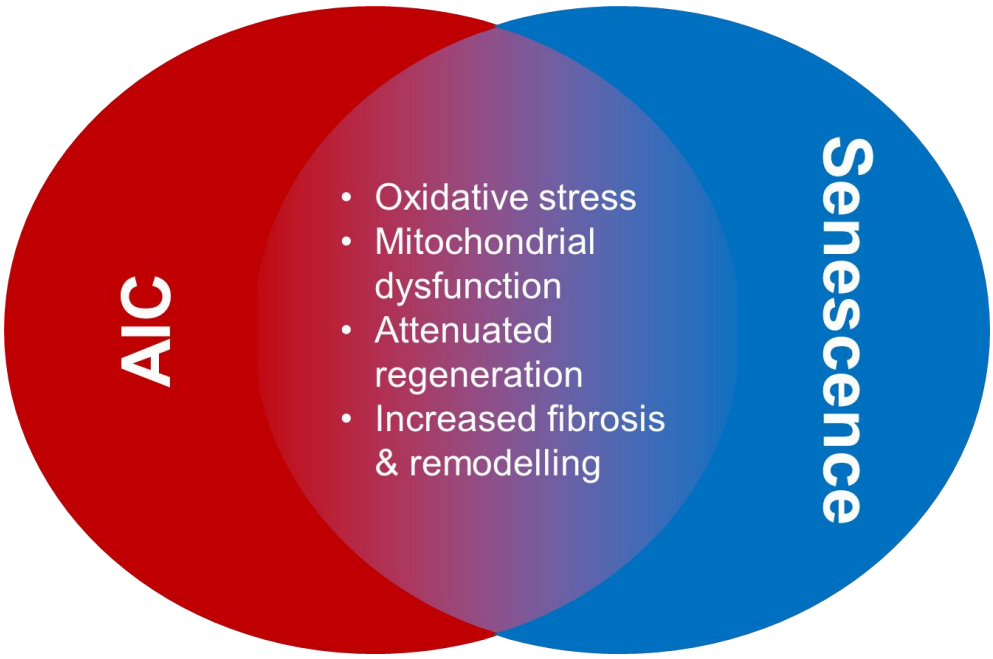

Figure 1.7 Representation of how aspects of the senescent phenotype align with observed aspects of anthracycline induced cardiotoxicity (AIC). Increased oxidative stress and mitochondrial dysfunction have been noted in both settings, alongside attenuated regenerative capacity, increased fibrosis & remodelling.

1.4.8 Anthracyclines impact non-cardiomyocyte populations in the heart – considerations for senescence induction

CMs have historically received the lion's share of attention in cardiotoxicity research but it has long been known that a large percentage of the cardiac environment is made up of non-CM cell types. In their seminal 1980 study, Asish C. Nag et al. performed a fine analysis of murine hearts to show five different non-muscle cell types and their distributions through the heart.[189] More recently, using analyses of large-scale single-cell and single-nucleus transcriptomes, Litviňuková et al. showed that the heart can be divided into six anatomical regions containing 11 different cell types: fibroblasts, pericytes, mesothelial, endothelial, smooth muscle, adipocytes, neuronal, myeloid, lymphoid and CMs (atrial and ventricular). Also, heterogeneity was seen even within cell types according to their atrial or ventricular locations.[190] The effects of anthracyclines upon these cells, their paracrine functions and cell-cell interactions is less well understood.

For instance, cardiac fibroblasts (CFs) are crucial to the formation and maintenance of extracellular matrix (ECM) in the cardiac microenvironment and are necessary for the proper contractility and function of CMs.[191] They are the most numerous cardiac-resident cell lineage,[48] and they release paracrine factors that are key to maintaining

the overall homeostasis of the cardiac microenvironment and coordinating cellular responses to external cues, be they pathological or physiological. In this sense, CFs can be seen to represent a physical and molecular link between various cell types in the myocardium. This was highlighted as early as 1998, when Gray et al. showed that Ang II stimulated CM hypertrophy through CF TGFβ and endothelin-1 signalling.[192]

Upon toxic drug insults, the fibroblast-mediated composition of ECM can change significantly through disrupted degradation/formation of matrix, which can induce cardiac dysfunction.[193] Recent studies have shown that pressure overload cardiac hypertrophy can activate an abnormal fibroblast phenotype, which degrades normal matrix and is resistant to apoptosis.[194] Incidentally, these characteristics bear a striking resemblance to the well-documented cancer-associated fibroblast phenotype, which has myriad functions.[195] In a similar vein, an earlier study showed that after rats were chronically exposed to DOX, CFs proliferated and ECM-remodelling matrix metalloproteinases (MMPs) were detected in circulation.[196] In this study, DOX also caused heterogeneous subcellular alterations of CMs, as well as structural disorganization of the cardiac extracellular environment.

CFs are but one example of a non-CM cell type involved in modifying and maintaining the structure of the cardiac environment. Others include endothelial cells, smooth muscle cells and mesenchymal stromal cells. Though key players in the cardiac milieu, these cell types have not been as rigorously studied as CMs in the context of AIC, and different molecular mechanisms of toxicity may play out in these cell types. For example, a recent study showed that mitophagy in CFs was prevented by the induction of p53 by DOX,[197] and overall, the authors concluded that DOX elicited a pathological phenotype in CFs that was distinct from other cell types.

Although, there have been no known clear demonstrations that anthracyclines induce CFs to senescence *in vivo*, DOX induces primary CFs to senescence *in vitro*,[198] and indeed DOX is routinely used to induce fibroblasts from other organ systems to senescence.[199] Further suggesting senescence contributes to cardiac fibrosis and remodelling, CFs lacking expression of p53 (a key controller of senescence) which were exposed to DOX demonstrated reduced cell cycle arrest, increased proliferation, displayed reduced migration, and attenuated expression of genes associated with dilated cardiomyopathy.[197] Fibrotic lesions are found in the hearts of patients treated with anthracyclines, and studies have demonstrated that rats chronically exposed to

DOX develop cardiac fibrosis because of increased collagen production and fibroblast survival.[51,200]

In vitro, DOX induces endothelial cells to a senescent-like phenotype which includes dysregulation of vascular tone, increased endothelium permeability, arterial stiffness, impairment of angiogenesis and vascular repair, and a reduction in mitochondrial biogenesis.[201,202] Endothelial cell senescence has been implicated in the development of CVDs including coronary artery disease, aortic aneurysm, and stenosis during ageing,[203-205] and therefore, it likely contributes to cardiac dysfunction following cancer therapy in this way, as reviewed previously.[206]

In summary, DOX can induce senescence in several relevant cardiac cell lineages including CMs, CFs, and endothelial cells. The senescent phenotype of each of these lineages is likely to be distinct but may contribute to mechanisms of disease in CVD and in AIC, in addition to the more widely studied CM cell type (**Figure 1.8**).

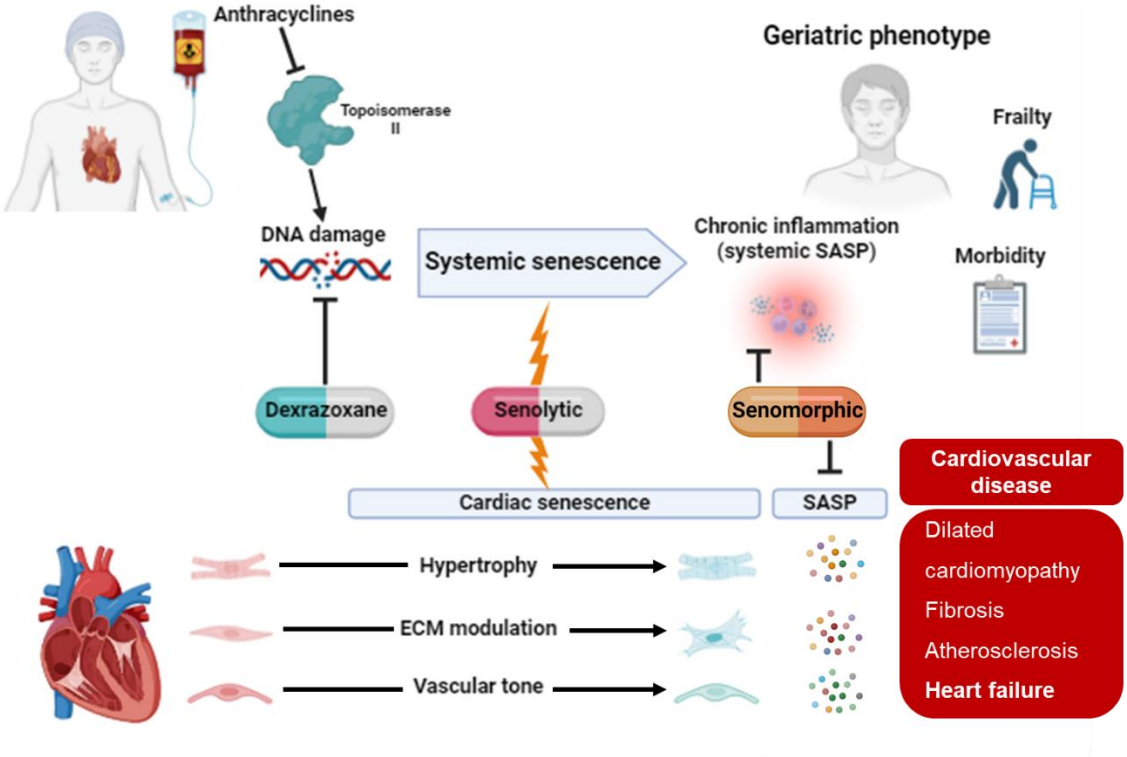

Figure 1.8 An overview of how senescence might occur and promote disease in anthracycline-induced cardiotoxicity (AIC). Anthracyclines induce systemic senescence and drive morbidities typically associated with a geriatric phenotype through several interdependent mechanisms, chief among them cumulative and persistent DNA damage, partly through the canonical inhibition of topoisomerase II enzymes. In the heart, senescence is induced in several cell populations which collectively contribute to age-related cardiovascular diseases (CVDs), including dilated cardiomyopathy and fibrosis (maladaptive myocardial remodelling), both directly and via expression of the senescence-associated secretory phenotype (SASP). Eliminating senescent cells via senolytic treatment or modulating the senescent phenotype (primarily the SASP) has shown promise in the context of senescence and other forms of CVDs but remains to be fully explored in AIC. Deeper understanding of how the senescent phenotype might contribute to pathology of AIC specifically, is necessary. Made using Biorender.com

1.4.9 The potential benefit of eliminating/modulating senescent cardiac cells in anthracycline-induced cardiotoxicity

If eliminating senescent cells in models of CVD is associated with improved outcomes, applying the same approach in AIC is an exciting prospect. However, it should be noted that the few *in vivo* studies exploring this have so far used whole-body elimination of senescent cells via systemic senolytic treatment, or by systemically eliminating p16-expressing cells (in the p16-3MR mouse). Therefore, the precise contribution of various senescent cardiac cell types to AIC pathology remains poorly understood. Furthermore, eliminating the senescent proportion of CMs in the myocardium is likely

an irreversible process due to the post-mitotic nature of this lineage, which may have detrimental effects on the structural integrity of the cardiac tissue long-term.

Another class of drugs termed senomorphics aim to modulate the senescent phenotype (particularly dampening the expression of the pro-inflammatory SASP) or prevent its onset altogether without inducing apoptosis (like senolytics), but this form of intervention is less well-established in AIC. Studies of the senomorphics 5-aminoimidazole-4-carboxamide ribonucleotide (AICAR) and resveratrol in monolayer cultures of DOX-treated induced pluripotent stem cell CMs (iPSC-CMs) showed promise: senescence onset was prevented and iPSC-CMs displayed improved viability and mitochondrial function.[182] When the senomorphic treatment was applied to a more sophisticated, DOX-treated 3D engineered heart tissue model, senescence was prevented but functional parameters (e.g. contractility) were not improved compared to tissues treated with DOX alone.[182] Therefore, targeting cellular senescence in broad strokes may not be effective in AIC. Rather, it may be more beneficial to gain a thorough understanding of which finer details of the senescent phenotype are likely to persistently promote cardiovascular pathology in AIC, and specifically target these molecular processes.

1.5 Conclusions

In summary, chronic AIC is an emerging health concern for the ever-expanding population of cancer survivors. Despite its long history, this toxicity is poorly understood and unpicking the molecular mechanisms at play is a research priority for developing additional specific and effective interventions. Recent findings of relevant working groups and reviews in the literature highlight the importance considering of cell-cell crosstalk and pathological mechanisms outside of cell death, which many historical studies have focused on.[207,208]

Anthracyclines have been demonstrated to induce senescence in cardiac cell populations, but their precise contribution towards cardiotoxicity is still poorly understood. Systemic elimination of senescent cells improves outcomes in animal models of AIC, but further mechanistic studies are required to establish the safety of this approach long-term and its relevance to human disease. A thorough understanding of the senescent CM phenotype induced by DOX is required to establish robust foundations for any interventions, such as senolytics or senomorphics, or indeed other

more selective therapies which target defined, disease-promoting molecular mechanisms of the phenotype.

1.6 Hypothesis

Based on the conclusions above, the hypothesis underpinning this project was that CMs are induced to senescence following a clinically relevant dose of DOX, and that these senescent cells consequently contribute to persistent AIC pathology.

1.7 Aims

The aims of this project are as follows:

1. Investigate the cytotoxicity of DOX upon cardiac and cancer cell types, and select a relevant exposure of DOX for mechanistic studies of cardiotoxicity going forwards
2. Establish and optimise an *in vitro* cell line model that can capture phenotypic changes in CMs following a relevant exposure of DOX, and test whether senescence is induced
3. Characterise the phenotype of CMs induced to senescence by DOX, to evaluate its potential contribution to chronic maladaptive remodelling in AIC
4. Translate findings from optimised cell line models into a gold-standard iPSC-CM model, to explore whether findings are consistent across models and build confidence in cell line studies

Chapter 2. Materials and Methods

2.1 Cell culture techniques

2.1.1 General maintenance

Across this project, five different cell types were used. Firstly, the AC10 and AC16 human CM cell lines (AC10 cell line kindly donated by Dr Barbara Savoldo from Texas Children's Hospital, Texas, USA, AC16 cell line purchased from Merck SCC109). These lines were originally developed by Mercy Davidson and colleagues by fusing primary CMs from adult human ventricular myocardium with simian virus 40 (SV40)-transformed, mitochondrial DNA-depleted human fibroblasts, then selecting, subcloning and screening the resulting clones for CM-specific markers.[209] The outcome was immortalised, proliferative cells which demonstrably express CM-specific markers (e.g. α-actinin, troponin I) and should contain CM-derived mitochondrial DNA, but which lack organised sarcomeres and contractile capability, instead displaying a endothelial/fibroblast-like morphology in culture.[209] Also used in this project were primary human cardiac fibroblasts (HCF, Promocell C-12375), MCF-7 breast cancer cell line (kindly provided by the Institute of Cancer Therapeutics, University of Bradford) and commercially purchased induced pluripotent stem cell-derived CMs (iPSC-CM, FujiFilm Diosynth 01434 #R1059). Cells were maintained in a humidified atmosphere at 37 °C, 5% CO_2, and cultured in a Biosafety Level Class II biological safety cabinet.

AC10 and AC16 CMs were cultured in DMEM F-12 (Gibco 11320-033) with 10% FBS (Gibco 10500-064) and 1% penicillin/streptomycin antibiotics (P/S, Gibco 15140-122). The only deviation from this was during conditioned media collection (see **4.2.5**), whereby AC16 CMs were cultured for 48 hours in 1% P/S phenol red-free DMEM/F-12 (Gibco 21041-025) without FBS, to avoid phenol red interfering with any downstream spectrophotometric applications and facilitate the detection of potentially low-abundance secreted cytokines. Primary HCF cultures were established in Fibroblast Growth Medium 3 (Promocell C-23025), and once established were cultured in DMEM/F-12 with 10% FBS and 1% P/S. MCF-7 cells were cultured in RPMI-1640 culture medium (Sigma R8758), with 10% FBS and 1% P/S. iPSC-CM cultures were thawed and plated using Plating Medium (FujiFilm Diosynth R1151) and at Day 1 post-plating were maintained using Maintenance Medium (Fujifilm Diosynth R1151). iPSC-CMs were thawed and maintained according to specialist manufacturer's protocols (see **5.2.1**).

According to the needs of the assay, cells were cultured in culture vessels of various sizes, including 175 cm^2, 75 cm^2, and 25 cm^2 flasks (Corning 431080, VWR 10062-860, VWR 734-2311, respectively), 96-, 48-, 24- and 6-well plates (Corning 3598, Greiner Bio-One 677180, Greiner Bio-One 662160, Corning 3516, respectively) and 8- and 4-well chambered slides (ibidi 80806, Thermo Scientific 154526PK, respectively).

2.1.2 Passaging cell cultures

The volumes listed here are representative of a 75 cm^2 cell culture flask, which were adjusted proportionally for various vessel sizes. AC10, AC16, MCF-7 and HCF cultures were passaged when cultures reached 80% confluence, as follows. In a sterile environment, culture media was gently aspirated. 10 mL of phosphate buffered saline (PBS, Gibco 10010-015) was added to generously cover the cell monolayer and wash away any traces of culture media, and then gently aspirated. 3 mL of trypsin/ethylenediaminetetraacetic acid (EDTA) (T/E, Sigma-Aldrich T3924) was added to cover the cell monolayer, and was incubated with the cells for approximately 4 minutes at 37 °C. Cells were gently agitated and checked under a light microscope to verify detachment. 7 mL of culture media (appropriate to the cell line, containing 10% FBS) was added to the T/E cell suspension, to quench the action of T/E. Cells were mixed into a homogenous suspension by pipetting up and down, then split into 1:10 ratio for onward culture – 1/10 of the cell suspension (1 mL) would be continued in culture and 9/10 (9 mL) of the cell suspension would be cryopreserved or discarded, as required. To establish a new 75 cm^2 flask of cells, 1 mL of cell suspension was added to 9 mL of appropriate culture media in a fresh 75 cm^2 culture flask. The flask was laid down inside the tissue culture hood for a short time to allow cells to settle onto the growth surface, before placing the flask into a humidified atmosphere at 37 °C, 5% CO_2.

2.1.3 Cryopreservation of cells

To maintain long-term stocks of cells, cultures were cryopreserved and stored at -196 °C in secure liquid nitrogen dewars. In a sterile environment cell suspension was gently mixed with dimethyl sulfoxide (DMSO, Sigma-Aldrich D8418-100ML) in a 9:1 ratio. The cell suspension:DMSO mixture was placed into cryovials (Starlab E3110-6122), which were immediately placed into a Mr. Frosty™ Freezing Container (Nalgene, Thermo Scientific 5100-0001) filled with propan-2ol (Fisher Bioreagents 17170576) and stored

at -80 °C, to achieve a cooling rate of approximately 1 °C per minute. After 1-3 days, the cryovials were placed at into liquid nitrogen until required.

2.1.4 Quantifying cells in culture

When it was necessary to seed specific numbers of cells per cm^2 of culture surface, the number of cells in a given suspension was counted manually using a haemocytometer. Post-trypsinisation, the resultant cell suspension was centrifuged at 400 x *g* for 5 minutes to obtain a pellet. The supernatant was aspirated, and the pellet resuspended: 1 mL of culture media would first be added to the pellet and a 1 mL micropipette used to resuspend, to ensure a homogenous distribution of cells and minimise clumping. Then, additional culture media would be added as appropriate to achieve a practical concentration of cells: an 80% confluent 75 cm^2 flask would typically be resuspended in approximately 10 mL of culture media in total. Then, 100 µL of well-mixed cell suspension was placed into a 1.5 mL Eppendorf tube and outside the safety cabinet, 10 µL of this sample was placed into the chamber of a clean cover-slipped haemocytometer (Hawksley, Scientific Laboratory Supplies HAE2118D2) via capillary action. Using a light microscope at 10X objective, cells were counted in each of the five grids present on the haemocytometer. Cells were only counted if they showed a viable appearance – bright and rounded in shape. The mean number of cells was calculated from the five counts (**Figure 2.1**) and using standard approaches (whereby the volume of the haemocytometer is known), the concentration of cells per mL of solution was deduced (by multiplying mean number of cells by 10^4). Total number of cells was calculated using the known total volume of suspension, and therefore seeding densities could be prepared appropriately.

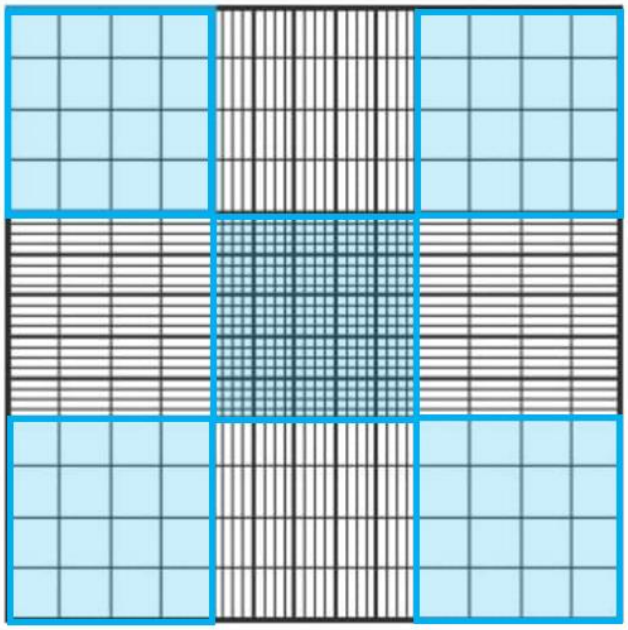

Figure 2.1 Schematic of haemocytometer used for cell counting. Depiction of a Neubauer-style haemocytometer gridded area. Cells are counted in each of the five areas highlighted in blue, and a mean average calculated. This number is multiplied by 10^4 to calculate the number of cells present per mL of cell suspension, according to the known dimensions of the counting chamber.

2.1.5 Trypan blue exclusion to assess viability of cells

When it was necessary to assess viability of cell cultures, a trypan blue exclusion was used. For instance, this technique was used each time a vial of iPSC-CMs was thawed from liquid nitrogen storage (see **5.2.1**). The protocol in **2.1.4** was followed up until 100 µL of well-mixed cell suspension was placed into a 1.5 mL Eppendorf tube. At this point, the 100 µL was combined with 0.4% Trypan Blue solution (Gibco 15250-061) and mixed gently. Then, 10 µL of this trypan blue/cell suspension mixture was placed into the chamber of a clean cover-slipped haemocytometer via capillary action as before. Non-viable cells whose membrane is compromised will take up the trypan blue dye and can be visualised under the microscope. By counting the number of cells which are trypan blue +ve/non-viable (e.g. 5), and the total number of cells (e.g. 21), the percentage of viability can be calculated (e.g. 76%). By applying the mean average percentage viability from all five squares to the total cell number, the number of viable cells can be deduced (**Figure 2.2**).

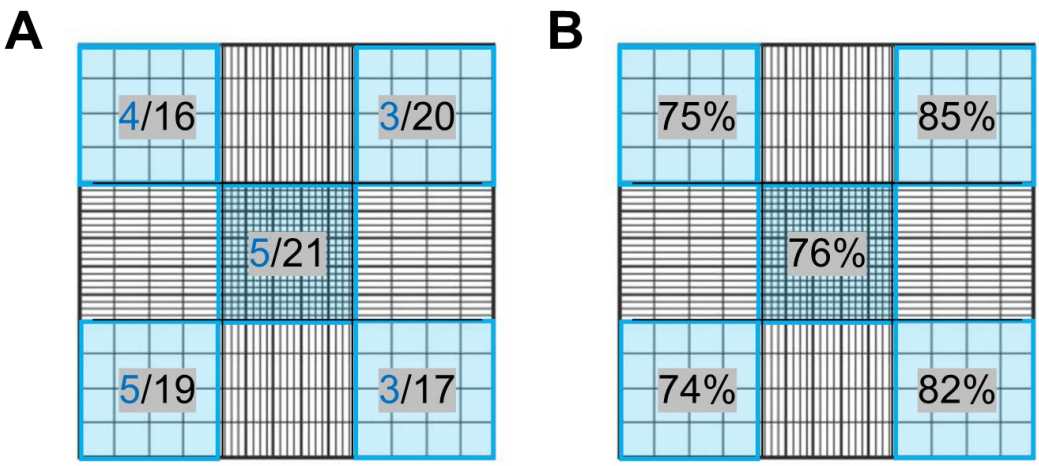

Figure 2.2 Schematic demonstrating the methodology for deducing number of viable cells. A) In each grid of the haemocytometer (highlighted in blue), the number of trypan blue-positive (non-viable) cells are counted, and the total number of cells (both trypan blue-positive and negative, non-viable and viable) are counted. **B)** Trypan blue and total cell counts from A) can be expressed as a proportion which reflects the percentage viability of cells. A mean average can be taken of the five calculated percentages, to deduce the number of viable cells in initial suspension.

2.1.6 10-day dose-recovery doxorubicin exposure regimen

In the optimised, chronic anthracycline-induced cardiotoxicity (AIC) *in vitro* model used throughout this thesis, cells were exposed to doxorubicin (DOX) or DMSO vehicle control for 3 hours before being allowed to recover in full culture media. Briefly, doxorubicin hydrochloride (Sigma D1515) was dissolved in DMSO to achieve a 100 μM stock solution and stored in aliquots at -20 °C until needed. Culture media was aspirated from cells gently and replaced with appropriate media containing DOX at a concentration of 500 nM (100 μM DOX stock solution diluted 1/20,000 using culture medium to achieve low levels of DMSO, 0.005% by volume), or 0.005% DMSO by volume alone. Cells were maintained in these DOX- or DMSO-containing media for 3 hours in a humidified atmosphere at 37 °C, 5% CO_2. Then, media was gently aspirated, cells were washed with appropriate buffer (Dulbecco's PBS for iPSC-CMs, Gibco 14040-133, PBS for all other cell types), and appropriate treatment-free culture medium replaced. Cells were then cultured for 10 days or until near confluence was reached, whichever came first, at which point the exposure regimen ended (**Figure 2.3**).

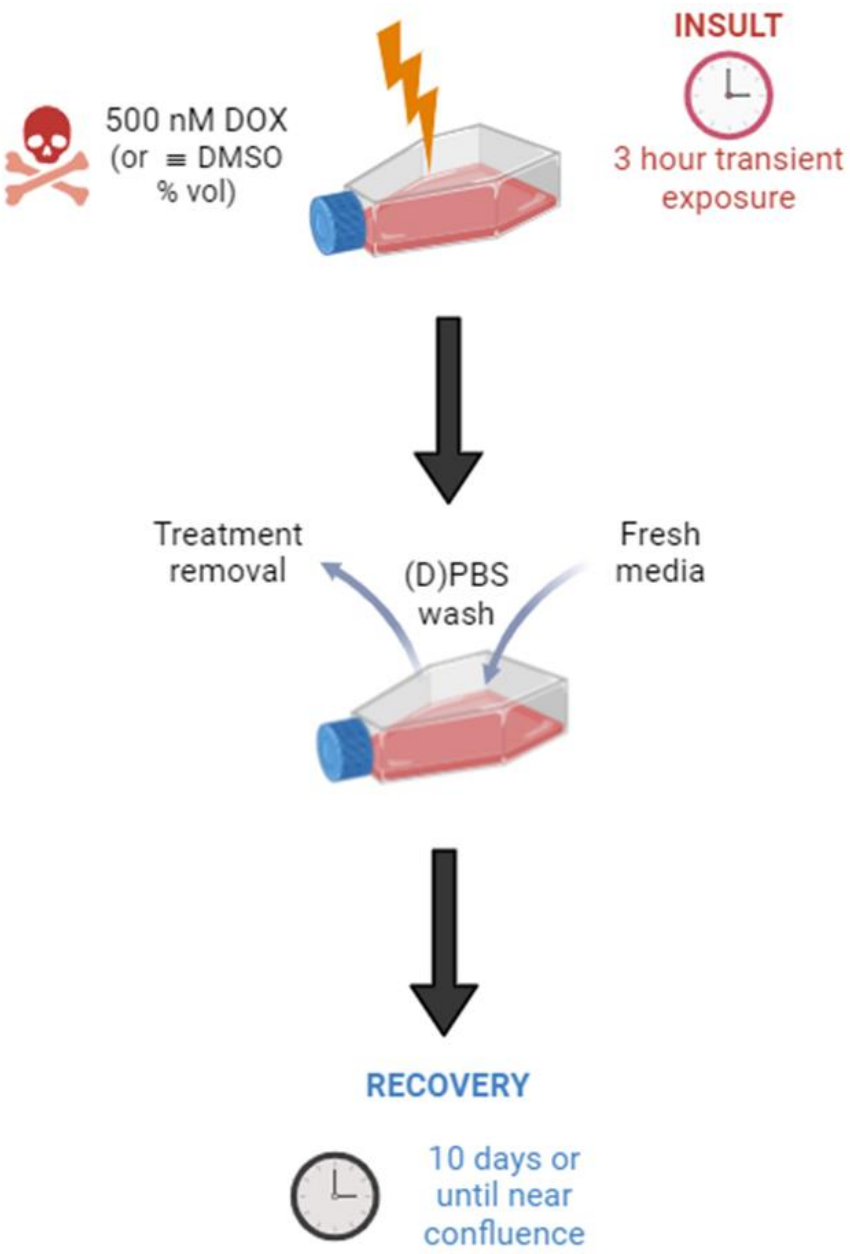

Figure 2.3 Schematic of the dosing regimen used to induce CMs to senescence with DOX. Comprises of a 3-hour exposure to 500 nM DOX or equivalent concentration by volume of DMSO vehicle control, followed by removal of the treatment and a recovery period. Made using Biorender.com

2.2 Molecular techniques

2.2.1 MTS viability assay

To evaluate viability, CellTiter 96® AQueous One Solution Cell Proliferation Assay (Promega) was used in an MTS assay, a variant of the original MTT assay. The colorimetric MTT assay is perhaps the most widely used method for establishing a substance's IC_{50} value *in vitro.*[210] The assay was developed by Mosmann and colleagues in 1983, and it remains a powerful molecular biology tool in studies today,[211] partly since colorimetric assays in a microplate format boast low procedural/technical error and good ease of use. MTS is a novel tetrazolium salt ([3-(4,5-dimethylthiazol-2-yl)-5-(3-carboxymethoxyphenyl)-2-(4-sulfophenyl)-2H-tetrazolium, inner salt), reduced by viable, metabolically active cells into a pigmented formazan product, which is soluble in cell culture medium (**Figure 2.4**). The assay relies on measuring the amount of pigmented tetrazolium salt generated by active cells in a bioreductive reaction, and so is a widely accepted proxy for number of viable cells in culture. The absorbance of formazan at 490 nm is proportional to the number of viable cells in culture, and so can be used to measure cell viability in toxicity studies.

MTS solution was prepared and combined with 1-methoxy phenazine methosulfate (PMS; Sigma) solution according to manufacturer's instructions. Immediately before beginning MTS assay, medium was gently aspirated from all wells and replaced with 100 µL of fresh medium. 20µL of MTS/PMS solution was then added to each well. The plate was incubated at 37°C/5% CO_2 for 4 hours before reading absorbance at 490 nm using Thermo Scientific Multiskan Go plate reader.

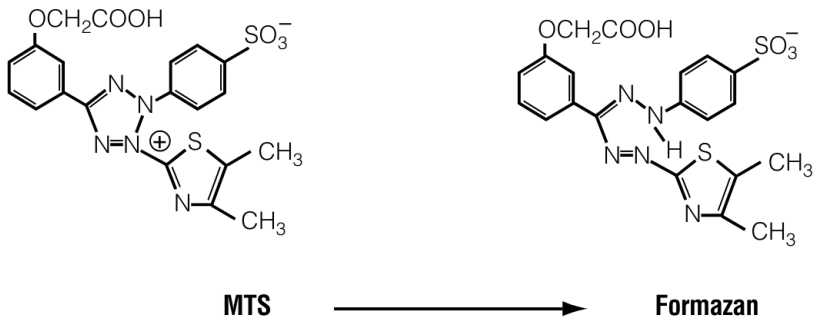

Figure 2.4 Chemical structures of MTS tetrazolium and its pigmented formazan salt product, which is soluble in culture medium. Colorimetric quantification of soluble formazan product is used as a readout for viable cell number in culture.

2.2.2 Pelleting cells for RNA isolation

In order to isolate RNA from AC16 CMs and HCFs, cells from culture were first pelleted. Cells were trypsinised and centrifuged to obtain a pellet, as previously described. Upon obtaining a cell pellet, the culture media supernatant was gently aspirated and discarded. The pellet was then washed using a 1 mL micropipette in ice-cold sterile PBS, to help remove traces of FBS-containing culture medium, given that composition FBS is notoriously uncharacterised and may interfere with high-sensitivity downstream analyses.[212,213] The PBS cell suspension was centrifuged at 4 °C for 5 minutes at 400 x *g*, before aspirating PBS supernatant and storing the cell pellet immediately at -80 °C until needed.

An adapted protocol was used to isolate RNA from iPSC-CMs for qPCR and RNA-Seq applications, which are detailed in **5.2.7** - **5.2.10** and **5.2.12** - **5.2.13**.

2.2.3 Total RNA isolation

Depending on cell number, RNA was isolated from cell pellets using either an RNeasy Mini kit (Qiagen 74134) or an RNeasy Micro kit (Qiagen 74034). For both kits, 350 µL Buffer RLT Plus was added to the cell pellet and vortexed for 30 seconds. The homogenised lysate was then transferred to a gDNA Eliminator spin column within a 2 mL collection tube and centrifuged for 30 seconds at 9,000 x *g*. The column was then discarded. 350 µL of 70 % ethanol (Nuclease-free water, Qiagen 1039498 + ethanol absolute, VWR 20821.321) was added to the flow-through, and the mixture was combined well by pipetting gently several times. The total mixture was transferred to an RNeasy Mini (Mini prep) **or** RNeasy MinElute (Micro prep) spin column within a 2 mL collection tube and centrifuged for 15 seconds at 9,000 x *g*. The flow-through was discarded. 700 µL of Buffer RW1 was then added to the RNeasy Mini spin column, and centrifuged for 15 seconds at 9,000 x *g*. 500 µL of Buffer RPE was then added to the RNeasy spin column and centrifuged at 9,000 x *g* for 15 seconds, and the flow-through was discarded. **From this point onwards the protocols diverged.** **For the Mini prep:** this Buffer RPE step was repeated but centrifuged for 2 minutes. The RNeasy spin column was then placed into a collection tube and 30 µL of RNase-free water was gently added directly to the spin column membrane. The column was centrifuged at 9,000 x *g* for 1 minute to elute RNA. **For the Micro prep:** 500 µL of 80% ethanol was added to the spin column and centrifuged for 2 minutes at 9,000 x *g* to wash the spin column membrane. The RNeasy MinElute spin column was placed into a new

collection tube with the spin column lid open and centrifuged at full speed (13,000 x *g*) for 5 minutes to dry the membrane. Finally, the RNeasy spin column was placed into a collection tube and 14 µL of RNase-free water was gently added directly to the spin column membrane. The column was centrifuged at full speed for 1 minute to elute RNA.

2.2.4 Quantifying RNA and quality assurance

Extracted RNA was quantified using a NanoDrop ND-8000 8-sample spectrophotometer (ThermoFisher) and its 260/280 ratio quality parameter was checked for closeness to 2.0.

2.2.5 cDNA synthesis

A given quantity of total RNA (1 µg where samples were sufficient, 100 ng where RNA was lower in concentration) was incorporated into a cDNA synthesis reaction using the Tetro cDNA Synthesis Kit (Meridian Bioscience BIO-65043). Random hexamers were used to prime the reaction, giving random coverage to all regions of the RNA, therefore generating a cDNA pool containing various lengths of cDNA. Synthesis was carried out according to manufacturer's instructions. Briefly, a single 20 µL cDNA synthesis reaction mixture comprised the following: random hexamer primer (1 µL), 10 mM dNTP mix (1 µL), 5x RT buffer (4 µL), RiboSafe RNase Inhibitor (1 µL), Tetro Reverse Transcriptase (1 µL @ 200 u/µL), total RNA (n µL, according to RNA concentration), DEPC-treated water (to 20 µL). Using a Biorad DNA Engine Tetrad 2 Peltier Thermal Cycler, reaction mixtures were then incubated as follows: 25 °C for 10 minutes, 45 °C for 30 minutes, 85 °C for 5 minutes, 4 °C thereafter. cDNA samples were stored at -20°C until required.

2.2.6 Primer design for quantitative polymerase chain reaction

Primer pairs were designed using the webtool Primer-BLAST (available at https://www.ncbi.nlm.nih.gov/tools/primer-blast/),[214] and then custom manufactured (Sigma Aldrich or Integrated DNA Technologies), or were commercially sourced as pre-designed "KiCqStart" primers (Sigma Aldrich).

In the case of Primer-BLAST, polymerase chain reaction (PCR) product size was restricted to 70-200 bp, which is considered optimal for quantitative PCR application as standard. Primer candidates were restricted to those spanning exon-exon junctions, to minimise the chance of amplifying contaminating genomic DNA, and organism was

set to Homo sapiens. All other parameters remained as default settings within the webtool. Upon return of primer pair candidates, selection was limited to those pairs with 40-60% GC ratio, and ideally 50-55%, alongside checking self-complementarity scores to minimise primer hairpin formation. To check specificity of primers to the desired gene transcripts before use, primer sequences were run back through the BLAST tool.[215]

2.2.7 Quantitative polymerase chain reaction standard workflow

qPCR reactions were carried out in a 384-welled plate format. Firstly, a master mix comprising Platinum™ SYBR™ Green qPCR SuperMix-UDG w/ROX (SYBR, Invitrogen 11744100), relevant forward and reverse primers at (10 µM), and water was made, and distributed into individual wells of the plate such that a single qPCR reaction in a well constituted 5 µL SYBR, 0.5 µL forward primer, 0.5 µL reverse primer, 1.5 µL RNase-free water. 2.5 µL of relevant test cDNA was then added to each reaction, or 2.5 µL to constitute a control reaction, to highlight any contamination in the experiment. The plate was covered with an adhesive sealing film (Thermo Scientific AB-0558) to minimise evaporation and cross-contamination. Using an Eppendorf 5430 Centrifuge, the 384-well plate was centrifuged at 100 x *g* for 1 minute to ensure all reagents were at the bottom of the well. PCR amplification was performed using the QuantStudio7 Flex Real-Time PCR System with standard Comparative Ct (ΔΔCt) and a standard run for 40 cycles (Applied Biosystems 4485701). 2-3 technical replicates were performed per target, per sample in a plate. Mean CT values of all targets were processed and expressed using the standard delta delta Ct (ddCt) algorithm: briefly, the mean CT value of a given housekeeper was calculated and if multiple housekeepers were utilised, these mean values were further combined into a generic housekeeper “grand average” value, for further rigour. The grand average housekeeper CT value was subtracted from the mean CT value of a given target of interest, to account for pipetting/other technical errors which may give rise to artificial variance in target amplification (ΔCT). This value was then expressed as $-2^{\Delta CT}$ and compared between treatment conditions (ddCt).

2.2.8 General fluorescence immunocytochemistry workflow

Throughout this thesis, fluorescence immunocytochemistry was used to test for the expression of various proteins of interest in cells. Specific protocols and reagents were used for each assay (listed in Materials and Methods sections within Chapters 3-5),

but all protocols followed the same basic conceptual workflow (**Figure 2.5A,** adapted from Im et al.).[216] Primary antibodies raised in a host species react to the target protein of interest and bind to it. After washing away non-bound primary antibody, a secondary antibody is employed, which is reactive to the species type of the primary antibody. The secondary antibody is conjugated to a fluorophore, which is excited by and then emits light at predetermined wavelengths of light (e.g. 499 and 520 nm respectively for Invitrogen A21206, **Figure 2.5B**). Nuclei are typically visualised using reagents such as Hoechst stain or 4′,6-diamidino-2-phenylindole (DAPI), which intercalate with DNA (particularly regions rich in adenine and thymine) and emit light around at around 461 nm wavelength.[217-219] DAPI is used throughout the fluorescence immunocytochemistry protocols in this thesis. The emission of these fluorescent signals together can be detected by fluorescence microscopy, and images can be captured by this process to be analysed downstream.

2.3 Miscellaneous

Data was collated and tidied using Microsoft Excel. Statistical analyses were performed using GraphPad Prism software, version 10. Where appropriate, analyses were performed to interrogate the normality of data distribution using the Shapiro-Wilk test. Non-parametric analyses were performed to analyse results when data failed to pass normality testing. For specific data analyses methods, see **3.2**, **4.2** and **5.2**. All cell lines used in this project are from commercial sources and all studies were approved by local ethics if required.

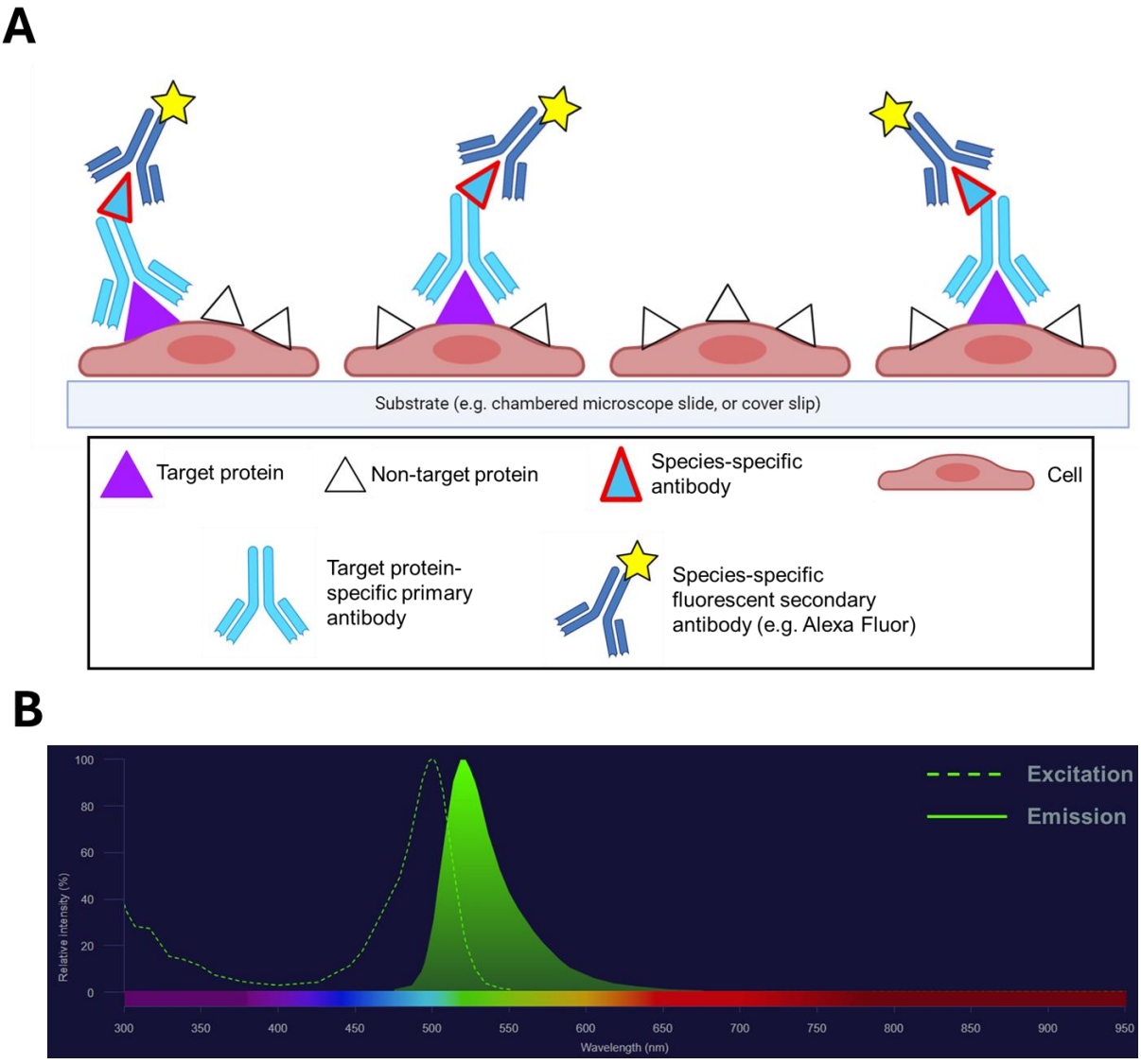

Figure 2.5 Fluorescence immunocytochemistry overview. A) Conceptual schematic of fluorescence immunocytochemistry techniques used throughout this thesis. Cells are exposed to primary antibodies which bind specifically to target protein (purple triangle). Secondary antibodies, conjugated to a fluorescent moiety (yellow star), are selective for the host species of the primary antibodies (blue triangle, red outline) and bind accordingly. Made using Biorender.com. **B)** A representative example of the specific excitation and emission characteristics of a fluorophore conjugated to secondary antibody. Here, excitation intensity peaks at 499 nm wavelength of light, and emission intensity peaks at 520 nm wavelength.

.

Chapter 3. Toxicity of Doxorubicin Upon Various Cell Types, and Induction of Senescence in an Immortalised Cardiomyocyte Cell Line

3.1 Introduction

3.1.1 Investigating the clinical cardiotoxicity of anthracyclines

Anthracyclines, particularly DOX, have demonstrated clinical success in the treatment of a wide range of malignancies but their use is hindered by the subsequent development of anthracycline-induced cardiotoxicity and progressive cardiac failure.

Despite this family of chemotherapeutics acting to directly damage nucleic acids and thus initiate a direct cytotoxic effect as their primary therapeutic mechanism against cancer cells, this is not believed to be so straightforward in the context of cardiotoxicity.[220] It is accepted that the initial exposure of the myocardium to DOX results in cytotoxicity of a proportion of cells within this tissue, analogous to its action against cancer cells, evidenced by increased serum biomarkers such as cardiac troponins.[221] Histopathology of post-mortem hearts from anthracycline cardiotoxicity patients indicate a proportion of CMs undergo cell death as a result of toxicity, leaving behind vacuoles.[222] Preclinical studies also indicate that CM apoptosis is upregulated following anthracycline exposure, and that heart weight is decreased 24 hours following DOX exposure.[138,139] However, exactly how this purported acute loss of cardiac cell number results in an asymptomatic pathology for an extended period of time, before progressing to chronic heart failure, remains unclear.

The progressive cardiotoxicity of anthracyclines is understood to be a consequence of either: a persistent genetic/biochemical change in the surviving cells within the myocardium post-exposure,[223,224] a reactionary response by specific cellular populations (such as cardiac fibroblasts or cardiac stem cells within the cardiac tissue),[207,225] or a response to sub-therapeutic and/or sublethal concentrations of anthracycline within the cardiac cellular environment, as a result of drug pharmacokinetics and drug administration cycles.[180,226]

The use of *in vitro* assays is well established to provide valuable insight into the pharmacological safety profiles of drugs, including cancer chemotherapeutics.[227] For

instance, *in vitro* screening studies are used to generate basic toxicity data which allow researchers to adopt relevant concentrations of a novel drug class (such as the relatively novel monoclonal antibodies), for downstream mechanistic biochemical studies.[228] Similarly, data from *in vitro* studies are a regulatory and ethical requirement for progression to preclinical *in vivo* safety studies, which are financially costly, labour-intensive, and which must be minimised in scale and harm, according to the 3Rs principles.[229] In order to interrogate the mechanistic basis of AIC, through *in vitro* cellular and molecular analyses, a greater understanding of the sensitivities and exposure profiles of cardiac cells to anthracyclines is firstly required.

3.1.2 Cytotoxicity of anthracyclines – translating the clinical scenario to cell culture

In the clinic, the first-line tool used by oncologists to reduce the potential for both acute and late-onset anthracycline cardiotoxicity is adherence to a lifetime cumulative dose limit of the drug. Historically, the optimised lifetime cumulative dose for DOX in adult breast cancer patients was defined as 550 mg/m^2,[33] but now even exposure to > 250 mg/m^2 of DOX can be considered clinically "high risk", prompting ongoing cardiac monitoring of the patient.[230] Gender-based differences in toxicity are notable in the paediatric population, with girls being more at risk for late-onset depression of LV contractility post-anthracycline treatment.[46] As such, it is now accepted that cardiovascular risk post-anthracycline chemotherapy is highly individual, and furthermore that there are no completely "safe" doses of anthracyclines, with even low-dose anthracycline exposure significantly increasing cardiovascular risk later in life.[230-232] Subsequently, there is an important precedent for the concentrations of anthracyclines applied in an *in vitro* setting to recapitulate and reflect the clinical situation.

Numerous clinical studies have been conducted over the past decade in which pharmacokinetic parameters of DOX have been evaluated in different cancer types and patient populations.[233-235] At the typical clinical dose of 30-70 mg/m^2 for DOX, the maximum systemic pharmacokinetic exposure (C_{max}) was calculated to range from 1.16 to 3.02 μM, with patient characteristics impacting this exposure to a degree, and some authors estimating the C_{max} to be lower still.[236] This data reflects systemic rather than cardiac exposure parameters for this drug but gives an indication of the maximal expected exposures of the cardiac tissue. With an ever-evolving cardio-oncology community publishing guidelines and position papers about this topic,[230] remaining

faithful to clinical parameters when designing a toxicity assay results in more relevant and impactful results.

Many *in vitro* studies have reported parameters of anthracyclines cytotoxicity, with these studies either focused on elucidation of cytotoxicity *per se* or evaluation of a specific signalling pathway. Although several methodologies have been employed in the context of cytotoxicity evaluations, the commonest parameter for recording such effects is the cytotoxicity IC_{50} value, representing the concentration of drug required to reduce the cellular activity or number by 50%.[237] In terms of the intended therapeutic action of DOX, the National Cancer Institute (NCI) have screened the efficacy of this drug against their panel of 60 cancer cell lines representing a range of cancer types, in the "NCI-60 Human Tumour Cell Lines Screen".[238] In this 48-hour exposure, DOX was shown to exhibit potent activity against the majority of cancer cell types, with the mean LC_{50} (concentration of drug inducing cytotoxicity in 50% of the population) across the panel determined to be 11.5 μM (**Figure 3.1A**), and the GI_{50} value (indicating the concentration at which a compound inhibits growth of a cell type by 50%) being 95.1 nM (**Figure 3.1B**).

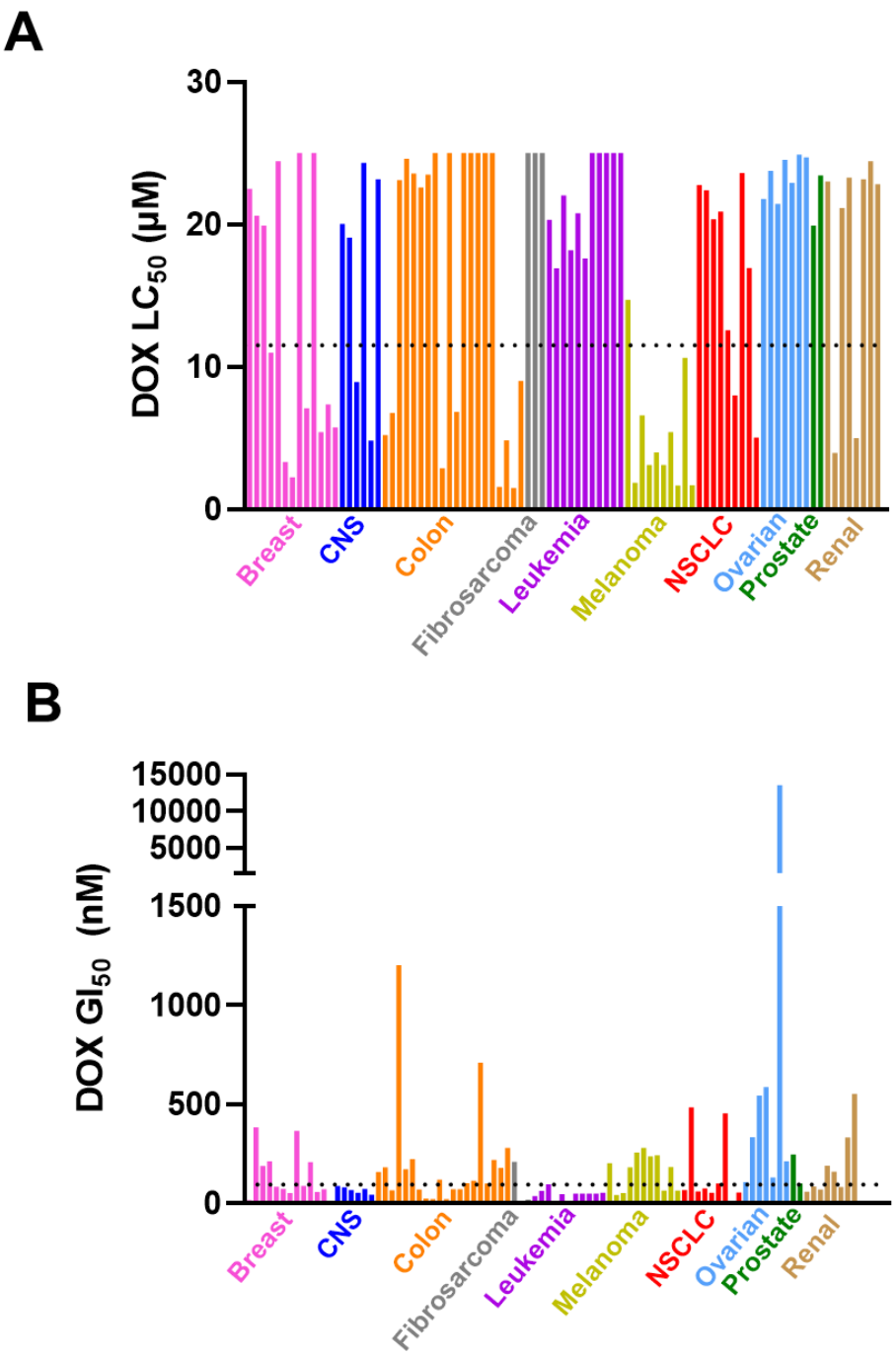

Figure 3.1 LC_{50} and GI_{50} data of DOX (compounds reference 123127) against 60 cancer cell lines according to NCI-60 data repository shows that DOX is broadly toxic to many cancer cell types *in vitro* (according to sulphorhodamine B cell protein assay). A) The average concentration at which DOX induced cytotoxicity in 50% of the cell population is 11.5 μM (marked with dotted line). **B)** The average concentration at which DOX inhibits growth in 50% of the cell population is 95.1 nM (marked with dotted line).

The Genomics of Drug Sensitivity in Cancer (GDSC) database also provides a good overview of DOX's anticancer efficacy *in vitro*.[239] From screening 870 genetically characterised human cancer cell lines, the mean IC_{50} of DOX in a 72-hour exposure setting is estimated to be 0.171 μM.

Mechanistic studies of DOX's action against cardiac cells *in vitro* have, to date, unfortunately been reported to lack alignment with the clinical exposure parameters – for instance, some seminal *in vitro* studies of DOX cardiotoxicity have been criticised for using non-clinically relevant concentrations of drug.[240] Although supraclinical concentrations have persisted in some studies, several more recent studies present clinically relevant dosing as a central strength of their investigations.[182,241,242]

However, an important overlooked factor even in these studies is the exposure duration (which range from 24-96 hours continuous exposure) and its relationship to clinical administration and dosing. Another important criterion for modelling of human cardiotoxicity is the use of the most appropriate cell line. Many previous studies have used the H9c2 and HL-1 cell lines. The origin and cell type of the H9c2 line is not ideal for modelling human AIC: this cell line is embryonic in character and derived from rat, whilst also better recapitulating the myoblast phenotype rather than CMs proper.[243,244] The HL-1 line is murine-derived and although it can robustly model contractile phenomena, the cell line is atrial in origin, so may not best model molecular mechanisms in AIC, which is associated more strongly with ventricular disease.[245] The AC10/AC16 human ventricular cell line and more recently human induced pluripotent stem cell derived CMs (iPSC-CMs) better address the ideal criteria for modelling AIC *in vitro*.[246] A range of IC_{50} values have independently been reported for DOX against these human cardiac cell lines, ranging from 0.46-1.67μM.[247-249]

3.1.3 Exposure time and concentration yield different cellular fates – implications for study design

Considering the aforementioned clinical administration and dosing of DOX and the late-onset nature of its cardiotoxicity, recent studies have highlighted the conceptual importance not just of cytotoxicity, but rather of the phenotypic changes in cells which may survive acute toxicity, and their contribution on long-term disease. In essence, though a large, supraclinical DOX exposure may promote apoptosis in CMs, a smaller DOX exposure may promote other cellular fates which persistently promote pathology.[250] A mechanism which has been highlighted in this paradigm is cellular

senescence: briefly, a phenotype defined as exit from the cell cycle accompanied by a pro-inflammatory secretome. Induction of senescence has been shown to contribute to the side effects of DOX both *in vivo* and *in vitro*,[179] and will be investigated throughout this thesis using *in vitro* models established in this chapter.

3.1.4 Aims and objectives

The purpose of this phase of the project is to determine the differential toxicity of DOX upon different cell types relevant to the context of cardiotoxicity after cancer treatment.

The sensitivity of the AC10 human ventricular cell line and human cardiac fibroblasts will be determined following exposure to the drug at clinically relevant concentrations for varying time periods, by using the MTS assay to evaluate cellular viability (see **2.2.1**). This will allow elucidation of any effect upon cellular viability and provide a representative model of the relationship between pharmacokinetic drug concentrations and cardiac cell lineages. In parallel, the response of the MCF-7 breast cancer cell line to DOX will also be assessed for comparison to cardiac cell types. The latter aim will be to develop a DOX exposure model which more faithfully emulates clinical exposures of DOX, and which recapitulates progressive cardiotoxicity onset rather than acute cell death. Following this more chronic exposure to DOX, cardiac cell types will then be assessed for cell fate changes which might persist in surviving cells, namely the induction of cellular senescence.

3.2 Materials and methods

3.2.1 Acute toxicity assay timeline

Briefly, across all cell types tested for acute DOX toxicity, cells were seeded on Day -1, treated with relevant concentrations of DOX or control substance on Day 0 (see **3.2.2**) and the experimental endpoint (cellular viability) was measured on Day 1, 2, 3 and 4 to generate IC_{50} values at 24-, 48-, 72- and 96-hours exposure (**Figure 3.2**).

3.2.2 Viability assay

Excepting the first column of the plate, 2500 cells were seeded into each well of a 96-well microplate (Corning) and allowed to adhere overnight. Each well was maintained in 180µL of appropriate culture medium and incubated at 37°C/5% CO_2 as standard. 20µL of a given substance was then added to various wells, which underwent a 1/10 dilution upon addition to the pre-existing 180 µL volume: appropriate culture medium (plate columns one and two), 1% w/v DMSO vehicle (column three), 100 µM DOX (column four). Column 4 was then serially diluted (1 in 10 dilution, 20 µL volume) across columns 5-12, giving a DOX dosage range of 10 µM-100 fM from columns 4-12 (**Figure 3.3**). Cell cultures were maintained at standard conditions for a given drug exposure time (24-96 hours) before evaluating viability via an MTS assay (see **2.2.1**).

3.2.3 4-day dose-recovery toxicity assay timeline

AC16 cells were seeded on Day -1, treated with 500 nM DOX or equivalent concentration of DMSO vehicle on Day 0, and the experimental endpoint (cellular viability) was measured on day 4 to evaluate cellular viability (**Figure 3.4**).

3.2.4 10-day dose-recovery exposure model

AC16 CMs were seeded into tissue culture plasticware at 2000 cells/cm^2 using standard cell culture techniques (see **2.1.4**) and left to adhere overnight. The next day, the 10-day recovery period began (see **2.1.6**).

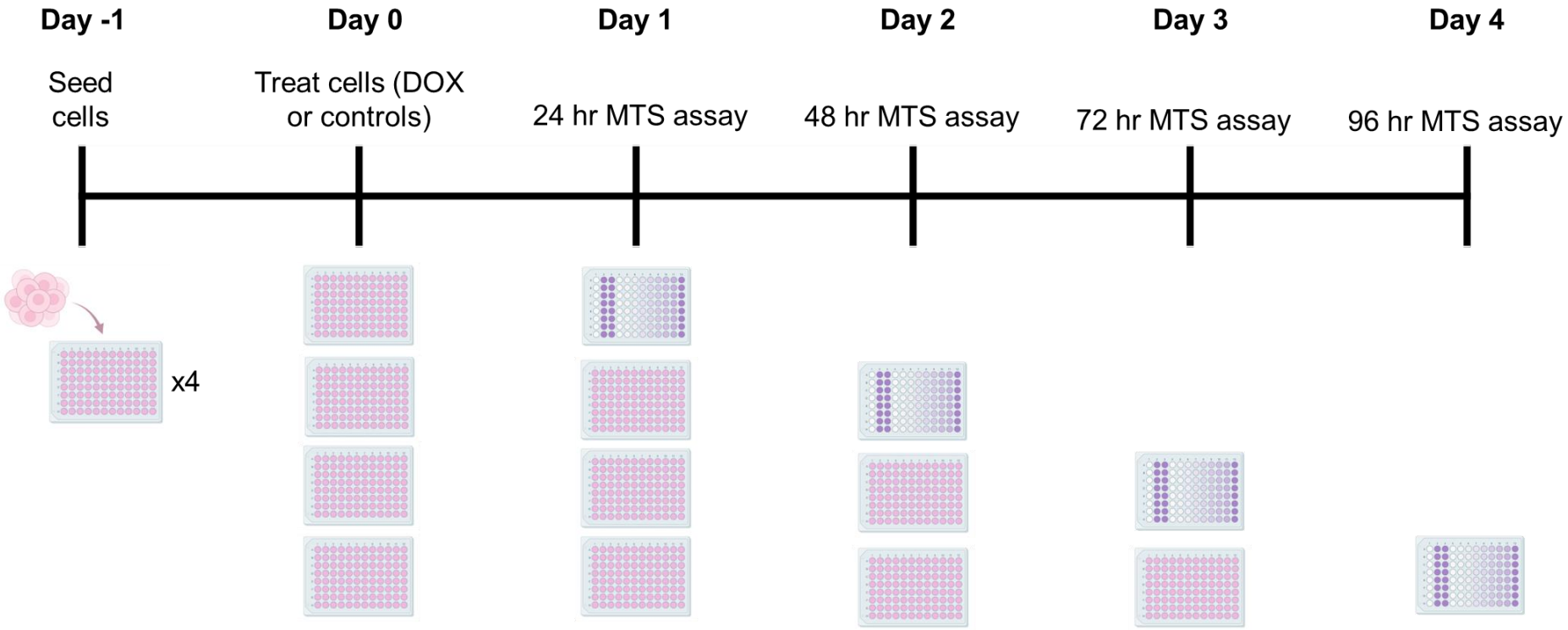

Figure 3.2 Schematic of acute DOX exposure for AC10, AC16 (96 hours only), HCF and MCF-7 cell lines. Cells are seeded into four 96-well microplates on day -1 and left to adhere overnight. Cells are treated with DOX or appropriate control continuously from day 0. On days 1, 2, 3 and 4, cells in microplates are assessed for viability using MTS assay. Made using Biorender.com.

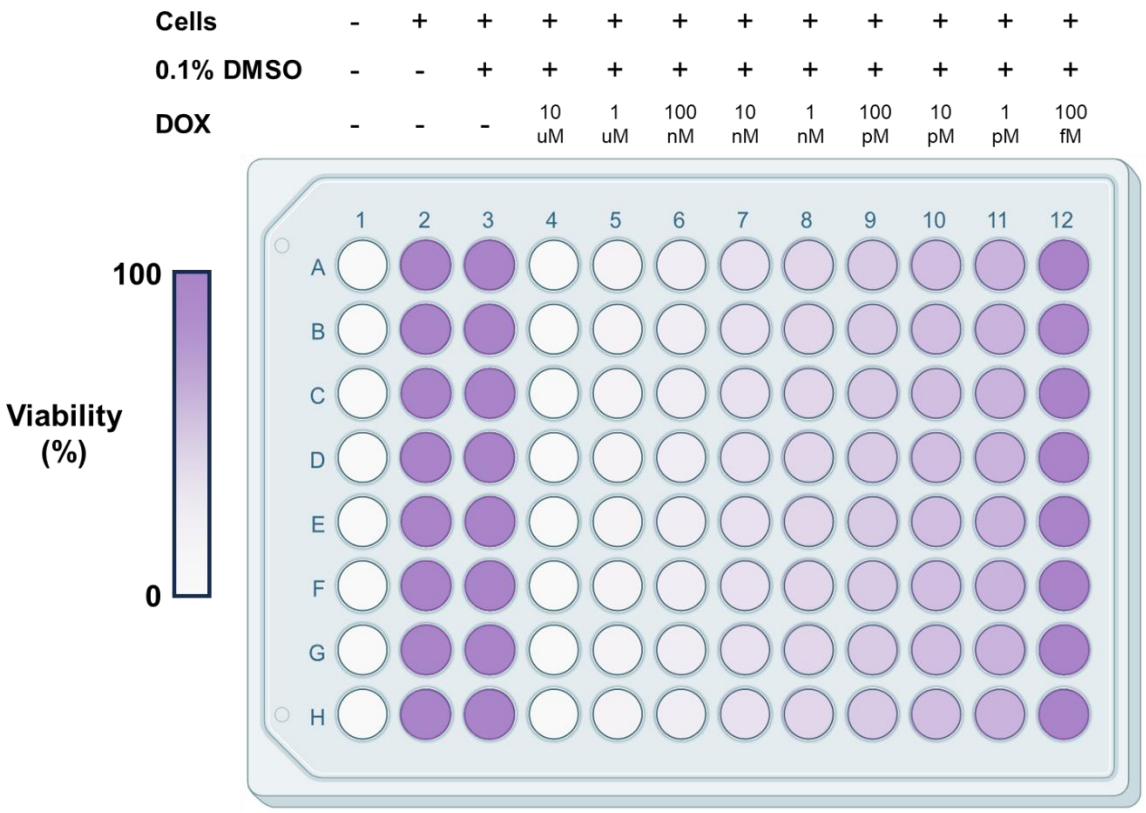

Figure 3.3 Schematic of a typical MTS assay 96-well plate layout used throughout this section of the study. A given cell type is seeded into all wells of the plate except the first column. The next day, appropriate culture medium is added to column two, DMSO is added to cells cultured in column three, and varying concentrations of DOX are added to columns 4-12 using a 1:10 serial dilution. A representative colour palette is used here which typifies the formazan product pigmentation readout of this assay, with an intense colouring indicating high cell viability. Made using Biorender.com

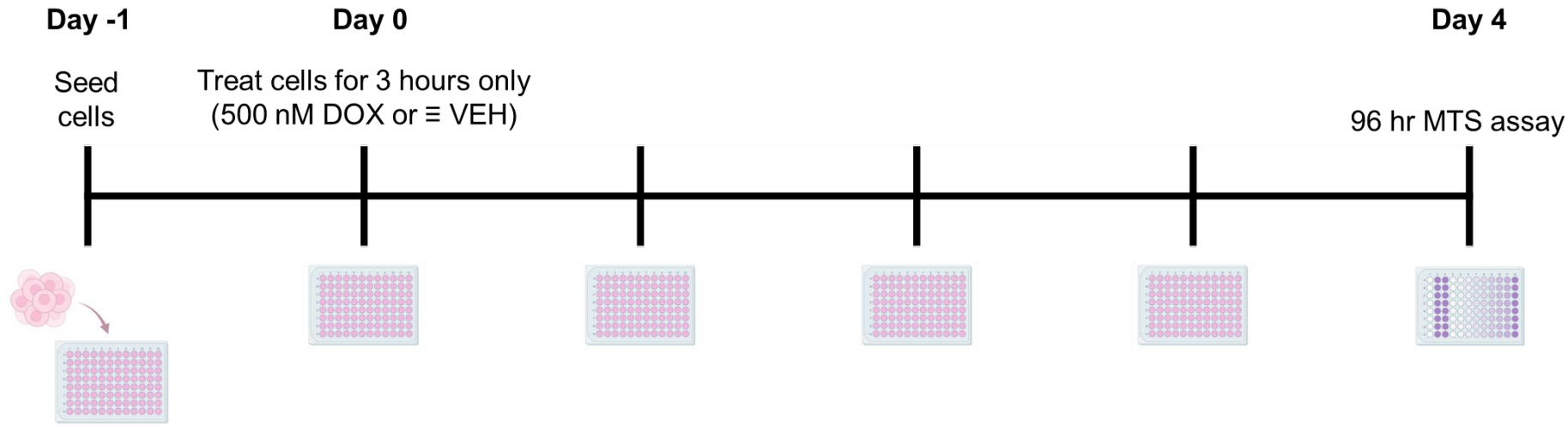

Figure 3.4 Schematic of 4-day dose-recovery DOX exposure for AC16 cells. Cells are seeded into a 96-well microplate on day -1 and left to adhere overnight. Cells are treated with 500 nM DOX or equivalent concentration DMSO vehicle control (VEH) for 3 hours only on day 0. On day 4, AC16 cells in microplate are assessed for viability using MTS assay. Made using Biorender.com.

3.2.5 Fluorescence immunocytochemistry for classical senescence markers

For immunofluorescent staining of senescence-associated proteins p16 and p21, AC16 cultures were fixed with warm 4% paraformaldehyde (PFA, Thermo Scientific J19943-K2) in PBS for 20 minutes at room temperature, then PFA was gently aspirated, and cells were washed three times (5 mins each) with ice-cold PBS (Gibco 10010-015, five-minute wash time). Cells were then permeabilised using a ten-minute incubation with 0.1% Triton X-100 (Sigma T8787-250ML) in PBS (Sigma Aldrich P4417-100TAB) at room temperature. Permeabilisation agent was aspirated gently, then cells were washed with PBS as before. Blocking of non-specific antibody binding was via 1% bovine serum albumin (BSA, Sigma Aldrich A7906-100G) in 0.1% Tween-20 (Sigma Aldrich P1379-250ML) PBS (PBST) for 30 minutes at room temperature. Blocking solution was then removed and primary antibodies against p16 (Roche Ventana 805-4713, mouse anti-human monoclonal, 1:1 dilution) or p21 (Abcam ab7960, rabbit anti-human polyclonal, 1:200) were added to cells. Cells were incubated with primary antibodies overnight at 4°C. Primary antibodies were then removed and cells were washed with PBS as before. Secondary fluorochrome conjugated IgG antibodies reactive to the primary antibody species were used to allow for detection. For anti-p16: Invitrogen A21202, Donkey anti-Mouse Alexa Fluor 488, 1:1000. For anti-p21: Invitrogen A21206, Donkey anti-Rabbit Alexa Fluor 488, 1:100. Cells were incubated with secondary antibodies for one hour at room temperature in the dark, antibodies were then gently aspirated, cells were washed thrice with PBS as before, and DAPI-containing mounting media applied (Invitrogen P36931). Samples were stored at 4°C. Images were acquired using a 10X objective on a Zeiss AxioImager instrument.

3.2.6 RNA isolation and quality/quantity evaluation

RNA was isolated from AC16 cell pellets using an RNeasy Mini kit (Qiagen 74134, see **2.2.2** and **2.2.3**), and the quality/quantity verified (see **2.2.4**). RNA was stored at -80 °C until required.

3.2.7 cDNA synthesis

cDNA was synthesised from RNA extracted from cell pellets using standard methods (see **2.2.5**) and stored at -20 °C until required.

3.2.8 Quantitative real-time polymerase chain reaction (qPCR)

Primers were designed using Primer-BLAST (see **2.2.6**) or commercially sourced as pre-designed "KiCqStart" primers (Sigma Aldrich) (**Table 3.1**). qPCR was carried out according to a standard workflow (see **2.2.7**). *ACTB* (β-actin), *RPLP0* (ribosomal protein lateral stalk subunit P0) and *HPRT1* (hypoxanthine phosphoribosyltransferase 1, HPRT1) were used as a combined endogenous control.

Table 3.1 Details of primer pairs used in RT-qPCR studies. Primer sequences were either designed using Primer-BLAST and commercially custom-manufactured, or primers purchased as a pre-designed commercial product ("KiCqStart").

Target gene transcript	Forward (5' → 3')	Reverse (5' → 3')	Manufacturer
Cyclin dependent kinase inhibitor 2A (*CDKN2A*)	GTCGGGTAGAGGAGGTGCG	CCCATCATCATGACCTGGATCG	Sigma-Aldrich custom
Cyclin dependent kinase inhibitor 1A (*CDKN1A*)	TCTCAGGGTCGAAAACGGC	GCAGAAGATGTAGAGCGGGC	Sigma-Aldrich custom
P53 Upregulated Regulator of P53 Levels (*PURPL*)	CGTGTGAAAAGAACCCAGGTA	CGCCTGGTAAAACAACCAGT	Sigma-Aldrich custom
Growth Differentiation Factor 15 (*GDF15*)	TCCGGATACTCACGCCAGAA	GTCACGTCCCACGACCTTG	Sigma-Aldrich custom
Apoptosis regulator Bcl-2	CGTTGCCTTATGCATTTGTTTTGGT	TGGTGTTTCCCCCTTGGCAT	Integrated DNA

BCL2)			Technologies (IDT) custom
ACTB	GACGACATGGAGAAAATCTG	ATGATCTGGGTCATCTTCTC	Sigma-Aldrich KiCqStart
RPLP0	TCGACAATGGACGCATCTAC	ATCCGTCTCCACAGACAAGG	Sigma-Aldrich custom
HPRT1	TGACCAGTCAACAGGGGAC	CTTCGTGGGGTCCTTTTCAC	Sigma-Aldrich custom

3.2.9 Fluorescence SA-β-Gal assay

β-gal fluorescent assay Kit (Abcam 287846) was used according to manufacturer's instructions, with modifications. AC16 cells were cultured and exposed to DOX or VEH as previously described. At day ten post-exposure, 7.6 x 10^5 cells per treatment group were collected and pelleted, then homogenised with 100 µL ice cold β-gal assay buffer and kept on ice for 10 mins. Samples were centrifuged at 10,000 x *g* for five minutes at 4°C and the supernatant was collected. 5 µL of β-galactosidase positive control was diluted 1:25 in assay buffer. A 96-well plate (Cellstar®, #655180) was prepared with sample wells containing 5 µL of sample per well (6 technical replicate wells per treatment group), and each well was made up to a 50 µL volume with assay buffer. A reaction master mix was prepared using β-gal substrate and assay buffer, and 50 µL of this was added to each well. A standard curve of known concentrations was generated using the provided fluorescein standard. Fluorescence of all samples at Ex/Em = 480/530 nm was measured using a Varioskan LUX microplate reader (ThermoFisher Scientific), as a readout of β-gal activity at five-minute intervals for 30 minutes. Data was quantified according to a standard curve, and processed according to manufacturer's instructions, to calculate β-gal activity (pmol/min/µL) in DOX- and VEH-treated samples.

3.2.10 Statistical analyses for DOX IC_{50} curve fitting

Eight wells (A-H) represented eight technical replicates for each condition tested in one column of the 96-well plate. The mean absorbance value was calculated for each plate column, then the mean absorbance of column one was subtracted from all other mean absorbances, as a background correction to account for phenol red absorbance in

culture media. All mean absorbances from DOX conditions were then normalised to the mean absorbance of column three, the vehicle control, to generate a normalised percentage survival. The resulting data from at least three independent experiments was combined to generate an average survival curve. Using GraphPad Prism 10, DOX concentrations were log-transformed to allow downstream curve fitting. Using the same software, nonlinear regression was used to fit a survival curve to this data and generate an IC_{50} value for DOX, which had the equation Y=100/(1+10^((LogIC_{50}-X)*HillSlope))). Goodness-of-fit of the nonlinear regression fitting was evaluated by interpretation of the R^2 value, where $R^2 = 1$ indicates a perfect goodness-of-fit.

3.2.11 General statistical analyses

To compare IC_{50} values of DOX in different cell lines, a one-way ANOVA was used with Tukey's correction for multiple comparisons. To analyse qPCR results, data were processed to the widely used ddCT form, whereupon they were statistically analysed using a paired t-test. As is common, data were graphed in the form 2^-ddCT format for easier visualisation and interpretation. To analyse β-gal activity, an unpaired t test was used. Microsoft Excel was used for basic data collection/tidying, and GraphPad Prism 10 was used to carry out statistical analysis and generate graphs. Significance was assigned as $p < 0.05$.

3.3 Results

3.3.1 Doxorubicin induces time-dependent cytotoxicity in the AC10 cardiomyocyte cell line

In order to identify the sensitivity of AC10 CMs to DOX, which will inform later studies, AC10 cells were exposed to DOX for 24-96 hours at a concentration range of 100 fM–10 μM. A sigmoidal survival curve was then fitted using non-linear regression (**Figure 3.5**). At 24 hours exposure, the estimated IC_{50} value of DOX was greater than the maximal exposure concentration (>10 μM). At 48, 72 and 96 hours the IC_{50} of DOX was calculated as 52.5 nM, 20.6 nM and 14.2 nM, respectively (**Figure 3.5**, **Table 3.2**).

Table 3.2 Calculated IC_{50} values of DOX in AC10 CM cell line following a given exposure time. Survival curves were fitted using linear regression, the goodness of fit of this model is expressed as the R^2 value.

DOX exposure time (hours)	IC_{50} (nM)	R^2 - curve goodness of fit
24	> 10000	-
48	52.5	0.9311
72	20.6	0.9818
96	14.2	0.9776

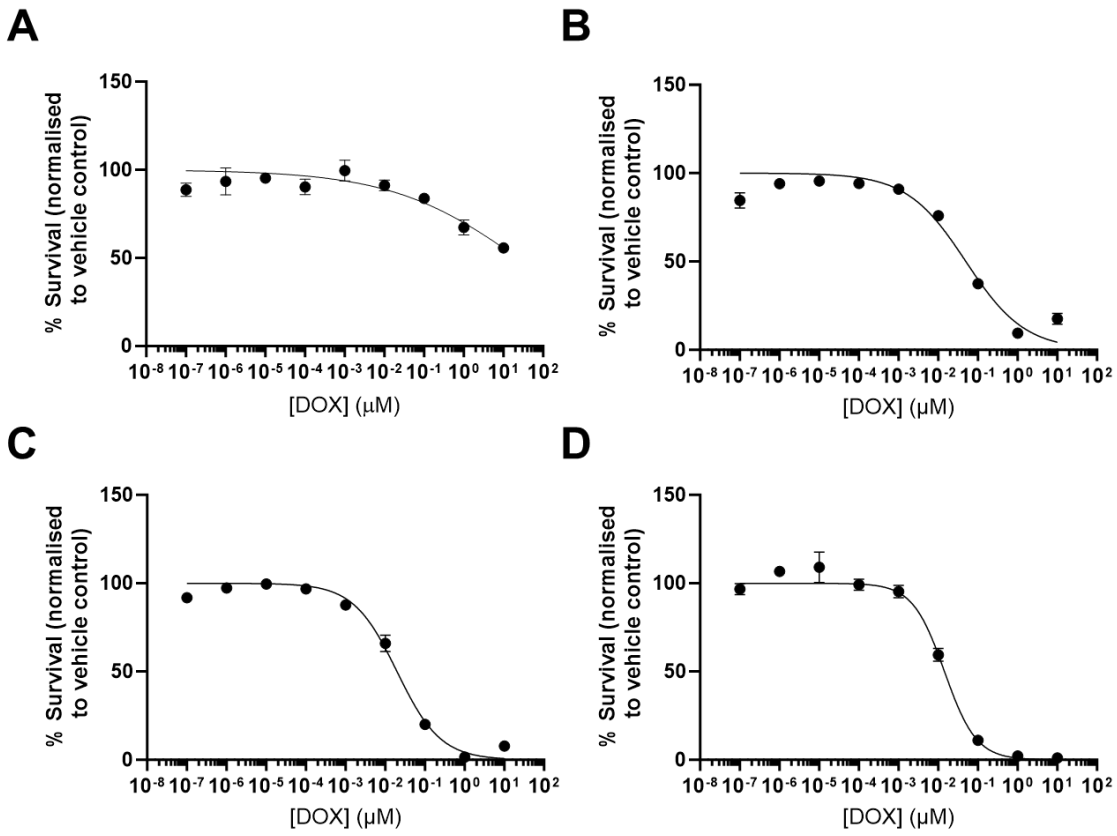

Figure 3.5 Percentage survival of AC10 CM cell line following various exposure times to a range of DOX concentrations, normalised to DMSO vehicle control, as indicated by MTS metabolism assay. A) Percentage survival after 24 hours exposure to DOX. **B)** Percentage survival after 48 hours exposure to DOX. **C)** Percentage survival after 72 hours exposure to DOX. **D)** Percentage survival after 96 hours exposure to DOX. Each data point = mean +/- SD, n ≥ 3.

3.3.2 Doxorubicin induces time-dependent cytotoxicity against primary human cardiac fibroblasts

Primary HCFs were exposed to DOX in a similar manner to AC10 CMs (see **3.3.1**). At 24 hours exposure, the estimated IC_{50} value of DOX was >10 μM, as was observed for AC10.The IC_{50} of DOX was calculated as 1181 nM, 222 nM and 148 nM at 48, 72 and 96 hours DOX exposure, respectively (**Table 3.3**, **Figure 3.6**).

Table 3.3 Calculated IC_{50} values of DOX in primary human cardiac fibroblasts following a given exposure time. Survival curves were fitted using linear regression, the goodness of fit of this model is expressed as the R^2 value.

DOX exposure time (hours)	IC_{50} (nM)	R^2 - curve goodness of fit
24	>10000	-
48	1181	0.8834
72	222	0.9316
96	148	0.9513

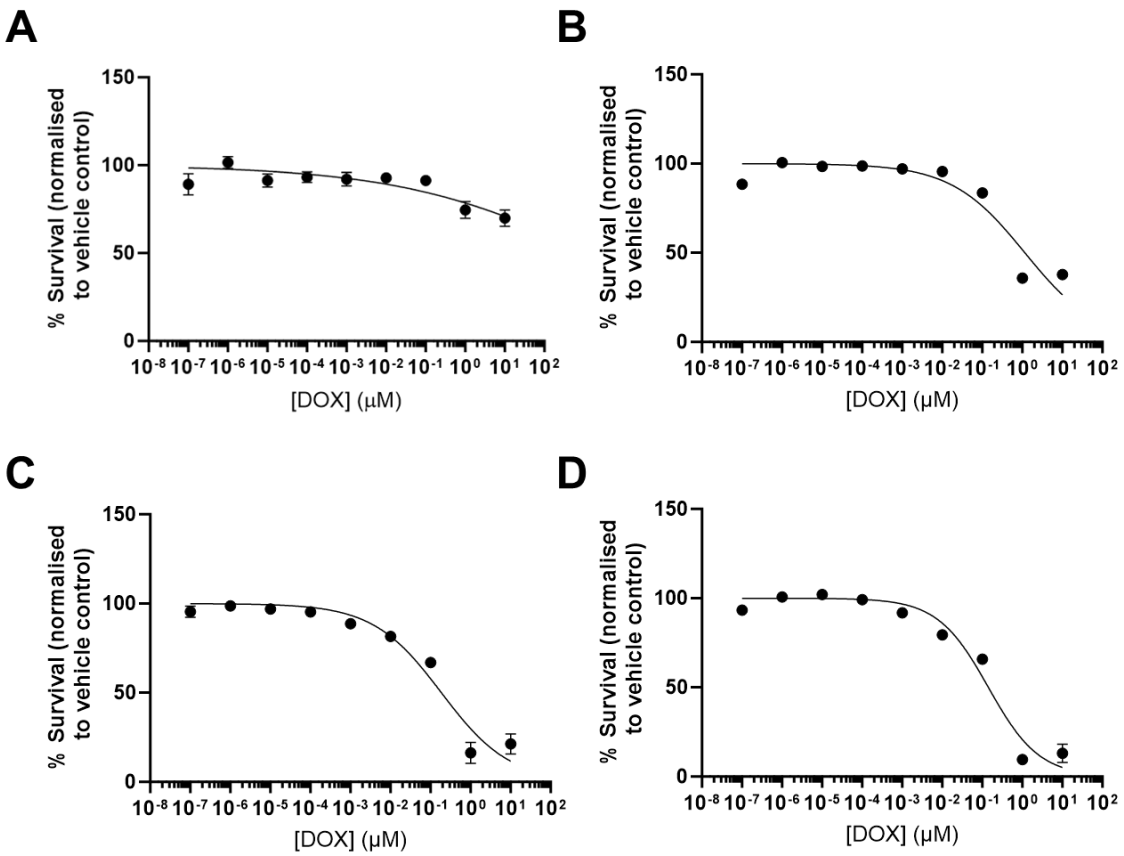

Figure 3.6 Percentage survival of primary human cardiac fibroblasts following various exposure times to a range of DOX concentrations, normalised to DMSO vehicle control, as indicated by MTS metabolism assay. A) Percentage survival after 24 hours exposure to DOX, with IC_{50} value >10 μM. **B)** Percentage survival after 48 hours exposure to DOX. **C)** Percentage survival after 72 hours exposure to DOX. **D)** Percentage survival after 96 hours exposure to DOX. Each data point = mean +/- SD, n = 3.

3.3.3 Doxorubicin induces time-dependent cytotoxicity against the MCF-7 breast cancer cell line

The breast cancer cell line MCF-7 was exposed to DOX in a similar manner to AC10 CMs and HCFs. At 24 hours exposure, the estimated IC_{50} value of DOX was again >10 μM. The estimated IC_{50} of DOX calculated as 1902 nM, 774 nM and 199 nM at 48, 72 and 96 hours exposure, respectively (**Table 3.4**, **Figure 3.7**).

Table 3.4 Calculated IC_{50} values of DOX in MCF-7 breast cancer cell line following a given exposure time. Survival curves were fitted using linear regression, the goodness of fit of this model is expressed as the R^2 value.

DOX exposure time (hours)	IC_{50} (nM)	R^2 - curve goodness of fit
24	>10000	-
48	1902	0.8956
72	774	0.8980
96	199	0.9783

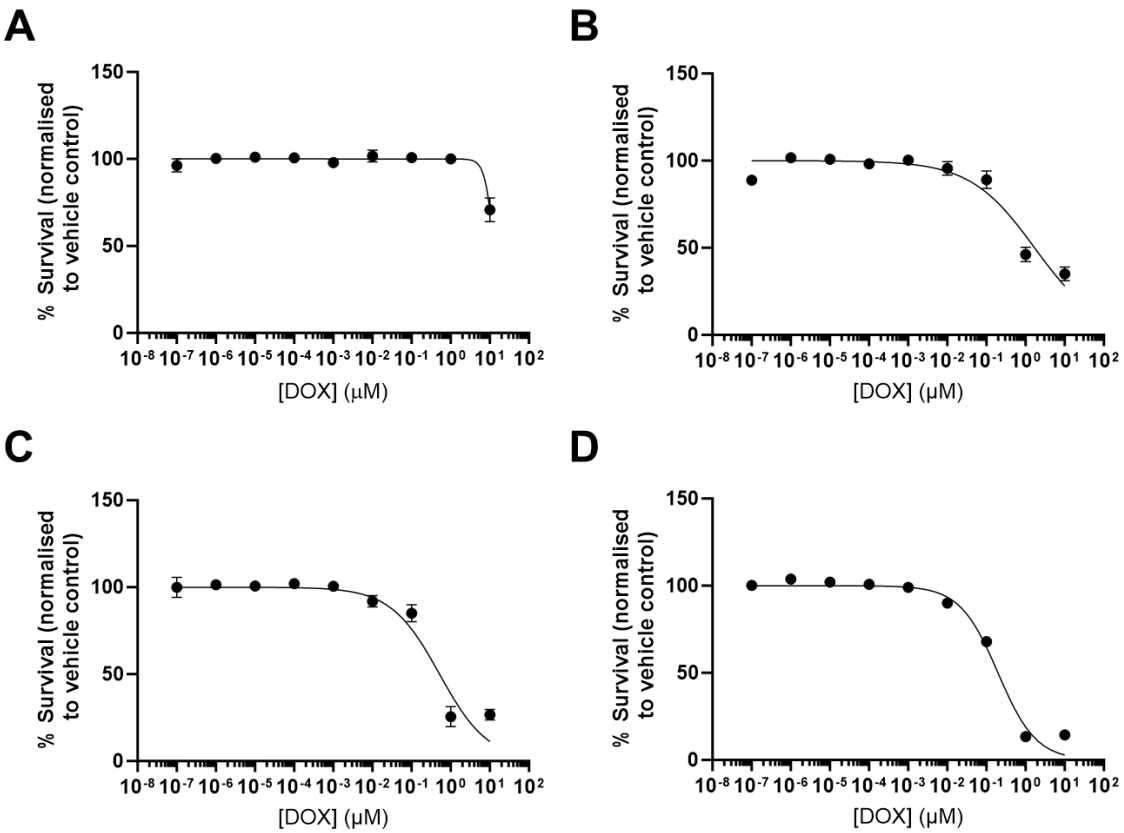

Figure 3.7 Percentage survival of the MCF-7 breast cancer cell line following various exposure times to a range of DOX concentrations, normalised to DMSO vehicle control, as indicated by MTS metabolism assay. A) Percentage survival after 24 hours exposure to DOX. **B)** Percentage survival after 48 hours exposure to DOX. **C)** Percentage survival after 72 hours exposure to DOX. **D)** Percentage survival after 96 hours exposure to DOX. Each data point = mean +/- SD, n = 3.

3.3.4 Comparison of doxorubicin sensitivity between cell types

As would be assumed for a known cytotoxic agent, longer exposure times to DOX generated a lower IC_{50} value within a single cell model. However, the AC10 CM cell line was particularly sensitive to DOX cytotoxicity, with IC_{50} values in the range of 14.2-52.5 nM. Though this is in agreement with previously published data on the AC10 cell line within our lab (indicating this result might not have arisen from human error or technical faults during the assay),[251] it is strikingly lower than the counterpart IC_{50} values for the MCF-7 breast cancer cell line obtained in this study (199-1900 nM), which would suggest DOX shows an approximately 10-fold higher cytotoxicity for CMs than cancer cells *in vitro*.

To explore whether this difference might be due to an artefact of the AC10 cell line in our hands, the sensitivity of AC16 cardiomyocytes to DOX was briefly investigated: AC10 and AC16 cells are subclones derived from the same cell line,[209] and there is no theoretical reason for them to display different sensitivities to DOX. AC16 CMs were exposed to DOX in a similar manner to AC10 CMs, HCFs and MCF-7 cells (see **3.3.1**, **3.3.2** and **3.3.3**), at a 96-hour exposure only, using a narrower range of DOX concentrations based on estimated IC_{50} from AC10 results. The estimated IC_{50} value of DOX in AC16s was consequently calculated as 144.4 nM (**Figure 3.8A**). Given the significantly lower IC_{50} of DOX against AC10 CMs (**Figure 3.8B**), and the fact that the AC16 cell line has emerged as the predominant cell line over AC10 for CM biology research due to its commercial availability and associated genetic verifications (AC10 cells are no longer available for purchase), it was decided to employ AC16 as a more verifiable model going forward, to maximise the comparability of later studies to published works.[252] Comparing the IC_{50} values of DOX against AC16 CMs, HCFs and MCF-7s, there was no significant difference between cell types (**Table 3.5**), indicating a similar sensitivity to DOX across the board.

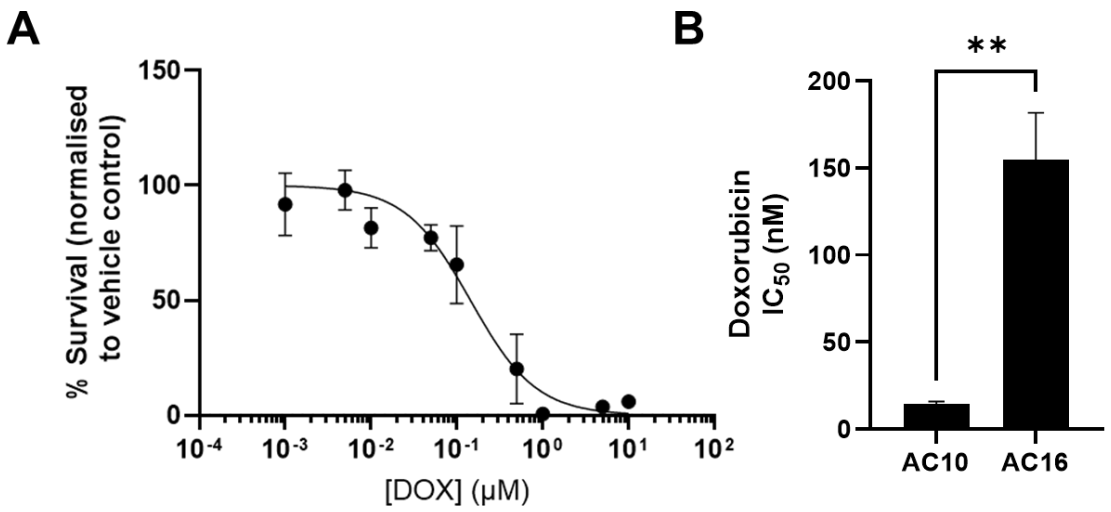

Figure 3.8 IC_{50} of DOX against AC10 and AC16 CM cell types. A) Percentage survival of the AC16 CM cell line following 96 hours exposure to a range of DOX concentrations, normalised to DMSO vehicle control, as indicated by MTS metabolism assay. Each data point = mean +/- SD, n = 6. **B)** Comparison of DOX IC_{50} values against AC10 and AC16 CM models, in a 96-hour exposure, calculated using an MTS viability assay (metabolism-based). Data represents the mean +/- SEM of n ≥ 3 independent experiments, analysed with an unpaired student's t test.

Table 3.5 Summary of DOX IC_{50} values across three relevant cell models. 96-hours exposure IC50 values are detailed, which were analysed using a one-way ANOVA with Tukey's correction for multiple comparisons. Data is presented as mean +/- SEM, n = ≥ 3 independent experiments).

Cell type	Mean IC_{50} +/- SEM (nM)	Significantly different to other cell types?
AC16	144 +/- 26.9	No
HCF	148 +/- 19.3	No
MCF-7	199 +/- 10.1	No

3.3.5 Response of AC16 cardiomyocytes to doxorubicin exposure and 4-day recovery period

A concern regarding anthracyclines is the delayed nature of their cardiotoxicity, which may not be accurately described by a dose-response curve in a classical acute study. Therefore, to better represent this, a dose-recovery ("hit and run") model was evaluated. After a three-hour DOX exposure, and 93-hour recovery period in culture, the mean IC_{50} +/- SEM of DOX was calculated as 624.5 +/- 105.3 nM (**Figure 3.9**, R^2 = 0.8704), which is below the mean reported C_{max} of DOX (2.32 +/- 0.58 μM) in clinical settings (see **3.1.2**). This model was subsequently employed to investigate the phenotype of these surviving CMs post-insult and how they might persistently contribute to the delayed onset nature of DOX-associated cardiotoxicity.

500 nM DOX was selected going forward, given that this is below the IC_{50} of DOX in a three-hour exposure setting, and is below the clinical C_{max} of DOX, but representative of clinical exposures within one to two pharmacokinetic terminal half-lives of this drug (reported to be 20-48 hours).[25,235,253]

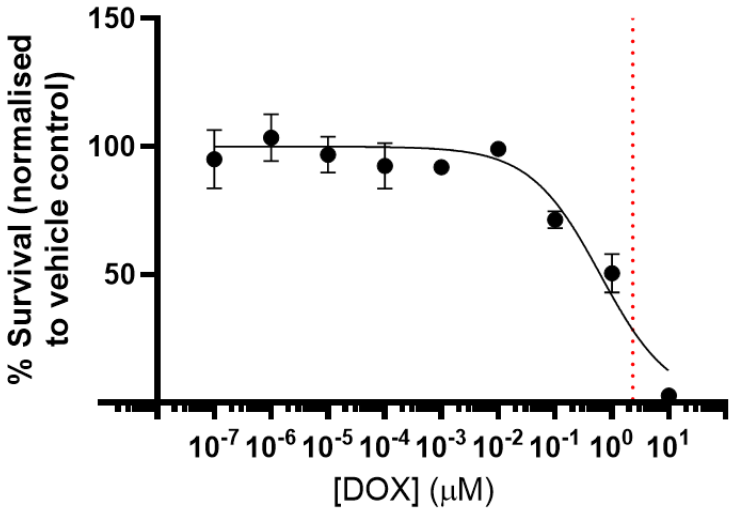

Figure 3.9 Percentage survival of the AC16 CM cell line following 3 hours exposure to a range of DOX concentrations and a 93-hour recovery period, normalised to DMSO vehicle control, as indicated by MTS metabolism assay. The clinical C_{max} value is indicated with a red dotted line. Each data point = mean +/- SEM, n = 3.

3.3.6 Assessment of senescence-related markers in AC16 cardiomyocytes 10 days following a sublethal exposure to DOX

As previously mentioned, studies investigating the impact of DOX upon CMs have previously used high doses that lead to cell death, which perhaps does not represent the clinical situation. The consequent hypothesis in this project was that sublethal DOX exposure leads to myocardial dysfunction due to senescence induction. As such, the next aim was to establish whether CMs subjected to a sublethal dosing regimen are indeed induced to senescence. Studies in the literature have shown that a 500 nM, 3 hour exposure to DOX is sufficient to induce phenotypic alterations to CMs *in vitro* which may contribute to disease.[180] 500 nM is within the range of DOX C_{max} measured in patient sera in the clinic,[235] and also tallies with seminal *in vitro* and *in vivo* studies implicating senescence as a driver of DOX cardiotoxicity.[179]

The expression of p16 and p21 proteins (classical senescence markers and controllers of the senescent phenotype) in AC16 cells was tested 10 days post 500 nM DOX or equivalent VEH exposure, using fluorescence immunocytochemistry approaches. Minimal expression of p16 was noted in AC16 cells post-VEH (**Figure 3.10A**). However, 10 days post-DOX, the vast majority of AC16 cells in culture expressed p16, with the staining pattern being diffuse and localised to both cytoplasmic and nuclear compartments (**Figure 3.10A**). In the case of p21 staining, this marker was not observed in VEH-treated cells (**Figure 3.10B**) but was seen in a small number of DOX-treated cells (**Figure 3.10B**). The staining pattern of p21 was notably different to p16, being instead clearly observed in the nuclear compartment and minimally observed in the cytoplasmic compartment. Next, the expression of these markers was quantified using RT-qPCR. These studies identified that p16 transcript (*CDKN2A*) was significantly increased post-DOX compared to VEH control (**Figure 3.10C**). Similarly, quantification of p21 transcript (*CDKN1A*) also showed a significant increase in DOX vs VEH treatment groups (**Figure 3.10D**).

Having established DOX induced the expression of two hallmark senescence controllers the quantification of additional genes which are associated with CM senescence was carried out. B-cell lymphoma 2 (Bcl-2) is a regulator of apoptosis, which inhibits formation of the apoptotic pore, and previous studies have demonstrated that *in vivo* treatment with Bcl-2 inhibitors induces senescent CMs to apoptosis, suggesting Bcl-2 is expressed by and important for senescent cell survival.[173,175,181] DOX-treated AC16 CMs demonstrated a significant increase in *BCL2* transcript

expression (**Figure 3.10E**). Similarly, DOX-treated CMs displayed a significant increase in *GDF15*, a cytokine identified as a component of the CM SASP (**Figure 3.10F**).[173] Recent studies have also identified that the expression of *PURPL*, a long non-coding RNA (lncRNA), is linked to the senescent phenotype,[157] although to date *PURPL* expression had not been investigated in the context of CM senescence. A significant increase in this novel lncRNA senescence marker was observed in DOX-treated CMs (**Figure 3.10G**)

Another "gold-standard" hallmark of cellular senescence is increased beta-galactosidase activity (senescence-associated beta-galactosidase, SA-β-Gal). Most mammalian cells, regardless of age phenotype show lysosomal β-Gal activity at pH 4, but senescent cells notably express lysosomal β-Gal activity at pH 6 – therefore robust β-Gal activity under higher pH conditions can be used to specifically detect senescent cells.[149] This is thought to be due to overexpression of GLB1, the gene encoding for lysosomal enzyme.[254] Using a commercially available fluorescent β-Gal activity assay, the activity of β-Gal in AC16 cell homogenate derived from cell cultures treated with DOX or VEH was tested, according to previous dosing regimens in this study. The activity of β-Gal in DOX-treated AC16 cultures was 6.2 pmol/min/μL, significantly higher than its activity in VEH-treated cultures, 1.3 pmol/min/μL (**Figure 3.10H**)

Taken together, these data provide strong evidence that sublethal DOX treatment induces senescence in AC16 CMs through activation of classical senescence pathways and indicates that senescent AC16 CMs express additional proteins associated with *in vivo* CM senescence.

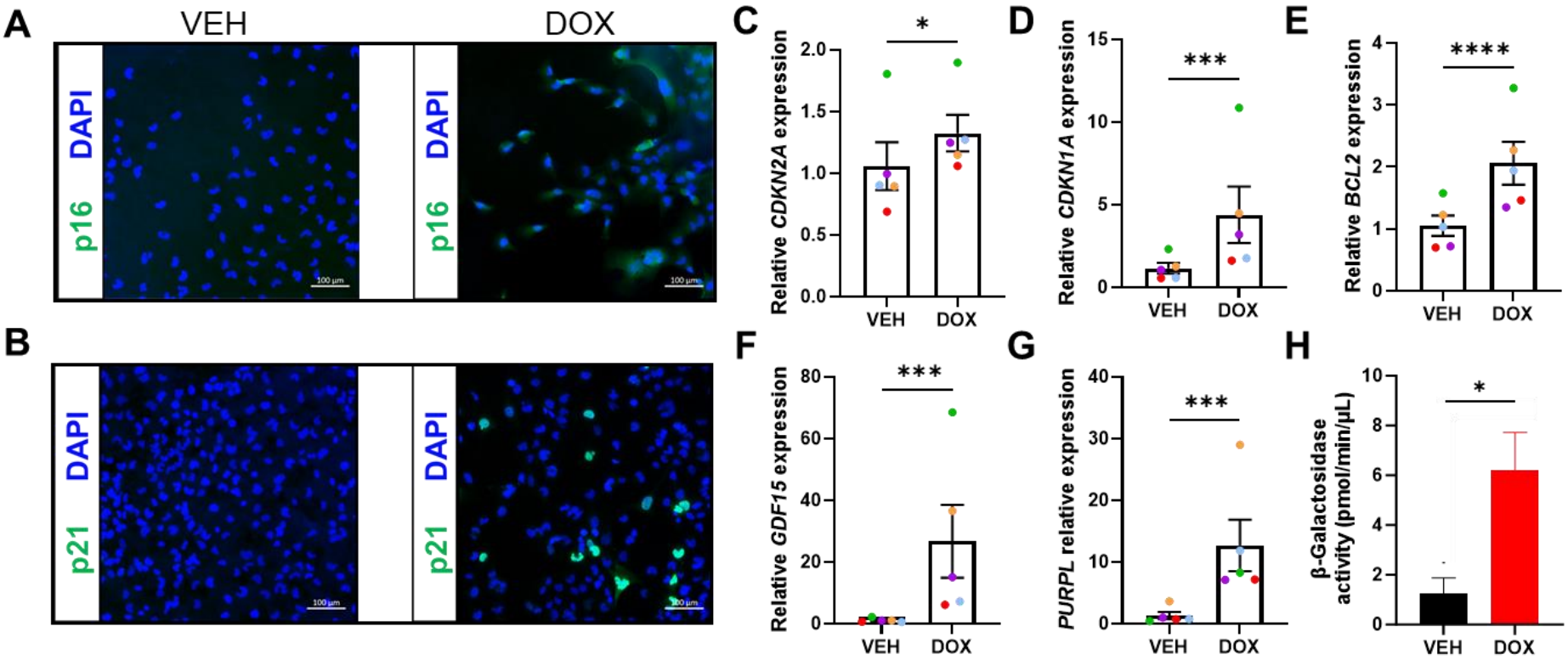

Figure 3.10 Sublethal DOX exposure induces expression of senescence markers in AC16 CMs. A) Representative image of immunofluorescent staining following recovery from VEH exposure (left) or DOX exposure (right) (p16 green, nuclei blue) **B)** Representative image of immunofluorescent staining following recovery from VEH exposure (left) or DOX exposure (right) (p21 green, nuclei blue). **C-H)** RT-qPCR expression analysis in DOX/VEH treated AC16 CMs: **C)** *CDKN2A* **D)** *CDKN1A* **E)** *BCL2* **F)** *GDF15* **G)** *PURPL*. Data is presented as mean +/- SEM from n = 5 independent experiments, where *HPRT1*, *ACTB* and *RPLP0* were used as endogenous controls. **** $p \leq 0.0001$. *** $p \leq 0.001$, * $p \leq 0.05$ using a paired student's t-test. **H)** Comparison of SA-β-galactosidase activity (pmol/min/μL) in the cellular lysates of DOX- and VEH-treated AC16 CMs. Data is presented as mean +/- SEM, n = 3 independent experiments. * $p \leq 0.05$ using an unpaired student's t-test. Scale bars = 100 μm.

3.4 Discussion

Development of cardiac toxicities is a major clinical problem with many cancer chemotherapeutics, especially the anthracycline family of drugs such as DOX. The aim of this chapter was to characterise and optimise a clinically relevant *in vitro* human cellular model to evaluate the mechanistic basis of DOX-induced cardiotoxicity.

3.4.1 Cytotoxicity of doxorubicin varies by exposure time and cell type

Against the AC10 human CM cell line DOX exhibited IC_{50} values of 52.5 +/- 6.91, 20.6 +/- 3.56, and 14.2 +/- 1.33 nM at 48, 72 and 96 hours respectively. These values are in agreement with the previous studies of Rockley et al. who reported an IC_{50} at 96 hours of 20 nM.[251] Relative to published data for cancer cell lines, AC10 cells appear comparatively sensitive to DOX. It could be speculated that this heightened sensitivity is due to the accumulation of DOX in CMs,[255] or the concept that DOX particularly targets the mitochondria of the energetically demanding CM due to the drug's cationic nature and resultant strong affinity for cardiolipin, a lipid found in the inner mitochondrial membrane.[256] However, before exploring these concepts further, this marked sensitivity was verified in the AC16 clone of the cell line.

AC10 and AC16 sensitivity to DOX was different, exhibiting cytotoxicity IC_{50} values at a 96-hour exposure of 14.2 +/- 1.33 nM and 144 +/- 26.9 nM, indicating underlying differences between the clones. Our lab's AC10 cell cultures were established from a gift from Dr Barbara Savoldo (Texas Children's Hospital, USA), have been employed by multiple users in the lab, and as the handling of the cell line increased over time, phenotypic drift (an unfortunately common, and somewhat inevitable, artefact of serially culturing immortalised cell lines) may have occurred and given rise to these differences.[257] For instance, these differences might be attributed to altered drug influx/efflux dynamics, heightened proliferation, attenuated antioxidant response, or some other biochemical changes, but these lay outside the scope of this study. On the other hand, our AC16 cultures were recently purchased from a commercial source (therefore quality-control tested by e.g. short tandem repeat profiling) and were then established completely in-house. For these reasons and to better align this work with studies in the literature, future work therefore transitioned from using AC10 CMs to AC16 CMs.

When comparing the sensitivities of AC16 CMs, HCFs and MCF-7s to DOX, there were no significant differences in IC_{50} values, suggesting similar sensitivities. Though these

monolayer culture assays are a basic model, the suggestion that cardiac-resident populations lose a similar proportion of viability as a cancer cell population following DOX exposure is striking, highlighting the flawed, nonselective nature of this therapy.

3.4.2 Cytotoxicity of doxorubicin on non-cardiomyocyte cells of the heart

Historically, CMs have long received the lion's share of attention in cardiotoxicity research, but it has long been known that a large percentage of the cardiac cellular population is made up of non-CM cell types, by number. The toxicity of DOX in these non-CM populations, such as HCFs, is less well-studied but is gaining attention.[258] Here, it was shown that HCFs had a similar sensitivity to DOX cytotoxicity as the AC16 CM cell line, underscoring these concepts. HCFs are crucial to the formation and maintenance of extracellular matrix (ECM) in the cardiac microenvironment and are necessary for the proper contractility and function of CMs.[191] The acute loss of cardiac fibroblasts in the acute phase of DOX exposure would therefore likely disrupt cell-cell crosstalk in the heart, and impact other cell types' functionality. A survey of the literature found no robust reports of an IC_{50} value for DOX in HCFs, but, in agreement with the data in this project, related studies have been conducted showing that HCFs *in vitro* are indeed sensitive to DOX after 24 hrs exposure (using an MTT/MTS approach).[259] An *in vivo* study highlighted how approximately 80% of all apoptotic cardiac cells derived from DOX-treated animals were fibroblasts, though rather than a cell type-specific sensitivity this may point to the fact that the majority of cells in the heart are fibroblasts.[48]

Unlike CMs, HCFs retain the ability to proliferate and replenish apoptotic HCFs lost in acute phases of toxicity, though this may require phenotypic shift towards an activated phenotype, akin to the proliferative burst observed post-myocardial infarction.[260,261] HCFs release paracrine factors that are key to maintaining the overall homeostasis of the cardiac microenvironment and coordinating cellular responses to external cues, be they pathological or physiological. HCFs can therefore be seen to represent a physical and molecular link between various cell types in the myocardium – and short of HCF cell death, even changes to the HCF phenotype may promote pathology: this will be discussed later in this thesis. HCFs are but one example of a non-CM cell type crucial for making up the myocardial cellular milieu. Others include endothelial cells, smooth muscle cells and mesenchymal stromal cells. It would be interesting to evaluate the IC_{50} of DOX against these cell types using similar viability assays, to inform on the various sensitivities of the heterogeneous and complex cell populations in the heart.

3.4.3 Considering the suitability of MCF-7 cell line for doxorubicin toxicity studies

Within the anthracycline drug family, DOX and epirubicin remain crucial treatments for breast cancer, and their efficacy against relevant cell lines *in vitro* is well-established. The IC_{50} values of DOX against MCF-7 breast cancer cells reported here (199 nM at 96 hours exposure, 774 nM at 72 hours exposure) broadly agree with values reported in the literature.[239,262,263] Some studies have highlighted how incorporation of this cell line into a 3D model,[262,264] which better mimics the true tumour environment, drastically reduces its sensitivity to DOX, so it is worth interpreting these IC_{50} values from monolayer cultures with caution. To gain a more holistic understanding of DOX efficacy against breast cancer, it would be prudent to: investigate more sophisticated models (e.g. 3D models incorporating multiple cell types), and consider the clinical incidence of drug-resistant breast cancer (by evaluating drug-resistant cell lines for e.g. epigenetic variation or single nucleotide polymorphisms in drug transporters).[265,266]

Furthermore, data from the NCI-60 screen highlights the diverse sensitivities of various cancer cell types to a single therapy like DOX. MCF-7 is but one tumour cell line which can be used to model breast cancer, commonly used due to its robust oestrogen receptor (ER) expression and thus, capacity for hormonal response.[267] Others include the MDA-MB-231 cell line (which is ER-negative),[268] the T47D cell line (which is progesterone-sensitive and derives from a ductal carcinoma rather than adenocarcinoma),[269] and the BT-549 cell line (derived from a papillary, metastatic ductal carcinoma). DOX has a range of LC_{50} and GI_{50} values listed between these breast cancer cell lines (data not shown), even before purpose-made drug-resistant cell lines are considered, or other tissue types. Therefore, the MCF-7 toxicity data should not be interpreted as a catch-all representation of DOX's anticancer efficacy in general.

3.4.4 The MTS assay for assessing cytotoxicity in vitro

For the assessment of cytotoxicity and subsequent comparisons to other studies, the MTS assay was utilised specifically within this study. This colorimetric method is comparable to both the sulphorhodamine B (SRB) assay used for the NCI-60 screening (more amenable to high-throughput screening than MTS) and the luminescence-based CellTiter-Glo viability assay (Promega) used by the GDSC (NCI-60 transitioning to this assay in 2024).[238,239,270] All of these methodologies provide an

indirect measurement of drug toxicity via representation of cell metabolic capacity (MTS), total protein mass (SRB), or ATP production (CellTiter-Glo), respectively, which theoretically can be affected by a drug impacting cellular metabolism in the absence of cell number changes.[271] However, previous studies with the AC10 (and more latterly the AC16) cell line have demonstrated a close relationship between readouts from the MTT/MTS assay and cell numbers, assessed via trypan blue exclusion assay and real-time cellular impedance assays, providing a degree of confidence in these results.[251]

3.4.5 Refining an in vitro exposure model to elucidate the molecular mechanisms of toxicity – senescence induction in cardiomyocyte cell types

As previously discussed, though acute toxicity assays are useful in some experimental contexts, their readouts may not be the most useful for exploring the mechanisms of delayed DOX cardiotoxicity when used in isolation. Informed by the clinical doses of DOX administered to patients and the delayed-onset nature of this toxicity, an important output in this study was the development a dose-recovery *in vitro* model. The MTS assay results from this model, with 3 hour DOX exposure followed by a 93 hour recovery period, were notably different to those obtained following 96-hour continuous acute exposure, which aligns with the concept that acute exposure to high doses of DOX may induce a different effect in CMs compared to a transient exposure to low doses of DOX.[272] Studies have highlighted how one effect of low dose DOX exposure is the induction of cellular senescence:[250] since it was discovered that participation in the mitotic cell cycle is not a prerequisite for cells attaining a senescent phenotype, cellular senescence has gained much attention as a mechanism in CVD more generally,[173] and within AIC specifically.[179] To explore the capacity of a sublethal dose of DOX to induce senescence in a human CM cell line, the recovery period following DOX exposure was increased to 10 days going forward (based on the time course of senescence onset in CVD models from this lab and others).[175,179]

In the AC16 cell line, markers of senescence were elevated at the transcript and protein level 10 days after a transient, sublethal DOX exposure. Cells showed p16 protein expression throughout the whole cell following DOX exposure, contrasting with the nuclear-only expression of p21. Given their roles in cell cycle regulation, p16 and p21 protein may traditionally be considered to be constrained to the nucleus, yet a survey of the literature returned no studies showing nuclear-only p16 expression in AC16 cells and other commonly used immortalised/cancer cells lines (e.g. HeLa, HepG2) via immunofluorescent methods – in fact, one study shows p16 localisation to the

cytoplasm and nucleus of A549 and HEK293T cells, similar to the AC16 studies herein.[273] There is robust evidence for elevated p21 protein expression to be localised to the nucleus in response to stress, as was noted in the results above.[274]

3.4.6 Considering other senescence-related markers

GDF15 and *PURPL* transcripts were increased in AC16 cells 10 days post-DOX, markers which have been associated with cellular senescence. GDF15, the protein encoded by *GDF15*, is emerging as a powerful circulating biomarker of cardiovascular stress in humans, with some studies showing its performance matches that of BNP.[275] GDF15 was recently identified as a CM-specific SASP protein,[173] and its elevation in this project's 10-day dose-response model alongside typical senescence markers p16, p21 and SA-β-Gal is also in accordance. The heterogeneity of the senescent phenotype is widely acknowledged as a challenge and research priority in the field. In a study aiming to identify more universal, useful transcript markers of senescence, the lncRNA *PURPL* was highlighted as a strong candidate, which performed well across various senescence-inducing stimuli, cell types and tissue types.[157] Therefore, its elevation in DOX-treated AC16 CMs is also supportive of the induction of the senescent phenotype.

SA-β-Gal has long been acknowledged as a robust protein marker of cellular senescence.[149] Here, a fluorescence-based assessment of SA-β-Gal levels in cell lysate was used, to provide a quantitative, orthogonal approach to the qualitative p16 and p21 immunostaining. There was a significant increase in SA-β-Gal activity within DOX-treated AC16 CMs. To explore the expression of these markers within this model further, it would be of interest to use an SA-β-Gal immunostain on fixed cells to shed light on the frequency at which these three historically gold-standard senescence markers co-stain within the same cells.

Landmark studies of senescence and DOX cardiotoxicity have so far focused more on whole-animal murine studies or non-cardiovascular human cell lineages,[179,180] whereas in this project the AC16 human ventricular cell line was used. Considering other comparable cell types; H9c2 cells are commonly utilised in basic cardiovascular research, but they better resemble skeletal muscle cells, despite their cardiac origin.[243,276] The HL-1 cell line is often used in studies and is advantageous in its contractile potential, but is also immortalised and furthermore, is atrial in origin rather than ventricular, which AC16s are.[209,245] Both HL-1 and H9c2 are murine-derived,

compared to AC16s which are human-derived. Therefore, certainly as a predecessor to more sophisticated models, the AC16 cell line is proposed to have utility in cardiotoxicity & senescence studies, especially given its capacity to show robust upregulation in p21 and p16, alongside SA-β-Gal activity in an orthogonal study post-DOX exposure, as shown here.

3.4.7 Conclusions

Overall, the toxicity assays detailed highlight the significance of exposure time and cell model choice when establishing IC_{50} values of a substance and these values' relevance to the literature. Furthermore, choosing a concentration and exposure time which is reflective of a real-world clinical context is crucial to beginning further studies into the molecular mechanisms of AIC. Considering the clinical pathology of DOX cardiotoxicity, the sublethal 10-day dose-recovery DOX exposure model used here indicates that CMs acquire a senescent phenotype in the days following exposure, a phenotype which may contribute towards progression of cardiovascular disease generally.

Chapter 4. Exploring the Doxorubicin-Induced Senescent Phenotype in a Cardiomyocyte Cell Line

4.1 Introduction

4.1.1 Cardiomyocyte hypertrophy in senescence and doxorubicin cardiotoxicity

At a whole-organ level, a decrease in total LV CM mass (CM atrophy) has been reported clinically following DOX treatment,[69] but studies suggest this is paired with an increased CM volume in the surviving cells (CM hypertrophy).[277] CM hypertrophy can occur physiologically, as a result of exercise or pregnancy, but more pertinent to this project, can also occur in pathology in response to a variety of small molecules, such as DOX.[278]

There are conflicting data as to whether CM senescence is associated with cellular and/or organ-level hypertrophy. In the context of ageing, CM senescence has been linked to pathological hypertrophy,[173,279] and in rat neonatal CMs *in vitro*, overexpressing $p16^{INK4a}$ and $p21^{CIP1/WAF1}$ using an adenovirus vector prevented cell enlargement upon serum stimulation and depressed the genetic expression of cardiac hypertrophy markers, indicating that these cell cycle inhibitors are required for induction of CM hypertrophy.[280] However, *in vivo* studies of acute CVD like IRI suggest that senescence is not a leading cause of hypertrophy, since CM-specific p16-knockout animals showed no change in CM area or LV mass compared to wild-type controls, post-IRI.[281] In the complex, acute disease setting of IRI therefore, other mechanisms may have a driving role in the regulation of CM hypertrophy, alongside cellular senescence. It may be speculated that chronic, DOX-induced changes in the senescent myocardium may follow a pathology similar to the ageing phenotype rather than IRI but nevertheless, the precise interactions between CM hypertrophy and senescence in the context of AIC are yet to be elucidated.

4.1.2 Mitochondrial morphology and dysfunction in senescent cells

Mitochondrial dysfunction has been touted as a major player in CM functional decline and heart disease more broadly.[282] DOX is known to damage CM mitochondria directly, and contribute to persistent dysfunction.[180,224] Being so energetically demanding, CMs are especially vulnerable to the impacts of mitochondrial dysfunction, and having a more limited antioxidant capacity, are also particularly vulnerable to the effects of mitochondrial ROS (mtROS).[283,284] Defective and damaged mitochondria can be

turned over via mitophagy (autophagy of mitochondria), but the attenuation of this important quality control process is a recognised feature of cellular senescence:[285] a lack of mitophagy is therefore thought to contribute to the accumulation of defective mitochondria within senescent cells.

Not only is the quality control of mitochondria affected in senescent cells, but also the morphology of the mitochondrial network more globally. Firstly, the mitochondrial footprint within senescent cells has widely been shown to increase compared to non-senescent controls.[187] However, this has mostly been shown in stress-induced senescence using ionising radiation or etoposide treatment as senescence stimuli or, when using DOX, in non-CM cell types.[187,286] Furthermore, the precise morphological characteristics of the network (e.g. branch length), which is crucial for proper function, is understudied in DOX-induced senescence in the CM context.

It is generally thought that mitochondrial fission/fusion dynamics are disrupted in senescent cells, with some authors suggesting that decreased fission-related protein PINK1 contributes to a more fused mitochondrial network.[287] A hyper-fused mitochondrial network which is less able to dynamically regulate fission/fusion events may be less able to adapt to metabolic demands, compromising the function of the cell. In CMs, decreased mitochondrial network branch length has separately been correlated with a decrease in maximal respiration rate and spare capacity (i.e. functional capacity).[288] However, there are few studies evaluating the mitochondrial network morphology of DOX-induced senescent CMs, and how this may impact cellular energy production and function.

4.1.3 Senescent cardiomyocytes are secretory – function of the SASP

One of the distinguishing features of senescent cells is their ability to secrete a pro-inflammatory SASP, as previously introduced (see **1.4**). Using a purified population of CMs, it was only recently demonstrated that CMs secrete a non-canonical, functional SASP.[173] Therefore, it is thought that the SASP previously attributed to CMs isolated from cardiac tissues may actually be derived from other cell populations, such as HCFs, which overgrow *ex vivo* CMs in culture over time. However, though this study highlighted novel CM SASP targets such as GDF15, Endothelin 3 and TGFβ2, these were only detected at the mRNA level and their functionality was only demonstrated by applying the recombinant proteins individually to fibroblast cultures.

True co-culture studies exploring the CM SASP's effects on cardiac fibroblasts are scant, but it is well-established that paracrine interactions between CMs and cardiac fibroblasts play a role in cardiovascular health and disease, including via the SASP.[289,290] Short of its functionality, better understanding the senescent CM SASP in circulation may enable the development of this secretome signature into a biomarker panel which is predictive or prognostic of cardiovascular disease. Clinically, circulating SASP proteins have shown encouraging results in their capacity to predict clinically important health outcomes in older adults, including death (combining GDF15, RAGE, VEGFA, PARC, and MMP2),[291] COVID-19 prognosis (using immunosenescence and inflammageing cytokine markers IL-6, IL-10, TNF-α),[292] and age-related health deficits and/or postsurgical outcomes (combining GDF15, FAS, osteopontin, TNFR1, ACTIVIN A, CCL3, and IL-15).[293] No SASP profile for DOX-induced senescence in CMs has been established as of yet,[182] so elucidating this SASP signature and its paracrine functionality is an unmet need in the field, alongside evaluating its clinical potential as a predictive circulating biomarker of AIC.

4.1.4 Aims and objectives

As previously detailed, senescence was classically defined by irreversible exit from the cell cycle by Hayflick and Moorhead. However, the field's understanding of the senescent phenotype, and its potential role in cardiovascular disease such as AIC, has since expanded to include many hallmarks.[155]

Having assessed DOX-exposed AC16 CMs for traditional senescence markers p16, p21 and SA-β-gal (see **1.4.1**), the aim now is to characterise other phenotypic hallmarks of senescent cells, namely cellular hypertrophy, mitochondrial network alterations, and the presence of a functional SASP, using cell imaging techniques, specialist bioimaging analyses and cytokine array following the 10-day dose-response DOX exposure regimen. Given the acknowledged heterogeneity of the senescent phenotype dependent on stimuli and cell type, these studies will inform on the specific phenotype of CMs induced to senescence by DOX, and how these features may contribute to pathology.

4.2 Materials and Methods

4.2.1 Hypertrophy image analysis

To quantify the size of AC16 CMs, cells were imaged using a Nikon Eclipse TS100 light microscope before VEH/DOX exposure. Then, VEH-treated cells were imaged at days

1 and 3, at which point cells became confluent in culture so were unsuitable for further imaging. DOX-treated cells were imaged at days 1, 3, 7 and 10 following exposure. At each time point, the size of 20 cells within one field of view were manually measured using ImageJ.

4.2.2 Cell culture, immunofluorescent labelling & qualitative imaging of the mitochondrial network

AC16 cells were seeded into 6-well plates, each well containing sterile glass cover slips (VWR 631-0150). Cells were allowed to adhere overnight then exposed to DOX or DMSO vehicle (VEH) according to the established protocol (see **2.1.6)** but with the adaptation that the cells were trypsinised and re-seeded at a lower density if the culture reached confluence, to prevent overgrowth during the 10-day recovery period.

AC16s were fixed at room temperature using a ten-minute incubation with a 1:1 mix of normal culture medium:4% PFA (Thermo Scientific 28906, diluted 1:4 with PBS), which was then replaced by 4% PFA only for a further ten minutes. Cover slips were washed three times with PBS (Gibco 10010-015), then cells were permeabilised for 15 minutes at room temperature with 0.2% Triton X-100 (Sigma X100) in PBS, with gentle rocking. Cells were washed thrice with PBS, then blocked with 5% goat serum (Sigma G9023) in PBST, at room temperature for one hour. Block was aspirated gently, then cells were incubated at 4°C overnight with a combination of primary antibodies, which were: Cell Signalling D5C8, rabbit anti-human TFAM, 1:500; Abcam ab14730, mouse anti-human ATP5B, 1:500. Primary antibodies were gently aspirated, cells were washed thrice with PBST for five minutes per wash, with gentle rocking. Cells were incubated for one hour at room temperature in the dark with a combination of secondary antibodies, which were: Invitrogen A21069, goat anti-rabbit Alexa Fluor 568, 1:500; Invitrogen A11001, goat anti-mouse Alexa Fluor 488, 1:500. Secondary antibodies were removed, and cells were washed twice with PBST, then incubated with 1 µg/mL DAPI (Invitrogen 62248) for 15 minutes at room temperature. Cells were washed twice with distilled, deionised water before mounting (Fisher Scientific 15586276) onto cover slips and sealing with nail varnish.

Images were acquired using a 63x oil immersion objective on a Zeiss Confocal LSM 980 multiphoton instrument, with Airyscan super resolution imaging.

4.2.3 High-content imaging of mitochondrial network morphology for quantification

The Newcastle University BioImaging Unit is acknowledged for their assistance with the generation of imaging data. Slides were visualized with an upright LSM 880 microscope with Airyscan detector (Carl Zeiss) using W Plan-Apochromat 40x/1.0 DIC VIS-IR M27 objective (equipment funded by Wellcome Trust 2017, 208339/Z/17/Z). For large images 3x3 or 4x4 tiles at zoom 1.8 were used to cover multiple cells, while z-slices were acquired with a z-step size of 6-7.5 µm. Airyscan processing was performed using the Airyscan processing function in the ZEN software.

4.2.4 Quantification of the mitochondrial network using MiNA

The Newcastle University BioImaging Unit is acknowledged for their assistance with analysis of mitochondrial network morphology. Mitochondrial network morphology in individual cells was analysed using the MiNa (Mitochondrial Network Analysis) script for the open-source software Fiji (ImageJ).[294] MiNA is a simplified workflow for analysing mitochondrial morphology,[295] here using 3D z-stacks of fluorescence images. The MiNA macro generated a skeleton of the mitochondrial network in each cell and calculated mitochondrial footprint volume, mitochondrial "doughnuts" per cell (toroidal mitochondria), and mean branch length of the network per cell. Original source code for the MiNA workflow can be found at https://github.com/StuartLab/MiNA, and the code used for this work can be found at https://github.com/NCL-ImageAnalysis/General_Fiji_Macros under the title MiNA_CustomScript.py (**Appendix A**).[296] Otsu was used to threshold images,[297] no other notable modifications were made to the original code.

4.2.5 Conditioned media collection from senescent AC16 cardiomyocytes

AC16 CMs were treated with DOX and VEH according to the previously described 10-day dose-recovery regimen (see **2.1.6**). Cells were cultured in T75 culture flasks (Corning). On day 8 post-exposure, a media change was performed, whereby media was aspirated, cells were washed gently with PBS, then 10 mL of fresh DMEM/F-12 media (Gibco 21041-025) was added into flasks. Media contained 1% P/S (Gibco 15140-122 100 mL) but contained no FBS and no phenol red, to minimise any interference in downstream LC-MS or cytokine array applications. After 48 hours, now-conditioned media was collected from senescent and non-senescent AC16 cultures

and centrifuged at 5,000 x *g* for 10 minutes to remove cell debris. Supernatant was decanted and stored at -20 °C until needed.

4.2.6 LCMS for detection of doxorubicin and doxorubicinol in conditioned media

The concentration of DOX and doxorubicinol (DOXol) was evaluated in conditioned media using a liquid chromatography mass spectrometry (LCMS) method.

LCMS was carried out by Martin Galler (Newcastle University, UK). To prepare samples for LCMS, 100 µL of either blank, standard, quality control (QC) or conditioned media sample was firstly pipetted into an Eppendorf tube (DOX for standards was obtained from Sigma, 44583-1mg, DOXol for standards was obtained from Chem Cruz, sc-495904). Standards were prepared fresh on the day of the assay, ranging from 5-500 ng/mL in blank plasma. The internal standard was idarubicin (Sigma I1656-10mg). 10 µL of internal standard working solution (0.5 µg/mL) was added. Then, 400 µL of acetonitrile was added to each tube and briefly vortexed, before being centrifuged at 14,000 rpm for 5 minutes at 20 °C. Supernatant was transferred to a 12 mm borosilicate tube and dried down at 30 °C under nitrogen. Residue was reconstituted in 200 µL 0.1% formic acid (aq), then vortexed. 170 µL was transferred to limited volume insert, then 10 µL was injected onto the column.

Chromatographic separation of DOX and DOXol was achieved using a Zorbax Eclipse Plus C18 2.1x50mm Rapid Resolution HD 1.8-Micro, ran for 7.5 minutes at a flow rate of 0.5 mL/minute (50:50 0.1% formic acid: acetonitrile). Reconstituted samples were analysed using an Agilent 1260/ ABSCIEX 4000 LC/MS system and Analyst Version 1.6.2 software (Applied Biosystems). The retention times and mass transitions (Q1/Q3) of DOX, DOXol and the internal standard were: DOX 3.05 min, 544/398; DOXol 3.00 min, 546/399; internal standard idarubicin 3.15 min, 498/130.

A standard curve of known DOX and DOXol samples (corrected for idarubicin internal standard) was created and used to calculate DOX and DOXol concentrations in conditioned media samples. To ensure the validity of the assay, DOX and DOXol QC samples (derived from separate drug stocks to DOX/DOXol standards) of known concentrations (15, 150 and 400 ng/mL) were ran simultaneously with experimental samples. Validity of the calculated concentrations from the assay was determined based on acceptance criteria for the clinical application of this method: for $\frac{3}{4}$ of the standards concentrations and $\frac{2}{3}$ of the QCs concentrations to lie between 75-125% of

expected values. Back-calculated concentrations of standards and QCs were within 69–124% of expected values for the run to be valid. Standard curves were linear between 0-500 ng/mL for DOX and DOXol with R^2 values > 0.99.

4.2.7 Culturing human cardiac fibroblasts in conditioned media

Human cardiac fibroblasts (C-12375) were seeded into T25 flasks (Corning) according to standard cell culture protocols (see **2.1.4**) at 5,000 cells/cm^2 and left to adhere overnight. DMEM/F-12 with 1% P/S and 10% FBS was used for culture. The next day, media was aspirated from cells, cells were washed with PBS, and conditioned media was applied from either senescent or non-senescent AC16 cell cultures. Media was changed every 3 days, until 10 days in culture was reached. At day 10, HCFs were trypsinised, pelleted and stored at -80 °C according to standard protocols (see **2.2.2**), for downstream RNA isolation

4.2.8 RNA isolation, quantification and quality assurance

RNA was isolated from HCF cell pellets using an RNeasy Micro Kit (Qiagen, see **2.2.3**). The quantity and quality of RNA was assessed (see **2.2.4**).

4.2.9 cDNA synthesis

cDNA was synthesised from HCF RNA according to standard methods (see **2.2.5**).

4.2.10 Quantitative real-time polymerase chain reaction (qPCR)

Primer pairs were custom-designed using the webtool Primer-BLAST or commercially sourced as pre-designed “KiCqStart” primers (Sigma Aldrich). Custom-designed primers were purchased from Sigma and Integrated DNA Technologies (IDT). RT-qPCR was carried out according to a standard workflow (see **2.2.7**). *ACTB* was used as an endogenous control.

Table 4.1 Details of primer pairs used in RT-qPCR studies. Primer sequences were designed using Primer-BLAST and commercially custom-manufactured.

Target gene transcript	Forward (5' → 3')	Reverse (5' → 3')	Manufacturer
Periostin (*POSTN*)	TCCCCGTGACTGT CTATAAGC	CCTTGGTGACCTCT TCTTGT	Sigma-Aldrich custom
Interleukin-8 (*IL8*)	CTCTTGGCAGCCT TCCTGATT	ACTCTCAATCACTCT CAGTTCT	IDT
ACTB	GACGACATGGAGA AAATCTG	ATGATCTGGGTCATC TTCTC	Sigma-Aldrich KiCqStart

4.2.11 Immunofluorescent probing & imaging of Ki67 in HCFs cultured in conditioned media

For immunofluorescent probing of proliferation marker Ki67, HCF cultures were fixed with warm 4% paraformaldehyde (PFA) in PBS for 20 minutes at room temperature, then PFA was gently aspirated, and cells were washed three times (5 mins each) with ice-cold PBS. Cells were then permeabilised using a ten-minute incubation with 0.1% Triton X-100 in PBS at room temperature. Permeabilisation agent was aspirated gently, then cells were washed with PBS as before. Blocking of non-specific antibody binding was via 1% bovine serum albumin (BSA) in 0.1% Tween-20 PBS (PBST) for 30 minutes at room temperature. Blocking solution was then removed and primary antibodies against Ki67 (Abcam ab15580, rabbit anti-human Ki67, 1:200 dilution) was added to cells. Cells were incubated with primary antibodies overnight at 4°C. Primary antibodies were then removed and cells were washed with PBS as before. Secondary fluorochrome conjugated IgG antibodies reactive to the primary antibody species were used to allow for detection (Invitrogen A21207, donkey anti-rabbit Alexa Fluor 594) Cells were incubated with secondary antibodies for one hour at room temperature in the dark, antibodies were then gently aspirated, cells were washed three times with PBS as before, and DAPI-containing mounting media applied (Invitrogen P36931). Samples were stored at 4°C. Images were acquired using a Zeiss AxioObserver Z1 instrument.

4.2.12 Quantification of Ki67-positive HCFs from immunostaining

20 images were taken per experiment using random fields of view. All nuclei in the field of view were quantified, then all Ki67-expressing nuclei in the field of view were quantified. For each field of view, the proportion of Ki67-positive cells was expressed as “Number of Ki67-positive nuclei”/”Number of DAPI-positive nuclei” * 100. The mean of 20 fields of view was calculated. Three independent experiments were conducted, and the mean average Ki67 expression was calculated from them. The data from senescent conditioned media-treated HCFs and non-senescent conditioned media-treated HCFs was compared using an unpaired student’s t test, where $p < 0.05$ was considered significant.

4.2.13 Cytokine array analysis of conditioned media

Conditioned media was collected from AC16 CMs (see **4.2.5**). Media was decanted into Eppendorf tubes after centrifugation and, to minimise the chance of secreted factors being below the lower limit of quantification for downstream applications, concentrated using Pierce Protein Concentrator spin columns (3K Molecular Weight Cut Off, Thermo Scientific 88525). 100 µL of concentrated conditioned media per experiments (n = 3 independent experiments) was then stored at -80°C until shipment to Eve Technologies (Calgary, Canada). Upon receipt, conditioned media was tested in technical duplicates for 71 different cytokines and chemokines in a multiplexed array format, using Eve Technologies’ 71-plex Human Cytokine 71-Plex Discovery Assay. A mean average observed concentration was calculated from 3 independent experiments per protein target.

4.2.14 Heatmap generation

The online webtool www.heatmappr.ca was used to generate a heatmap of the cytokine array results. The clustering method was average linkage, which was applied to both protein targets (rows) and conditioned media samples (columns). Distance measurement method was Euclidean. 50 colour shades were used to represent Z-scores between -2 (blue), 0 (white), and 2 (red).

4.2.15 Statistical analyses

To determine the significance of AC16 CM hypertrophy in **4.3.1**, a Brown-Forsythe and Welch’s ANOVA was used. Equal SD of data from each time point was not assumed and multiple comparisons were corrected for using the Dunnett’s T3 test. An unpaired

student’s t-test was used to determine the significance of differences in mitochondrial network analysis outputs in **4.3.2** and differences in Ki67 immunostaining in **4.3.3**. To analyse qPCR results in **4.3.3**, data were processed to the widely used ddCT form, whereupon they were statistically analysed using a paired t-test. As is common, data were graphed in the form 2^-ddCT format for easier visualisation and interpretation.

4.3 Results

4.3.1 Senescent AC16 cardiomyocytes show persistent hypertrophy during a 10-day recovery period from DOX exposure

Previously, a link has been established between senescence and hypertrophy.[298,299] To ascertain if DOX treatment and the induction of senescence in AC16 CMs was associated with hypertrophy, AC16 CMs were imaged at various timepoints across the 10-day recovery period following sublethal 500 nM, 3-hour DOX exposure (the previously established dosing regimen to induce senescence), and measured cell area. Compared to cells at the pre-DOX treatment timepoint Day 0, DOX-exposed cells at Days 1, 3, 7 and 10 showed a persistently larger mean area (**Figure 4.1A**), even in the absence of DOX stimulus. Furthermore, when compared to the final timepoint of VEH-exposed AC16 CMs before cultures became confluent, DOX-exposed AC16 CMs were significantly larger in size (**Figure 4.1B**).

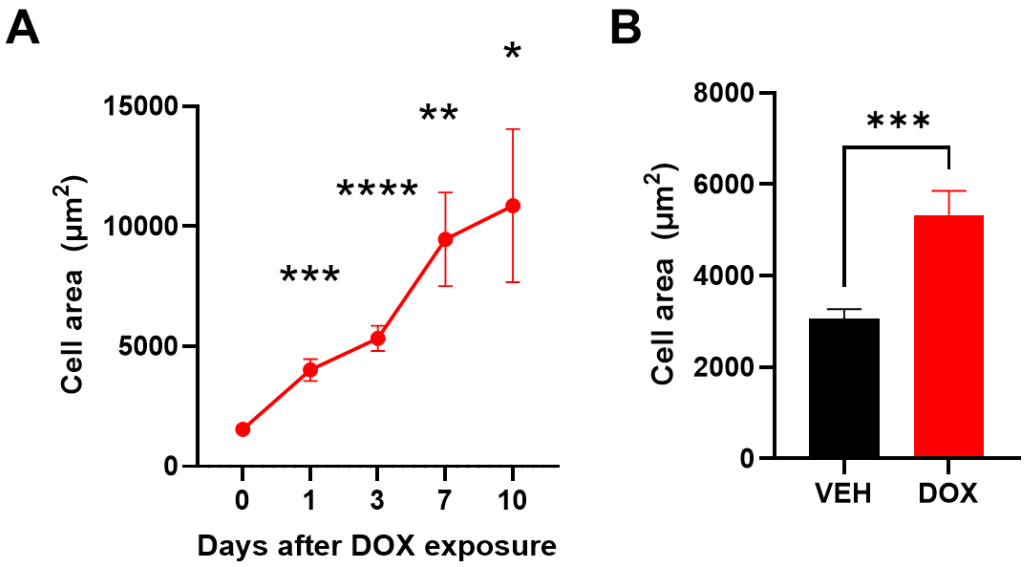

Figure 4.1 Senescent AC16 CMs show a persistent and time-dependent increase in size after DOX exposure. A) Cell area is significantly higher at each time point when compared to pre-treatment timepoint Day 0. Data are represented as mean +/- SEM, n = 20 cells. * $p \leq 0.05$, ** $p \leq 0.01$, *** $p \leq 0.001$ compared to Day 0, as determined by a Brown-Forsythe and Welch's ANOVA (equal SD of data from each time point not assumed and multiple comparisons corrected for using Dunnett's T3 test). **B)** At Day 3 post-VEH or DOX exposure, DOX-treated AC16 CMs are significantly larger than VEH-treated counterparts, as determined by an unpaired student's t test. *** $p \leq 0.001$.

4.3.2 Senescent AC16 cardiomyocytes display expansion of the mitochondrial network and quantitative changes in branch length

The mitochondrial network is a complex 3D structure which is affected by a number of dynamic processes such as mitochondrial biogenesis and the balance of fission/fusion, which are perturbed as a result of toxicity generally, and during ageing and cellular senescence.[300,301] Namely, senescent cells have been reported to have increased mitochondrial copy number & volume per cell (global mitochondrial mass), decreased mitochondrial fission, and impaired mitophagy.[287,302]

To assess whether senescence induction in AC16 CMs via DOX was associated with alterations in mitochondrial morphology (that might be indicative of changes in mitochondrial dynamics or function), the mitochondrial network of these cells was firstly immunostained and imaged. AC16 cells were induced to senescence with DOX as before, then using fluorescence immunocytochemistry, the mitochondrial network and mitochondrial DNA of cells was imaged using antibodies against ATP5B (a complex V protein) and TFAM (a mtDNA-specific transcription factor) following a recovery period. In both treatment conditions, the staining pattern of ATP5B revealed an interconnected tubular mitochondrial network with some small separate tubules also observed (**Figure 4.2**).

In non-senescent cells, broadly speaking, mtDNA staining co-localised with the mitochondrial network. In senescent cells, several differences are noted. Firstly, in agreement with the aforementioned hypertrophy data, senescent cells had a markedly larger cell and nuclear area. In addition, senescent AC16 CMs displayed differences in their mitochondrial architecture than controls. Senescent cells appeared to have much denser mitochondrial architecture than non-senescent counterparts, qualitatively. Thirdly, there are some instances of mtDNA not being co-localised to the mitochondrial network (white arrow), which may support the notion of mtDNA release into the cytoplasm in CMs after DOX exposure.[303]

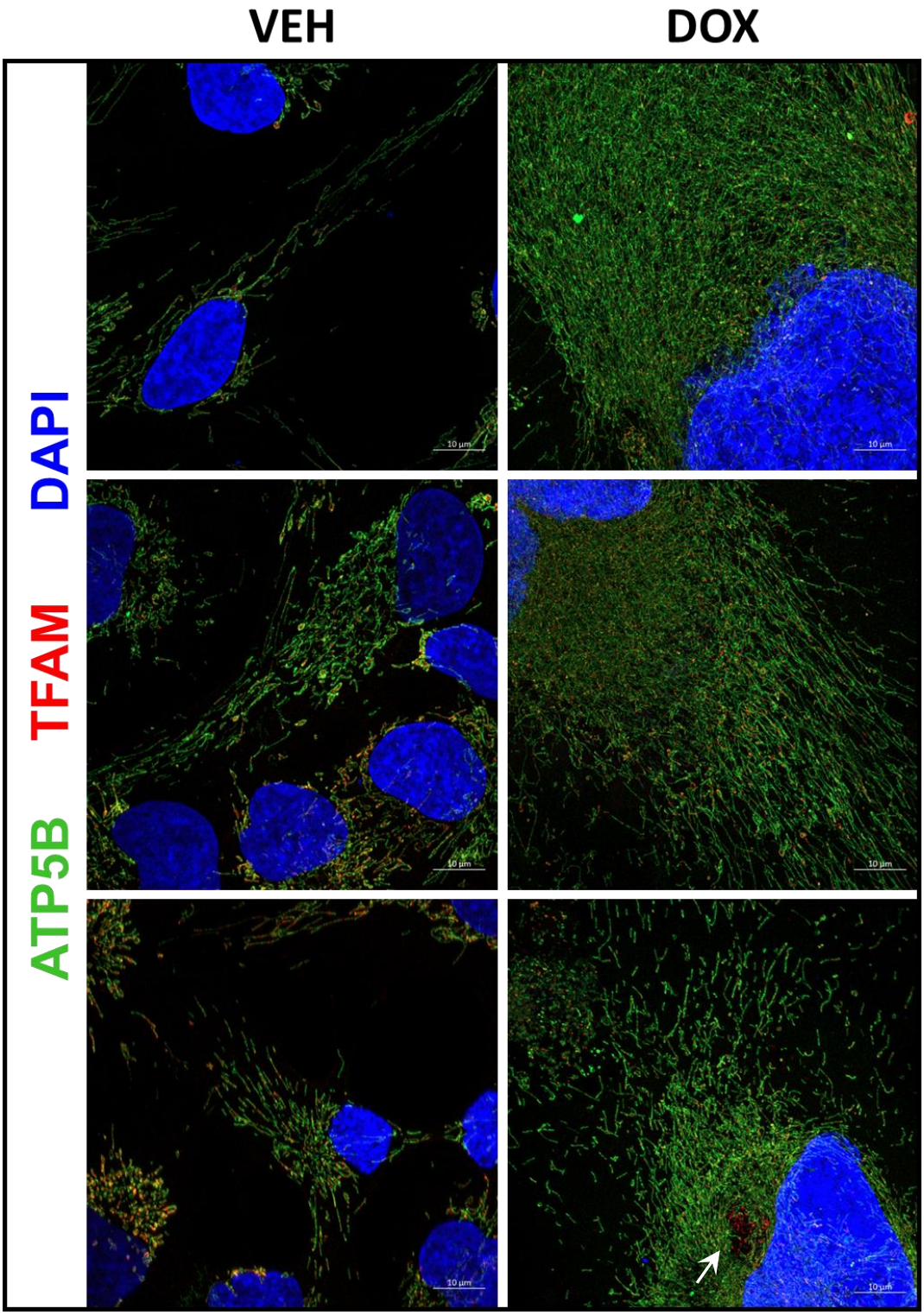

Figure 4.2 Imaging of the mitochondrial network and mitochondrial DNA within senescent vs non-senescent AC16 CMs (treated with DOX or VEH as previously described and analysed 10 days post-exposure). CMs were labelled with anti-ATP5B (a subunit of complex V) (green) and anti-TFAM (a mitochondrial DNA transcription factor) (red). Nuclei are labelled with DAPI (blue). Scale bar = 10 µm.

To more accurately explore the putative changes to mitochondrial network morphology in senescent AC16 CMs, the MiNA (Mitochondrial Network Analysis) workflow was applied to immunofluorescent images. MiNA analysis showed that the mitochondrial footprint of senescent AC16 CMs was significantly larger than non-senescent CMs (**Figure 4.3A**, 10118 +/- 2056 vs 439.9 +/- 147.1 μm^3 mean mitochondrial signal per cell +/- SEM). Furthermore, more toroidal mitochondria (coined "doughnuts")[304] were observed in senescent CMs relative to non-senescent CMs (**Figure 4.3B**, 6.444 +/- 1.469 vs 0.2222 +/- 0.1008 mean doughnuts per cell +/- SEM). However, given that senescent CMs are known to be larger in area than non-senescent CMs (and likely volume), it is important to normalise the number of doughnuts per cell to account for this confounding variable. When the number of doughnuts per cell was normalised to the appropriate cellular mitochondrial footprint volume, no significant difference was found between the frequency of doughnuts in senescent and non-senescent populations (**Figure 4.3C**, 0.0009282 +/- 0.0002530 vs 0.0007234 +/- 0.0003916 mean doughnuts/μm^3 mitochondrial volume +/- SEM). Interestingly, independent of cell volume of mitochondrial footprint, the mean length of a mitochondrial network branch was shorter in senescent CMs than non-senescent counterparts (**Figure 4.3D**, 1.418 +/- 0.05299 vs 1.780 +/- 0.04880 μm mean branch length +/- SEM).

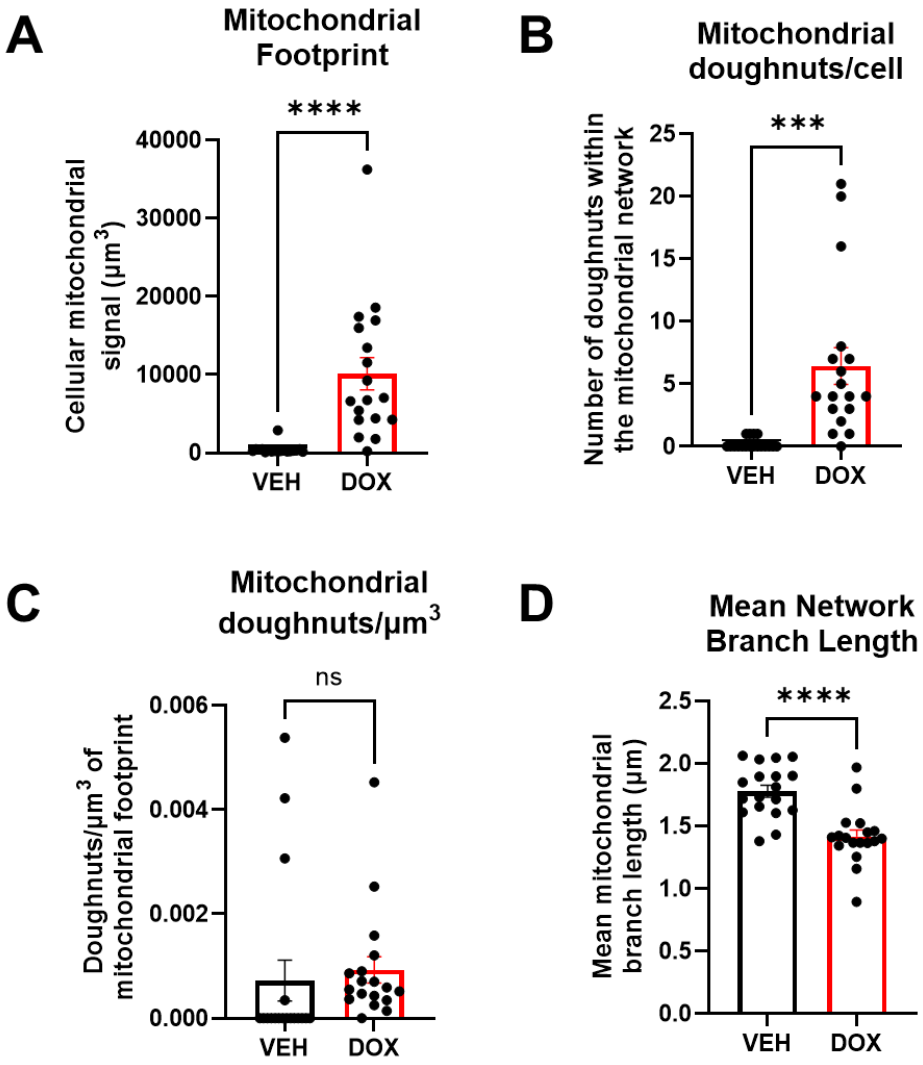

Figure 4.3 Quantitative analysis of mitochondrial network in senescent and non-senescent AC16 CMs (n = 18 cells per group), various output parameters from MiNA workflow A) Cellular mitochondrial footprint (μm^3) **B)** Mitochondrial doughnuts (toroidal mitochondria) per cell **C)** Number of doughnuts normalised to mitochondrial footprint volume of a cell **D)** Mean mitochondrial branch length. Data is represented as mean +/- SEM, n = 18 regions of interest (18 cells). *** $p \leq 0.001$ **** $p \leq 0.0001$ using student's unpaired t-test.

4.3.3 Conditioned media from senescent AC16 cardiomyocyte cultures is free from doxorubicin, yet induces phenotypic changes in primary human cardiac fibroblasts

A key part of the senescent cellular phenotype is the SASP, which typically comprises a cocktail of pro-inflammatory cytokines. The CM SASP has its own distinct molecular signature, the selected individual components of which (TGFβ, GDF15 and Endothelin 3) are demonstrably functional *in vitro*, as shown in previous studies outside the setting of DOX cardiotoxicity.[173] To ascertain whether DOX-induced senescent CMs also secrete a SASP, and explore whether the SASP is functional after DOX (or its metabolites) is removed from the environment, conditioned media taken from senescent AC16 CM cultures (exposed to DOX according to the established 10-day regimen) was applied to primary human cardiac fibroblasts, which were then cultured in this media for 10 days.

Firstly, it was verified that conditioned media was indeed free from DOX or DOXol (the main metabolite of DOX) using liquid chromatography mass spectrometry. Nominal DOX standards matched the calculated DOX concentration well (**Figure 4.4A**): a linear regression curve fitted the data with equation $y = 0.00608x + 0.00883$ (where y = analyte area/internal standard area and x = analyte concentration/internal standard concentration), and a goodness-of-fit R^2 value of 0.9922. All samples of conditioned media from senescent CMs contained 0 mg/mL DOX or a concentration below the lower limit of quantification (LLOQ, **Figure 4.4A**). In the case of DOXol, nominal standards also matched the calculated DOXol concentration well (**Figure 4.4B**): a linear regression curve fitted the data with equation $y = 0.0338x - 0.000813$, and a goodness-of-fit R^2 value of 0.9951. All samples of conditioned media were similarly free from DOXol, with concentrations measured as 0 mg/mL or below the LLOQ (**Figure 4.4B**).

To assess whether conditioned media was functional in a paracrine capacity, the expression of interleukin-8 (*IL8*) and periostin (*POSTN*) transcript in human cardiac fibroblasts was measured – these being two key markers of the activated myofibroblast phenotype, which is associated with inflammation and fibrosis. On day 10 of culture in conditioned media, human cardiac fibroblasts showed a large, significant increase trend in interleukin-8 transcript (**Figure 4.5A**) and a significant increase in periostin transcript (**Figure 4.5B**). To assess whether the proliferative capacity of these cells was impacted by the conditioned media, HCFs were immunofluorescently probed for

Ki67, a classical marker of cellular proliferation. Anti-Ki67 fluorescence signal was localised to the nucleus and stained in a characteristic punctate pattern (**Figure 4.5C**) There was no significant difference between the treatment groups (5.51 +/- 2.77 % vs 2.92 +/- 1.95% Ki67^{+ve} nuclei in DOX cmed vs VEH cmed) (**Figure 4.5D**).

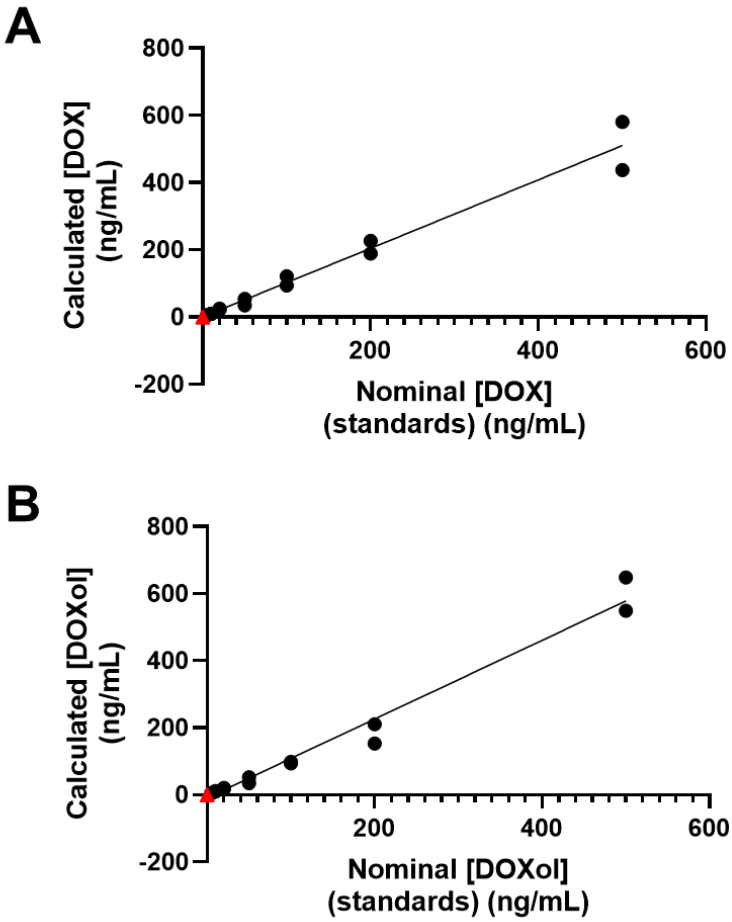

Figure 4.4 Liquid Chromatography Mass Spectrometry to quantify DOX and DOXol concentration. A) Nominal concentrations of DOX in standards match well to calculated DOX concentrations via LCMS (black dots). Five test samples of conditioned media contained 0 ng/mL of DOX or a concentration below the lower limit of quantification (red triangles). **B)** Nominal concentrations of DOXol in standards match well to calculated DOXol concentrations via LCMS (black dots). Five test samples of conditioned media contained 0 ng/mL of DOXol or a concentration below the lower limit of quantification (red triangles). Test samples of conditioned media (red triangles) represent n = 5 independent experiments. Nominal standard concentrations of DOX or DOXol represent n = 2 technical replicates.

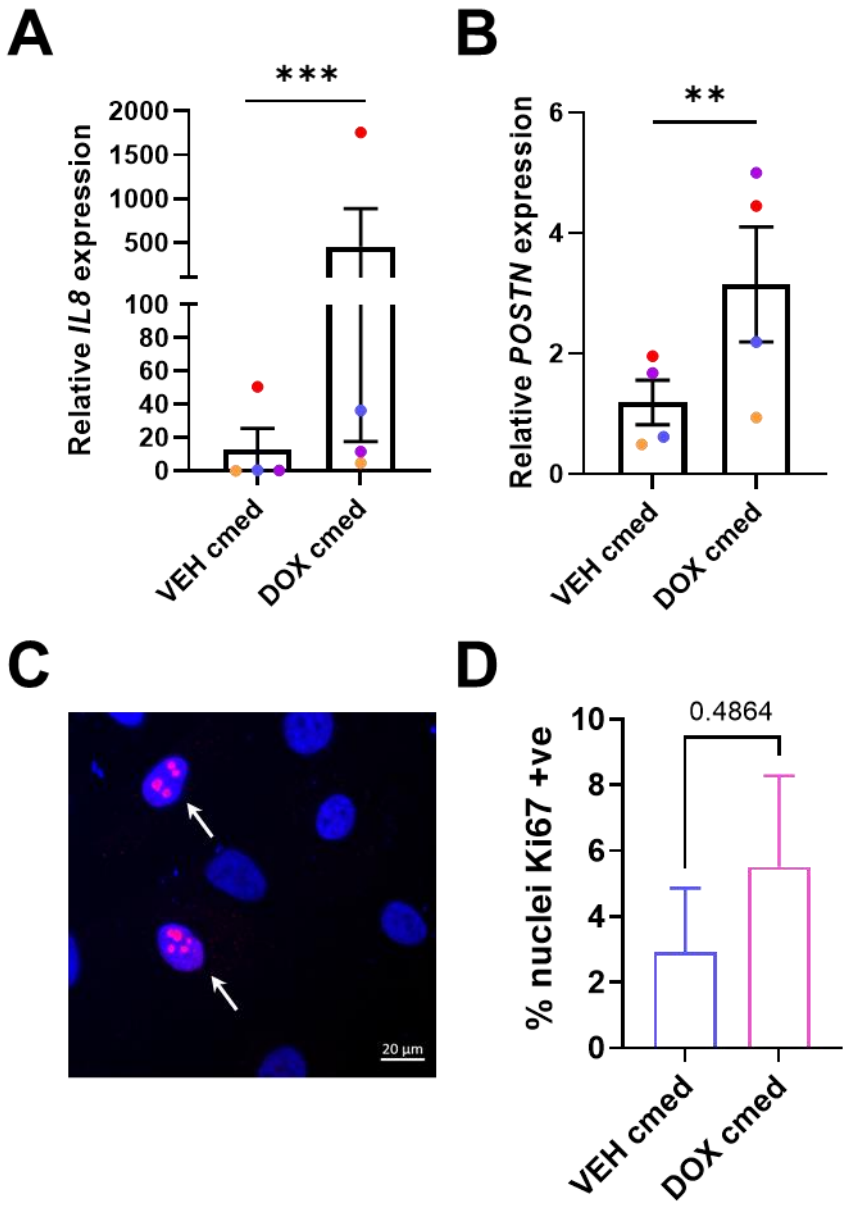

Figure 4.5 Compared to conditioned media from non-senescent AC16 CMs (VEH cmed), conditioned media from senescent AC16 CMs (DOX cmed) induces transcript-level changes in human cardiac fibroblasts (HCFs) but is not associated with an alteration in proliferation (as measured by Ki67 expression). A) qPCR analysis showed a significant increase in *IL8* gene transcript in HCFs cultured in DOX cmed compared to VEH cmed. **B)** qPCR analysis showed a significant increase in periostin transcript in HCFs cultured in DOX cmed compared to VEH cmed. **C)** Representative anti-Ki67 fluorescence signal (red), localised to the nucleus (DAPI, blue) in HCFs **D)** There was no significant difference in Ki67 expression in HCFs cultured in DOX cmed compared to VEH cmed, indicating no change in the proliferation of cells. qPCR data in **A-B)** represents n = 4 independent experiments +/- SEM, where *ACTB* was used as an endogenous control. Immunofluorescence Ki67 data in **C)** represents n = 3 independent experiments +/- SEM.

4.3.4 Conditioned media from senescent AC16 cardiomyocytes contains various pro-inflammatory cytokines

To identify which proteins in the conditioned media of senescent AC16 CMs may contribute to the induction of a pro-myofibroblast phenotype in human cardiac fibroblasts, conditioned media was analysed using a commercially available 71-plex cytokine array. 35 of the 71 cytokines in the array were detectable in media from either senescent or non-senescent AC16 CMs. It should be noted that to enable robust detection of cytokines in conditioned media, conditioned media was concentrated (see **4.2.13**). Therefore, cytokine concentrations are proportionally larger than the concentration that would be found in the original unconcentrated conditioned media – the raw pg/mL values of cytokines are not representative. Though there was variability seen between three independent experiments in a treatment group, overall, there was an increased cytokine expression profiles in DOX-treated AC16s, notably containing higher levels of factors such as VEGF, IL-6, IL-8, FGF-2, MCSF and MCP-1 (**Table 4.2**). Using a heatmap to visualise and cluster the cytokines and samples, it was observed that conditioned media samples from VEH-treated, non-senescent AC16s markedly clustered together, as did the conditioned media samples from DOX-treated, senescent AC16s (**Figure 4.6**). Some clustering of cytokines could be seen but this was less pronounced. For instance, the concentrations of M-CSF and MCP-1 across samples were distinct between treatment groups in a similar way, so clustered together.

At first glance, many proteins showed higher concentrations in conditioned media from senescent AC16s than that from non-senescent AC16 CMs (see **Appendix A**, **Figure S1A**), but when data was taken together and analysed with corrections for multiple comparisons, the only cytokines which were statistically significantly different between treatment groups were IL-17F, MCP-1, M-CSF and TNFα (**Figure 4.7**) – all were significantly higher in conditioned media from senescent AC16 CM culture.

Table 4.2 Concentrations of 35 cytokines detected in conditioned media from senescent ("DOX") or non-senescent ("VEH") AC16 CM cultures. A 71-plex cytokine array was used to detect targets. N = 3 independent experiments. Cytokines highlighted in blue have statistically significant differences in concentrations between treatment groups (**Fig 4.7**).

Cytokine name	Non-senescent conditioned media ("VEH") mean observed conc. +/- SD (pg/mL)	Senescent conditioned media ("DOX") mean observed conc. +/- SD (pg/mL)
EGF	0.47 +/- 0.81	0.36 +/- 0.63
Eotaxin	2.38 +/- 0.63	0.76 +/- 0.43
FGF-2	7.2 +/- 3.25	41.29 +/- 21.02
FLT-3L	0.09 +/- 0.03	0.43 +/- 0.18
Fractalkine	0.0 +/- 0.0	2.72 +/- 2.7
GROα	0.15 +/- 0.26	2.13 +/- 2.11
IL-1α	0.27 +/- 0.2	1.33 +/- 0.48
IL-1β	0.0 +/- 0.0	0.12 +/- 0.21
IL-1RA	0.06 +/- 0.1	0.07 +/- 0.06
IL-4	0.0 +/- 0.0	0.09 +/- 0.07
IL-6	0.0 +/- 0.0	22.46 +/- 12.42
IL-7	1.17 +/- 0.07	0.75 +/- 0.11
IL-8	0.18 +/- 0.11	31.02 +/- 25.53
IL-10	0.0 +/- 0.0	0.0 +/- 0.01
IL-12p40	0.0 +/- 0.0	0.04 +/- 0.07
IL-13	0.0 +/- 0.0	0.84 +/- 0.73
IL-15	0.0 +/- 0.0	0.65 +/- 0.31
IL-17F	0.0 +/- 0.0	0.14 +/- 0.03
IL-18	0.12 +/- 0.07	0.0 +/- 0.0
MCP-1	1.98 +/- 0.7	469.93 +/- 83.91
MCP-3	0.0 +/- 0.0	7.16 +/- 6.73
M-CSF	6.18 +/- 2.08	105.35 +/- 19.31
MDC	0.01 +/- 0.01	0.0 +/- 0.01
PDGF-AA	0.0 +/- 0.0	7.75 +/- 4.73
RANTES	0.0 +/- 0.0	4.92 +/- 3.14
TNFα	0.06 +/- 0.1	0.61 +/- 0.06
TNFβ	0.0 +/- 0.0	0.08 +/- 0.14
VEGF-A	0.0 +/- 0.0	28.11 +/- 19.02
ENA-78	0.0 +/- 0.0	1.36 +/- 2.36
Eotaxin 2	0.35 +/- 0.13	0.41 +/- 0.19
I-309	0.09 +/- 0.01	0.1 +/- 0.01
IL-20	0.32 +/- 0.55	1.63 +/- 2.83
IL-23	1.74 +/- 3.01	0.0 +/- 0.0
SDF-1α&β	26.07 +/- 8.46	47.76 +/- 14.28
TRAIL	0.21 +/- 0.05	0.14 +/- 0.02

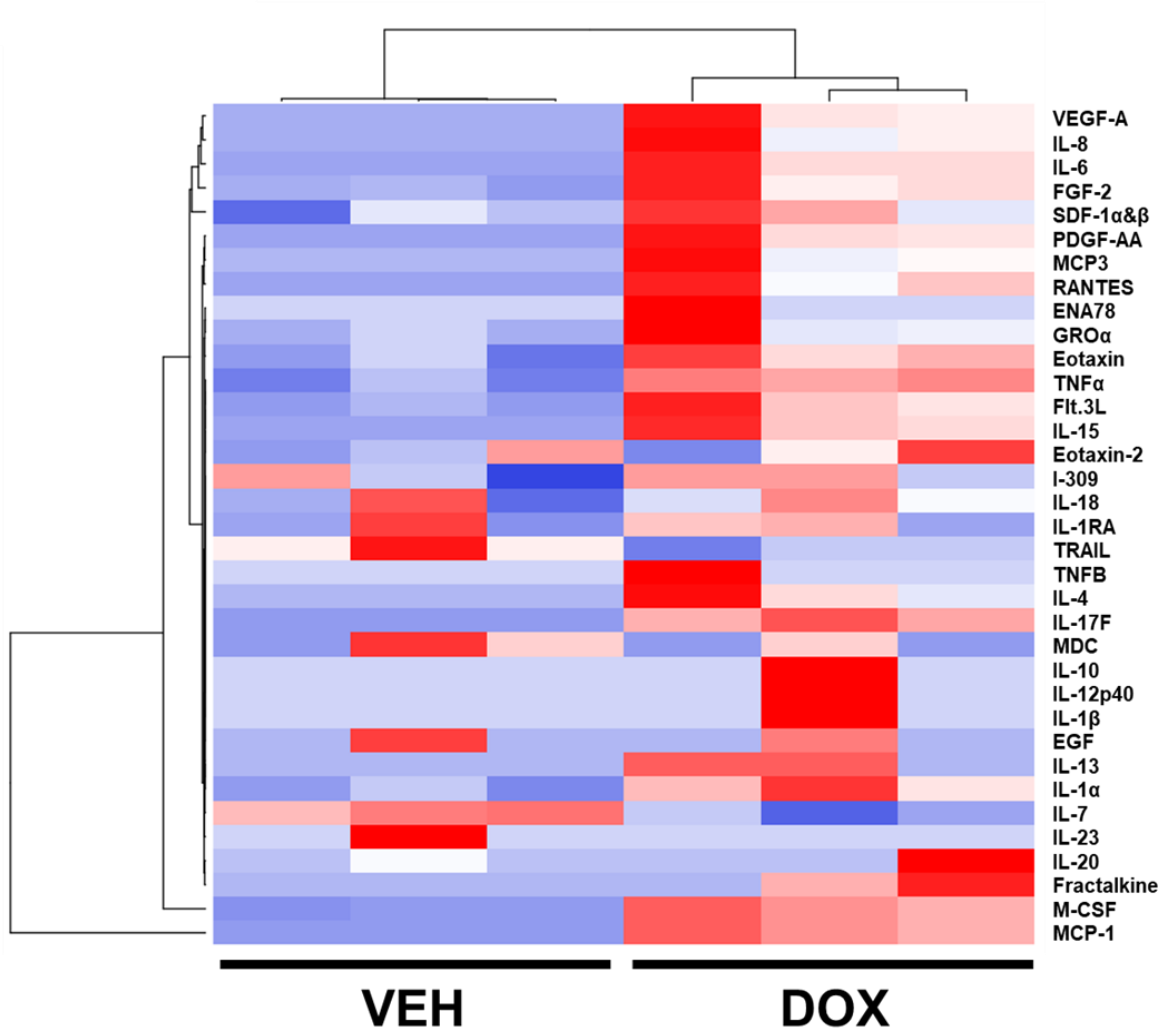

Figure 4.6 Cytokine array results expressed in heatmap form, summarising detected cytokines in the conditioned media from senescent AC16 CMs. 35 cytokines were detected in conditioned media using a cytokine array. Factors such as VEGF-A, IL-8 and IL-6 show the trend of being more highly expressed in senescent AC16 CM conditioned media vs non-senescent AC16 CM conditioned media. Blue represents a lower concentration of cytokine, red represents a higher concentration of cytokine. Data are represented as n = 3 independent experiments per treatment group, with concentrations being z-score normalised to allow for like-for-like comparisons between cytokines.

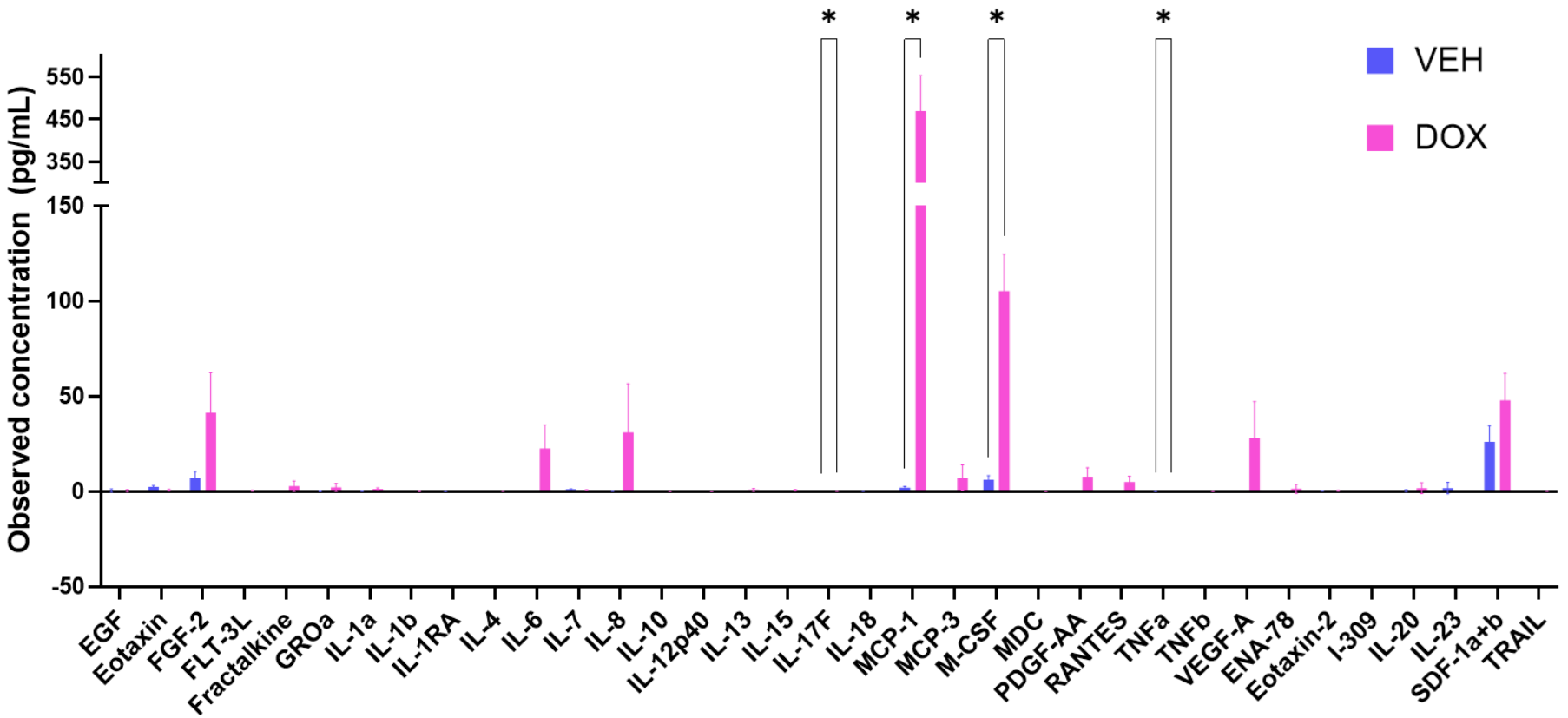

Figure 4.7 Cytokine array results from conditioned media of senescent vs non-senescent AC16 CMs. Concentrations of 35 detected cytokines within conditioned media from non-senescent AC16 CM cultures ("VEH cmed", purple) compared to those from senescent AC16 CM cultures ("DOX cmed", pink). Data is represented as mean observed concentration (pg/mL) +/- SD, n = 3 independent experiments. * $p < 0.05$ from multiple unpaired student's t tests, multiple comparisons corrected for by Holm-Šídák method

4.3 Discussion

4.3.1 Senescent AC16 cardiomyocytes are hypertrophic, and show a markedly increased mitochondrial footprint

The first finding was that senescent AC16 CMs had a persistently larger cell area across the 10-day recovery period from DOX exposure. CM hypertrophy can occur in physiology but is notably a hallmark of cellular stress in a spectrum of cardiovascular pathologies, from *in vitro* models through to cardiovascular tissue from patients with HFpEF.[305] This morphology has also been observed in CMs exposed to low-dose DOX *in vitro*.[306]

Several candidates have been reported as modulators of CM hypertrophy, including the Epac1 protein (a member of the "exchange protein directly activated by cAMP" protein family), the NAD^+-dependent deacetylase Sirtuin 1, and the AE3 Cl^-/HCO_3^- ion exchange protein.[307-310] However, the causal role of CM hypertrophy in disease is complex – the hypertrophy of neighbouring cells following loss of CMs in acute disease is necessary for proper integrity and function of the cardiac tissue. The way in which cardiac tissue consequently remodels in three dimensions is multifactorial and involves several cell types (e.g. cardiac fibroblasts which establish interstitial fibrosis). Therefore, when considering the results here from a basic monolayer culture, it may be more productive to consider why AC16 CMs acquire a hypertrophic morphology after DOX exposure, rather than the consequences of this phenotype downstream in the timeline of pathology.

Qualitative immunofluorescent (IF) data supported the notion that senescent CMs are more mitochondria-rich than non-senescent CMs. A general caveat of the approach used here is that ATP5B was used as a marker of the mitochondrial network, but to be precise, ATP5B is a complex V marker which may be upregulated irrespective of mitochondrial organelle content. Other common mitochondrial markers used in the context of IF are voltage-dependent anion channel (VDAC), COX IV and commercially available MitoTracker probes. This may become imbalanced upon acquisition of the senescent phenotype – a widely-acknowledged hallmark of which is disrupted metabolism, often accompanied by an increase in mitochondrial content.[311]

4.3.2 Mitochondrial network morphology of senescent AC16 cardiomyocytes, and considerations of functionality

Mitochondrial network morphology can change in disease states, which has recently been reviewed.[312] Upon quantifying the morphology of the mitochondrial network of senescent AC16s, it was found here that the mitochondrial footprint per cell was higher in senescent cells, which is in agreement with published literature by Passos and colleagues.[302]

The number of mitochondrial doughnuts, that is, toroidal mitochondria, was also higher per cell. Mitochondrial doughnuts are thought to be an early indicator of cellular stress, and studies have shown that the formation of these structures is associated with increased mitochondrial ROS levels (which was not assessed here but would certainly merit future studies, using complementary techniques like MitoSOX immunofluorescent probes).[313] The reversible formation of mitochondrial doughnuts may allow a cell to adaptively increase mitochondrial surface area for organelle contacts or resist mitophagy.[314,315] Importantly, according to modelling, doughnut-shaped mitochondria have been reported to represent a conformation with a lower-energy state than a tubular conformation in terms of Gibbs free energy – i.e. this conformation of system is generally more energetically favourable and can perform more work.[316] It should be noted that imaging mitochondrial doughnuts is challenging, and the fluorescence techniques used here in best efforts may mistakenly identify other shapes of mitochondria as doughnuts – therefore these results should be interpreted with caution.[317]

However, when it is considered, on reflection, that senescent AC16 CMs are larger than non-senescent counterparts, it cannot definitively be stated that senescent AC16 cells have a denser mitochondrial network *per se* (this would require a measurement of cell volume), nor that they have more doughnuts (this may be increased solely due to larger cell size and the accompanying, perhaps proportional, larger mitochondrial footprint). To account for this, the number of doughnuts in each cell was normalised to each cell's mitochondrial footprint and compared this output in each treatment group. This more conservative analysis revealed that there was no significant difference in the incidence of mitochondrial doughnuts between treatment groups, suggesting that there may be equal changes, e.g. adaptation to stress, resistance to mitophagy, between groups. However, independent of mitochondrial network footprint, network branch length was still significantly shorter in senescent AC16 CMs, suggestive of a

change to the architecture of the mitochondrial network. Decreased branch length may indicate increased fission rates, but further studies would certainly be merited to investigate this – evaluating the expression of Drp1 protein (required for mitochondrial fission)[318] via Western blot, would be a sensible starting point. On the other hand, studies have pointed to DOX directly integrating with mtDNA to induce interlinking of mitochondria, an effect which was shown to be dependent on MFN1 and OPA1 pro-fusion proteins - this may also warrant investigation.[319]

Lastly, it is important to consider how acquisition of a hypertrophic phenotype and accompanying (perhaps proportional) expansion of the mitochondrial network may affect energetic output of a cell. Mature CMs characteristically generate the majority of their required ATP via mitochondrial oxidation of free fatty acids, rather than glycolysis.[320] This shift is accompanied by a consequent increase in free fatty acid content, and decrease in ATP level.[308] Studies have shown that fatty acids are not the major energy substrate for pathologically hypertrophic CMs, whereas they remain to be so in physiologically hypertrophic CMs. In senescent vs non-senescent CMs, evaluating any shifts from oxidative phosphorylation to glycolysis, changes in free fatty acids, and assessing the balance of anabolic and catabolic cellular processes, would be of interest in future studies.

Future work to elucidate the functional, metabolic performance of senescent CMs would also be warranted, for instance via Seahorse Metabolism assays or evaluating ATP production in culture – it may be that mitochondria are not functioning as efficiently as a result of senescence induction. On the other hand, impaired mitophagy may contribute to an accumulation of (perhaps poor-quality) mitochondria observed here, which has also been implicated in the senescent phenotype[321] – though studies so far have largely focused on non-CMs. In future work, measuring these parameters in a dynamic, real-time manner will be crucial, to accurately inform on the characteristics of the mitochondrial network morphology and functionality of live cells – this is a central strength of e.g. the seahorse Metabolism assay and common ATP assays, but imaging the mitochondrial network in real-time is still a developing and technically challenging methodology, falling outside of the capacity of this project.[322,323]

Qualitative IF imaging captured a notable instance of a lack of co-localisation between the mitochondrial network and mtDNA. Though purely inferential at this stage, mtDNA release into the cytoplasm is noted as a marker of cellular senescence which activates the cGAS-STING pathway, contributing to sterile inflammation and propagation of the

senescent phenotype in disease.[303] To test for the presence of mitochondrially encoded transcripts (such as *MT-ND1* and *MT-ND5*), subcellular fractionation of senescent and non-senescent CMs (similarly induced via DOX exposure) could be undertaken to isolate cytoplasmic, mitochondrial and nuclear compartments of the cell lysate, which could be analysed via qPCR.

4.3.3 The composition of senescent AC16 cardiomyocyte SASP

Conditioned media collected from senescent AC16 CM cultures contained several cytokines of note, including VEGF, IL-6, IL-8, FGF-2, MCSF and MCP-1. Substantial variability was seen across the three independent experiments per treatment group, which may have arisen due to stress/variation either in the AC16 recovery period prior to conditioned media collection, or indeed in the 10-day period of HCF exposure to conditioned media.

MCP-1 (also known as CCL2) and M-CSF are classically responsible for recruiting immune cells to sites of injury in an inflammatory response, and stimulating monocyte differentiation into macrophages, respectively. Both showed a particularly large increase in conditioned media collected from senescent AC16 CMs, compared to non-senescent controls. In the context of heart failure, *in vitro* studies have shown how oxidised low-density lipoprotein can induce the genetic expression of MCP-1 in HL-1 CMs.[324] MCP-1 also has demonstrated pro-inflammatory SASP activity in mesenchymal stromal cells (MSCs): when recombinant MCP-1 was applied to MSCs, senescence was induced, with p53 and p21 protein expression increasing via ROS.[325] M-CSF has been named as a SASP factor generally, but interestingly, the upregulation of M-CSF in the Nrf2 axis was shown to promote cancer cell senescence and consequent resistance to DOX chemotherapy – tallying with propositions by Demaria and colleagues than not only does senescence and the SASP promote delayed-onset cardiotoxicity of DOX, but also that they contribute to cancer relapse.[179,326]

Other factors which showed an increased, non-significant trend in senescent AC16 CM conditioned media included IL-6, IL-8, VEGF-A and FGF-2. IL-6 and IL-8 in particular are often named as major components of the SASP, but when Anderson and colleagues tested for the expression of these components and others commonly associated with the SASP in a purified CM population, there were very few changes between young, non-senescent cells and old, senescent cells – the SASP from this purified CM population was deemed novel and “non-canonical”, and authors suggested

that traditional SASP factors from past studies may derive from non-CM populations.[173] Therefore, the presence of these same canonical SASP factors in the results here may speak to the fibroblast contribution to the phenotype of AC16 cells. To strengthen this work in the future, using iPSC-CM cells (or, though technically challenging, isolated human CMs) and a more unbiased methodology such as bulk proteomics, would be of use.

4.3.4 The ability of the SASP to enact changes in neighbouring cell types

It is established that the SASP is able to enact inflammatory, paracrine responses and the senescent phenotype to non-senescent cells in the environment.[327] To test whether senescence induction in CMs might promote changes in non-myocyte cell types which could accelerate tissue remodelling and disease in AIC, HCFs were exposed to conditioned media from senescent AC16 CM cultures. HCFs showed large increases in interleukin-8 and periostin transcripts, key markers of the activated myofibroblast phenotype which promotes ECM modulation, collagen deposition and fibrosis.[328,329] The expression of Ki67 was no different between treatment groups, suggesting no association with exit from the cell cycle or senescence induction, though further validation of this using previously detailed markers p16, p21 and SA-β-Gal would be required to bolster this conclusion.

Following injury, inflammation induction and inflammation resolution, a pro-fibrotic response is warranted in the acute phase of injury response: a well-studied example of this is the healing process after myocardial infarction (MI). Following MI, the tissue repair phase of the healing response facilitates scar formation, then maturation, to preserve the structural integrity of the ischaemic tissue under strain.[330] A parallel could be drawn here with AIC, where it is thought that cytotoxicity of chemotherapy results in the acute loss of CMs, then accumulation of fibrotic tissue to fill the vacuoles left behind. With both these contexts however, the timely resolution of these physiologically phasic responses is crucial. At autopsy or transplant, marked global interstitial fibrosis is noted in the myocardium of paediatric AIC patients,[51,331] which likely contributes to a stiffness in the tissue and may lead to HFrEF. Extended inflammation or fibrotic responses can lead to pathology – if either of these two processes are inappropriately stimulated long-term by the presence of highly secretory senescent CMs, maladaptive tissue remodelling, and fibrosis may be promoted in AIC.

4.3.5 Conclusions

Overall, these results show that compared to non-senescent controls, AC16 CMs induced to senescence by DOX exposure are hypertrophic, have an apparently larger mitochondrial footprint, and a mitochondrial network with shorter branch lengths on average. Also, senescent AC16 CMs release cytokines which are classically attributed to a canonical SASP, which can induce transcriptional changes in naïve HCFs.

Chapter 5. Exploring the Transcriptome of Induced Pluripotent Stem Cell-Derived Cardiomyocytes Induced to Senescence by Doxorubicin

5.1 Introduction

5.1.1 In vitro cardiomyocyte models for cellular senescence and anthracycline-induced cardiotoxicity

True mature human CMs are post-mitotic in nature and show little proliferation.[48] Exactly how human CMs decrease their proliferation to this level in the postnatal period remains poorly understood, but the downregulation of key cell-cycle promoting cyclins has been implicated.[332] Murine models suggest that cyclins D1, E, A and B1 are downregulated in late embryonic and postnatal stages, alongside cyclin-dependent kinases (CDKs) 4, 2 and 1 - synchronously, the formation and activity of cyclin-CDK complexes also appears to be downregulated.[333] In this study, authors noted that from the P5 murine developmental stage onwards, CDK activities were also likely inhibited by other factors, in addition to downregulated endogenous expression. Studies suggest that mature CMs exhibit little telomerase expression, which may also contribute to cell cycle exit.[334] As a result of these changes and others, maturing CMs are thought to arrest at G1/S transition.[335] Recent studies show that mature murine CMs undergo senescence via irreversible telomere damage, which is independent of telomere length or telomerase activity.[173]

Historically, most studies investigating senescence and AIC have used the proliferative, immortalised cell lines H9c2, HL-1, and the AC cell lines. The proliferative nature of these cell lines contrasts with that of true CMs but makes them useful for pilot senescence studies due to their ease of culturing, and the fact that senescence can be identified by lack of proliferation. However, the effect of immortalisation upon the cell cycle when senescence is induced is debated. It is not clear whether, for instance 1) SV40 immortalisation promotes telomere maintenance and thus grants extended proliferative capacity to cells, free from replicative senescence, or 2) telomeres are eroded as replication occurs, which is sensed by the cell, but replicative senescence is not activated as normal. Some studies show that SV40 immortalisation resulting in overexpression of large T antigen (used in the AC and HL-1 cell lines) associates with aberrant universal upregulation of p16, while the p21 pathway is not perturbed, remaining tightly regulated and responsive to senescence-inducing stress.[336]

Modelling the interplay of senescence induction and the post-mitotic phenotype in immortalised, proliferative cell models is therefore complex and not fully characterised.

More recently, induced pluripotent stem cells (iPSCs) have become available to researchers as a source of many cell types – this has been particularly useful in the context of CM culture, where the postmitotic nature of these cells has made isolation/maintenance of meaningful numbers of CMs from tissue technically challenging. Now, validated iPSC-derived CMs (iPSC-CMs) can be purchased commercially, and protocols have also been published to differentiate CMs from iPSCs in-house.[337] These concepts have been leveraged to create patient-derived cell models in several disease contexts. In the field of AIC, patient-derived iPSC-CMs were elegantly used to show that these models can recapitulate the disposition of a patient to develop AIC clinically, therefore implicating a genetic basis for the toxicity.[338] From a more basic standpoint, robust iPSC-CM models generally display a non-proliferative phenotype, true to that of *bona fide* post-mitotic human CMs – this is a clear strength when modelling the particular senescent phenotype of CMs. Therefore, iPSC-CMs offer an exciting opportunity to explore patient-specific vulnerabilities to cardiotoxicity (e.g. pharmacogenomics). Although sophisticated 3D microtissues incorporating iPSC-CMs with other cell types show interesting data about myocardial contractility and targeting senescence in AIC within a complex multicellular system,[182] the drawback of these models is the difficulty in attributing dysfunction or pathology to the senescent phenotype of an individual cell type. Therefore, using purely iPSC-CMs in a monoculture can improve understanding about the interplay of CM senescence and AIC.

5.1.2 The transcriptomic profile of senescent cells

As previously introduced, the senescent phenotype is heterogeneous according to cell type, stimulus, and other factors. On a more technical note, attempts to characterise the senescent phenotype of CMs may also be hindered by imperfect isolation from tissue: it has historically been common for contaminating fibroblast populations to overgrow CMs in *ex vivo* culture.[339] Novel protocols to try and address this have been published even in recent years.[340,341] This has impacts on mechanistic studies: CMs were recently found to display a “non-canonical SASP”, which contrasted with previous studies.[173] Authors suggested that this discrepancy could be due to a previously imperfect CM isolation, which was contaminated with non-myocyte cell types. Recent landmark studies have produced unifying gene panels which aim to characterise

senescent cells via their transcriptome, regardless of species (human vs mouse), senescence-inducing stimuli or cell type.[156] But in light of the acknowledged heterogeneity of the senescent phenotype, it would be more useful specifically to understand the specific transcriptomic signature of CMs induced to senescence by DOX *per se*, guided by these unifying studies in the literature.

5.1.3 Aims and objectives

To build on findings from previous studies, here the aim was to validate results from the AC16 cell model, which showed that DOX exposure leads to the induction of senescence, in a more sophisticated iPSC-CM cell model. The induction of senescence markers p16 and p21 was re-assessed in DOX-exposed iPSC-CMs, along with other senescence-associated transcripts. Having confirmed their expression, the transcriptomic signature of iPSC-CMs exposed to sublethal DOX was then explored, to elucidate the molecular mechanisms of the CM senescent phenotype and discuss how this may drive the pathology of AIC.

5.2 Materials and Methods

5.2.1 iPSC-CM thawing and culture

iPSC-CMs (iCell Cardiomyocytes^2) were purchased as a kit from Fujifilm Diosynth (donor ID 01434 (female, apparently healthy normal), cat. no. R1059) and stored immediately in liquid nitrogen. Relevant culture media from the kit was stored immediately at -20 °C until required (iCell Cardiomyocyte Plating Medium and Maintenance Medium, Fujifilm Diosynth). The day before thawing cells, plating media was placed at 4 °C overnight to thaw. The next day, plating media was equilibrated to room temperature. Cell culture vessels were then prepared by coating with 5 µg/mL fibronectin solution (in sterile water) and storing at 37 °C for up to 1-4 hours, until cells were ready to be thawed.

iPSC-CMs were removed from liquid nitrogen and placed onto dry ice during transport. Then, the vial was thawed in a 37 °C water bath for 2 minutes. The cryovial was cleaned with 70% ethanol and now working in a sterile environment, the contents gently transferred to a 50 mL centrifuge tube (Falcon). The vial was rinsed with 650 µL plating medium, and this was transferred dropwise to the 50 mL centrifuge tube over 90 seconds, whilst gently swirling. 1 mL of plating medium was the added to the 50 mL centrifuge tube dropwise over 40-60 seconds, whilst swirling gently. The solution was gently pipetted twice to ensure maximum viability, and cell suspension volume was noted for later. To evaluate viability of cells post-thaw, 5 µL of cell suspension was decanted from the 50 mL suspension tube and 45 µL of plating media was added dropwise. 50 µL of 0.4% Trypan Blue solution (Gibco 15250-061) was added to this suspension and mixed gently by pipetting. This mixture was added to a haemocytometer and cell viability was calculated as a percentage (see **2.1.4** and **2.1.5**). The individual lot certificate of analysis (CoA) for iPSC-CMs was checked and the number of live cells post-thaw calculated using viability percentage * CoA cell number. Cell suspension was diluted accordingly to adjust plating density to 156,000 cells/cm^2 (manufacturer recommendation to form a functional syncytium). Fibronectin solution was gently aspirated from plasticware, and cell suspension dispensed into vessels. iPSC-CMs were cultured at 37 °C/5% CO_2 for 4-24 hrs.

The next day, Maintenance Media was equilibrated to 37 °C. Plating media was very gently aspirated from iPSC-CM cultures (with great care taken not to disturb the sensitive CM monolayer) and replaced with maintenance media. Maintenance media

was replaced gently every other day going forward, and iPSCs were cultured at 37 °C/5% CO_2. Provided good contractility and morphology was observed, at day 4 post-thaw, iPSC-CMs were deemed ready for assays (manufacturer recommendation).

5.2.2 10-day dose-recovery doxorubicin exposure regimen for iPSC-CMs

iPSC-CMs were exposed to DOX similar to AC16 cells (see **2.1.6**). On day 4 post-thaw, iPSC-CMs were exposed to 500 nM DOX or equivalent concentration of DMSO vehicle control (diluted in iPSC-CM Maintenance Medium) for 3 hours only, followed by a 10-day recovery period.

5.2.3 iPSC-CM immunofluorescent staining

For all immunofluorescent staining endpoints, iPSC-CMs were cultured in chambered polymer cover slips suitable for inverted microscopy imaging (ibidi 80806).

iPSC-CMs were fixed in culture by gently aspirating Maintenance Media and adding warm 4% PFA in PBS for 20 minutes at room temperature. PFA was then gently aspirated, and cells were washed three times with ice-cold PBS (five-minute wash time). Cells were then permeabilised using a ten-minute incubation with 0.1% Triton X-100 in PBS at room temperature. Permeabilisation agent was aspirated gently, then cells were washed with PBS as before. Blocking of non-specific antibody binding was via 1% BSA in 0.1% PBST for 30 minutes at room temperature.

Blocking solution was then removed and cells were incubated with primary antibodies in the following “triple-stain” combinations. In the first case (n = 1): α-actinin (Abcam ab50599, rat anti-human α-actinin 1:200), p16 (Roche Ventana 805-4713, mouse anti-human p16, 1:1 dilution) p21 (Abcam ab7960, rabbit anti-human p21, 1:200). In the second case (n = 4): Troponin-C (Abcam ab30807, goat anti-human cardiac Troponin-C, 1:200), 2. p16 (Roche, as before) and 3. p21 (Abcam, as before).

iPSC-CMs were incubated with primary antibodies overnight at 4 °C. The next day, primary antibodies were aspirated, and cells washed three times with PBS as before. Secondary fluorochrome conjugated IgG antibodies reactive to the primary antibody species were used to allow for detection in the following “triple-stain” combinations. In the first case: For α-actinin, Invitrogen A21247 goat anti-rat Alexa Fluor 647 1:1000; For p16, Invitrogen A21202 donkey anti-mouse Alexa Fluor 488, 1:1000; For p21, Invitrogen A21207 donkey anti-rabbit Alexa Fluor 594, 1:1000. In the second case: For Troponin-C, Invitrogen A11055, donkey anti-goat Alexa Fluor 488, 1:1000; For p16,

Invitrogen A21203, donkey anti-mouse Alexa Fluor 594, 1:1000; For p21, Invitrogen A21443, chicken anti-rabbit Alexa Fluor 647, 1:1000.

Cells were incubated with secondary antibodies for one hour at room temperature in the dark, antibodies were then gently aspirated, cells were washed three times with PBS as before, and DAPI-containing mounting media was applied (Invitrogen P36931). Samples were stored at 4°C. To capture cTnC striations, Nikon A1R Confocal microscope was used in laser scanning mode, with a 40x oil immersion objective. Using NIS Elements software, images were processed to generate a maximum intensity projection and transformed to reduce noise and improve clarity. To capture α-actinin, p21 and p16 staining, a Zeiss AxioObserver Z1 inverted epifluorescent microscope was used with a 40x oil immersion objective.

5.2.4 General comments: iPSC-CM immunofluorescence quantification

For all iPSC-CM immunofluorescence studies, 20 images of iPSC-CMs were taken in random areas per experiment (20 fields of view, FOVs). There were 5 independent experiments (n = 5).

5.2.5 Quantification of nuclear p21 fluorescence intensity in DOX- or VEH-treated iPSC-CMs

To check for differences in p21 expression between treatment groups, mean nuclear p21 intensity of iPSC-CMs in 20 FOVs were combined into a grand average per experiment (n = 5) and analysed statistically. p21 nuclear intensity was measured using a semi-automated ImageJ segmentation analysis, quantifying the intensity of p21 fluorescence signal co-localised with a DAPI-positive area using a macro (see **Appendix A**). Briefly, the nuclear fluorescence channel was used for segmentation (the Otsu method was used for auto thresholding nuclear shapes),[297] and then the fluorescence intensity in the p21 fluorescence channel was measured within the nuclear area. Finally, the background fluorescence was manually subtracted from the mean nuclear p21 fluorescence intensity for all images.

5.2.6 Quantification of nuclear p16 punctate immunostaining in DOX- or VEH-treated iPSC-CMs

To check for differences in nuclear punctate p16 expression between treatment groups, the number of nuclei showing p16-positive punctate staining was manually counted per FOV – p16-positive punctate staining was not counted if it was not localised to a

DAPI-positive nucleus. Mean nuclear punctate p16 expression of iPSC-CMs in 20 FOVs were combined into a grand average per experiment (n = 5) and analysed statistically.

5.2.7 Harvesting iPSC-CMs for RNA isolation: RT-qPCR

At the end of the 10-day exposure to DOX, iPSC-CMs were harvested for RNA. Firstly, Maintenance Media was gently aspirated, and cells were washed once with DPBS. Then, T/E (Sigma-Aldrich T3924-100ML) was added to cells for 5-6 minutes, before gently agitating the welled plate and using a pipette to wash the T/E over the iPSC-CM monolayer. T/E was quenched in a 1:1 ratio using Maintenance media, and wells were washed twice with maintenance media to maximise number of cells lifted from the culture surface. Cell suspensions were then centrifuged at 400 x *g* for 5 minutes to obtain a pellet, and supernatant was carefully aspirated. Pellet was then resuspended in ice-cold PBS (Gibco 10010-015) using gentle pipetting and centrifuged at 400 x *g* for 5 minutes again. Supernatant was aspirated and pellets were stored at -80 °C until needed.

5.2.8 RNA isolation: RT-qPCR

For RNA isolation for RT-qPCR studies, RNA was isolated from iPSC-CM cell pellets using an RNeasy Micro Kit (Qiagen 74034, see **2.2.3**). Concentration of iPSC-CM RNA was measured and quality checked according to standard methods (see **2.2.4**).

5.2.9 cDNA synthesis

cDNA was synthesised using RNA extracted from iPSC-CMs according to standard methods (see **2.2.5**). 100 ng of total RNA was incorporated into each cDNA synthesis reaction.

5.2.10 Quantitative polymerase chain reaction (qPCR) for senescence-associated transcripts

Primer pairs were designed for qPCR using the webtool Primer-BLAST (see **2.2.6**) or commercially sourced as pre-designed “KiCqStart” primers (Sigma). Primers were purchased from Sigma and Integrated DNA Technologies (IDT). RT-qPCR was carried out according to a standard workflow (see **2.2.7**). *ACTB* and *HPRT1* were used together as endogenous controls.

Table 5.1 Details of primer pairs used in RT-qPCR studies. Primer sequences were designed using Primer-BLAST and commercially custom-manufactured.

Target gene transcript	Forward (5' → 3')	Reverse (5' → 3')	Manufacturer
CDKN2A	GTCGGGTAGAG GAGGTGCG	CCCATCATCATG ACCTGGATCG	Sigma-Aldrich custom
CDKN1A	TCTCAGGGTCG AAAACGGC	GCAGAAGATGTA GAGCGGGC	Sigma-Aldrich custom
PURPL	CGTGTGAAAAG AACCCAGGTA	CGCCTGGTAAAA CAACCAGT	Sigma-Aldrich custom
GDF15	TCCGGATACTCA CGCCAGAA	GTCACGTCCCA CGACCTTG	Sigma-Aldrich custom
NPPB	ATTAAGAGGAAG TCCTGGC	AAATGAGTCACT TCAAAGGC	Sigma-Aldrich KiCqStart
HPRT1	TGACCAGTCAA CAGGGGAC	CTTCGTGGGGT CCTTTTCAC	Sigma-Aldrich custom
ACTB	GACGACATGGA GAAAATCTG	ATGATCTGGGTC ATCTTCTC	Sigma-Aldrich KiCqStart

5.2.11 Quantification of nuclei number and morphology of DOX- or VEH-treated iPSC-CMs

Standard methods were adapted from Willet and Johnson.[342] Using Fiji (ImageJ),[294] 20 FOVs per experiment were individually, manually thresholded until nuclei were sufficiently captured. Then, the images were binarized. Then, each nucleus in an image was separated using Process > Binary > Watershed. Analyse > Analyse Particles was then used to evaluate the area of each nucleus, with "exclude on edges" enabled. Particle size was thresholded at 50-1500 μm^2 and circularity was thresholded at 0.00-1.00. This analysis also generated the number of nuclei per FOV. The mean size of nucleus in each of the 20 FOVs per experiment was noted. To check for differences in the number of nuclei observed in an average FOV between treatment groups, mean number of nuclei in 20 FOVs were combined into a grand average per experiment (n = 5) and analysed statistically. To compare mean nuclear size and the spread of data, all FOV data per treatment group was pooled and used in a violin plot, for more comprehensive visualisation of data spread (n = 110-123).

5.2.12 Sample preparation for RNA-Seq

Following consultation with the manufacturers of iPSC-CMs (Fujifilm Diosynth) and Azenta, who carried out RNA Seq, the following protocol was developed to obtain optimal samples for RNA Seq pipeline. iPSC-CMs were cultured and treated with DOX or VEH as previously described, in a 24-welled plate format (Greiner Bio-One 662160). At day 10 post-treatment, 350 µL of Buffer RLT (Qiagen) was added directly to each well, plate was placed on ice, and cells were incubated with Buffer RLT for up to 5 minutes with gentle agitation via pipetting. Lysed cells were stored at -80°C before transporting to Azenta Life Sciences (Essex, UK) (packaged in solid CO_2), for onward processing.

5.2.13 RNA extraction from iPSC-CMs for RNA-Seq, assessment of RNA quality/quantity

RNA was extracted by Azenta Life Sciences. Total RNA was extracted from lysed cells in buffer RLT using RNeasy Micro kit following manufacturer's instructions (Qiagen, Hilden, Germany). RNA samples were quantified using Qubit 4.0 Fluorometer (ThermoFisher Scientific, Waltham, MA, USA). RNA integrity was checked with 5600 Fragment Analyzer (Agilent Technologies, Palo Alto, CA, USA).

5.2.14 RNA Seq workflow

Bulk RNA Seq was carried out by Azenta Life Sciences.

Library preparation: To better enable sequencing of long non-coding RNAs, rRNA was depleted from total RNA. To enhance confidence in fold change measurements, Mix1 of External RNA Controls Consortium (ERCC) control was spiked in.

Sequencing: 11-nucleotide unique molecular identifiers (UMIs) (New England Biolabs) were ligated to transcripts, to more accurately profile the transcriptome during amplification. Paired end 150 bp sequencing was used on an Illumina NovaSeq 6000 platform. Sequencing depth was 10 million read pairs per sample.

Data analysis: Raw data was trimmed to remove adapter sequences and low-quality reads, and then aligned to human reference genome GRCh38.[343] Read counts were further annotated and normalised in a manner proprietary to Azenta Life Sciences. Using DESeq2, a comparison of gene expression between DOX- and VEH-treated iPSC-CMs was performed. The Wald test was used to generate p-values and $\log_2$ fold

changes. Genes with an adjusted p-value of < 0.05 and absolute log_2 fold change > 1 were considered as differentially expressed genes.

5.2.15 Gene set enrichment analysis

Briefly, gene set enrichment analysis (GSEA) is used to calculate an enrichment score (ES) for a given *a priori* defined gene set, which indicates any overrepresentation of the gene set (e.g. Hallmark Gene Pathways) in gene expression data from VEH or DOX-treated iPSC-CMs. This is done by checking how the genes in a specific gene set are distributed in the ranked list of all genes in the bulk RNA Seq, nearer the top or nearer the bottom. A higher ES indicates positive enrichment (i.e. genes from the predefined gene set cluster near the top of the total gene expression data). Once all gene sets have been evaluated, the ES is normalised (NES) to account for different numbers of genes constituting various gene panels. The NES of any given predetermined gene set can then be compared and corrected for multiple hypothesis testing.

GSEA was performed using two approaches, via the GSEA online software and via the R bioinformatics program. Maria Camacho Encina (Newcastle University, UK) assisted with GSEA design, wrote R code and carried out analysis. To perform GSEA for senescence gene panels, normalised gene expression data were analysed for enrichment using GSEA software (Broad Institute, version 4.3.3). The GMT files for SAUL_SEN_MAYO and FRIDMAN_SENESCENCE_UP gene sets were downloaded from the Molecular Signatures Database (MSigDB, version 2023.2.Hs).[344,345] To perform GSEA for hallmark pathway gene panels, gene expression data were analysed for enrichment using the fgsea package in R (version 4.3.0). Hallmark pathways were downloaded from MSigDB (version 2023.2.Hs). Packages used are available from Bioconductor.

5.2.16 Gene Ontology analysis

Maria Camacho Encina carried out Gene Ontology (GO) analyses. The compareCluster function within the R package org.Hs.eg.db was used to perform GO enrichment analysis (i.e., specifying the “enrichGO” function on the fun argument, which will return the enrichment GO categories after FDR control) in the list of upregulated or downregulated genes. List of genes was generated as follows: upregulated (DOX vs VEH) if log_2(fold change) > 0.7 and padj < 0.05, downregulated if log_2(fold change) < - 0.7 and padj < 0.05. The three gene ontology categories,

Molecular Function, Cellular Compartment and Biological Process, were assessed. Packages used are available from Bioconductor.

5.2.17 Statistical analyses

An unpaired student's t-test was used to compare mean number of nuclei, p16 immunostaining expression and p21 immunostaining expression between iPSC-CM treatment groups. A Welch's t-test was used to compare the mean nuclear size between iPSC-CM treatment groups (F test of the data was statistically significant, indicating different variances between the data sets). Data concerning nuclear size of iPSC-CMs per FOV (n = 110-123) failed normality testing (Shapiro-Wilk), so a Mann-Whitney test was employed to test for the presence of difference in nuclear size. To analyse qPCR results, data were processed to the widely used ddCT form, whereupon they were statistically analysed using a paired t-test. As is common, data were graphed in the form 2^-ddCT format for easier visualisation and interpretation.

5.3 Results

5.3.1 Induced pluripotent stem cell-derived cardiomyocytes express cardiac markers α-actinin and cardiac troponin C

Though the AC16 cell line is a useful model in certain contexts, it is acknowledged that a more sophisticated model for true CMs is iPSC-CMs. To ensure this work remained impactful and mimics the clinical situation as closely as possible, some of our previous AC16 studies were validated and furthered in this “gold-standard” cell type.

Though the cells in the following studies were purchased from a commercial source and boast assurances of CM purity and phenotype, cells were first checked for proper differentiation by assessing the presence of two basic CM-typic proteins, α-actinin and cTnC, using fluorescence immunocytochemistry. Fluorescence microscopy confirmed the presence of α-actinin (magenta), and though the focal plane was not even across the field of view, outlines of cell clusters can broadly be made out within the confluent cell culture (**Figure 5.1A**). Confocal microscopy was used to validate the presence of cTnC (green) and allowed the observation of its organisation into striated filaments, which are crucial for the contractile phenotype of this cell model (**Figure 5.1B**). No cells, based on DAPI-nuclear labelling, lacked expression of these markers, which is in line with the purity assurances provided by the commercial source of these cells.

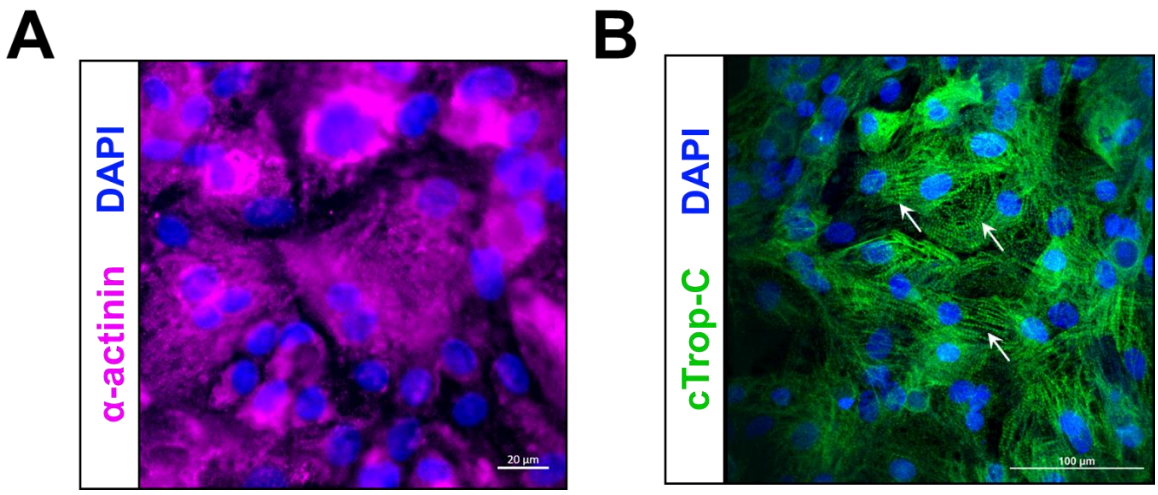

Figure 5.1 α-actinin and cardiac troponin C expression in iPSC-CMs. A) iPSC-CMs labelled with anti-α-actinin antibody (magenta), nuclei labelled with DAPI (blue), visualised using epifluorescent microscope. Scale bar = 20 µm. **B)** iPSC-CMs labelled with anti-troponin-C antibody (green), nuclei labelled with DAPI (blue), visualised by confocal microscopy. Arrows highlight striated filaments in culture. Scale bar = 100 µm.

5.3.2 Various markers of senescence are elevated in iPSC-CMs at day 10 post-DOX, relative to post-VEH

Using fluorescence immunocytochemistry, it was next ascertained if, as per the results using AC16 cells (see **3.3.7**), the 10-day DOX dose-response regimen induced iPSC-CMs to senescence. Expression of p16 was observed at some degree in both VEH and DOX-treated CMs. Cells displayed bright punctate p16 expression in their nuclei (**Figure 5.2A,** white arrows) – from representative images this was notably more prevalent in DOX-treated cells. A criterion for positive p16 staining was therefore defined, in which nuclei containing ≥ 1 $p16^{+ve}$ puncta were considered $p16^{+ve}$, which were then manually quantified as a proportion of total nuclei per field of view. Using this approach, significantly more $p16^{+ve}$ nuclei were identified per field of view following DOX treatment compared to VEH-treated iPSC-CM controls (63.3 ± 5.5% vs 12.4 ± 1.5%) (**Figure 5.2A**).

Regarding p21, diffuse nuclear expression of p21 was observed in both VEH and DOX treatment conditions (**Figure 5.2B**, white arrows). The anti-p21 signal was observed to varying intensity within the nuclei observed in a single field of view (**Figure 5.2B**). Given the variety of nuclear anti-p21 signal intensity in a single field of view, it was difficult to justify a threshold to manually categorise a nucleus as p21-positive or p21-negative. Therefore, an unbiased semi-automated segmentation approach was used

to quantify p21 nuclear signal intensity rather than manual quantification. Fold-change in mean nuclear p21 fluorescent signal was significantly high in DOX-treated iPSC-CMs compared to VEH-treated counterparts (1.3-fold increase) (**Figure 5.2B**).

Using the same primers as in AC16 studies, RT-qPCR results showed that in the absence of DOX exposure, iPSC-CMs did not express the transcript encoding p16 protein, *CDKN2A*. *CDKN2A* expression appeared to increase in DOX-treated iPSC-CMs but this result did not reach statistical significance. A wide range of expression levels were indicated by a large SEM: across five independent experiments, expression varied greatly from undetectable to 0.05-times the expression of the averaged *HPRT1* and *ACTB* expression (**Figure 5.2C**). In summary, RT-qPCR approaches did not measure any statistically significant change in iPSC-CM *CDKN2A* transcript between DOX or VEH treatment groups – the low expression levels perhaps indicate that the transcript cannot be reliably detected by this method at all. However, *CDKN1A*, which encodes p21, was robustly detected using these methods and a significant increase in p21 expression was observed following DOX treatment when compared to VEH control (**Figure 5.2D**). Similar to the AC16 line data, the putative senescence markers *PURPL* and *GDF15*, were both significantly upregulated in DOX-treated iPSC-CMs (**Figure 5.2E, F**). The classical CVD marker *NPPB* (see **1.2.5**) was also examined and was significantly upregulated in DOX-treated iPSC-CMs (**Figure 5.2G**).

It was next explored whether exposure to DOX induced morphometric changes associated with the senescent phenotype. Previous studies have suggested that senescent cells undergo changes in their nuclei structure leading to larger, irregular shaped nuclei,[346,347] therefore iPSC-CM nuclear size was quantified in both treatment conditions. At day 10 in the DOX treatment condition, significantly fewer DAPI-positive nuclei were observed per individual field of view than in VEH treated cultures (**Figure 5.3A, B**), with 31.7± 2.2 nuclei per field of view in the DOX treatment condition and 54.3 ± 3.3 nuclei per field of view in the VEH treatment condition (**Figure 5.3C**). DOX-treated iPSC-CMs had significantly larger nuclei as measured by semi-automated analyses, with the median nuclear size of DOX-exposed CMs being 161.3 μm^2 compared to 139.0 μm^2 in the control condition (**Figure 5.3D**). Furthermore, there was more heterogeneity in nuclear size following DOX treatment than in the control: a Welch's t test returned an F test p value of < 0.0001, indicating that variance in nuclear size was not equal between DOX-treated iPSC-CMs and VEH-treated iPSC-CMs.

This data together provides a strong indication that iPSC-CMs are induced to senescence following DOX exposure.

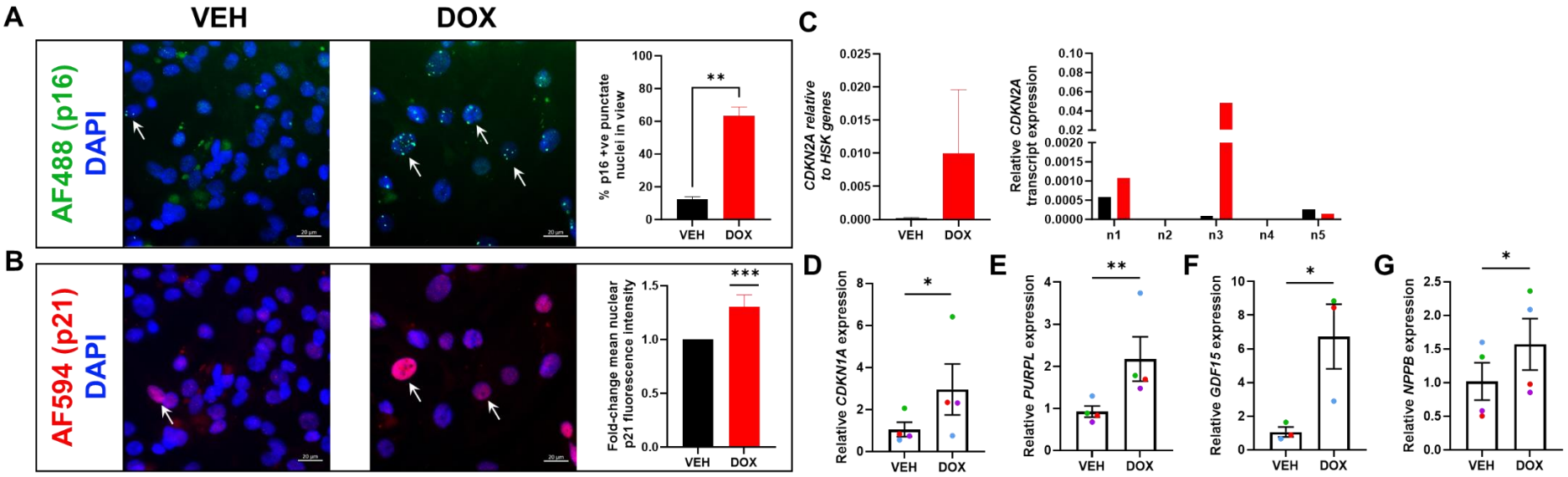

Figure 5.2 Markers of senescence are elevated in iPSC-CMs 10 days post-DOX compared to controls A) A minority of VEH-treated iPSC-CM nuclei display punctate p16 staining (solid arrows). Many DOX-treated iPSC-CMs show multiple anti-p16 puncta (solid arrows) localised to the nuclei. Quantification of the number of nuclei containing >1 anti-p16^{+ve} puncta shows that anti-p16 puncta^{+ve} cells are significantly more numerous in DOX treatment condition than VEH treatment condition. Scale bar = 20 μm. **B)** Fluorescence immunostaining of senescence marker p21 in VEH- and DOX-treated iPSC-CMs, at 10 days post-drug exposure. VEH-treated and DOX-treated iPSC-CMs show nuclear, diffuse anti-p21 signal, seen more strongly in some nuclei than others (solid arrows). Semi-automated segmentation analysis of nuclear anti-p21 signal intensity shows that anti-p21 signal is more intense in the nuclei of iPSC-CMs treated with DOX compared to those treated with VEH treatment condition. Scale bar = 20 μm. * $p < 0.05$ **C-G)** RT-qPCR studies exploring senescence markers **C)** *CDKN2A* **D)** *CDKN1A* **E)** *PURPL* **F)** *GDF15* **G)** *NPPB*. For all RT-qPCR experiments *HPRT1* and *ACTB* were used as endogenous controls. Data represents mean ± SEM from n = 3-4 independent experiments. ** $p \leq 0.01$, * $p \leq 0.05$ using unpaired (immunofluorescence) or paired (RT-qPCR) student's t-test.

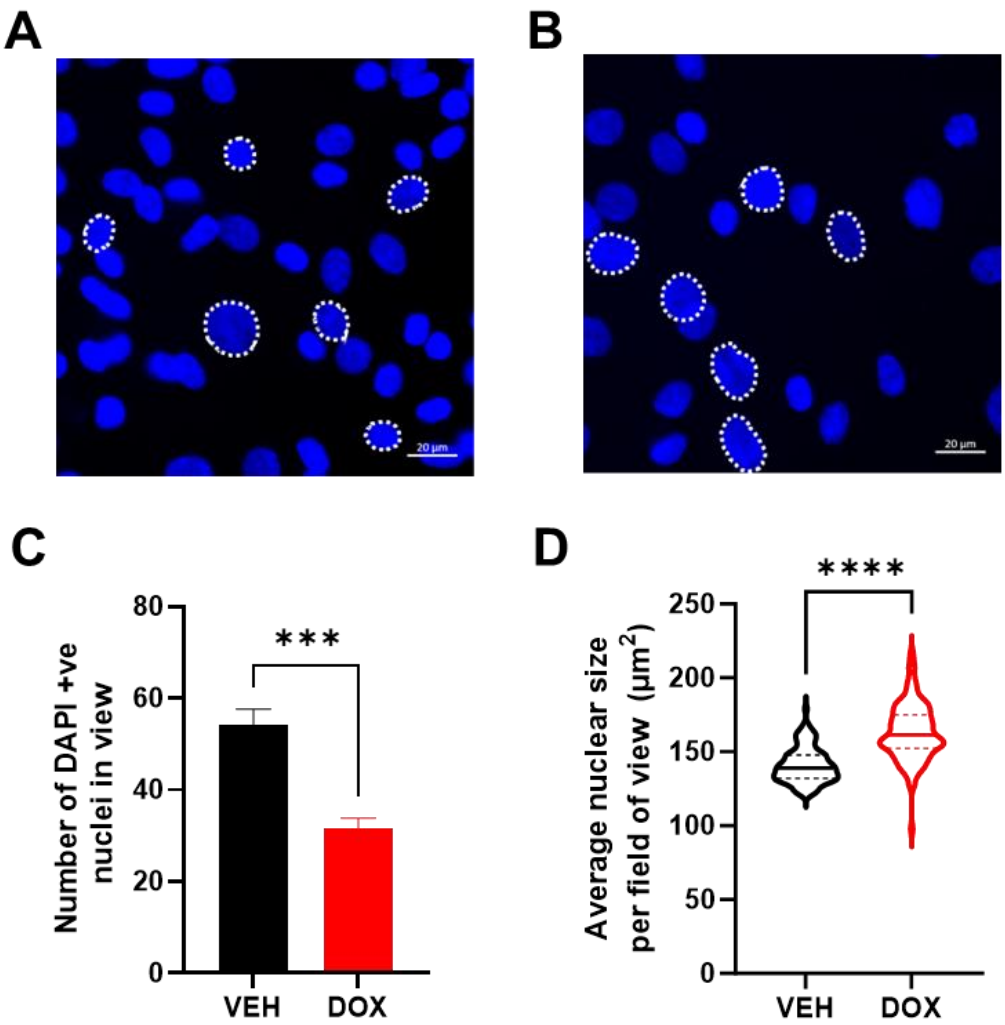

Figure 5.3 DOX treatment associates with nuclear enlargement in iPSC-CMs. A and B) Representative images of CM nuclei labelled with DAPI (blue) for both experimental conditions at 10 days post-treatment (white dashed outlines showing examples of individual nuclei). Scale bars 20 µm. **C)** Graph showing total number of nuclei per field of view. Data are mean of five independent experiments +/- SEM. *** $p \leq 0.001$. **D)** Graph showing median nuclear size and nuclear size distribution as measured by semi-automated analyses, dashed horizontal lines within the plot indicate the 25th and 75th quartiles. Solid horizontal line indicates the median nuclear size value. Data is comprised of 110-123 individual fields of view across five independent experiments, analysed for difference in mean values via a Mann-Whitney test. **** $p \leq 0.0001$.

5.3.3 Quality and quantity evaluation of RNA isolated from iPSC-CMs for bulk RNA-Seq

To integrate the transcription profile of senescence CMs in an unbiased manner, more unbiased, high-throughput methods were then employed in the form of bulk RNA-Seq.

To test whether the total RNA extracted from iPSC-CM cell pellets was sufficient in quality and quantity for downstream RNA sequencing, RNA was run through a denaturing agarose gel. The assay readout gel was free of smears and showed sharp, clear rRNA bands at 28S and 18S sizes (approx. 5000 and 2000 nucleotides, respectively) in all samples (**Figure 5.4**). The ratio of 28S:18S band fluorescence intensity was measured (**Figure 5.5**) and was calculated as approximately 2.0 in all samples.

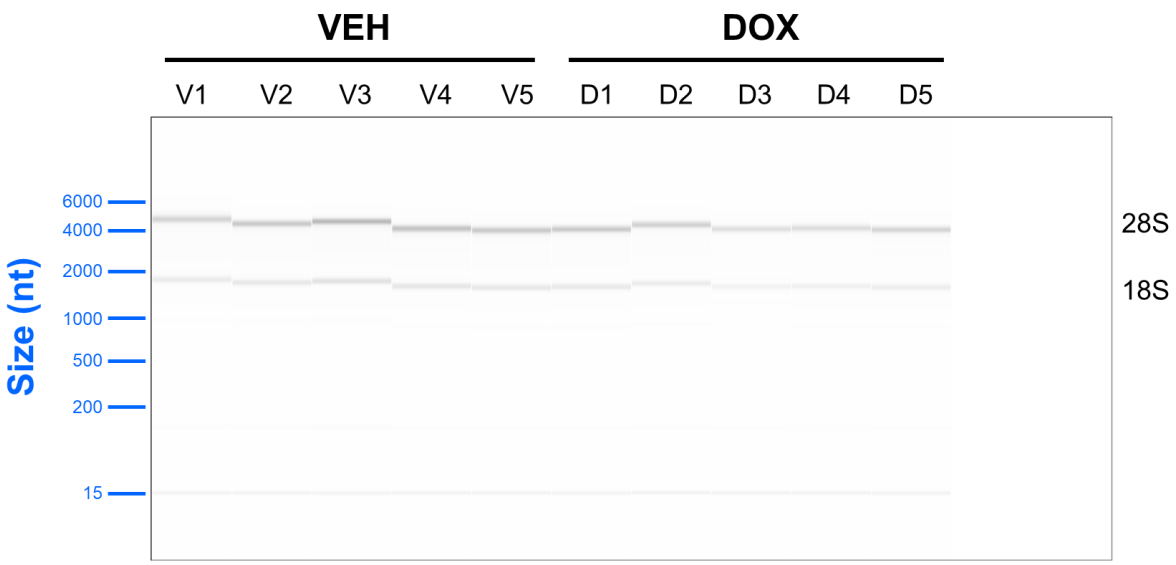

Figure 5.4 Gel image from iPSC-CM total RNA quality assessment (Agilent Fragment Analyser). Non-senescent (V1-5) and senescent (D1-5) iPSC-CM total RNA was run on a denaturing agarose gel. Good quality RNA is indicated by sharp and clear chemiluminescent 28S and 18S rRNA bands (indicated) at the expected size in nucleotides (nt) (approx. 5000 and 2000, respectively), with 28S rRNA bands qualitatively appearing more intense than 18S bands.

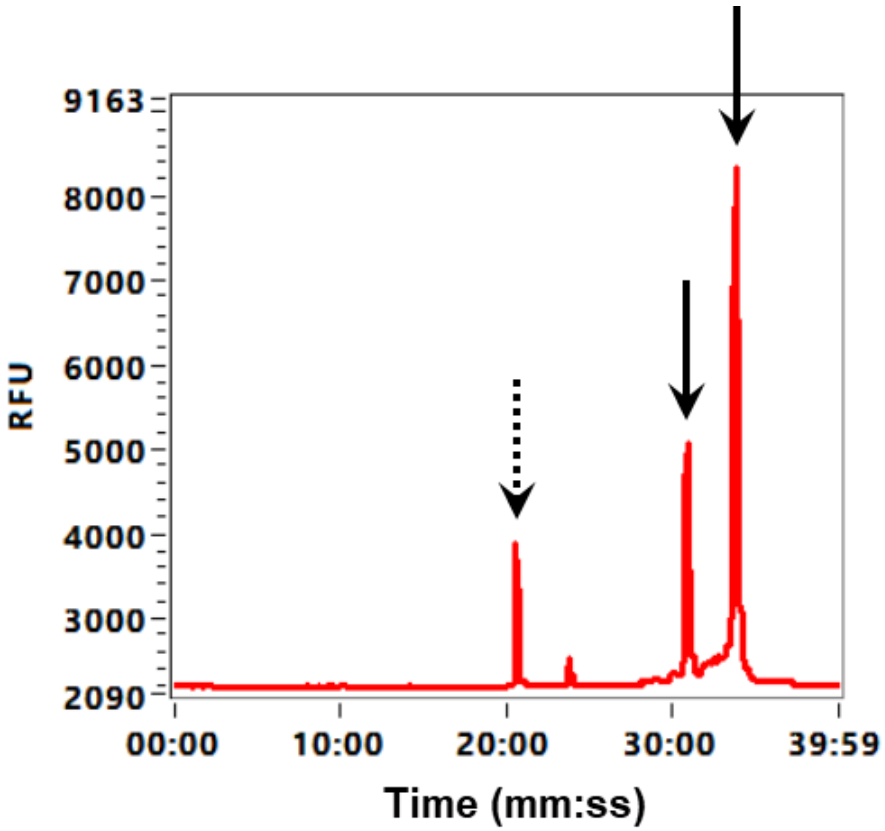

Figure 5.5 Representative plot of the relative fluorescence quantification of total RNA quality assessment gel bands (sample V1). Dashed arrow at approx. 20 minutes indicates lower molecular weight marker (15 nucleotides on gel), solid arrows at approximately 30 and 35 minutes represent 18S and 28S rRNA bands respectively. RFU = relative fluorescence units.

Total RNA quantity was assessed fluorometrically, showing that RNA concentration was sufficient for downstream processing in all cases (36.0-73.1 ng/μL range) (**Table 5.2**). The quality of RNA was robust in all samples, shown by the assignment of RNA Quality Number 10.0, derived from the 28S/18S rRNA ratio of approximately 2.0 (**Table 5.2**).

Table 5.2 Overview of total RNA quantity and quality, as assessed by Qubit instrument and Fragment analyser 28S/18S ratio, respectively. RNA concentration was sufficient for downstream bulk-RNA applications. All samples were deemed sufficiently high quality with RNA Quality Numbers (RQN) of 10.0 (10.0 being the highest quality possible, 1.0 being the lowest quality possible).

Sample ID	Total RNA concentration (µg/µL)	RQN score
V1	57.8	10.0
V2	52.2	10.0
V3	73.1	10.0
V4	61.3	10.0
V5	60.9	10.0
D1	50.1	10.0
D2	51.6	10.0
D3	42.4	10.0
D4	36.0	10.0
D5	43.8	10.0

5.3.4 Evaluating the variance in RNA from DOX-treated or VEH-treated iPSC-CMs

Upon completing the RNA-Seq workflow, analysis of the RNA from VEH- or DOX-treated iPSC-CMs shows that when considering variance, samples cluster strongly according to treatment group, with 85% of the variance being explained by this variable (**Figure 5.6**). Interestingly, more variance was seen within the VEH treatment condition than the DOX treatment condition – samples within the VEH group do not cluster as tightly. However, this intra-treatment variance still only contributes 6% of the total variance across all samples, being far outweighed by inter-treatment variance (**Figure 5.6**).

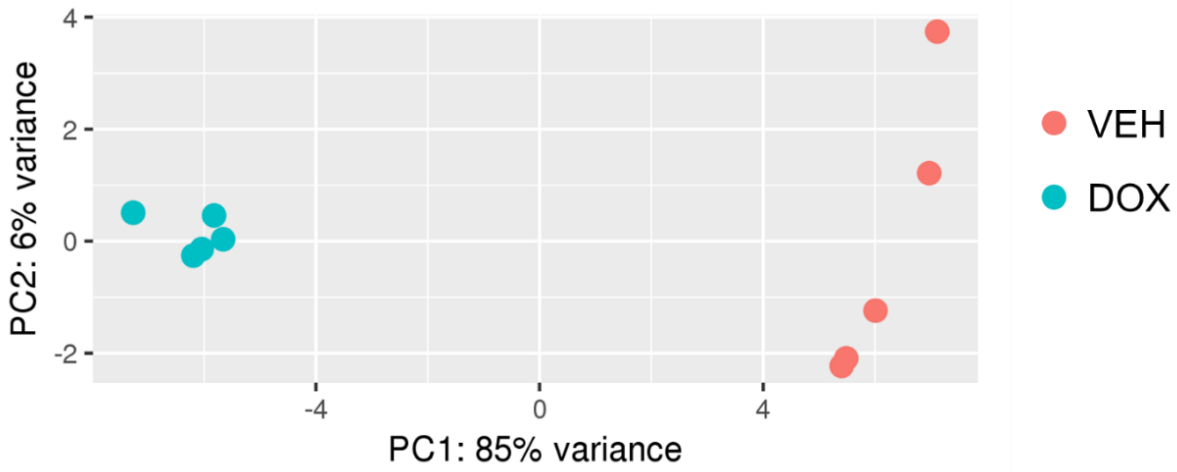

Figure 5.6 Principal component analysis of non-senescent ("VEH", red dots) and senescent ("DOX", blue dots) iPSC-CM RNA data. 85% of the variance amongst all samples can be attributed to treatment group. More variance is seen within the non-senescent, VEH treatment group than within the senescent, DOX treatment group, but these intra-group differences only explain 6% of the variance overall. PC = principal component. N = 5 per treatment group.

5.3.5 Individual gene-level analysis of RNA-Seq data from DOX- or VEH-treated iPSC-CMs

RNA Seq analysis identified 14,976 transcripts as expressed in one or both of the non-senescent or senescent iPSC-CM treatment groups (**Figure 5.7**, all dots). On an individual gene level, 513 genes were significantly differentially expressed, using the thresholds log2 fold change > 1 or < -1, and adjusted p-value < 0.05. 428 genes were downregulated in senescent vs non-senescent samples, with the most significance/greatest fold-change observed in cell cycle-related genes such as *MKI67*,

NEK2, *TOP2A* and *ASPM* (**Figure 5.7**, blue dots). 85 genes were upregulated in senescent vs non-senescent samples, with the most significance/greatest fold-change observed in *CDKN1A* (encoding p21), *NPPB* (encoding BNP) and *GDF15* - all commonly associated with senescence and/or CVD, alongside more novel targets such as the lncRNA *LINC01164* (**Figure 5.7**, red dots). *CDKN2A*, encoding p16 protein, was not detected in either iPSC-CM treatment group (absent from data).

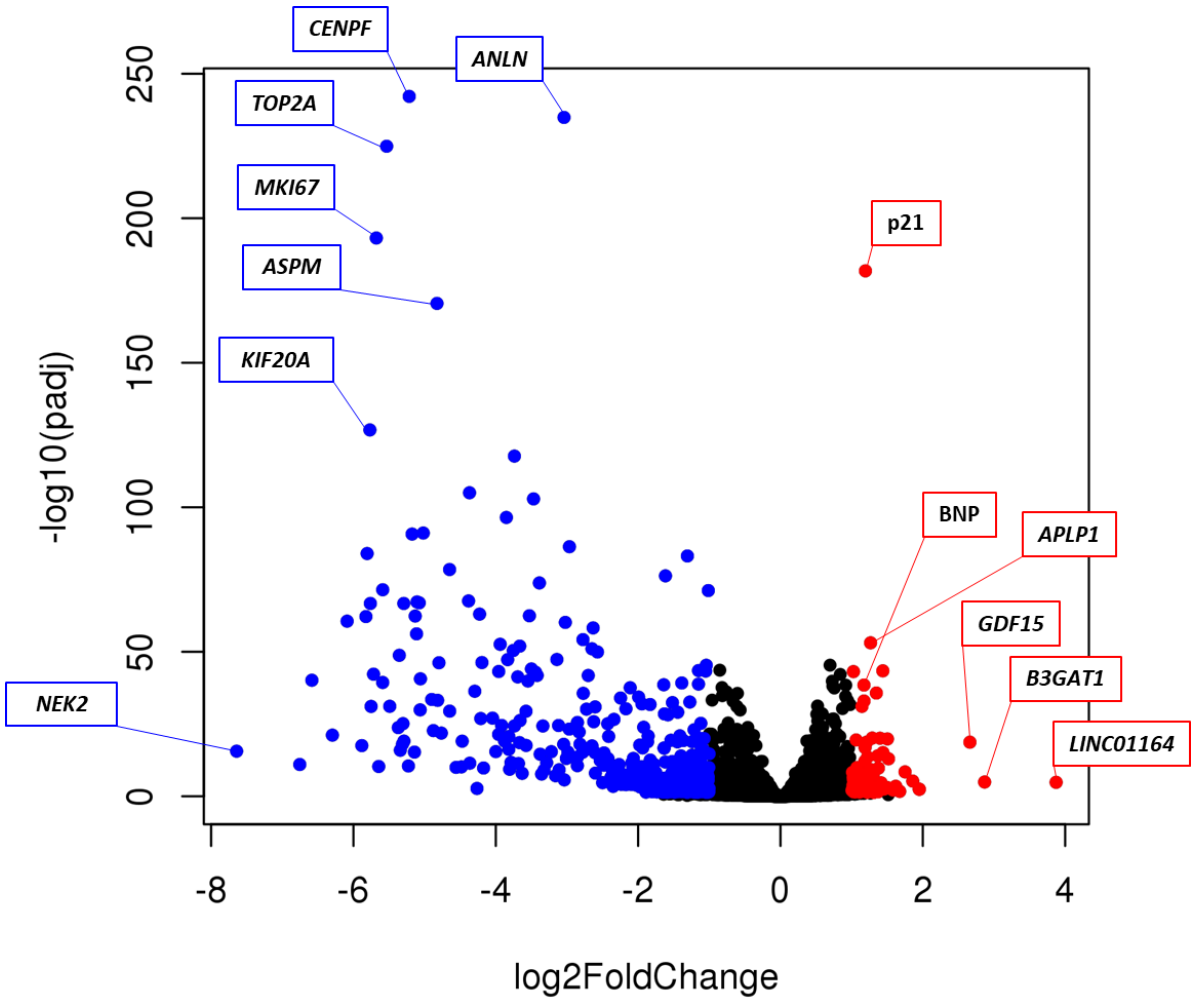

Figure 5.7 Volcano plot displaying all 14,976 gene transcripts detected in one of both of non-senescent and senescent iPSC-CM RNA, with notable genes labelled. Each dot represents a gene, 428 blue dots are genes significantly downregulated in senescent vs non-senescent samples (such as *KIF20A*, *TOP2A*, *NEK2*, *MKI67*) 85 red dots are genes significantly upregulated in senescent vs non-senescent samples (such as *BNP*, *APLP1*, *GDF15*, *LINC01164*). -log10(padj) = adjusted p-value of mean gene expression change, expressed in log base 10. Log2FoldChange = Mean fold-change of gene in senescent condition vs non-senescent condition, expressed in log base 2.

5.3.6 Gene Set Enrichment analysis of the transcriptome of DOX- vs VEH-treated iPSC-CMs reveals an enrichment for senescence-associated transcripts

To gain a better understanding of how differentially expressed individual genes may collectively affect cellular processes, Gene Set Enrichment Analysis (GSEA) was performed. The transcriptomes of DOX- and VEH-treated samples were compared to two well-established gene panels of cellular senescence. Comparing this data with the gene set compiled and published by Fridman and colleagues, the DOX-treated iPSC-CM group was highly enriched for targets in this panel, with an enrichment score (ES) of 0.521 (**Figure 5.8A**). Concordantly, there was greater enrichment for the more recently published SenMayo gene panel in the DOX treatment group compared with the VEH treatment group, indicated by a positive ES of 0.658 (**Figure 5.8B**).

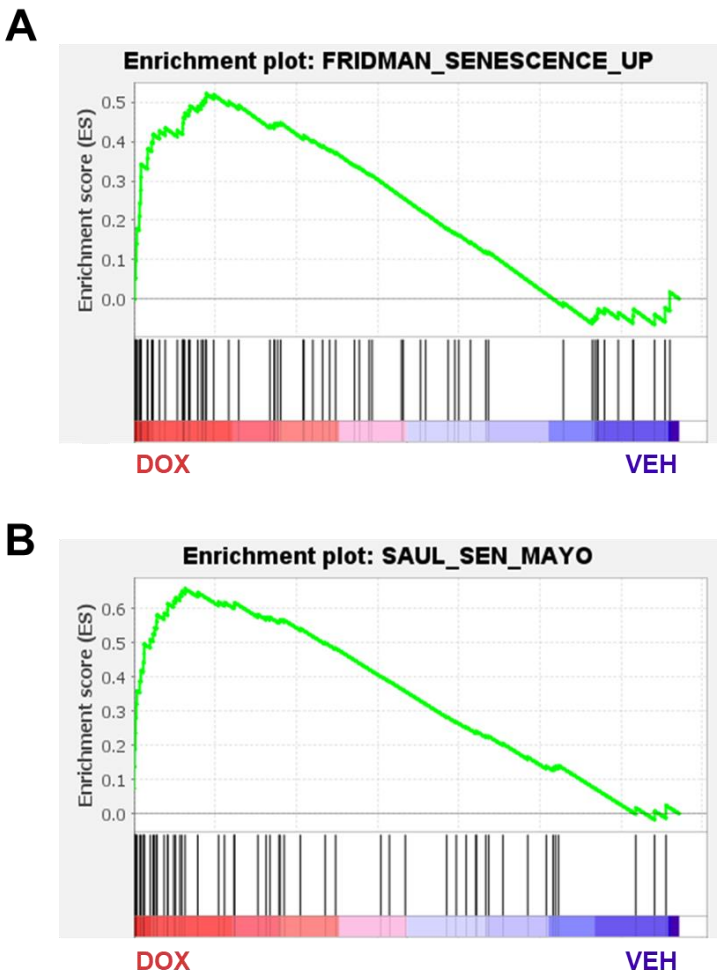

Figure 5.8 GSEA determined significant enrichment in published senescence gene sets for DOX-treated iPSC-CMs compared to VEH-treated iPSC-CMs. A) iPSC-CM RNA sequencing results were compared to gene markers established as being upregulated in senescence, by Fridman et al. DOX-treated iPSC-CMs showed a higher enrichment than VEH-treated cells, indicated by a positive enrichment score (ES) of 0.521. **B)** iPSC-CM RNA sequencing results were compared to the SenMayo gene set panel using GSEA, showing that there was notably more enrichment against this panel in DOX treatment group vs VEH treatment group, with an ES of 0.658.

5.3.7 Gene Set Enrichment Analysis shows that senescent iPSC-CMs are differentially enriched for several validated hallmark pathways compared to non-senescent controls

Having established that DOX-treated iPSC-CMs indeed display a senescent transcriptomic signature in accordance with published data, enriched pathways in senescent iPSC-CMs were then identified, by comparing RNA Seq data with the comprehensive Molecular Signatures Database (MSigDB) hallmark pathways, a collection of defined gene sets which convey specific biological states or processes. Gene set enrichment analysis (GSEA) revealed that the most upregulated pathways in senescent iPSC-CMs according to NES were “p53”, “oxidative phosphorylation”, “epithelial mesenchymal transition” and “TNFα signalling via NFκB”, amongst others (**Figure 5.9**).The most downregulated pathways were “G2M checkpoint”, “E2F targets”, “mitotic spindle” and “MYC targets” (**Figure 5.9**). Pathways of notable NES but having statistically non-significant p-values were “TGFβ signalling”, “UV response up”, “interferon α response” (upregulated); and “UV response down”, “oestrogen response - late” (downregulated) (**Figure 5.9**).

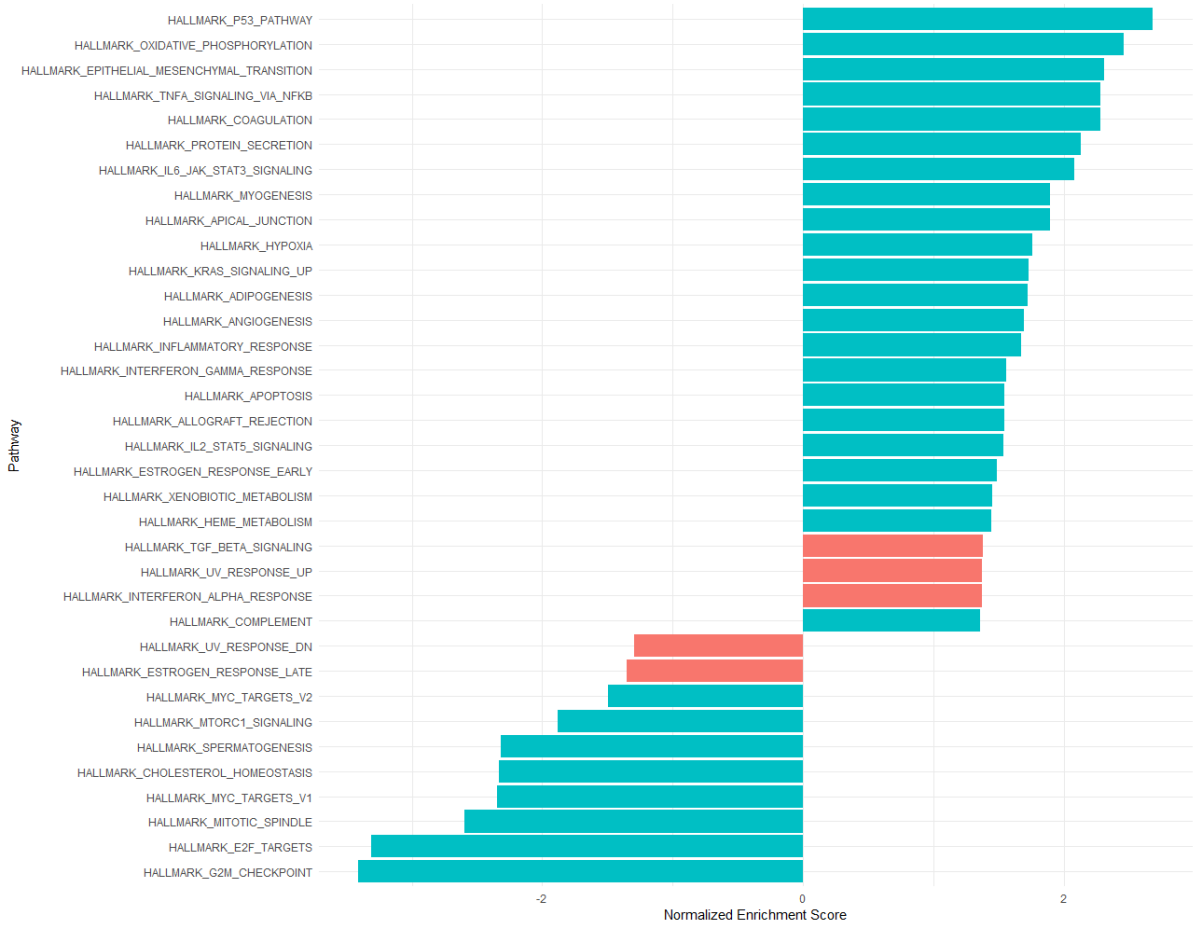

Figure 5.9 GSEA of RNA sequencing from senescent vs non-senescent iPSC-CMs, exploring differentially regulated pathways. With a normalised enrichment score of > 0, several pathways were highlighted as significantly upregulated in senescent iPSC-CMs, notably the “p53”, “oxidative phosphorylation”, “epithelial to mesenchymal transition”, and “TNFα signalling via NFκB” pathways. With a normalised enrichment score of < 0, the “G2M checkpoint”, “E2F targets” and “mitotic spindle” pathways were significantly downregulated in senescent iPSC-CMs vs VEH. Blue bars represent pathways which are statistically significantly regulated, red bars represent pathways which are not statistically significantly regulated. Significance was determined by adjusted p value < 0.05.

5.3.8 Gene Ontology approaches highlight several differentially regulated processes in senescent vs non-senescent iPSC-CMs

Gene Ontology (GO) analysis is commonly used to interpret RNA-Seq data sets, which aims to computationally shed light on the functions of gene products. Senescent and non-senescent iPSC-CMs bulk RNA-Seq data was analysed using GO terms, firstly in the context of molecular function (in the GO, “a process that can be carried out by the action of a single macromolecular machine, via direct physical interactions with other molecular entities”). Many GO terms were significantly different between treatment groups: 188 were upregulated and 452 were downregulated in senescent vs non-senescent iPSC-CMs (**Figure 5.10**). Upregulated terms in the senescent group included “signalling receptor regulator activity”, “signalling receptor activator activity” and “receptor ligand activity”. Significantly downregulated terms in the senescent group include “single stranded DNA binding”, “microtubule motor activity” and “microtubule binding” (**Figure 5.10**).

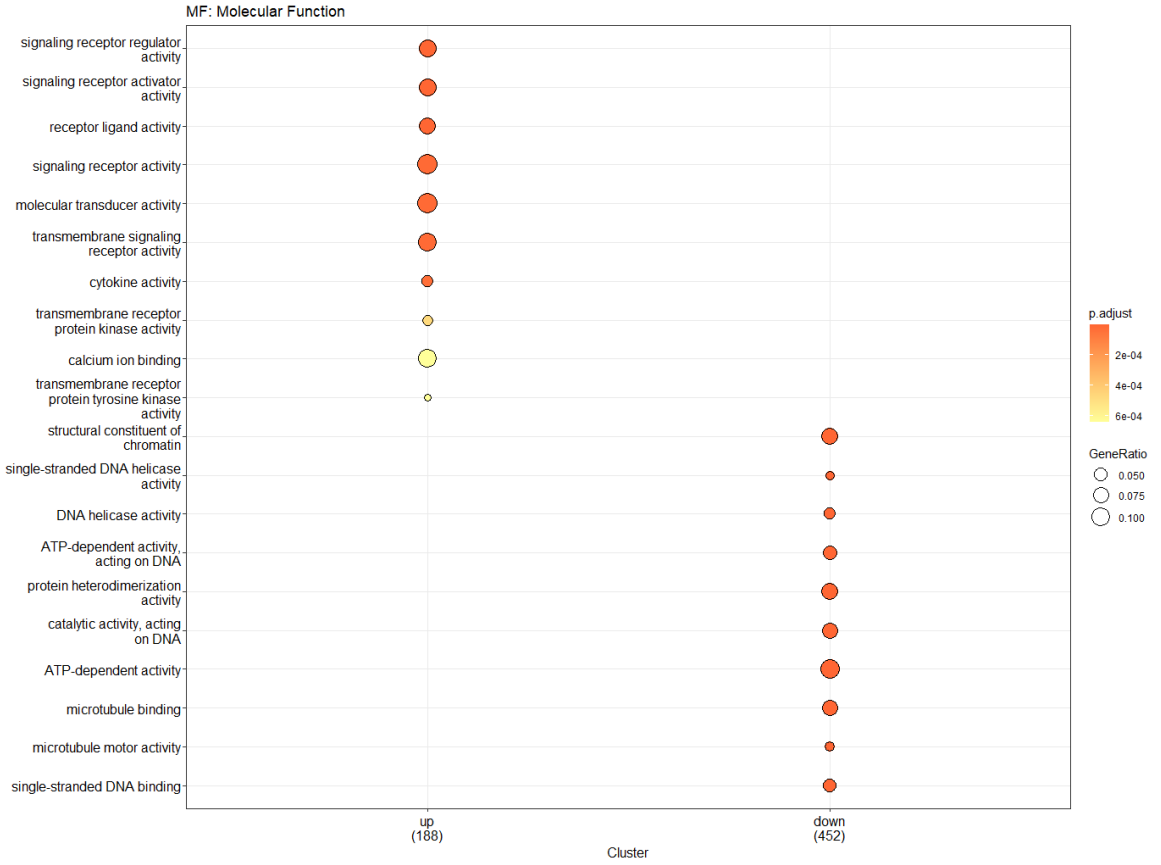

Figure 5.10 Bubble plot showing selected results from Gene Ontology analysis of RNA from senescent vs non-senescent iPSC-CMs in the paradigm of molecular function. Significantly upregulated GO terms in the senescent group included “signalling receptor regulator activity”, “signalling receptor activator activity” and “receptor ligand activity”. Significantly downregulated terms in the senescent group included “single stranded DNA binding”, “microtubule motor activity” and “microtubule binding”. The size of a bubble (“GeneRatio”) indicates how many gene products in each pathway are significantly differentially regulated between treatment groups - the more components are present from the pathway, the larger the gene ratio, and the larger the bubble. The colour of a bubble indicates the adjusted p-value of a given pathway being significantly differentially regulated (“p.adjust”), where red is a lower p-value, and yellow is a higher p-value (all p-values displayed are < 0.05).

To explore the subcellular localisation of differentially regulated gene products, the same data was then analysed in the GO cellular compartment context. There were 198 upregulated terms and 461 downregulated terms in senescent vs non-senescent iPSC-CMs (**Figure 5.11**). Significantly upregulated terms in the senescent group included “external encapsulating structure”, “extracellular matrix” and “collagen-containing extracellular matrix”. Significantly downregulated pathways in the senescent group included “nuclear chromosome”, “spindle” and “kinetochore” (**Figure 5.11**).

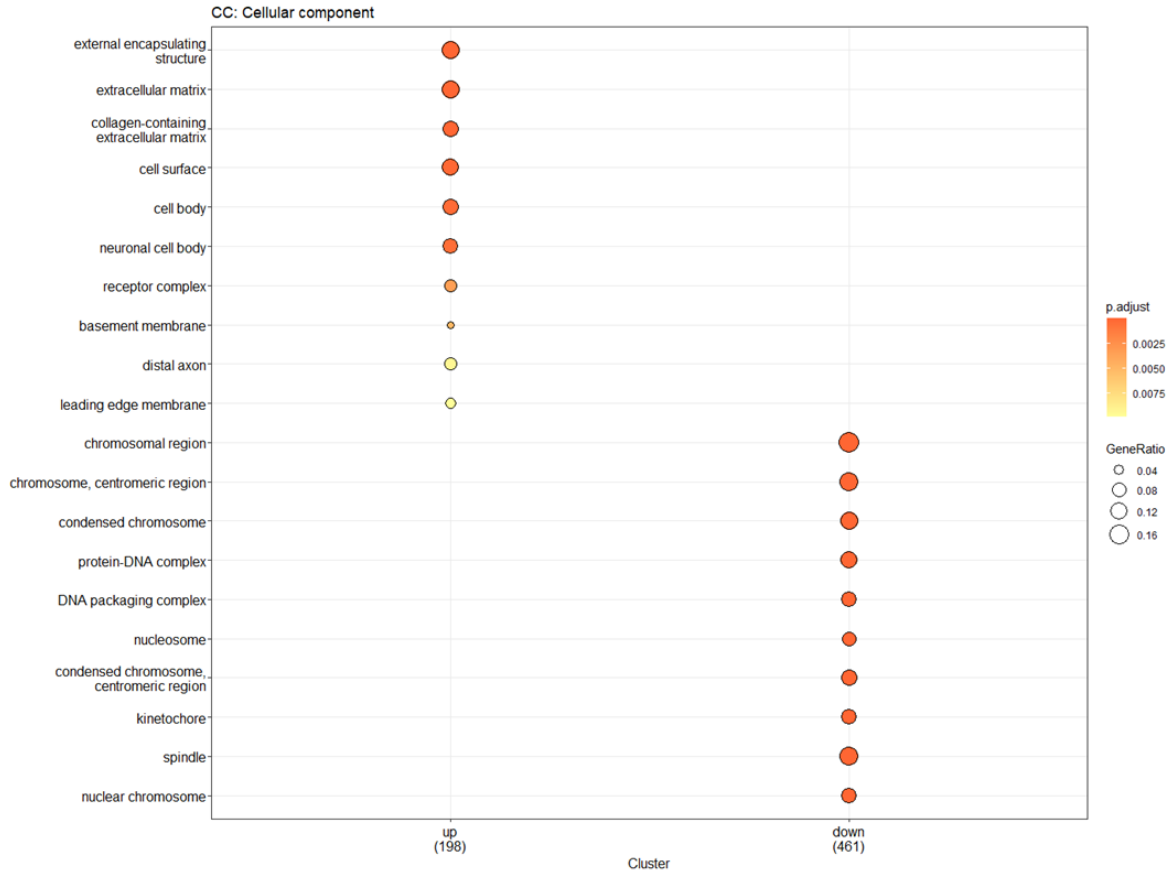

Figure 5.11 Senescent iPSC-CMs display enrichment in cellular compartments and hallmark pathways which suggest elevated signalling, and extracellular matrix modifications. Bubble plot showing Gene Ontology analysis of senescent vs non-senescent iPSC-CM RNA in the paradigm of cellular component, describing the specific location within the cell in which a gene product carries out a molecular function. Significantly upregulated pathways in the senescent group included “external encapsulating structure”, “extracellular matrix” and “collagen-containing extracellular matrix”. Significantly downregulated pathways in the senescent group included “nuclear chromosome”, “spindle” and “kinetochore”. The size of a bubble (“GeneRatio”) indicates how many gene products in each pathway are significantly differentially regulated between treatment groups - the more components are present from the pathway, the larger the gene ratio, and the larger the bubble. The colour of a bubble indicates the adjusted p-value of a given pathway being significantly differentially regulated (“p.adjust”), where red is a lower p-value, and yellow is a higher p-value (all p-values displayed are < 0.05).

Lastly, the “biological process” paradigm of GO analysis was used to evaluate the larger, more complex biological objectives that differentially regulated genes and their molecular processes contribute to, in a higher-level fashion. There were 189 upregulated terms and 448 downregulated terms in senescent vs non-senescent iPSC-CMs. Significantly upregulated pathways in the senescent group included “mitotic G1 DNA damage checkpoint signalling”, “mitotic G1/S transition checkpoint signalling” and “DNA damage response, signal transduction by p53-class mediator resulting in cell cycle arrest”. Significantly downregulated pathways in the senescent treatment group included “cell cycle phase transition”, “mitotic sister chromatid segregation” and “DNA-templated DNA replication” (**Figure 5.12**). GO analyses are summarised in **Table 5.3**.

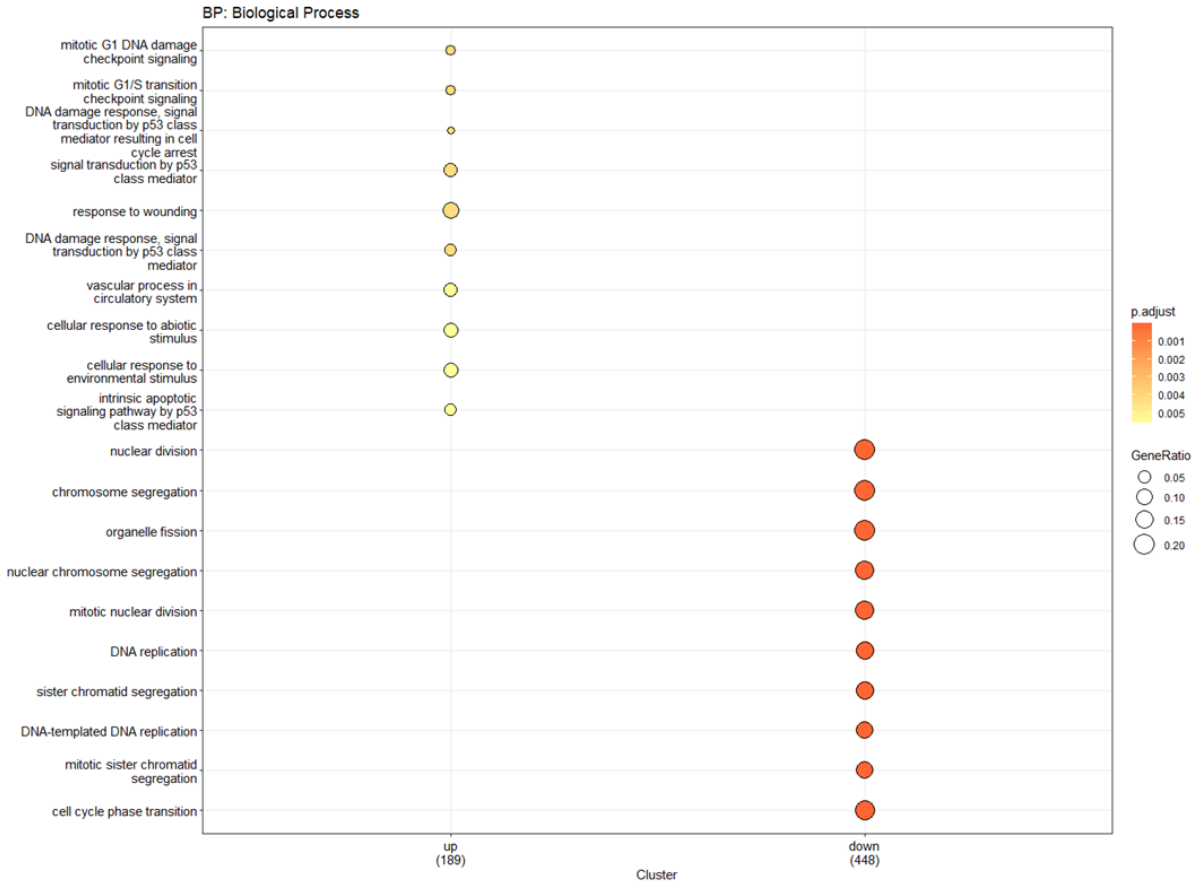

Figure 5.12 Bubble plot showing Gene Ontology analysis of RNA derived from senescent vs non-senescent iPSC-CMs in the paradigm of biological process, which describes the larger, more complex biological objectives that differentially regulated genes and their molecular processes contribute to. Significantly upregulated pathways in the senescent group included “mitotic G1 DNA damage checkpoint signalling”, “mitotic G1/S transition checkpoint signalling” and “DNA damage response, signal transduction by p53-class mediator resulting in cell cycle arrest”. Significantly downregulated pathways in the senescent group included “cell cycle phase transition”, “mitotic sister chromatid segregation” and “DNA-templated DNA replication”. The size of a bubble (“GeneRatio”) indicates how many gene products in each pathway are significantly differentially regulated between treatment groups - the more components are present from the pathway, the larger the gene ratio, and the larger the bubble. The colour of a bubble indicates the adjusted p-value of a given pathway being significantly differentially regulated (“p.adjust”), where red is a lower p-value, and yellow is a higher p-value (all p-values displayed are < 0.05).

Table 5.3 Overview of differentially expressed GO terms between senescent and non-senescent iPSC-CMs. Terms are grouped according to GO paradigm (Molecular Function, Cellular Component and Biological Process).

GO paradigm	Upregulated in senescent iPSC-CMs	Downregulated in senescent iPSC-CMs
Molecular Function	• Signalling receptor regulator activity • Signalling receptor activator activity • Receptor ligand activity	• Single stranded DNA binding • Microtubule motor activity • Microtubule binding
Cellular Component	• External encapsulating structure • Extracellular matrix • Collagen-containing extracellular matrix	• Nuclear chromosome • Spindle • Kinetochore
Biological Process	• Mitotic G1 DNA damage checkpoint signalling • Mitotic G1/S transition checkpoint signalling • DNA damage response, signal transduction by p53-class mediator resulting in cell cycle arrest	• Cell cycle phase transition • Mitotic sister chromatid segregation • DNA-templated DNA replication

5.4 Discussion

In the experimental results above, it was established that iPSC-CMs exhibit classical cardiac proteins and show several changes at the transcript and protein level following DOX exposure: some concordant with previous findings in the AC16 model, others divergent. On a whole-transcriptome level, iPSC-CMs treated with DOX are strikingly different than their VEH-treated counterparts. Hundreds of gene transcripts were differentially expressed, and they displayed a strong senescence-associated transcriptome signature, alongside enrichment in: cell signalling molecular functions, externally localised component activity, and cell cycle checkpoint processes.

5.4.1 iPSC-CMs express α-actinin and cardiac troponin C, supportive of their use as a model of bona fide cardiomyocytes

It was firstly noted that iPSC-CMs express α-actinin and cTnC at the protein level. Though AC16 CMs were not immunostained for these proteins in this thesis, similar work has been explored in other published studies, which found that iPSC-CMs and AC16 CMs expressed α-actinin, but only iPSC-CMs expressed cTnT.[247] In the publication detailing the establishment of the AC16 cell line, Davidson and colleagues show how the line express a-actinin and troponin I using immunofluorescence.[209] On troponins, three main forms of troponin are expressed by CMs: cTnC, cTnI, and cTnT: cTnI and cTnT are released by necrotic CMs and as previously discussed, are clinically used as a circulating biomarker of, for example, MI. However, as cTnC has an identical amino acid structure to the muscular (skeletal) troponin C, it is not used as a clinical biomarker of CVD since increased levels in circulation could originate from skeletal muscle.[348]

It was also found by Linn and colleagues that iPSC-CMs express more α-actinin protein than AC16 CMs, on average. In one study, iPSC-CMs were found to more closely resemble the transcriptomic profile of human heart tissue (though this tissue would have comprised multiple cell types, as CMs were not purified).[252] Overall, though the AC16 cell line certainly has utility, iPSC-CMs show more favourable findings in the literature in their likeness to true human CMs. This extends to their contractile capabilities, which were not explored in this study, reflected in their expression of cTnC into striated filamentous apparatus.

5.4.2 iPSC-CMs show upregulation in senescence and CVD-associated transcripts and proteins, 10 days post-DOX

Shown by qPCR, transcripts *NPPB, GDF15*, and *PURPL*, associated with CVD and CM senescence (as previously discussed, see **1.2.5**, **1.4.5**, **3.4.6**), were elevated in iPSC-CMs 10 days post-DOX. *GDF15* and *PURPL* were also elevated in foundational AC16 qPCR studies, cementing the concept that *GDF15* and lncRNA *PURPL* might be especially useful transcriptional biomarkers in identifying CM senescence induction following DOX exposure. *NPPB* was also significantly increased in iPSC-CMs 10 days post-exposure, which indicates CM stress. Interestingly, BNP increases in circulation during "healthy" ageing in humans, but is also positively correlated with frailty index.[349,350] BNP production has been linked with senescence in preclinical models,[299,351] but a clear link between the two in humans is yet to be established. Furthermore, its reliability as an early, predictive clinical biomarker of AIC specifically is still debated.[352]

Studies of senescence markers p16 and p21 in iPSC-CMs broadly supported the findings in AC16 cells, both at the transcript (qPCR) and protein (fluorescence immunocytochemistry) level. Conspicuously however, p16 transcript could not be detected by qPCR methods in iPSC-CMs, yet its protein form was robustly detected via immunofluorescence, and this was significantly more highly expressed in the DOX treatment group. The staining pattern is also similar to that observed in the literature, in aged, & diseased human hearts.[353] This aligns with the historical observations that p16 protein is all but undetectable in mature CMs and, from more recent studies, that it is upregulated in senescence.[176,354,355] "Baseline" vs "senescent" levels of p16 transcript and protein in other post-mitotic cell types such as neurons, osteocytes, and post-mitotic cochlear cells have been described in various recent studies, showing mixed levels of expression and activation.[166,170,356,357] Based on the minimal transcript detected by RT-qPCR but a significant increase of the p16 protein following DOX exposure, it may be assumed that in this context, upregulation of p16 occurs at the translational level in iPSC-CMs, the possible mechanisms of which have been introduced earlier in this thesis and reviewed elsewhere.[358] Future studies would aim to optimise immunofluorescent staining of iPSC-CMs, exploring detergent-based washes, species-specific serum blocking solution, and titrations of antibody dilutions, with the goal of minimising the extranuclear, non-specific signal observed here.

5.4.3 iPSC-CMs display nuclear changes 10 days post-DOX compared to 10 days post-VEH which support the acquisition of the senescent phenotype

At day 10 post-DOX, less nuclei were observed per field of view in immunofluorescent imaging than at day 10 post-VEH. Though the aim was to use a dose of DOX which does not overly induce acute loss of viability and rather induces a persistent phenotypic change in CMs which might contribute to chronic AIC, this decrease in nuclei number shows there is indeed some loss of viability over time associated with DOX exposure. Nuclear size was also significantly larger in iPSC-CMs post-DOX compared to post-VEH, which may be indicative of acquisition of the senescent phenotype. There was also a greater spread of data in the nuclear size of DOX-treated iPSC-CMs compared to VEH-treated counterparts, perhaps suggesting that senescence is not induced in a uniform manner across the culture.

Studies have shown that senescent cells have larger and more disorganised nuclear structure than non-senescent cells, which might be attributed to the accumulation of intracellular RNA and proteins (due to attenuated proteasome-mediated processes and RNA turnover),[346] and loss of lamin B1, which helps regulate nuclear size, stability and circularity.[347] Indeed, nuclear morphology and size are now being reported as predictive markers of senescence onset, which are also useful in identifying senescent cells in culture using high-throughput deep-learning analyses of DAPI-stained cultures.[359,360] Enlargement in nuclei post-DOX has been observed in H9c2 rat myoblasts at concentrations of ≥ 1μM DOX up to 24 hours post-exposure,[361] and others have shown more specifically that 2 hours post-exposure, H9c2 cells show nuclear condensation (indicating acute apoptosis) but at 24 hours, cells show nuclear swelling,[362] similar to the aforementioned study and the findings in this thesis. This has been reproduced more recently in human iPSC-CMs treated with DOX, following a conceptually similar dosing regimen to the one used in this thesis.[185]

5.4.4 RNA-Seq studies highlight individual transcript changes in iPSC-CMs support the acquirement of a senescent phenotype 10 days post-sublethal DOX exposure

Many individual gene transcripts were elevated in RNA-Seq data from DOX-treated iPSC-CMs compared to VEH controls, 10 days post-treatment. *CDKN1A*, encoding for senescence marker p21, was significantly upregulated, suggesting this cell type has a robust p53 signalling system. However, *CDKN2A*, encoding another gold-standard

hallmark of senescence p16, was undetectable in both treatment groups, in concordance with RT-qPCR results earlier in this thesis and findings in by other groups.[156]

Also supporting previous qPCR findings in iPSC-CMs and AC16 CMs, classical CVD marker *NPPB* and novel cardiovascular senescence marker *GDF15* were significantly upregulated in RNA-seq data from DOX-treated iPSC-CMs. Physiologically, GDF15 is expressed at a low level by a multitude of cell types across various tissues, and its production/secretion is generally upregulated in several organ systems under conditions of stress.[363-367] In CVD, the clinical utility of GDF15 as a predictive serum biomarker has been proposed, and it has also garnered attention in the related fields of geroscience and mitochondrial disease.[368,369] In particular, our group has proposed *GDF15* to be a CM-specific SASP factor in age-related senescence.[173] More recently, Linders and colleagues' elegant studies using dynamic engineered heart tissues (comprising CMs, cardiac fibroblasts and collagen) showed that *GDF15* was upregulated at the transcript level following chronic DOX treatment.[182]

Notably, transcript encoding for Ki67, *MKI67*, was significantly downregulated in senescent iPSC-CMs. Ki67 is commonly used as a marker of cellular proliferation, so it is interesting and perhaps counterintuitive to observe its expression in purportedly non-proliferative iPSC-CMs at all. Positive Ki67 expression can indeed indicate cell cycle activity but can also indicate binucleation or changes in ploidy, which are common phenomena in mature mammalian CMs.[370] Indeed, it is thought that the rare occurrences of true adult CM proliferation occur in a paradigm outside the canonical cell cycle, which Ki67 is associated with. To truly assess iPSC-CM proliferation, a direct measure such as cell counting could be employed, or a method for measuring nucleation and ploidy could be used (a combination immunostain for cell borders [e.g. using wheat-germ-agglutinin] and nuclei [e.g. using DAPI] would inform on nucleation, and a EdU/BrdU labelling assay would inform on ploidy).[370] Other conspicuous transcripts which were differentially expressed between treatment groups were TopII-encoding transcripts *TOP2A* and *TOP2B*: both were significantly downregulated in senescent iPSC-CMs but in accordance with current thinking in the field (see **1.3.1**), the overall expression level of *TOP2B* was much higher than *TOP2A* in both conditions (data not shown). Given that DOX is canonically thought to target the TopII enzymes at a protein level, further investigations into why it is associated with downregulated transcript expression may be warranted.

Earlier in this thesis, a cytokine array was used to examine cytokines secreted into conditioned media by senescent AC16 CMs, which might represent a CM SASP (see **4.3.4**). Cytokines which were notably upregulated included VEGF, IL-6, IL-8, FGF-2, MCSF and MCP-1. While secreted proteins do not always match transcriptomic expression like-for-like, it is worth noting that not all of these senescent AC16 secreted factors were represented in the RNA-Seq transcriptome from senescent iPSC-CMs. For instance, the transcripts encoding IL-6, IL-8 and MCP-1 were not detected in either population of iPSC-CMs (though a signal transducer for IL-6, *IL6ST*, was expressed and upregulated in senescence). FGF-2 transcript was not significantly upregulated in senescent iPSC-CMs, though FGF-1 was. On the other hand, transcripts for VEGF-A and M-CSF were significantly upregulated in senescent iPSC-CMs. These differences may speak to the partially fibroblast-like phenotype of AC16s influencing the secretome of the cell type: carrying out a similar cytokine array on iPSC-CM conditioned media would help to resolve these differences between the models.

RNA-seq data also highlighted several more novel transcript markers which were significantly upregulated in DOX-treated iPSC-CMs, which might serve as new markers specifically of the DOX-induced senescent CM signature. For instance, *B3GAT1* and long intergenic non-coding RNA gene *LINC01164* were identified to be upregulated transcripts. *B3GAT1* has no established link with DOX-induced cardiotoxicity in the literature. It encodes for 3-beta-glucuronosyltransferase 1, which creates the cell surface CD57 epitope. Interestingly, when a subpopulation of effector memory T cells terminally differentiates (termed TEMRA cells), this can be identified by the subpopulation acquiring expression of CD57 and losing expression of CD27 & CD28 epitopes. CD57 can be used to identify T cells with the shortest telomeres, which are considered senescent following repeated antigenic stimulation and which show impaired functionality.[371] Immunosenescence and its link with CVD has gained attention in recent years, and remains to be fully understood.[372] There is very little published on *LINC01164*, excepting its potential as a biomarker in hepatocellular carcinoma.[373] Despite the large and statistically significant fold-changes in these two transcripts between treatment conditions, it is important to note that both are expressed at a very low level in terms of normalised reads (data not shown), which is not adequately conveyed in the commonly-used volcano plot format. Therefore, these findings must be interpreted with caution as their differential regulation may not result in impactful biological changes. *APLP1*, however, is expressed at a robust number of

raw reads and was significantly upregulated following DOX treatment and may therefore represent a more biologically relevant target of interest. This gene has been implicated in DOX toxicity to renal podocytes and HUVECs, but excitingly, has not yet been studied in CM cell types.[374,375]

5.4.5 DOX-exposed iPSC-CMs are enriched for published senescence gene panels compared to VEH-exposed controls

Taking a higher-level view, DOX-treated iPSC-CMs were enriched for two well-regarded gene panels describing cellular senescence. The Fridman panel derives from Supplemental Table 2 of Fridman and Tainsky's 2008 comprehensive review of critical pathways in cellular senescence,[376] and the SenMayo panel derives from Saul et al's 2022 study which defined a gene set to identify senescent cells across tissues.[156] Crucially, Saul and colleagues evidenced their gene set as being senescence-defining rather than generic ageing-defining by showing in preclinical models that selective clearance of senescent cells results in a reduction in the SenMayo panel. Concordant with the results in this chapter, the authors highlight in their study using human donor bone/marrow samples that *CDKN2A* did not show an increase with increasing donor age, which was attributed to its comparatively low expression.

5.4.6 GSEA reveals significantly enriched and de-enriched hallmark biological pathways in senescent iPSC-CMs

Considering the RNA-Seq data via the lens of GSEA, upregulated pathways in senescent CMs included p53. p53 is often dubbed "the guardian of the genome" and is negatively regulated by the E3 ubiquitin ligase MDM2. p53 is near universally activated in response to intrinsic or extrinsic cellular stressors including telomere erosion, senescence, DNA damage, mitophagy, and others - resulting in a number of outcomes including cell cycle arrest, apoptosis, senescence, DNA repair and others. Thus, p53 and MDM2 together form a node for multitudes of cellular stress signals and responses, which makes mechanistic decisions in ways that are not yet fully understood.[377] p53 therefore partly regulates senescence and it has long been known that senescent cells develop persistent p53-positive foci in their nuclei, signalling irreparable DNA damage.[378] Downstream of the p53/MDM2 node is p21, a classical marker of senescence (see **1.4.1**).

Mature CMs generate approximately 80% of their ATP from fatty acid oxidation (FAO) feeding the oxidative phosphorylation (OXPHOS) metabolic pathway.[379,380] It is thought

that during CM ageing and canonical senescence, the cell displays a shift from OXPHOS to glycolysis,[381,382] which contrasts with the results in this thesis, where the OXPHOS pathway was one of the most highly upregulated in data from senescent iPSC-CMs. This may simply indicate an adaptive uptick in energy production in senescent CMs as an response to DOX exposure, which is known to impair ATP production via direct interaction with OXPHOS complexes.[383] However, some investigations have highlighted that the metabolic profile of senescent cells can vary depending on senescence-inducing stimuli, e.g. cells induced to Ras-induced senescence show greater oxidation of fatty acids compared to cells induced to replicative senescence.[384] In therapy-induced (etoposide-treated) senescent tumour cells, authors showed how there was a deregulation of glycolipid processing and aberrant lipid metabolism.[385] Overall, it is thought that lipid droplets accumulate in senescent cells and that these play a role in SASP generation.[386] Given how CMs in particular rely so heavily on FAO to feed the OXPHOS pathway, it may be that their metabolic reprogramming under senescence differs from that of other cell types. It would be interesting to further analyse the RNA seq data to a finer level of detail, analysing for enrichment of KEGG pathways such as the AMPK signalling pathway or fatty acid degradation, to compare this data with some of the more nuanced findings of these studies.

Many other pathways which were differentially enriched in the GSEA analysis speak to a cellular phenotype which is “putting the brakes on” due to stress, most obviously the downregulation of cell cycle-associated hallmark pathways “G2M checkpoint” and “mitotic spindle”, and transcription-associated hallmark pathway “E2F targets”. MTORC1, which is a part of the far-reaching TOR signalling cascade, is also downregulated. This would generally be associated with the inhibition of macromolecular/protein synthesis, which can be triggered in response to energy deprivation, amongst other stimuli.[387] mTOR signalling has recently been reviewed specifically in the context of DOX cardiotoxicity: the 30 *in vivo* studies included in the review show mixed conclusions about the regulation of mTORC1 in this pathology, but surmise that this signalling axis has a crucial role to play in the mechanisms of toxicity.[388]

Lastly, several other upregulated hallmark pathways suggest an enrichment in remodelling and inflammatory pathways, such as “epithelial to mesenchymal transition” (EMT), “TNFα signalling via NFκB”, “IL-6/JAK-STAT signalling”, and “IL-2/STAT5

signalling". Cellular EMT classically involves several requisite steps such as changes in morphology, functionality, cell-cell interactions and polarity. These changes are characterised as a switch to an embryonic/foetal gene program, which can be activated in the epicardium after injury.[389,390] Some *in vitro* studies have implicated EMT in AIC pathology,[391,392] though studies focusing on the activation of this gene program in CMs, rather than endothelial cells, are more limited. The activation of EMT processes are classically thought to be regulated by the TGFβ superfamily of proteins.[393] Interestingly, the TGFβ signalling pathway is not significantly upregulated in RNA-seq data from senescent CMs, though *TGFB1* and *TGFB2* transcripts were individually significantly upregulated by 1.6 and 1.5-fold, respectively (data not shown).

On the other hand, "TNFα signalling via NFκB", "IL-6/JAK-STAT signalling" and "IL-2/STAT5 signalling" pathways were all upregulated. TNFα signalling has been shown as upregulated in rats treated with DOX, and is implicated as an inducer of both CM enlargement and the foetal gene programme.[394,395] The IL-6/JAK-STAT signalling axis also has been implicated as an inducer of the EMT.[396] Both these pathways therefore offer an alternative stimulus for the EMT enrichment previously described. IL-2/STAT5 promotes inflammation generally and can modulate immune response,[397,398] and interestingly is demonstrably an activator of Bcl-XL, a pro-survival protein often activated in senescent cells.[399]

Further studies exploring the time course of the EMT program activation in DOX-exposed CMs would be of interest – whether the activation of this program resolves appropriately over time or is chronically activated. The time course of the pro-inflammatory profile of iPSC-CMs could also be explored, and its necessity for maintenance of the senescent phenotype. For instance, by targeting elements of the IL-2/STAT5 signalling pathway, Bcl-XL expression in senescent iPSC-CMs might be attenuated and apoptosis therefore brought about – this could present a novel target for senolytic development. In the context of AIC, further questions remain surrounding the IL-2/STAT5 axis and its ability to modulate immune cells (e.g. T_{reg} cells) in a paracrine manner: this could be investigated *in vitro* by co-culturing senescent iPSC-CMs with T_{reg} cells and measuring T cell motility/recruitment. Functionally, it would be an open question as to whether their recruitment would, over time, result in a protective/injury resolving-type outcome, or a continuously inflammatory/deleterious outcome for CMs after DOX exposure – to incorporate the multiple peripheral cell types

necessary to orchestrate this response, this question may be best addressed in an *in vivo* model.

In summary, iPSC-CMs induced to senescence by DOX exposure display enrichment in EMT, which may be promoted by non-canonical signalling pathways TNFα-NFKB and IL-6/JAK-STAT (rather than the classical TGFβ stimulus) – this is accompanied by activation of the IL-2/STAT5 axis, which may have a pro-inflammatory, immune recruiting role. Based on these transcript-level studies, further studies would be warranted to explore these interactions at a functional, protein level.

5.4.7 GO analyses show upregulated and downregulated GO terms in senescent iPSC-CMs across molecular function, cellular component and biological pathway paradigms

Lastly, RNA-Seq data was analysed using Gene Ontology (GO) approaches, to elucidate the impact of senescence induction upon the molecular function, cellular component and biological pathway paradigms in iPSC-CMs. Molecular function GO analysis closely reflected the GSEA analysis, flagging “signalling receptor regulator activity”, “signalling receptor activator activity” and “receptor ligand activity” as upregulated in senescent iPSC-CMs (concordant with increased IL/JAK/STAT signalling), and “single stranded DNA binding”, “microtubule motor activity” and “microtubule binding” as downregulated (concordant with decreased transcriptional activity and cell cycle processes). This was also mirrored in the GO analyses within the paradigm of biological processes, which describes the larger, more complex biological objectives that differentially regulated genes and their molecular processes contribute to: the upregulated and downregulated terms in this analysis further supported the notion that cell cycle processes are downregulated primarily due to DNA damage response being activated.

More interestingly, when the cellular component that the differentially enriched GO terms were associated with is considered, several terms were highlighted in senescent cells which spoke to a secretory, pro-inflammatory phenotype, which may also modulate the extracellular environment: “extracellular matrix” and “collagen-containing extracellular matrix”, for instance. Indeed, the ECM-remodelling enzymes matrix metalloproteinases, are often contained in the canonical SASP.[150] It should be noted that manner in which senescent HCFs alter collagen deposition in the microenvironment is more well understood than the paracrine ability of CMs to

modulate this phenotype in a paracrine manner, particularly in the specific context of AIC.[400] To interrogate this concept further, a natural next step from the studies in this project would be to expose HCFs to conditioned media from iPSC-CMs induced to senescence with DOX, and then assess the collagen deposition of said HCFs, for instance by evaluating the deposited ratio of collagen I and III matrix (from preclinical studies, a larger collagen I/III ratio can be indicative of fibrosis in AIC).[401]

Furthermore, “external encapsulating structures” were highlighted. This term may refer to a variety of heterogeneous structures, collectively termed extracellular vesicles (EVs). EVs are sometimes termed as cellular “carrier pigeons”, due to their ability to convey signals in a paracrine fashion via their cargo, which can encompass DNA, RNA, lipids, metabolites, and cytosolic and cell-surface proteins.[402] The composition of EV cargo from senescent CMs is still understudied, but it has been shown that cancer cells induced to senescence by DOX produce pro-tumorigenic exosomes.[403] By comparing the data in this thesis with the “inflammatory response” hallmark pathway, it was found that senescent iPSC-CMs are enriched for genes in this pathway. When taken together with the promotion of signalling and enrichment of external encapsulating structures, this may suggest that senescent iPSC-CMs are able to induce a pro-inflammatory response, modulate non-myocyte cell types and affect their microenvironment accordingly. Altogether, due to the significant changes which the “surfaceome” undergoes during induction of senescence, surface biomarkers are emerging as candidate senotherapeutic targets, which may also enable the high-throughput identification of senescent cells via flow cytometry.[404]

5.4.8 Conclusions

Overall, the studies in this chapter were undertaken with the aim of assessing iPSC-CMs for phenotypic changes 10 days following sublethal DOX exposure. RT-qPCR and immunofluorescence studies support the notion that iPSC-CMs acquire a senescent phenotype. The transcriptomic profile of DOX-treated iPSC-CMs was also assessed, in an unbiased manner using bulk RNA-Seq. The RNA-Seq workflow was carried out successfully, and results highlighted that a transcriptomic profile typical of senescence was indeed present in the DOX-treated group. By employing GSEA and GO analyses, it was demonstrated that these senescent iPSC-CMs downregulated many typical cell-cycle processes, and possibly altered OXPHOS metabolism. The surfaceome was flagged as a notably changed cellular compartment in senescent CMs, and inflammation, ECM modulation and secretion were all enriched in this

population, which may have ramifications when considering the role of CMs in maladaptive remodelling, in the progressive cardiotoxicity of DOX.

Chapter 6. General Discussion

6.1 Opening remarks

With 1 in 2 UK adults now predicted to develop cancer at some point in their lives,[2] it is essential that cancer care as a whole continues to improve. Given that many more patients now survive their diagnosis for longer, it is particularly important that cancer survivorship (that is, staying well after cancer treatment/remission) is considered a priority in the field. The development of CVD is emerging as a major cause of mortality in cancer survivor populations.[405] In some cases, the development of CVD later in life after cancer has been linked to cancer treatment itself. Though many anticancer therapies are considered cardiotoxic, anthracycline chemotherapies are particularly notorious for their cardiotoxicity, and this impedes their usefulness in an oncology setting. With ever more patients surviving cancer for longer post-anthracycline treatment, it is feared that "today's cancer patients are tomorrow's heart failure patients". It is therefore of increasing importance that the cardiotoxic mechanisms of the anthracycline family of chemotherapeutics, including DOX, are better understood.

Senescence was classically defined as irreversible exit from the cell cycle following replicative exhaustion (akin to an ageing phenotype),[146] but only relatively recently is the field beginning to understand the complexities of this phenotype. This includes the accompanying secretory phenotype termed the SASP, and the concept that senescence can occur in post-mitotic cells such as CMs. CM senescence in particular is thought to be independent of telomere length, with senescence-inducing stimuli hinging on mitochondrially-derived ROS species,[173] but upstream of this it is thought that irradiation, oncogene activation and pathologies associated with oxidative/genotoxic stress such as diabetes, MI, IRI or chemotherapy can also serve as stimuli.[406] Senescent cells can therefore promote a prematurely aged phenotype due to accumulation following stressors, rather than accumulation purely due to replicative senescence in ageing (i.e. senescence is the increase in "biological age", which is not always associated with "chronological age").[186]

Senescent cells have been shown to play an active role in the promotion of CVD, within and outside of the ageing context.[281,407] CM senescence is also thought to play a role in AIC – this has been demonstrated in a variety of *in vitro* and *in vivo* studies in recent years.[179,180,182] Treatment of dynamically-engineered heart tissues with DOX results in the upregulation of senescence mechanism, alongside reduced force generation and

tissue dilatation.[182] Mitochondria isolated from DOX-treated CMs display mitochondrial DNA (mtDNA) damage, which was associated with increased cell death.[180] Impaired cardiac function in mice was associated with the persistent accumulation of senescent cells – when pharmacogenetically removed, cardiac dysfunction was prevented.[179]

However, several questions remain unaddressed when considering AIC toxicity and the contribution of senescent CMs to AIC pathology. Firstly, several *in vitro* studies have historically used supraclinical concentrations of DOX and acute exposure time courses, which can hinder the understanding of surviving, persistently dysfunctional cardiac cells which likely contribute to chronic disease. Secondly, cell models which faithfully emulate *bona fide* postmitotic CMs are only recently becoming more commonplace – this is a challenge throughout the field of CVD *in vitro* research but is particularly relevant to senescence research given its involvement in cell cycle perturbations. Lastly, the mechanistic understanding of how the CM senescent phenotype might contribute to disease is still poorly understood. Utilising a CM-specific model would allow for selective removal of senescent CMs and pinpointing of any improvements to this cell type specifically, which would add a great deal of insight to current knowledge obtained from systemic p16-knockout mouse models.

The data from this study provide evidence firstly that the AC16 CM cell line has utility as a model of CM senescence. AC16s were able to upregulate the cell cycle inhibitors and classical senescence markers p21 & p16 in response to DOX exposure. AC16s also showed upregulation in complementary senescence-associated transcripts, providing more evidence that this model can be used to capture a senescent phenotype. Secondly, it was demonstrated here that the acquisition of the senescent phenotype in CMs was associated with changes in cell morphology, mitochondrial network morphology, and the cell secretome: senescent AC16 CMs were able to produce a SASP-like secretome which induced promyofibroblast-like changes in human cardiac fibroblasts. Lastly, these concepts were built upon using the gold-standard *in vitro* cell model of iPSC-CMs. The data from this study showed that these cells also display senescence markers after DOX exposure, and they recapitulate previously published senescent transcriptomic signatures well, supporting their work in future mechanistic studies.

6.2 The cytotoxicity of doxorubicin in cardiac cell lineages – "cure at any cost" is no longer the mantra in oncology drug discovery

In the early stages of the project, it was established that DOX is equivalently toxic to the AC10 CM cell line and cardiac fibroblast cells, as it is to a breast cancer cell line, which might be interpreted unfavourably when beginning to consider the drug's safety profile in a cardiovascular context.

When DOX was first synthesised at the end of the 1960s, its safety profile was not assessed in the same way as it would be today, with a standardised battery of chronic *in vitro* and *in vivo* toxicity assays prior to first-in-human trials. Indeed in 1967, a Phase I clinical trial of daunomycin (the biosynthetic precursor to DOX, also cardiotoxic) against leukaemia in a paediatric cohort (n = 28) reported that some patients developed cardiopulmonary symptoms, in some cases congestive heart failure, but stated *"these patients had evidence of wide spread cancer and in most cases, there were adequate explanations for their clinical difficulties. Because these findings occurred, however, in patients who received more than 25 mg/kg of daunomycin, it was necessary to consider the possibility that death was due to a late toxic effect of daunomycin".*[28] Consequent histopathological autopsies on this small cohort were inconclusive, but the finding prompted investigation of the late effects of daunomycin in dogs, and dose limitation in patients going forward. The "cure at any cost" approach in oncology drug discovery at the time contrasts greatly with modern drug safety science approaches, where long-term safety studies are now a prerequisite in the development pipeline.

Years later, it is now known that DOX and its sister anthracycline compounds are indeed toxic to a variety of cell types due to their nonspecific cytotoxic mechanisms, primarily intercalation with DNA and TopII poisoning. This was reflected in the results in this thesis, where TopII-encoding transcripts *TOP2A* and *TOP2B* were significantly downregulated in iPSC-CMs following DOX exposure, and that CMs and cardiac fibroblasts are, unfortunately, equally as vulnerable to acute DOX toxicity as a breast cancer cell line *in vitro*. An MTS assay, as used here, is one standard way of evaluating toxicity of a compound *in vitro*, but to better align with high-throughput screenings of cancer drugs in the literature,[238,239] validating this using luminescence-based CellTiter-Glo methods might better futureproof these acute toxicity results.

However, these acute studies might not recapitulate the molecular mechanisms which contribute to late-onset AIC (as opposed to acute). Therefore, designing an *in vitro* assay with clinical exposures in mind is crucial to investigate how the cytotoxicity of DOX might realistically manifest as late-onset adverse effects in the clinic. For instance, this project focused on the persistent cellular effects which might contribute to chronic AIC, given the delayed-onset nature of this toxicity. It was shown that although some loss in cell viability likely occurs following a DOX exposure, some CMs can survive acute toxicity, but their phenotype is altered chronically - they acquire a senescent phenotype.

6.3 The utility of p16/CDKN2A as a marker of doxorubicin-induced senescence in mature human cardiomyocytes

In agreement with other studies in the literature, results in this thesis found that AC16s were a useful model of cellular senescence.[408,409] AC16s induced the senescence marker p16 at the transcript and protein level following DOX exposure, which contrasts with the findings of Kastury and colleagues, who found that p16 was decreased following senescence-inducing stimuli.[408] Other studies have found that AC16s are capable of increasing p16 expression following stress, but cells did show a strong level of p16 protein expression even in control conditions.[409] Therefore, the results in this thesis fall somewhere outside the findings of these publications.

Some studies show that SV40 immortalisation leads to the constitutive expression of p16.[336] In agreement with this, in both VEH and DOX treatment groups *CDKN2A* transcript was expressed at comparable levels (cycle threshold) to the *RPLP0* housekeeper gene in RT-qPCR experiments, indicating some transcript expression in the absence of senescence-inducing stimulus (data not shown). Contrastingly, results in this project found no detectable expression of p16 protein in non-senescent AC16 CMs using immunofluorescence approaches. Western blotting would offer a more categorical assessment of p16 expression in this cell line, shored up by testing various anti-p16 antibodies which have been previously validated in the literature.

Separate from technical artefacts in immortalised cell lines, the expression of *CDKN2A* transcript in *bona fide* mature adult CMs is debated. RNA-Seq data from senescent iPSC-CMs showed no detectable expression of *CDKN2A* transcript, but robust protein expression in immunocytochemistry studies was seen. Recent seminal studies of the senescent cell transcriptome are concordant with the data in this thesis showing that

CDKN2A is not detectable.[156] Indeed, recent studies of human CM senescence (and separately AIC) more commonly document p16 expression at the protein level: Linders and colleagues provide an elegant, holistic overview of senescence induction using human multicellular models *in vitro* (comprising myocytes and non-myocytes) and AIC patient cardiac tissue samples from autopsy – *CDKN2A* expression is not discussed in autopsy samples, only in the heterogeneous multicellular models.[182] From their findings, it might be speculated that *CDKN2A* is not transcribed at detectable levels in mature human CMs and induction instead occurs at the protein level. Furthermore, it may be hypothesised that increased *CDKN2A* expression in a senescent cardiac microenvironment may originate from non-myocyte populations. These concepts should be considered for future work, where a human CM-specific "checklist" of senescence markers might be developed, which may not incorporate the canonical *CDKN2A* marker. Furthermore, the unbiased transcriptomic techniques used here with senescent iPSC-CMs might be replicated in other cardiac cell lineages (e.g. cardiac fibroblasts, endothelial cells) which might contribute to *CDKN2A* expression throughout the heart.

Though its transcript *CDKN2A* is not as useful as a senescence marker in mature human CMs, p16 in its protein form has been used as a generic marker of senescent cells to generate transgenic mouse models, whereupon p16-expressing cells are induced to apoptosis upon pharmacological stimulation (e.g. Ganciclovir treatment in the p16-3MR model).[161] This whole-body elimination of p16-expressing cells has proved beneficial in mouse models of AIC,[179] but like in other CVD contexts, it is difficult to know which senescent cell population's elimination contributes to improved outcomes. Indeed, senescent circulating CD4+ T cells have been shown to promote cardiac inflammatory shifts which are in line with pathological "inflammageing",[372] so it is worth considering that disease-promoting senescent populations may not even be cardiac-resident.

An alternative model has been developed which allows the knockout of p16 in CMs specifically (driven by the cardiac-specific Myh6 protein).[281] Studies using this mouse line showed that p16 knockout was associated with better outcomes in cardiac remodelling post-MI, which suggests that p16 expression is important for CM senescence driving pathology following MI. Models such as these have been better able to attribute molecular mechanisms of pathology to senescent CMs specifically, separate to other cardiac-resident lineages.[281] Using a CM-specific approach in the

context of AIC *in vivo* models would allow for the unpicking of the role of senescence in CMs and other cell types, within the chronic pathology of AIC.

6.4 Phenotypic changes in senescent cardiomyocytes after doxorubicin exposure – mitochondrial network and function

The phenotype of senescent AC16 CMs following DOX exposure was explored, and it was firstly found that cells were hypertrophic, and that their mitochondrial network seemed comparatively dense, only to discover with more nuanced analyses that the differences in morphology were milder than at first glance. Some authors suggest that a more fragmented network (which may be indicated by the mean shorter branch length in senescent CMs, shown in this thesis), suggests that fission events dominate fusion events.[410] In any case crucially, functional assays were not undertaken in this project, which would be informative about the efficiency of the mitochondrial network in senescent CMs. It may be that despite appearances, the network in DOX-induced senescent CMs is equally as productive as non-senescent CMs.

On a more global scale, the metabolism of senescent CMs could be assessed using the Seahorse system. This would allow the nuanced evaluation of energetic output parameters in DOX-induced senescent vs non-senescent CMs, including maximal respiration, proton leak and ATP-linked respiration, by serially & specifically inhibiting different complexes of the electron transport chain (**Figure 6.1**).

To further explore the underpinning, dynamic characteristics of the mitochondrial network, fission/fusion events and mitophagy events might be examined – these processes must be delicately balanced to effectively maintain the network. Firstly, measuring fission/fusion events is technically challenging but possible: for instance, cell lines can separately be transfected with two different fluorescent probes localised to the mitochondrial matrix, and fusion events can be assessed by quantifying the instances of fluorescent probe co-localisation in isolated mitochondria, and fission events can be assessed using electron microscopy protocols.[410]

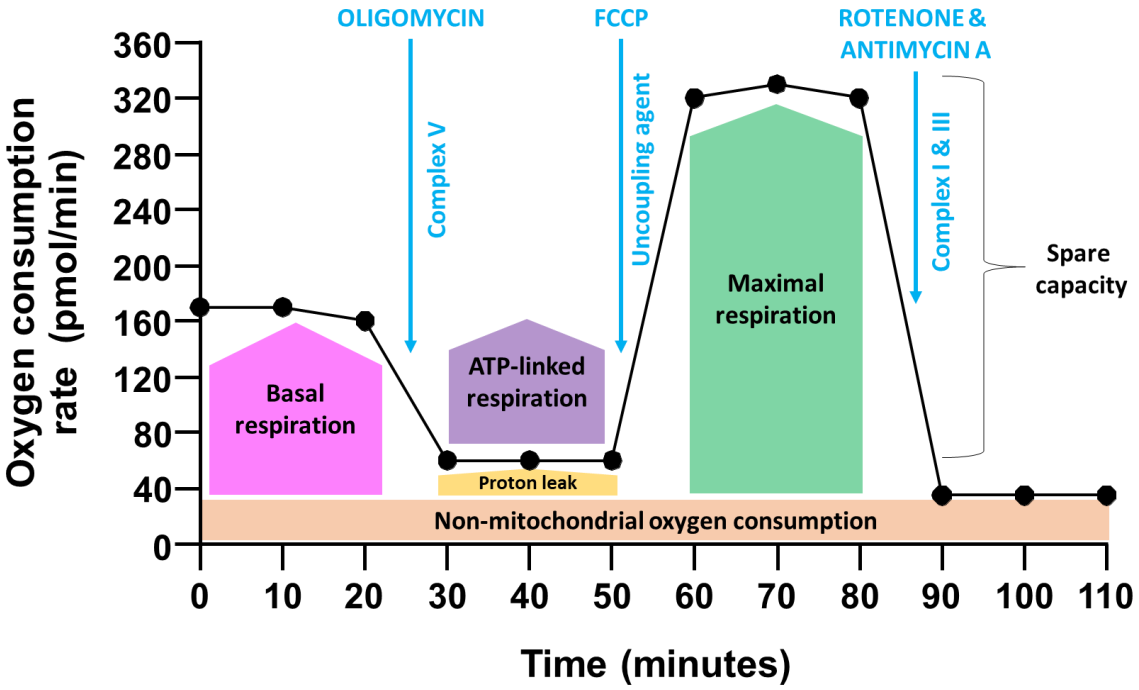

Figure 6.1 Time course schematic of the Seahorse mitochondrial function stress test, outlining parameters which can be measured with the assay. Blue arrows indicate the compounds used to inhibit specific complexes in the electron transport chain, which allows more nuanced investigation of specific parameters rather than energetic output as an amalgamated whole.

With regards to mitophagy, senescent cells are thought to display dampened mitophagy processes, which can be regulated by the PINK1/Parkin pathway.[411] In CMs induced to senescence via DOX, the phosphorylation levels of PINK1 (which increases to induce mitophagy) might be examined using phos-tag approaches or using phospho-specific antibodies. Or recruitment of its downstream signal amplifier Parkin to mitochondria might be tested, by imaging the co-localisation of fluorescent antibody staining, or by fractionating cell lysates to obtain mitochondrial/cytosolic fractions, then probing each for Parkin protein expression. Given that mitophagy is a dynamic process, these approaches might be built upon by measuring mitophagy events in real-time using the fluorescence mt-mKeima reporter, a pH-sensitive mitochondria-targeted fluorescent protein used to monitor delivery of mitochondria (440 nm mt-mKeima excitation at neutral pH) to the lysosome (586 nm excitation at acidic pH).[412]

Finally, there is a strong and long-standing evidence base to suggest that DOX is particularly damaging to mtDNA, more so than nuclear DNA.[413] This has been shown

in preclinical models,[180] but crucially, also in human hearts at autopsy following AIC.[414] Direct damage to mtDNA by DOX, which has been demonstrated at low doses *in vitro*,[180] may be an initiating event which promotes mitochondrial dysfunction downstream via consequent ROS generation (which may contribute to senescence induction) and disruption of mitochondrially-encoded products.

6.5 Looking to the future – the potential of senolytics and senomorphics in treatment of anthracycline-induced cardiotoxicity

There is still a lack of treatment interventions in AIC which specifically target mechanisms of cardiotoxicity. Dexrazoxane remains the only clinically utilised cardioprotective drug in AIC, but its molecular mechanism is still debated today,[415] and it is administered only to certain patient groups, e.g. those receiving a high lifetime cumulative dose of anthracycline.[83] Making the situation more complex, in the subpopulation of patients who develop symptomatic cardiotoxicity, pathological molecular mechanisms may be set into play soon after anthracyclines treatment but remain asymptomatic until a later time – when interventions are less effective, and prognosis is often poorer. It is therefore difficult to know which patients one might administer interventions to in the earlier stages of cardiotoxicity, where disease might be attenuated. Targeting senescent CMs may provide novel therapeutic options in AIC treatment.

To recap, senescent cells can accumulate in the human body with increased age and increased stressor exposure, and these senescent cells contribute to disease (which often tallies with age-related pathologies).[167,298] Senescent cells have specifically been shown to accumulate in the heart after DOX exposure and contribute to side effects of chemotherapy.[179] It is still debated as to how this knowledge might be leveraged to target senescent CMs in the hopes of attenuating toxicity. Senolytic drugs (interventions which induce senescent cells to apoptosis, such as navitoclax, venetoclax and D&Q) and senomorphic drugs (interventions which modulate/prevent the onset of the senescent cell phenotype, such as AICAR, resveratrol and rapamycin) show promise in preclinical models of CVD, but studies in AIC are less common and less well-understood.

The senolytic navitoclax (which targets the BCL-2 family of pro-survival proteins) has been successfully used in a murine model of DOX toxicity – in the navitoclax-treated mice, data showed a significant decrease in senescence and cardiotoxicity markers,

alongside restoration of cardiac function as measured by echocardiography.[181] Importantly, this study used a co-treatment of navitoclax and DOX, i.e. a prophylactic treatment to target senescence/disease as it develops, rather than waiting for symptoms to appear, the latter which might not translate favourably into the clinic. Though it was not shown by the authors which senescent cells were removed by the systemic navitoclax treatment, myocardial senescence was shown to decrease overall. It is likely that this treatment eliminated multiple senescent cell types at once, and with them their pro-inflammatory SASP – this may attenuate inflammation and myocardial remodelling, which has been shown to reduce both fibrosis and hypertrophy in the context of ageing and IRI.[173,174] Regarding the transcript levels of BCL-2 family members in RNA-Seq data, in senescent AC16 CMs post-DOX *Bcl2* was significantly upregulated (see **3.3.6**), but in the iPSC-CM model *Bcl2* was non-significantly upregulated in senescence and furthermore was expressed at a relatively low level in terms of normalised reads. However, *BCL2L1* (which encodes for BCL-XL protein) and *BCL2L2* (which encodes for BCL-W protein), were both significantly upregulated in senescence and robustly expressed overall (data not shown). Therefore, BCL-2 protein family inhibitors such as navitoclax may be effective in eliminating senescent CMs in the context of AIC, but further studies should verify that these transcriptomic changes translate to the protein level in the first instance.

According to a phase II clinical trial, the safety profile of navitoclax appears promising in the treatment of myelofibrosis (as an additive to the standard-of-care JAK inhibitor ruxolitinib) – although thrombocytopaenia was acknowledged as an adverse (but manageable) effect of navitoclax, no notable adverse cardiovascular effects were reported.[168] Importantly however, it was noted that in some patients, the beneficial effect of adding to navitoclax to ruxolitinib treatment was achieved as late as week 72 post-treatment, suggesting that this combination therapy may have a positive impact which takes longer than 24 weeks to manifest – therefore longer-term follow up of the benefit and safety profile of navitoclax in these patients may be warranted (> 29 months in the trial). Given that senolytics eliminate senescent cells via the induction of apoptosis, and that the heart has limited regenerative potential,[48] questions remain regarding the long-term safety of senolytics since myocardial cell death (particularly in the CM population) is usually associated with adverse outcomes.[4,16]

To this end, senomorphic drugs have attracted attention as a more favourable therapeutic strategy. Encouraging studies have shown that the senomorphic drug

metformin (which reduces cardiovascular mortality and cardiovascular events in patients suffering from coronary heart disease, and has demonstrated senomorphic activity suppressing senescence and SASP expression in a variety of cell populations)[417-420] has a cardioprotective effect in small animal models of AIC.[421] Although the precise mechanisms by which metformin elicits its cardioprotective effect are not fully understood, it is possible that interference with the senescent phenotype may contribute. However, even senomorphic drugs are not without controversy. Linders and colleagues recently demonstrated that although treatment of contractile engineered human heart tissues with senomorphics AICAR and resveratrol alongside DOX prevented onset of senescence, the tissues exhibited increased apoptosis and fibrosis.[182] This was associated with no improvement in function (resveratrol) or diminished function (AICAR, worsened contractility and dilation). These findings challenge the notion that inhibition of the senescent phenotype would be beneficial in AIC.

Senescence, for all its involvement in the promotion of CVD in ageing and AIC, does have a physiological role to play in some contexts. Murine models have shown that elimination of $p16^{+ve}$ liver sinusoid cells was not followed by the generation of non-senescent cells to replace them, and this contributed to liver and perivascular tissue fibrosis – i.e. $p16^{+ve}$ liver sinusoid cells were both structurally and functionally important at the whole-organ level.[422] In a cardiovascular context, inhibiting the early induction of senescence in myofibroblasts in a model of pressure overload-induced cardiac hypertrophy was shown to be associated with aggravated myocardial fibrosis and impaired cardiac function.[423] The adverse effects of inhibiting the fundamental cellular phenotype of senescence, which contributes to both pathology and physiology must therefore always be considered. Indeed, these studies together highlight the pleiotropic antagonism of this phenotype: attenuating senescence in a targeted manner at the right time may ameliorate mechanisms of disease in AIC, but further studies are needed to solidify the understanding of this intervention.

References

1. Smittenaar CR, Petersen KA, Stewart K, Moitt N. Cancer incidence and mortality projections in the UK until 2035. *Br J Cancer*. 2016;115:1147-1155. doi: 10.1038/bjc.2016.304

2. Ahmad AS, Ormiston-Smith N, Sasieni PD. Trends in the lifetime risk of developing cancer in Great Britain: comparison of risk for those born from 1930 to 1960. *British Journal of Cancer*. 2015;112:943-947. doi: 10.1038/bjc.2014.606
3. National Cancer Institute. Survivorship. In: *NCI Dictionary of Cancer Terms*.
4. Hart NH, Crawford-Williams F, Crichton M, Yee J, Smith TJ, Koczwara B, Fitch MI, Crawford GB, Mukhopadhyay S, Mahony J, et al. Unmet supportive care needs of people with advanced cancer and their caregivers: A systematic scoping review. *Critical Reviews in Oncology/Hematology*. 2022;176:103728. doi: https://doi.org/10.1016/j.critrevonc.2022.103728
5. Mandelblatt JS, Small BJ, Luta G, Hurria A, Jim H, McDonald BC, Graham D, Zhou X, Clapp J, Zhai W, et al. Cancer-Related Cognitive Outcomes Among Older Breast Cancer Survivors in the Thinking and Living With Cancer Study. *Journal of Clinical Oncology*. 2018;36:3211-3222. doi: 10.1200/jco.18.00140
6. Oeffinger KC, Mertens AC, Sklar CA, Kawashima T, Hudson MM, Meadows AT, Friedman DL, Marina N, Hobbie W, Kadan-Lottick NS, et al. Chronic Health Conditions in Adult Survivors of Childhood Cancer. *New England Journal of Medicine*. 2006;355:1572-1582. doi: 10.1056/NEJMsa060185
7. Delaney A, Howell CR, Krull KR, Brinkman TM, Armstrong GT, Chemaitilly W, Wilson CL, Mulrooney DA, Wang Z, Lanctot JQ, et al. Progression of Frailty in Survivors of Childhood Cancer: A St. Jude Lifetime Cohort Report. *JNCI: Journal of the National Cancer Institute*. 2021;113:1415-1421. doi: 10.1093/jnci/djab033
8. Walter AW, Mulhern RK, Gajjar A, Heideman RL, Reardon D, Sanford RA, Xiong X, Kun LE. Survival and Neurodevelopmental Outcome of Young Children With Medulloblastoma at St Jude Children's Research Hospital. *Journal of Clinical Oncology*. 1999;17:3720-3728. doi: 10.1200/jco.1999.17.12.3720
9. Chevignard M, Câmara-Costa H, Doz F, Dellatolas G. Core deficits and quality of survival after childhood medulloblastoma: a review. *Neuro-Oncology Practice*. 2016;4:82-97. doi: 10.1093/nop/npw013
10. Mertens AC, Yasui Y, Neglia JP, Potter JD, Nesbit Jr ME, Ruccione K, Smithson WA, Robison LL. Late mortality experience in five-year survivors of childhood and adolescent cancer: the Childhood Cancer Survivor Study. *Journal of Clinical Oncology*. 2001;19:3163-3172.

11. Tukenova M, Guibout C, Oberlin O, Doyon F, Mousannif A, Haddy N, Guérin S, Pacquement H, Aouba A, Hawkins M. Role of cancer treatment in long-term overall and cardiovascular mortality after childhood cancer. *J Clin Oncol*. 2010;28:1308-1315.
12. Blaes AH, Konety SH. Cardiovascular Disease in Breast Cancer Survivors: An Important Topic in Breast Cancer Survivorship. *JNCI: Journal of the National Cancer Institute*. 2020;113:105-106. doi: 10.1093/jnci/djaa097
13. Greenlee H, Iribarren C, Rana JS, Cheng R, Nguyen-Huynh M, Rillamas-Sun E, Shi Z, Laurent CA, Lee VS, Roh JM, et al. Risk of Cardiovascular Disease in Women With and Without Breast Cancer: The Pathways Heart Study. *Journal of Clinical Oncology*. 2022;40:1647-1658. doi: 10.1200/jco.21.01736
14. Abdel-Qadir H, Thavendiranathan P, Austin PC, Lee DS, Amir E, Tu JV, Fung K, Anderson GM. The Risk of Heart Failure and Other Cardiovascular Hospitalizations After Early Stage Breast Cancer: A Matched Cohort Study. *JNCI: Journal of the National Cancer Institute*. 2019;111:854-862. doi: 10.1093/jnci/djy218
15. Lu Z, Teng Y, Ning X, Wang H, Feng W, Ou C. Long-term risk of cardiovascular disease mortality among classic Hodgkin lymphoma survivors. *Cancer*. 2022;128:3330-3339. doi: https://doi.org/10.1002/cncr.34375
16. Vaz-Luis I, Masiero M, Cavaletti G, Cervantes A, Chlebowski RT, Curigliano G, Felip E, Ferreira AR, Ganz PA, Hegarty J, et al. ESMO Expert Consensus Statements on Cancer Survivorship: promoting high-quality survivorship care and research in Europe. *Annals of Oncology*. 2022;33:1119-1133. doi: https://doi.org/10.1016/j.annonc.2022.07.1941
17. Brockmann H, Bauer K. *Naturwissenschaften*. 1950:492.
18. Grein A, Spalla C, Di Marco A, Canevazzi G. Descrizione e Classificazione di un Atinomicete (Streptomyces peucetius sp. nova) Produttore di una Sostanza ad Attivita Antitumorale: La Daunomicina. *Giornale di microbiologia*. 1963;11:109.
19. D'bost M, Ganter P, Maral R, Ninet L, Pinnert S, Preud'Homme J, Werner GH. Un novel antibiotique a proprietes cytostatiques: la rubidomycine. *CR Acad Sci Agric Bulg*. 1963;257:1813-1815.
20. Di Marco A, Gaetani M, Orezzi P, Scarpinato BM, Silvestrini R, Soldati M, Dasdia T, Valentini L. 'Daunomycin', a New Antibiotic of the Rhodomycin Group. *Nature*. 1964;201:706-707. doi: 10.1038/201706a0

21. Patrick GL. Nucleic Acids as Drug Targets. In: *An Introduction to Medicinal Chemistry*. Oxford University Press; 2013:120-134.
22. Capranico G, Tinelli S, Austin CA, Fisher ML, Zunino F. Different patterns of gene expression of topoisomerase II isoforms in differentiated tissues during murine development. *Biochimica et Biophysica Acta (BBA) - Gene Structure and Expression*. 1992;1132:43-48. doi: https://doi.org/10.1016/0167-4781(92)90050-A
23. World Health Organization. World Health Organization Model List of Essential Medicines, 21st List, 2019. In: Geneva: World Health Organization; 2019; 2019.
24. Baxter Healthcare Corporation. DOXIL: Doxorubicin Hydrochloride Liposome Injection, for intravenous use. In: U.S. Food and Drug Administration; 2022.
25. Pfizer. DOXORUBICIN HYDROCHLORIDE injection, for intravenous use. In: *FDA*. 2019.
26. Luqmani YA. Mechanisms of Drug Resistance in Cancer Chemotherapy. *Med Princ Pract*. 2005;14(suppl 1):35-48. doi: 10.1159/000086183
27. Herman EH, Schein P, Farmar RM. Comparative cardiac toxicity of daunomycin in three rodent species. *Proc Soc Exp Biol Med*. 1969;130:1098-1102. doi: 10.3181/00379727-130-33727
28. Tan C, Tasaka H, Yu K-P, Murphy ML, Karnofsky DA. Daunomycin, an antitumor antibiotic, in the treatment of neoplastic disease. Clinical evaluation with special reference to childhood leukemia. *Cancer*. 1967;20:333-353. doi: https://doi.org/10.1002/1097-0142(1967)20:3<333::AID-CNCR2820200302>3.0.CO;2-K
29. Lefrak EA, Pit'ha J, Rosenheim S, Gottlieb JA. A clinicopathologic analysis of adriamycin cardiotoxicity. *Cancer*. 1973;32:302-314. doi: 10.1002/1097-0142(197308)32:2<302::AID-CNCR2820320205>3.0.CO;2-2
30. O'Bryan RM, Luce JK, Talley RW, Gottlieb JA, Baker LH, Bonadonna G. Phase II evaluation of adriamycin in human neoplasia. *Cancer*. 1973;32:1-8. doi: 10.1002/1097-0142(197307)32:1<1::aid-cncr2820320101>3.0.co;2-x
31. Von Hoff DD, Layard MW, Basa P, Davis HL, Von Hoff AL, Rozencweig M, Muggia FM. Risk Factors for Doxorubicin-Induced Congestive Heart Failure. *Ann Intern Med*. 1979;91:710-717. doi: 10.7326/0003-4819-91-5-710
32. Doxorubicin hydrochloride [Specialist drug]. National Institute for Healthcare Excellence: British National Formulary. https://bnf.nice.org.uk/drugs/doxorubicin-hydrochloride-specialist-

drug/#:~:text=Healthcare%20professionals%20are%20advised%20to,dose%20should%20not%20be%20exceeded.

33. Swain SM, Whaley FS, Ewer MS. Congestive heart failure in patients treated with doxorubicin. *Cancer*. 2003;97:2869-2879. doi: https://doi.org/10.1002/cncr.11407
34. Bansal N, Amdani SM, Hutchins KK, Lipshultz SE. Cardiovascular disease in survivors of childhood cancer. *Current Opinion in Pediatrics*. 2018;30.
35. Lipshultz SE, Colan SD, Gelber RD, Perez-Atayde AR, Sallan SE, Sanders SP. Late cardiac effects of doxorubicin therapy for acute lymphoblastic leukemia in childhood. *N Engl J Med*. 1991;324:808-815. doi: 10.1056/NEJM199103213241205
36. Giantris A, Abdurrahman L, Hinkle A, Asselin B, Lipshultz SE. Anthracycline-induced cardiotoxicity in children and young adults. *Critical Reviews in Oncology Hematology*. 1997;27:53-68.
37. Cardinale D, Colombo A, Bacchiani G, Tedeschi I, Meroni CA, Veglia F, Civelli M, Lamantia G, Colombo N, Curigliano G, et al. Early Detection of Anthracycline Cardiotoxicity and Improvement With Heart Failure Therapy. *Circulation*. 2015;131:1981-1988. doi: doi:10.1161/CIRCULATIONAHA.114.013777
38. D'Agostino RB, Vasan RS, Pencina MJ, Wolf PA, Cobain M, Massaro JM, Kannel WB. General Cardiovascular Risk Profile for Use in Primary Care. *Circulation*. 2008;117:743-753. doi: doi:10.1161/CIRCULATIONAHA.107.699579
39. Chow EJ, Chen Y, Armstrong GT, Baldwin LM, Cai CR, Gibson TM, Hudson MM, McDonald A, Nathan PC, Olgin JE, et al. Underdiagnosis and Undertreatment of Modifiable Cardiovascular Risk Factors Among Survivors of Childhood Cancer. *Journal of the American Heart Association*. 2022;11:e024735. doi: doi:10.1161/JAHA.121.024735
40. Goldberg JF, Ness KK, Chi X, Santucci AK, Plana JC, Joshi VM, Luepker RV, Durand JB, Partin RE, Howell RM, et al. Cardiovascular Family History Increases Risk for Late-Onset Adverse Cardiovascular Outcomes in Childhood Cancer Survivors: A St. Jude Lifetime Cohort Report. *Cancer Epidemiol Biomarkers Prev*. 2021;30:123-132. doi: 10.1158/1055-9965.Epi-20-0809
41. Díaz-Gavela AA, Figueiras-Graillet L, Luis Á M, Salas Segura J, Ciérvide R, Del Cerro Peñalver E, Couñago F, Arenas M, López-Fernández T. Breast

Radiotherapy-Related Cardiotoxicity. When, How, Why. Risk Prevention and Control Strategies. *Cancers (Basel)*. 2021;13. doi: 10.3390/cancers13071712

42. Screever EM, Meijers WC, Moslehi JJ. Age-Related Considerations in Cardio-Oncology. *Journal of Cardiovascular Pharmacology and Therapeutics*. 2021;26:103-113. doi: 10.1177/1074248420968689
43. Lipshultz SE, Lipsitz SR, Mone SM, Goorin AM, Sallan SE, Sanders SP, Orav EJ, Gelber RD, Colan SD. Female sex and higher drug dose as risk factors for late cardiotoxic effects of doxorubicin therapy for childhood cancer. *N Engl J Med*. 1995;332:1738-1743. doi: 10.1056/NEJM199506293322602
44. Fradley MG. Heart Failure in Patients With Cancer Treated With Anthracyclines—Revisiting the Foundation of Cardio-Oncology. *JAMA Network Open*. 2023;6:e2254677-e2254677. doi: 10.1001/jamanetworkopen.2022.54677
45. Larsen CM, Garcia Arango M, Dasari H, Arciniegas Calle M, Adjei E, Rico Mesa J, Scott CG, Thompson CA, Cerhan JR, Haddad TC, et al. Association of Anthracycline With Heart Failure in Patients Treated for Breast Cancer or Lymphoma, 1985-2010. *JAMA Network Open*. 2023;6:e2254669-e2254669. doi: 10.1001/jamanetworkopen.2022.54669
46. Lipshultz SE, Lipsitz SR, Sallan SE, Dalton VM, Mone SM, Gelber RD, Colan SD. Chronic progressive cardiac dysfunction years after doxorubicin therapy for childhood acute lymphoblastic leukemia. *J Clin Oncol*. 2005;23:2629-2636. doi: 10.1200/JCO.2005.12.121
47. Lipshultz SE, Scully RE, Stevenson KE, Franco VI, Neuberg DS, Colan SD, Silverman LB, Moslehi JJ, Cheng S, Sallan SE. Hearts too small for body size after doxorubicin for childhood ALL: Grinch syndrome. *J Clin Orthod*. 2014;32:10021-10021. doi: 10.1200/jco.2014.32.15_suppl.10021
48. Bergmann O, Zdunek S, Felker A, Salehpour M, Alkass K, Bernard S, Sjostrom SL, Szewczykowska M, Jackowska T, Dos Remedios C, et al. Dynamics of Cell Generation and Turnover in the Human Heart. *Cell*. 2015;161:1566-1575. doi: 10.1016/j.cell.2015.05.026
49. Billingham ME, Mason JW, Birstow MR, Daniels JR. Anthracycline Cardiomyopathy Monitored by Morphologic Changes. *Cancer Treat Rep*. 1978;62:865-872.

50. BRISTOW MR, MASON JW, BILLINGHAM ME, DANIELS JR. Doxorubicin cardiomyopathy: evaluation by phonocardiography, endomyocardial biopsy, and cardiac catheterization. *Annals of internal medicine*. 1978;88:168-175.
51. Bernaba BN, Chan JB, Lai CK, Fishbein MC. Pathology of late-onset anthracycline cardiomyopathy. *Cardiovascular Pathology*. 2010;19:308-311. doi: https://doi.org/10.1016/j.carpath.2009.07.004
52. Jefferies JL, Mazur WM, Howell CR, Plana JC, Ness KK, Li Z, Joshi VM, Green DM, Mulrooney DA, Towbin JA, et al. Cardiac remodeling after anthracycline and radiotherapy exposure in adult survivors of childhood cancer: A report from the St Jude Lifetime Cohort Study. *Cancer*. 2021;127:4646-4655. doi: https://doi.org/10.1002/cncr.33860
53. Chan BYH, Roczkowsky A, Cho WJ, Poirier M, Sergi C, Keschrumrus V, Churko JM, Granzier H, Schulz R. MMP inhibitors attenuate doxorubicin cardiotoxicity by preventing intracellular and extracellular matrix remodelling. *Cardiovascular Research*. 2020;117:188-200. doi: 10.1093/cvr/cvaa017
54. Lushnikova EL, Klinnikova MG, Molodykh OP, Nepomnyashchikh LM. Morphological manifestations of heart remodeling in anthracycline-induced dilated cardiomyopathy. *Bulletin of Experimental Biology and Medicine*. 2004;138:607-612. doi: 10.1007/s10517-005-0138-0
55. Meléndez GC, Jordan JH, D'Agostino RB, Jr., Lesnefsky EJ, Hundley WG. Accelerated Left Ventricular Interstitial Collagen Deposition After Receiving Doxorubicin in Hypertension. *J Am Coll Cardiol*. 2018;72:1555-1557. doi: 10.1016/j.jacc.2018.07.028
56. Bruggink AH, de Jonge N, van Oosterhout MFM, Van Wichen DF, de Koning E, Lahpor JR, Kemperman H, Gmelig-Meyling FHJ, de Weger RA. Brain Natriuretic Peptide is Produced Both by Cardiomyocytes and Cells Infiltrating the Heart in Patients with Severe Heart Failure Supported by a Left Ventricular Assist Device. *The Journal of Heart and Lung Transplantation*. 2006;25:174-180. doi: https://doi.org/10.1016/j.healun.2005.09.007
57. Sutanto H, Dobrev D, Heijman J. Angiotensin Receptor-Neprilysin Inhibitor (ARNI) and Cardiac Arrhythmias. *International Journal of Molecular Sciences*. 2021;22:8994.
58. Cheng V, Kazanagra R, Garcia A, Lenert L, Krishnaswamy P, Gardetto N, Clopton P, Maisel A. A rapid bedside test for B-type peptide predicts treatment outcomes in patients admitted for decompensated heart failure: a pilot study.

Journal of the American College of Cardiology. 2001;37:386-391. doi: doi:10.1016/S0735-1097(00)01157-8

59. Maisel AS, McCord J, Nowak RM, Hollander JE, Wu AHB, Duc P, Omland T, Storrow AB, Krishnaswamy P, Abraham WT, et al. Bedside B-Type natriuretic peptide in the emergency diagnosis of heart failure with reduced or preserved ejection fraction. *Journal of the American College of Cardiology*. 2003;41:2010-2017. doi: doi:10.1016/S0735-1097(03)00405-4
60. Yamamoto K, Burnett JC, Jougasaki M, Nishimura RA, Bailey KR, Saito Y, Nakao K, Redfield MM. Superiority of Brain Natriuretic Peptide as a Hormonal Marker of Ventricular Systolic and Diastolic Dysfunction and Ventricular Hypertrophy. *Hypertension*. 1996;28:988-994. doi: doi:10.1161/01.HYP.28.6.988
61. Rothenburger M, Wichter T, Schmid C, Stypmann J, Tjan TDT, Berendes E, Etz C, Pioux A, Löher A, Wenzelburger F, et al. Aminoterminal pro type B natriuretic peptide as a predictive and prognostic marker in patients with chronic heart failure. *The Journal of Heart and Lung Transplantation*. 2004;23:1189-1197. doi: https://doi.org/10.1016/j.healun.2004.07.006
62. Gomes AV, Potter JD, Szczesna-Cordary D. The role of troponins in muscle contraction. *IUBMB Life*. 2002;54:323-333. doi: 10.1080/15216540216037
63. Park KC, Gaze DC, Collinson PO, Marber MS. Cardiac troponins: from myocardial infarction to chronic disease. *Cardiovascular Research*. 2017;113:1708-1718. doi: 10.1093/cvr/cvx183
64. Austin D, Maier RH, Akhter N, Sayari M, Ogundimu E, Maddox JM, Vahabi S, Humphreys AC, Graham J, Oxenham H. Preventing Cardiac Damage in Patients Treated for Breast Cancer and Lymphoma: The PROACT Clinical Trial. *JACC: CardioOncology*. 2024.
65. Ponikowski P, Voors AA, Anker SD, Bueno H, Cleland JGF, Coats AJS, Falk V, González-Juanatey JR, Harjola VP, Jankowska EA, et al. 2016 ESC Guidelines for the diagnosis and treatment of acute and chronic heart failure: The Task Force for the diagnosis and treatment of acute and chronic heart failure of the European Society of Cardiology (ESC)Developed with the special contribution of the Heart Failure Association (HFA) of the ESC. *Eur Heart J*. 2016;37:2129-2200. doi: 10.1093/eurheartj/ehw128
66. Nagiub M, Nixon JV, Kontos MC. Ability of Nonstrain Diastolic Parameters to Predict Doxorubicin-Induced Cardiomyopathy: A Systematic Review With Meta-

Analysis. *Cardiology in Review*. 2018;26:29-34. doi: 10.1097/crd.0000000000000161

67. Upshaw JN, Finkelman B, Hubbard RA, Smith AM, Narayan HK, Arndt L, Domchek S, DeMichele A, Fox K, Shah P, et al. Comprehensive Assessment of Changes in Left Ventricular Diastolic Function With Contemporary Breast Cancer Therapy. *JACC: Cardiovascular Imaging*. 2020;13:198-210. doi: doi:10.1016/j.jcmg.2019.07.018
68. Upshaw J. HFpEF After Cancer Therapy. https://www.acc.org/latest-in-cardiology/articles/2020/10/26/13/08/hfpef-after-cancer-therapy. 2020.
69. Ferreira de Souza T, Quinaglia T, Neilan TG, Coelho-Filho OR. Assessment of Cardiotoxicity of Cancer Chemotherapy: The Value of Cardiac MR Imaging. *Magn Reson Imaging Clin N Am*. 2019;27:533-544. doi: 10.1016/j.mric.2019.04.001
70. Mabudian L, Jordan JH, Bottinor W, Hundley WG. Cardiac MRI assessment of anthracycline-induced cardiotoxicity. *Front Cardiovasc Med*. 2022;9:903719. doi: 10.3389/fcvm.2022.903719
71. Rector TS, Kubo SH, Kohn JN. Patient's Self-Assessment of Their Congestive Heart Failure: Content, reliability and validity of a new measure, the Minnesota Living with Heart Failure Questionnaire. *Heart failure*. 1987;3:198-209.
72. Garin O, Ferrer M, Pont À, Rué M, Kotzeva A, Wiklund I, Van Ganse E, Alonso J. Disease-specific health-related quality of life questionnaires for heart failure: a systematic review with meta-analyses. *Quality of Life Research*. 2009;18:71-85. doi: 10.1007/s11136-008-9416-4
73. Malhotra R, Bakken K, D'Elia E, Lewis GD. Cardiopulmonary Exercise Testing in Heart Failure. *JACC: Heart Failure*. 2016;4:607-616. doi: doi:10.1016/j.jchf.2016.03.022
74. Chow EJ, Leger KJ, Bhatt NS, Mulrooney DA, Ross CJ, Aggarwal S, Bansal N, Ehrhardt MJ, Armenian SH, Scott JM, et al. Paediatric cardio-oncology: epidemiology, screening, prevention, and treatment. *Cardiovascular Research*. 2019;115:922-934. doi: 10.1093/cvr/cvz031
75. Henriksen PA. Anthracycline cardiotoxicity: an update on mechanisms, monitoring and prevention. *Heart*. 2018;104:971-977. doi: 10.1136/heartjnl-2017-312103
76. Armenian SH, Hudson MM, Mulder RL, Chen MH, Constine LS, Dwyer M, Nathan PC, Tissing WJ, Shankar S, Sieswerda E. Recommendations for

cardiomyopathy surveillance for survivors of childhood cancer: a report from the International Late Effects of Childhood Cancer Guideline Harmonization Group. *The Lancet Oncology*. 2015;16:e123-e136.

77. Lu X, Zhao Y, Chen C, Han C, Xue L, Xing D, Huang O, Tao M. BNP as a marker for early prediction of anthracycline-induced cardiotoxicity in patients with breast cancer. *Oncol Lett*. 2019;18:4992-5001. doi: 10.3892/ol.2019.10827
78. Wallace KB, Hausner E, Herman E, Holt GD, Macgregor JT, Metz AL, Murphy E, Rosenblum IY, Sistare FD, York MJ. Serum Troponins as Biomarkers of Drug-Induced Cardiac Toxicity. *Toxicologic Pathology*. 2004;32:106-121. doi: 10.1080/01926230490261302
79. Langer SW. Dexrazoxane for the treatment of chemotherapy-related side effects. *Cancer Manag Res*. 2014;6:357-363. doi: 10.2147/cmar.S47238
80. Herman E, Ferrans V. Influence of vitamin E and ICRF-187 on chronic doxorubicin cardiotoxicity in miniature swine. *Laboratory investigation; a journal of technical methods and pathology*. 1983;49:69-77.
81. Herman E, Ferrans V, Young R, Hamlin R. Pretreatment with ICRF-187 allows a marked increase in the total cumulative dose of doxorubicin tolerated by beagle dogs. *Drugs under experimental and clinical research*. 1988;14:563-570.
82. Herman EH, Ferrans VJ. Preclinical animal models of cardiac protection from anthracycline-induced cardiotoxicity. Paper/Poster presented at: Seminars in oncology; 1998;
83. Pfizer. ZINECARD® (dexrazoxane) for injection - FDA. In: U.S. Food and Drug Administration; 1995.
84. European Medicines Agency. Questions and Answers on Cardioxane (dexrazoxane, powder for solution for injection, 500 mg). In; 2017.
85. Tebbi CK, London WB, Friedman D, Villaluna D, Alarcon PAD, Constine LS, Mendenhall NP, Sposto R, Chauvenet A, Schwartz CL. Dexrazoxane-Associated Risk for Acute Myeloid Leukemia/Myelodysplastic Syndrome and Other Secondary Malignancies in Pediatric Hodgkin's Disease. *Journal of Clinical Oncology*. 2007;25:493-500. doi: 10.1200/jco.2005.02.3879
86. Lipshultz SE, Scully RE, Lipsitz SR, Sallan SE, Silverman LB, Miller TL, Barry EV, Asselin BL, Athale U, Clavell LA, et al. Assessment of dexrazoxane as a cardioprotectant in doxorubicin-treated children with high-risk acute lymphoblastic leukaemia: long-term follow-up of a prospective, randomised,

multicentre trial. *The Lancet Oncology*. 2010;11:950-961. doi: https://doi.org/10.1016/S1470-2045(10)70204-7

87. Chow EJ, Aggarwal S, Doody DR, Aplenc R, Armenian SH, Baker KS, Bhatia S, Blythe N, Colan SD, Constine LS, et al. Dexrazoxane and Long-Term Heart Function in Survivors of Childhood Cancer. *Journal of Clinical Oncology*. 2023;41:2248-2257. doi: 10.1200/jco.22.02423
88. Schuler MK, Gerdes S, West A, Richter S, Busemann C, Hentschel L, Lenz F, Kopp HG, Ehninger G, Reichardt P, et al. Efficacy and safety of Dexrazoxane (DRZ) in sarcoma patients receiving high cumulative doses of anthracycline therapy - a retrospective study including 32 patients. *BMC Cancer*. 2016;16:619. doi: 10.1186/s12885-016-2654-x
89. Lyu YL, Kerrigan JE, Lin C-P, Azarova AM, Tsai Y-C, Ban Y, Liu LF. Topoisomerase IIbeta mediated DNA double-strand breaks: implications in doxorubicin cardiotoxicity and prevention by dexrazoxane. *Cancer Res*. 2007;67:8839-8846. doi: 10.1158/0008-5472.CAN-07-1649
90. Brown NJ, Vaughan DE. Angiotensin-Converting Enzyme Inhibitors. *Circulation*. 1998;97:1411-1420. doi: doi:10.1161/01.CIR.97.14.1411
91. Yusuf S, Pitt B, Davis CE, Hood WB, Cohn JN. Effect of enalapril on survival in patients with reduced left ventricular ejection fractions and congestive heart failure. *N Engl J Med*. 1991;325:293-302. doi: 10.1056/nejm199108013250501
92. Effects of enalapril on mortality in severe congestive heart failure. Results of the Cooperative North Scandinavian Enalapril Survival Study (CONSENSUS). *N Engl J Med*. 1987;316:1429-1435. doi: 10.1056/nejm198706043162301
93. Singh KD, Karnik SS. Angiotensin Type 1 Receptor Blockers in Heart Failure. *Curr Drug Targets*. 2020;21:125-131. doi: 10.2174/1389450120666190821152000
94. Masarone D, Martucci ML, Errigo V, Pacileo G. The Use of β-Blockers in Heart Failure with Reduced Ejection Fraction. *J Cardiovasc Dev Dis*. 2021;8. doi: 10.3390/jcdd8090101
95. Lipshultz SE, Lipsitz SR, Sallan SE, II VCS, Shaikh SL, Mone SM, Gelber RD, Colan SD. Long-Term Enalapril Therapy for Left Ventricular Dysfunction in Doxorubicin-Treated Survivors of Childhood Cancer. *Journal of Clinical Oncology*. 2002;20:4517-4522. doi: 10.1200/jco.2002.12.102
96. Heck SL, Mecinaj A, Ree AH, Hoffmann P, Schulz-Menger J, Fagerland MW, Gravdehaug B, Røsjø H, Steine K, Geisler J, et al. Prevention of Cardiac

Dysfunction During Adjuvant Breast Cancer Therapy (PRADA): Extended Follow-Up of a 2×2 Factorial, Randomized, Placebo-Controlled, Double-Blind Clinical Trial of Candesartan and Metoprolol. *Circulation*. 2021;143:2431-2440. doi: doi:10.1161/CIRCULATIONAHA.121.054698

97. Attar A, Behnagh AK, Hosseini M, Amanollahi F, Shafiekhani P, Kabir A. Beta-Blockers for Primary Prevention of Anthracycline-Induced Cardiac Toxicity: An Updated Meta-Analysis of Randomized Clinical Trials. *Cardiovasc Ther*. 2022;2022:8367444. doi: 10.1155/2022/8367444
98. Henriksen PA, Hall P, MacPherson IR, Joshi SS, Singh T, Maclean M, Lewis S, Rodriguez A, Fletcher A, Everett RJ, et al. Multicenter, Prospective, Randomized Controlled Trial of High-Sensitivity Cardiac Troponin I–Guided Combination Angiotensin Receptor Blockade and Beta-Blocker Therapy to Prevent Anthracycline Cardiotoxicity: The Cardiac CARE Trial. *Circulation*. 2023;148:1680-1690. doi: doi:10.1161/CIRCULATIONAHA.123.064274
99. Shugh SB, Ryan TD. Heart transplantation in survivors of childhood cancer. *Transl Pediatr*. 2019;8:314-321. doi: 10.21037/tp.2019.06.02
100. Bock MJ, Pahl E, Rusconi PG, Boyle GJ, Parent JJ, Twist CJ, Kirklin JK, Pruitt E, Bernstein D. Cancer recurrence and mortality after pediatric heart transplantation for anthracycline cardiomyopathy: A report from the Pediatric Heart Transplant Study (PHTS) group. *Pediatric transplantation*. 2017;21:e12923.
101. NHS Blood and Transplant. Annual Report on Heart Transplantation 2022/2023. In; 2023.
102. Gille L, Nohl H. Analyses of the Molecular Mechanism of Adriamycin-Induced Cardiotoxicity. *Free Radical Biology and Medicine*. 1997;23:775-782. doi: https://doi.org/10.1016/S0891-5849(97)00025-7
103. Licata S, Saponiero A, Mordente A, Minotti G. Doxorubicin Metabolism and Toxicity in Human Myocardium: Role of Cytoplasmic Deglycosidation and Carbonyl Reduction. *Chemical Research in Toxicology*. 2000;13:414-420. doi: 10.1021/tx000013q
104. Powis G. Free radical formation by antitumor quinones. *Free Radical Biology and Medicine*. 1989;6:63-101. doi: https://doi.org/10.1016/0891-5849(89)90162-7

105. Minotti G, Recalcati S, Menna P, Salvatorelli E, Corna G, Cairo G. Quinones and Quinone Enzymes. In: Sies H, Packer L, eds. *Quinones and Quinone Enzymes*. Elsevier Academic Press; 2004.
106. Fiallo M, Laigle A, Garnier-Suillerot A, Amirand C, Ballini J-P, Chinsky L, Duquesne M, Jolles B, Sureau F, Turpin P-Y, et al. Interactions of iron-anthracycline complexes with living cells: A microspectrofluorometric study. *Biochimica et Biophysica Acta (BBA) - Molecular Cell Research*. 1993;1177:236-244. doi: https://doi.org/10.1016/0167-4889(93)90119-A
107. Myers CE, Gianni L, Simone CB, Klecker R, Greene R. Oxidative destruction of erythrocyte ghost membranes catalyzed by the doxorubicin-iron complex. *Biochemistry*. 1982;21:1707-1713.
108. Minotti G, Menna P, Salvatorelli E, Cairo G, Gianni L. Anthracyclines: Molecular Advances and Pharmacologic Developments in Antitumor Activity and Cardiotoxicity. *Pharmacol Rev*. 2004;56:185-229. doi: 10.1124/pr.56.2.6
109. Ichikawa Y, Ghanefar M, Bayeva M, Wu R, Khechaduri A, Naga Prasad SV, Mutharasan RK, Naik TJ, Ardehali H. Cardiotoxicity of doxorubicin is mediated through mitochondrial iron accumulation. *J Clin Invest*. 2014;124:617-630. doi: 10.1172/JCI72931
110. Lebrecht D, Setzer B, Ketelsen U-P, Haberstroh J, Walker UA. Time-dependent and tissue-specific accumulation of mtDNA and respiratory chain defects in chronic doxorubicin cardiomyopathy. *Circulation*. 2003;108:2423-2429. doi: 10.1161/01.CIR.0000093196.59829.DF
111. Lebrecht D, Walker UA. Role of mtDNA lesions in anthracycline cardiotoxicity. *Cardiovasc Toxicol*. 2007;7:108-113. doi: 10.1007/s12012-007-0009-1
112. Hasinoff BB, Patel D, Wu X. The oral iron chelator ICL670A (deferasirox) does not protect myocytes against doxorubicin. *Free Radic Biol Med*. 2003;35:1469-1479. doi: 10.1016/j.freeradbiomed.2003.08.005
113. Atwal M, Swan RL, Rowe C, Lee KC, Lee DC, Armstrong L, Cowell IG, Austin CA. Intercalating TOP2 Poisons Attenuate Topoisomerase Action at Higher Concentrations. *Molecular Pharmacology*. 2019;96:475-484. doi: 10.1124/mol.119.117259
114. Zhang S, Liu X, Bawa-Khalfe T, Lu L-S, Lyu YL, Liu LF, Yeh ETH. Identification of the molecular basis of doxorubicin-induced cardiotoxicity. *Nature Medicine*. 2012;18:1639-1642. doi: 10.1038/nm.2919

115. Martin E, Thougaard AV, Grauslund M, Jensen PB, Bjorkling F, Hasinoff BB, Tjørnelund J, Sehested M, Jensen LH. Evaluation of the topoisomerase II-inactive bisdioxopiperazine ICRF-161 as a protectant against doxorubicin-induced cardiomyopathy. *Toxicology*. 2009;255:72-79. doi: https://doi.org/10.1016/j.tox.2008.10.011

116. Myrehaug S, Pintilie M, Yun L, Crump M, Tsang RW, Meyer RM, Sussman J, Yu E, Hodgson DC. A population-based study of cardiac morbidity among Hodgkin lymphoma patients with preexisting heart disease. *Blood*. 2010;116:2237-2240. doi: 10.1182/blood-2010-01-263764

117. Gigli M, Rasoanaivo TWD, Millot J-M, Jeannesson P, Rizzo V, Jardillier J-C, Arcamone F, Manfait M. Correlation between Growth Inhibition and Intranuclear Doxorubicin and 4′-Deoxy-4′-iododoxorubicin Quantitated in Living K562 Cells by Microspectrofluorometry. *Cancer Research*. 1989;49:560-564.

118. Tokarska-Schlattner M, Zaugg M, Zuppinger C, Wallimann T, Schlattner U. New insights into doxorubicin-induced cardiotoxicity: The critical role of cellular energetics. *Journal of Molecular and Cellular Cardiology*. 2006;41:389-405. doi: https://doi.org/10.1016/j.yjmcc.2006.06.009

119. Gianni L, Herman EH, Lipshultz SE, Minotti G, Sarvazyan N, Sawyer DB. Anthracycline Cardiotoxicity: From Bench to Bedside. *Journal of Clinical Oncology*. 2008;26:3777-3784. doi: 10.1200/jco.2007.14.9401

120. Houtkooper RH, Vaz FM. Cardiolipin, the heart of mitochondrial metabolism. *Cell Mol Life Sci*. 2008;65:2493-2506. doi: 10.1007/s00018-008-8030-5

121. Chicco AJ, Sparagna GC. Role of cardiolipin alterations in mitochondrial dysfunction and disease. *Am J Physiol Cell Physiol*. 2007;292:C33-44. doi: 10.1152/ajpcell.00243.2006

122. Schlame M, Ren M. Barth syndrome, a human disorder of cardiolipin metabolism. *FEBS Lett*. 2006;580:5450-5455. doi: 10.1016/j.febslet.2006.07.022

123. Moulin M, Solgadi A, Veksler V, Garnier A, Ventura-Clapier R, Chaminade P. Sex-specific cardiac cardiolipin remodelling after doxorubicin treatment. *Biol Sex Differ*. 2015;6:20. doi: 10.1186/s13293-015-0039-5

124. Pereira GC, Pereira SP, Tavares LC, Carvalho FS, Magalhães-Novais S, Barbosa IA, Santos MS, Bjork J, Moreno AJ, Wallace KB, et al. Cardiac cytochrome c and cardiolipin depletion during anthracycline-induced chronic

depression of mitochondrial function. *Mitochondrion*. 2016;30:95-104. doi: 10.1016/j.mito.2016.07.005

125. Xu Y, Phoon CKL, Berno B, D'Souza K, Hoedt E, Zhang G, Neubert TA, Epand RM, Ren M, Schlame M. Loss of protein association causes cardiolipin degradation in Barth syndrome. *Nat Chem Biol*. 2016;12:641-647. doi: 10.1038/nchembio.2113
126. Speyer JL, Green MD, Kramer E, Rey M, Sanger J, Ward C, Dubin N, Ferrans V, Stecy P, Zeleniuch-Jacquotte A, et al. Protective Effect of the Bispiperazinedione ICRF-187 against Doxorubicin-Induced Cardiac Toxicity in Women with Advanced Breast Cancer. *N Engl J Med*. 1988;319:745-752. doi: 10.1056/NEJM198809223191203
127. Anversa P, Kajstura J. Ventricular Myocytes Are Not Terminally Differentiated in the Adult Mammalian Heart. *Circ Res*. 1998;83:1-14. doi: doi:10.1161/01.RES.83.1.1
128. Soonpaa MH, Field LJ. Survey of Studies Examining Mammalian Cardiomyocyte DNA Synthesis. *Circ Res*. 1998;83:15-26. doi: doi:10.1161/01.RES.83.1.15
129. Beltrami AP, Urbanek K, Kajstura J, Yan S-M, Finato N, Bussani R, Nadal-Ginard B, Silvestri F, Leri A, Beltrami CA, et al. Evidence That Human Cardiac Myocytes Divide after Myocardial Infarction. *New England Journal of Medicine*. 2001;344:1750-1757. doi: 10.1056/nejm200106073442303
130. Quaini F, Urbanek K, Beltrami AP, Finato N, Beltrami CA, Nadal-Ginard B, Kajstura J, Leri A, Anversa P. Chimerism of the Transplanted Heart. *New England Journal of Medicine*. 2002;346:5-15. doi: 10.1056/NEJMoa012081
131. Drazen JM. Expression of Concern: Beltrami AP et al. Evidence That Human Cardiac Myocytes Divide after Myocardial Infarction. N Engl J Med 2001;344:1750-7 and Quaini F et al. Chimerism of the Transplanted Heart. N Engl J Med 2002;346:5-15. *New England Journal of Medicine*. 2018;379:1870-1870. doi: doi:10.1056/NEJMe1813801
132. Bergmann O, Bhardwaj RD, Bernard S, Zdunek S, Barnabé-Heider F, Walsh S, Zupicich J, Alkass K, Buchholz BA, Druid H, et al. Evidence for cardiomyocyte renewal in humans. *Science*. 2009;324:98-102. doi: 10.1126/science.1164680
133. Mohamed TMA, Ang Y-S, Radzinsky E, Zhou P, Huang Y, Elfenbein A, Foley A, Magnitsky S, Srivastava D. Regulation of Cell Cycle to Stimulate Adult

Cardiomyocyte Proliferation and Cardiac Regeneration. *Cell*. 2018;173:104-116.e112. doi: https://doi.org/10.1016/j.cell.2018.02.014

134. Parmacek MS, Epstein JA. Cardiomyocyte renewal. *N Engl J Med*. 2009;361:86-88. doi: 10.1056/NEJMcibr0903347
135. Bergmann O, Jovinge S. Cardiac regeneration in vivo: mending the heart from within? *Stem Cell Res*. 2014;13:523-531. doi: 10.1016/j.scr.2014.07.002
136. Derks W, Bergmann O. Polyploidy in Cardiomyocytes. *Circ Res*. 2020;126:552-565. doi: doi:10.1161/CIRCRESAHA.119.315408
137. Senyo SE, Steinhauser ML, Pizzimenti CL, Yang VK, Cai L, Wang M, Wu T-D, Guerquin-Kern J-L, Lechene CP, Lee RT. Mammalian heart renewal by pre-existing cardiomyocytes. *Nature*. 2013;493:433-436. doi: 10.1038/nature11682
138. Kotamraju S, Konorev EA, Joseph J, Kalyanaraman B. Doxorubicin-induced apoptosis in endothelial cells and cardiomyocytes is ameliorated by nitrone spin traps and ebselen: role of reactive oxygen and nitrogen species. *Journal of Biological Chemistry*. 2000;275:33585-33592.
139. Pereira GC, Pereira SP, Pereira CV, Lumini JA, Magalhães J, Ascensão A, Santos MS, Moreno AJ, Oliveira PJ. Mitochondrionopathy Phenotype in Doxorubicin-Treated Wistar Rats Depends on Treatment Protocol and Is Cardiac-Specific. *PLOS ONE*. 2012;7:e38867. doi: 10.1371/journal.pone.0038867
140. Ellison GM, Vicinanza C, Smith AJ, Aquila I, Leone A, Waring CD, Henning BJ, Stirparo GG, Papait R, Scarfò M, et al. Adult c-kit(pos) cardiac stem cells are necessary and sufficient for functional cardiac regeneration and repair. *Cell*. 2013;154:827-842. doi: 10.1016/j.cell.2013.07.039
141. Gojo S, Gojo N, Takeda Y, Mori T, Abe H, Kyo S, Hata J-i, Umezawa A. In vivo cardiovasculogenesis by direct injection of isolated adult mesenchymal stem cells. *Experimental Cell Research*. 2003;288:51-59. doi: https://doi.org/10.1016/S0014-4827(03)00132-0
142. Jackson KA, Majka SM, Wang H, Pocius J, Hartley CJ, Majesky MW, Entman ML, Michael LH, Hirschi KK, Goodell MA. Regeneration of ischemic cardiac muscle and vascular endothelium by adult stem cells. *J Clin Invest*. 2001;107:1395-1402. doi: 10.1172/JCI12150
143. Wu SM, Fujiwara Y, Cibulsky SM, Clapham DE, Lien C-L, Schultheiss TM, Orkin SH. Developmental origin of a bipotential myocardial and smooth muscle cell

precursor in the mammalian heart. *Cell*. 2006;127:1137-1150. doi: 10.1016/j.cell.2006.10.028

144. Piegari E, De Angelis A, Cappetta D, Russo R, Esposito G, Costantino S, Graiani G, Frati C, Prezioso L, Berrino L, et al. Doxorubicin induces senescence and impairs function of human cardiac progenitor cells. *Basic Res Cardiol*. 2013;108:334. doi: 10.1007/s00395-013-0334-4
145. De Angelis A, Piegari E, Cappetta D, Russo R, Esposito G, Ciuffreda LP, Ferraiolo FAV, Frati C, Fagnoni F, Berrino L, et al. SIRT1 activation rescues doxorubicin-induced loss of functional competence of human cardiac progenitor cells. *Int J Cardiol*. 2015;189:30-44. doi: 10.1016/j.ijcard.2015.03.438
146. Hayflick L, Moorhead PS. The serial cultivation of human diploid cell strains. *Experimental Cell Research*. 1961;25:585-621. doi: https://doi.org/10.1016/0014-4827(61)90192-6
147. Serrano M, Lin AW, McCurrach ME, Beach D, Lowe SW. Oncogenic ras provokes premature cell senescence associated with accumulation of p53 and p16INK4a. *Cell*. 1997;88:593-602.
148. Shay JW, Pereira-Smith OM, Wright WE. A role for both RB and p53 in the regulation of human cellular senescence. *Experimental Cell Research*. 1991;196:33-39. doi: https://doi.org/10.1016/0014-4827(91)90453-2
149. Dimri GP, Lee X, Basile G, Acosta M, Scott G, Roskelley C, Medrano EE, Linskens M, Rubelj I, Pereira-Smith O. A biomarker that identifies senescent human cells in culture and in aging skin in vivo. *Proceedings of the National Academy of Sciences*. 1995;92:9363-9367. doi: doi:10.1073/pnas.92.20.9363
150. Lopes-Paciencia S, Saint-Germain E, Rowell M-C, Ruiz AF, Kalegari P, Ferbeyre G. The senescence-associated secretory phenotype and its regulation. *Cytokine*. 2019;117:15-22. doi: https://doi.org/10.1016/j.cyto.2019.01.013
151. Coppé J-P, Patil CK, Rodier F, Sun Y, Muñoz DP, Goldstein J, Nelson PS, Desprez P-Y, Campisi J. Senescence-Associated Secretory Phenotypes Reveal Cell-Nonautonomous Functions of Oncogenic RAS and the p53 Tumor Suppressor. *PLOS Biology*. 2008;6:e301. doi: 10.1371/journal.pbio.0060301
152. Zhu Y, Tchkonia T, Pirtskhalava T, Gower AC, Ding H, Giorgadze N, Palmer AK, Ikeno Y, Hubbard GB, Lenburg M. The Achilles' heel of senescent cells: from transcriptome to senolytic drugs. *Aging cell*. 2015;14:644-658.

153. Wang E. Senescent human fibroblasts resist programmed cell death, and failure to suppress bcl 2 is involved. *Cancer research*. 1995;55:2284-2292.
154. González-Gualda E, Baker AG, Fruk L, Muñoz-Espín D. A guide to assessing cellular senescence in vitro and in vivo. *FEBS J*. 2020. doi: 10.1111/febs.15570
155. Hernandez-Segura A, Nehme J, Demaria M. Hallmarks of Cellular Senescence. *Trends in Cell Biology*. 2018;28:436-453. doi: 10.1016/j.tcb.2018.02.001
156. Saul D, Kosinsky RL, Atkinson EJ, Doolittle ML, Zhang X, LeBrasseur NK, Pignolo RJ, Robbins PD, Niedernhofer LJ, Ikeno Y, et al. A new gene set identifies senescent cells and predicts senescence-associated pathways across tissues. *Nature Communications*. 2022;13:4827. doi: 10.1038/s41467-022-32552-1
157. Casella G, Munk R, Kim KM, Piao Y, De S, Abdelmohsen K, Gorospe M. Transcriptome signature of cellular senescence. *Nucleic Acids Research*. 2019;47:7294-7305. doi: 10.1093/nar/gkz555
158. Paramos-de-Carvalho D, Jacinto A, Saúde L. The right time for senescence. *eLife*. 2021;10:e72449. doi: 10.7554/eLife.72449
159. Muñoz-Espín D, Cañamero M, Maraver A, Gómez-López G, Contreras J, Murillo-Cuesta S, Rodríguez-Baeza A, Varela-Nieto I, Ruberte J, Collado M, et al. Programmed Cell Senescence during Mammalian Embryonic Development. *Cell*. 2013;155:1104-1118. doi: https://doi.org/10.1016/j.cell.2013.10.019
160. Collado M, Serrano M. Senescence in tumours: evidence from mice and humans. *Nature Reviews Cancer*. 2010;10:51-57. doi: 10.1038/nrc2772
161. Demaria M, Ohtani N, Youssef SA, Rodier F, Toussaint W, Mitchell JR, Laberge R-M, Vijg J, Van Steeg H, Dollé ME. An essential role for senescent cells in optimal wound healing through secretion of PDGF-AA. *Developmental cell*. 2014;31:722-733.
162. Tuttle CS, Waaijer ME, Slee-Valentijn MS, Stijnen T, Westendorp R, Maier AB. Cellular senescence and chronological age in various human tissues: a systematic review and meta-analysis. *Aging cell*. 2020;19:e13083.
163. Blasco MA. Telomeres and human disease: ageing, cancer and beyond. *Nature Reviews Genetics*. 2005;6:611-622.
164. Childs BG, Durik M, Baker DJ, van Deursen JM. Cellular senescence in aging and age-related disease: from mechanisms to therapy. *Nature Medicine*. 2015;21:1424-1435. doi: 10.1038/nm.4000

165. Chen Q, Liu K, Robinson AR, Clauson CL, Blair HC, Robbins PD, Niedernhofer LJ, Ouyang H. DNA damage drives accelerated bone aging via an NF-κB–dependent mechanism. *Journal of Bone and Mineral Research*. 2012;28:1214-1228. doi: 10.1002/jbmr.1851
166. Farr JN, Fraser DG, Wang H, Jaehn K, Ogrodnik MB, Weivoda MM, Drake MT, Tchkonia T, LeBrasseur NK, Kirkland JL, et al. Identification of Senescent Cells in the Bone Microenvironment. *Journal of Bone and Mineral Research*. 2016;31:1920-1929. doi: 10.1002/jbmr.2892
167. Baker DJ, Wijshake T, Tchkonia T, LeBrasseur NK, Childs BG, van de Sluis B, Kirkland JL, van Deursen JM. Clearance of p16Ink4a-positive senescent cells delays ageing-associated disorders. *Nature*. 2011;479:232-236. doi: 10.1038/nature10600
168. Harrison CN, Garcia JS, Somervaille TCP, Foran JM, Verstovsek S, Jamieson C, Mesa R, Ritchie EK, Tantravahi SK, Vachhani P, et al. Addition of Navitoclax to Ongoing Ruxolitinib Therapy for Patients With Myelofibrosis With Progression or Suboptimal Response: Phase II Safety and Efficacy. *J Clin Oncol*. 2022;40:1671-1680. doi: 10.1200/jco.21.02188
169. Eichhorst B, Niemann CU, Kater AP, Fürstenau M, Tresckow Jv, Zhang C, Robrecht S, Gregor M, Juliusson G, Thornton P, et al. First-Line Venetoclax Combinations in Chronic Lymphocytic Leukemia. *New England Journal of Medicine*. 2023;388:1739-1754. doi: doi:10.1056/NEJMoa2213093
170. Musi N, Valentine JM, Sickora KR, Baeuerle E, Thompson CS, Shen Q, Orr ME. Tau protein aggregation is associated with cellular senescence in the brain. *Aging Cell*. 2018;17:e12840. doi: https://doi.org/10.1111/acel.12840
171. Kumari R, Jat P. Mechanisms of Cellular Senescence: Cell Cycle Arrest and Senescence Associated Secretory Phenotype. *Frontiers in Cell and Developmental Biology*. 2021;9. doi: 10.3389/fcell.2021.645593
172. Levine ME. Modeling the Rate of Senescence: Can Estimated Biological Age Predict Mortality More Accurately Than Chronological Age? *The Journals of Gerontology: Series A*. 2012;68:667-674. doi: 10.1093/gerona/gls233
173. Anderson R, Lagnado A, Maggiorani D, Walaszczyk A, Dookun E, Chapman J, Birch J, Salmonowicz H, Ogrodnik M, Jurk D, et al. Length-independent telomere damage drives post-mitotic cardiomyocyte senescence. *EMBO J*. 2019;38. doi: 10.15252/embj.2018100492

174. Walaszczyk A, Dookun E, Redgrave R, Tual-Chalot S, Victorelli S, Spyridopoulos I, Owens A, Arthur HM, Passos JF, Richardson GD. Pharmacological clearance of senescent cells improves survival and recovery in aged mice following acute myocardial infarction. *Aging Cell*. 2019;18:e12945. doi: https://doi.org/10.1111/acel.12945

175. Dookun E, Walaszczyk A, Redgrave R, Palmowski P, Tual-Chalot S, Suwana A, Chapman J, Jirkovsky E, Donastorg Sosa L, Gill E, et al. Clearance of senescent cells during cardiac ischemia–reperfusion injury improves recovery. *Aging Cell*. 2020;19:e13249. doi: https://doi.org/10.1111/acel.13249

176. Lewis-McDougall FC, Ruchaya PJ, Domenjo-Vila E, Shin Teoh T, Prata L, Cottle BJ, Clark JE, Punjabi PP, Awad W, Torella D, et al. Aged-senescent cells contribute to impaired heart regeneration. *Aging Cell*. 2019;18:e12931. doi: https://doi.org/10.1111/acel.12931

177. Stojanović SD, Fiedler J, Bauersachs J, Thum T, Sedding DG. Senescence-induced inflammation: an important player and key therapeutic target in atherosclerosis. *European Heart Journal*. 2020;41:2983-2996. doi: 10.1093/eurheartj/ehz919

178. Holdt LM, Sass K, Gäbel G, Bergert H, Thiery J, Teupser D. Expression of Chr9p21 genes CDKN2B (p15INK4b), CDKN2A (p16INK4a, p14ARF) and MTAP in human atherosclerotic plaque. *Atherosclerosis*. 2011;214:264-270. doi: https://doi.org/10.1016/j.atherosclerosis.2010.06.029

179. Demaria M, O'Leary MN, Chang J, Shao L, Liu S, Alimirah F, Koenig K, Le C, Mitin N, Deal AM, et al. Cellular Senescence Promotes Adverse Effects of Chemotherapy and Cancer Relapse. *Cancer Discov*. 2017;7:165-176. doi: 10.1158/2159-8290.CD-16-0241

180. Mitry MA, Laurent D, Keith BL, Sira E, Eisenberg CA, Eisenberg LM, Joshi S, Gupte S, Edwards JG. Accelerated cardiomyocyte senescence contributes to late-onset doxorubicin-induced cardiotoxicity. *Am J Physiol Cell Physiol*. 2020;318:C380-C391. doi: 10.1152/ajpcell.00073.2019

181. Lérida-Viso A, Estepa- Fernández A, Morellá-Aucejo Á, Lozano-Torres B, Alfonso M, Blandez JF, Bisbal V, Sepúlveda P, García-Fernández A, Orzáez M, et al. Pharmacological senolysis reduces doxorubicin-induced cardiotoxicity and improves cardiac function in mice. *Pharmacological Research*. 2022;183:106356. doi: https://doi.org/10.1016/j.phrs.2022.106356

182. Linders AN, Dias IB, Ovchinnikova ES, Vermeer MCSC, Hoes MF, Mavrogenis GM, Deiman FE, Gomez KFA, Bliley JM, Nehme J, et al. Evaluation of Senescence and Its Prevention in Doxorubicin-Induced Cardiotoxicity Using Dynamic Engineered Heart Tissues. *JACC: CardioOncology*. 2023;5:298-315. doi: doi:10.1016/j.jaccao.2023.03.012
183. Dai D-F, Chiao Y-A, Martin G, Marcinek D, Basisty N, Quarles E, Rabinovitch P. Mitochondrial-targeted catalase: extended longevity and the roles in various disease models. *Progress in Molecular Biology and Translational Science*. 2017;146:203-241.
184. Kang YJ, Chen Y, Epstein PN. Suppression of doxorubicin cardiotoxicity by overexpression of catalase in the heart of transgenic mice (∗). *Journal of Biological Chemistry*. 1996;271:12610-12616.
185. Morris S, Molina-Riquelme I, Barrientos G, Bravo F, Aedo G, Gómez W, Lagos D, Verdejo H, Peischard S, Seebohm G, et al. Inner mitochondrial membrane structure and fusion dynamics are altered in senescent human iPSC-derived and primary rat cardiomyocytes. *Biochimica et Biophysica Acta (BBA) - Bioenergetics*. 2023;1864:148949. doi: https://doi.org/10.1016/j.bbabio.2022.148949
186. López-Otín C, Blasco MA, Partridge L, Serrano M, Kroemer G. Hallmarks of aging: An expanding universe. *Cell*. 2023;186:243-278. doi: https://doi.org/10.1016/j.cell.2022.11.001
187. Correia-Melo C, Marques FD, Anderson R, Hewitt G, Hewitt R, Cole J, Carroll BM, Miwa S, Birch J, Merz A, et al. Mitochondria are required for pro-ageing features of the senescent phenotype. *The EMBO Journal*. 2016;35:724-742. doi: https://doi.org/10.15252/embj.201592862
188. Zhu F, Li Y, Zhang J, Piao C, Liu T, Li H-H, Du J. Senescent cardiac fibroblast is critical for cardiac fibrosis after myocardial infarction. *PloS one*. 2013;8. doi: 10.1371/journal.pone.0074535
189. Nag AC. Study of non-muscle cells of the adult mammalian heart: a fine structural analysis and distribution. *Cytobios*. 1980;28:41-61.
190. Litviňuková M, Talavera-López C, Maatz H, Reichart D, Worth CL, Lindberg EL, Kanda M, Polanski K, Heinig M, Lee M, et al. Cells of the adult human heart. *Nature*. 2020;588:466-472. doi: 10.1038/s41586-020-2797-4

191. DeLeon-Pennell KY, Barker TH, Lindsey ML. Fibroblasts: The arbiters of extracellular matrix remodeling. *Matrix Biol*. 2020;91-92:1-7. doi: 10.1016/j.matbio.2020.05.006
192. Gray MO, Long CS, Kalinyak JE, Li HT, Karliner JS. Angiotensin II stimulates cardiac myocyte hypertrophy via paracrine release of TGF-beta 1 and endothelin-1 from fibroblasts. *Cardiovasc Res*. 1998;40:352-363. doi: 10.1016/s0008-6363(98)00121-7
193. Weber KT, Sun Y, Bhattacharya SK, Ahokas RA, Gerling IC. Myofibroblast-mediated mechanisms of pathological remodelling of the heart. *Nat Rev Cardiol*. 2013;10:15-26. doi: 10.1038/nrcardio.2012.158
194. Oatmen KE, Cull E, Spinale FG. Heart failure as interstitial cancer: emergence of a malignant fibroblast phenotype. *Nat Rev Cardiol*. 2020;17:523-531. doi: 10.1038/s41569-019-0286-y
195. Sahai E, Astsaturov I, Cukierman E, DeNardo DG, Egeblad M, Evans RM, Fearon D, Greten FR, Hingorani SR, Hunter T, et al. A framework for advancing our understanding of cancer-associated fibroblasts. *Nat Rev Cancer*. 2020;20:174-186. doi: 10.1038/s41568-019-0238-1
196. Ivanová M, Dovinová I, Okruhlicová L, Tribulová N, Simončíková P, Barteková M, Vlkovičová J, Barančík M. Chronic cardiotoxicity of doxorubicin involves activation of myocardial and circulating matrix metalloproteinases in rats. *Acta Pharmacol Sin*. 2012;33:459-469. doi: 10.1038/aps.2011.194
197. Mancilla TR, Davis LR, Aune GJ. Doxorubicin-induced p53 interferes with mitophagy in cardiac fibroblasts. *PLoS One*. 2020;15:e0238856. doi: 10.1371/journal.pone.0238856
198. Espitia-Corredor JA, Shamoon L, Olivares-Silva F, Rimassa-Taré C, Muñoz-Rodríguez C, Espinoza-Pérez C, Sánchez-Ferrer CF, Peiró C, Díaz-Araya G. Resolvin E1 attenuates doxorubicin-induced cardiac fibroblast senescence: A key role for IL-1β. *Biochimica et Biophysica Acta (BBA) - Molecular Basis of Disease*. 2022;1868:166525. doi: https://doi.org/10.1016/j.bbadis.2022.166525
199. Bientinesi E, Lulli M, Becatti M, Ristori S, Margheri F, Monti D. Doxorubicin-induced senescence in normal fibroblasts promotes in vitro tumour cell growth and invasiveness: The role of Quercetin in modulating these processes. *Mechanisms of Ageing and Development*. 2022;206:111689. doi: https://doi.org/10.1016/j.mad.2022.111689

200. Levick SP, Soto-Pantoja DR, Bi J, Hundley WG, Widiapradja A, Manteufel EJ, Bradshaw TW, Meléndez GC. Doxorubicin-Induced Myocardial Fibrosis Involves the Neurokinin-1 Receptor and Direct Effects on Cardiac Fibroblasts. *Heart, Lung and Circulation*. 2019;28:1598-1605. doi: https://doi.org/10.1016/j.hlc.2018.08.003
201. Wolf MB, Baynes JW. The anti-cancer drug, doxorubicin, causes oxidant stress-induced endothelial dysfunction. *Biochimica et Biophysica Acta (BBA) - General Subjects*. 2006;1760:267-271. doi: https://doi.org/10.1016/j.bbagen.2005.10.012
202. Jia G, Aroor AR, Jia C, Sowers JR. Endothelial cell senescence in aging-related vascular dysfunction. *Biochimica et Biophysica Acta (BBA) - Molecular Basis of Disease*. 2019;1865:1802-1809. doi: https://doi.org/10.1016/j.bbadis.2018.08.008
203. Childs BG, Baker DJ, Wijshake T, Conover CA, Campisi J, van Deursen JM. Senescent intimal foam cells are deleterious at all stages of atherosclerosis. *Science*. 2016;354:472-477. doi: doi:10.1126/science.aaf6659
204. Roos CM, Zhang B, Palmer AK, Ogrodnik MB, Pirtskhalava T, Thalji NM, Hagler M, Jurk D, Smith LA, Casaclang-Verzosa G. Chronic senolytic treatment alleviates established vasomotor dysfunction in aged or atherosclerotic mice. *Aging cell*. 2016;15:973-977.
205. Balint B, Yin H, Nong Z, Arpino J-M, O'Neil C, Rogers SR, Randhawa VK, Fox SA, Chevalier J, Lee JJ, et al. Seno-destructive smooth muscle cells in the ascending aorta of patients with bicuspid aortic valve disease. *eBioMedicine*. 2019;43:54-66. doi: 10.1016/j.ebiom.2019.04.060
206. Abdelgawad IY, Agostinucci K, Zordoky BN. Cardiovascular ramifications of therapy-induced endothelial cell senescence in cancer survivors. *Biochimica et Biophysica Acta (BBA) - Molecular Basis of Disease*. 2022;1868:166352. doi: https://doi.org/10.1016/j.bbadis.2022.166352
207. Tocchetti CG, Ameri P, de Boer RA, D'Alessandra Y, Russo M, Sorriento D, Ciccarelli M, Kiss B, Bertrand L, Dawson D, et al. Cardiac dysfunction in cancer patients: beyond direct cardiomyocyte damage of anticancer drugs: novel cardio-oncology insights from the joint 2019 meeting of the ESC Working Groups of Myocardial Function and Cellular Biology of the Heart. *Cardiovasc Res*. 2020;116:1820-1834. doi: 10.1093/cvr/cvaa222

208. Wagner JUG, Dimmeler S. Cellular cross-talks in the diseased and aging heart. *J Mol Cell Cardiol*. 2020;138:136-146. doi: 10.1016/j.yjmcc.2019.11.152
209. Davidson MM, Nesti C, Palenzuela L, Walker WF, Hernandez E, Protas L, Hirano M, Isaac ND. Novel cell lines derived from adult human ventricular cardiomyocytes. *J Mol Cell Cardiol*. 2005;39:133-147. doi: 10.1016/j.yjmcc.2005.03.003
210. Niepel M, Hafner M, Mills CE, Subramanian K, Williams EH, Chung M, Gaudio B, Barrette AM, Stern AD, Hu B, et al. A Multi-center Study on the Reproducibility of Drug-Response Assays in Mammalian Cell Lines. *Cell Systems*. 2019;9:35-48.e35. doi: 10.1016/j.cels.2019.06.005
211. Mosmann T. Rapid colorimetric assay for cellular growth and survival: Application to proliferation and cytotoxicity assays. *Journal of Immunological Methods*. 1983;65:55-63. doi: https://doi.org/10.1016/0022-1759(83)90303-4
212. Liu S, Yang W, Li Y, Sun C. Fetal bovine serum, an important factor affecting the reproducibility of cell experiments. *Scientific Reports*. 2023;13:1942. doi: 10.1038/s41598-023-29060-7
213. van der Valk J. Fetal bovine serum—a cell culture dilemma. *Science*. 2022;375:143-144. doi: doi:10.1126/science.abm1317
214. Ye J, Coulouris G, Zaretskaya I, Cutcutache I, Rozen S, Madden TL. Primer-BLAST: a tool to design target-specific primers for polymerase chain reaction. *BMC Bioinformatics*. 2012;13:134. doi: 10.1186/1471-2105-13-134
215. Altschul SF, Madden TL, Schäffer AA, Zhang J, Zhang Z, Miller W, Lipman DJ. Gapped BLAST and PSI-BLAST: a new generation of protein database search programs. *Nucleic Acids Res*. 1997;25:3389-3402.
216. Im K, Mareninov S, Diaz MFP, Yong WH. An Introduction to Performing Immunofluorescence Staining. *Methods Mol Biol*. 2019;1897:299-311. doi: 10.1007/978-1-4939-8935-5_26
217. Weisblum B, Haenssler E. Fluorometric properties of the bibenzimidazole derivative hoechst 33258, a fluorescent probe specific for AT concentration in chromosomal DNA. *Chromosoma*. 1974;46:255-260. doi: 10.1007/BF00284881
218. Kapuściński J, Skoczylas B. Simple and rapid fluorimetric method for DNA microassay. *Analytical Biochemistry*. 1977;83:252-257. doi: https://doi.org/10.1016/0003-2697(77)90533-4
219. Invitrogen. DAPI and Hoechst Nucleic Acid Stains. https://www.thermofisher.com/order/catalog/product/D1306.

220. Hoeger CW, Turissini C, Asnani A. Doxorubicin Cardiotoxicity: Pathophysiology Updates. *Current Treatment Options in Cardiovascular Medicine*. 2020;22:52. doi: 10.1007/s11936-020-00842-w

221. Pudil R, Mueller C, Čelutkienė J, Henriksen PA, Lenihan D, Dent S, Barac A, Stanway S, Moslehi J, Suter TM, et al. Role of serum biomarkers in cancer patients receiving cardiotoxic cancer therapies: a position statement from the Cardio-Oncology Study Group of the Heart Failure Association and the Cardio-Oncology Council of the European Society of Cardiology. *European Journal of Heart Failure*. 2020;22:1966-1983. doi: https://doi.org/10.1002/ejhf.2017

222. Takemura G, Fujiwara H. Doxorubicin-Induced Cardiomyopathy: From the Cardiotoxic Mechanisms to Management. *Progress in Cardiovascular Diseases*. 2007;49:330-352. doi: https://doi.org/10.1016/j.pcad.2006.10.002

223. Richard C, Ghibu S, Delemasure-Chalumeau S, Guilland J-C, Des Rosiers C, Zeller M, Cottin Y, Rochette L, Vergely C. Oxidative stress and myocardial gene alterations associated with doxorubicin-induced cardiotoxicity in rats persist for 2 months after treatment cessation. *Journal of Pharmacology and Experimental Therapeutics*. 2011;339:807-814.

224. Zhou S, Starkov A, Froberg MK, Leino RL, Wallace KB. Cumulative and Irreversible Cardiac Mitochondrial Dysfunction Induced by Doxorubicin1. *Cancer Research*. 2001;61:771-777.

225. De Angelis A, Piegari E, Cappetta D, Marino L, Filippelli A, Berrino L, Ferreira-Martins J, Zheng H, Hosoda T, Rota M, et al. Anthracycline Cardiomyopathy Is Mediated by Depletion of the Cardiac Stem Cell Pool and Is Rescued by Restoration of Progenitor Cell Function. *Circulation*. 2010;121:276-292. doi: 10.1161/CIRCULATIONAHA.109.895771

226. Ferreira LL, Cunha-Oliveira T, Veloso CD, Costa CF, Wallace KB, Oliveira PJ. Single nanomolar doxorubicin exposure triggers compensatory mitochondrial responses in H9c2 cardiomyoblasts. *Food and Chemical Toxicology*. 2019;124:450-461. doi: https://doi.org/10.1016/j.fct.2018.12.017

227. Bowes J, Brown AJ, Hamon J, Jarolimek W, Sridhar A, Waldron G, Whitebread S. Reducing safety-related drug attrition: the use of in vitro pharmacological profiling. *Nature Reviews Drug Discovery*. 2012;11:909-922. doi: 10.1038/nrd3845

228. Brennan FR, Kiessling A. In vitro assays supporting the safety assessment of immunomodulatory monoclonal antibodies. *Toxicology in Vitro*. 2017;45:296-308. doi: https://doi.org/10.1016/j.tiv.2017.02.025
229. MacArthur Clark J. The 3Rs in research: a contemporary approach to replacement, reduction and refinement. *British Journal of Nutrition*. 2018;120:S1-S7. doi: 10.1017/S0007114517002227
230. Lyon AR, López-Fernández T, Couch LS, Asteggiano R, Aznar MC, Bergler-Klein J, Boriani G, Cardinale D, Cordoba R, Cosyns B, et al. 2022 ESC Guidelines on cardio-oncology developed in collaboration with the European Hematology Association (EHA), the European Society for Therapeutic Radiology and Oncology (ESTRO) and the International Cardio-Oncology Society (IC-OS): Developed by the task force on cardio-oncology of the European Society of Cardiology (ESC). *European Heart Journal*. 2022;43:4229-4361. doi: 10.1093/eurheartj/ehac244
231. Bansal N, Amdani S, Lipshultz ER, others. Chemotherapy-induced cardiotoxicity in children. *Expert Opinion on Drug*. 2017.
232. Drafts BC, Twomley KM, D'Agostino R, Lawrence J, Avis N, Ellis LR, Thohan V, Jordan J, Melin SA, Torti FM, et al. Low to Moderate Dose Anthracycline-Based Chemotherapy Is Associated With Early Noninvasive Imaging Evidence of Subclinical Cardiovascular Disease. *JACC: Cardiovascular Imaging*. 2013;6:877-885. doi: doi:10.1016/j.jcmg.2012.11.017
233. Speth PAJ, Linssen PCM, Boezeman JBM, Wessels HMC, Haanen C. Cellular and plasma adriamycin concentrations in long-term infusion therapy of leukemia patients. *Cancer Chemotherapy and Pharmacology*. 1987;20:305-310. doi: 10.1007/BF00262581
234. Muller C, Chatelut E, Gualano V, De Forni M, Huguet F, Attal M, Canal P, Laurent G. Cellular pharmacokinetics of doxorubicin in patients with chronic lymphocytic leukemia: comparison of bolus administration and continuous infusion. *Cancer Chemotherapy and Pharmacology*. 1993;32:379-384. doi: 10.1007/BF00735923
235. Barpe DR, Rosa DD, Froehlich PE. Pharmacokinetic evaluation of doxorubicin plasma levels in normal and overweight patients with breast cancer and simulation of dose adjustment by different indexes of body mass. *European Journal of Pharmaceutical Sciences*. 2010;41:458-463. doi: https://doi.org/10.1016/j.ejps.2010.07.015

236. Linders AN, Dias IB, López Fernández T, Tocchetti CG, Bomer N, Van der Meer P. A review of the pathophysiological mechanisms of doxorubicin-induced cardiotoxicity and aging. *npj Aging*. 2024;10:9. doi: 10.1038/s41514-024-00135-7

237. CORTÉS A, CASCANTE M, CÁRDENAS ML, CORNISH-BOWDEN A. Relationships between inhibition constants, inhibitor concentrations for 50% inhibition and types of inhibition: new ways of analysing data. *Biochemical Journal*. 2001;357:263-268. doi: 10.1042/bj3570263

238. Shoemaker RH. The NCI60 human tumour cell line anticancer drug screen. *Nature Reviews Cancer*. 2006;6:813-823. doi: 10.1038/nrc1951

239. Yang W, Soares J, Greninger P, Edelman EJ, Lightfoot H, Forbes S, Bindal N, Beare D, Smith JA, Thompson IR, et al. Genomics of Drug Sensitivity in Cancer (GDSC): a resource for therapeutic biomarker discovery in cancer cells. *Nucleic Acids Research*. 2012;41:D955-D961. doi: 10.1093/nar/gks1111

240. Auner HW, Tinchon C, Linkesch W, Halwachs-Baumann G, Sill H. Correspondence re: O. J. Arola et al., Acute Doxorubicin Cardiotoxicity Involves Cardiomyocyte Apoptosis. Cancer Res., 60: 1789–1792, 2000. *Cancer Research*. 2001;61:2335-2336.

241. Nicoletto RE, Ofner CM. Cytotoxic mechanisms of doxorubicin at clinically relevant concentrations in breast cancer cells. *Cancer Chemotherapy and Pharmacology*. 2022;89:285-311. doi: 10.1007/s00280-022-04400-y

242. Mody H, Vaidya TR, Ait-Oudhia S. In vitro to clinical translational pharmacokinetic/pharmacodynamic modeling of doxorubicin (DOX) and dexrazoxane (DEX) interactions: Safety assessment and optimization. *Scientific Reports*. 2023;13:3100. doi: 10.1038/s41598-023-29964-4

243. Kimes BW, Brandt BL. Properties of a clonal muscle cell line from rat heart. *Experimental Cell Research*. 1976;98:367-381. doi: https://doi.org/10.1016/0014-4827(76)90447-X

244. Branco AF, Pereira SP, Gonzalez S, Gusev O, Rizvanov AA, Oliveira PJ. Gene Expression Profiling of H9c2 Myoblast Differentiation towards a Cardiac-Like Phenotype. *PLOS ONE*. 2015;10:e0129303. doi: 10.1371/journal.pone.0129303

245. Claycomb WC, Lanson NA, Jr., Stallworth BS, Egeland DB, Delcarpio JB, Bahinski A, Izzo NJ, Jr. HL-1 cells: a cardiac muscle cell line that contracts and

retains phenotypic characteristics of the adult cardiomyocyte. *Proc Natl Acad Sci U S A*. 1998;95:2979-2984. doi: 10.1073/pnas.95.6.2979

246. Wang PH, Fang YH, Liu YW, Yeh ML. Merits of hiPSC-Derived Cardiomyocytes for In Vitro Research and Testing Drug Toxicity. *Biomedicines*. 2022;10. doi: 10.3390/biomedicines10112764
247. Linn AK, Manopwisedjaroen S, Kanjanasirirat P, Borwornpinyo S, Hongeng S, Phanthong P, Thitithanyanont A. Unveiling the Antiviral Properties of Panduratin A through SARS-CoV-2 Infection Modeling in Cardiomyocytes. *International Journal of Molecular Sciences*. 2024;25:1427.
248. Livingston M, Armstrong A, Meyer N, Carlson C, Vaidyanathan R, Rieger C. Society of Toxicology Annual Meeting. Paper/Poster presented at: Society of Toxicology; 2021;
249. Li J, Zhou L, Jiang Y, Gao H, Maierhaba T, Gong H. Long noncoding RNA RMRP ameliorates doxorubicin-induced apoptosis by interacting with PFN1 in a P53-Dependent manner. *Molecular and Cellular Probes*. 2023;72:101937. doi: https://doi.org/10.1016/j.mcp.2023.101937
250. Maejima Y, Adachi S, Ito H, Hirao K, Isobe M. Induction of premature senescence in cardiomyocytes by doxorubicin as a novel mechanism of myocardial damage. *Aging Cell*. 2008;7:125-136. doi: https://doi.org/10.1111/j.1474-9726.2007.00358.x
251. Rockley KL. In Vitro Evaluation of Anthracycline-induced Cardiotoxicity and Mitigation by Perturbation of Angiotensin Signalling. In: *School of Medicine and Health*. eTheses: Durham University; 2018:324.
252. Onódi Z, Visnovitz T, Kiss B, Hambalkó S, Koncz A, Ágg B, Váradi B, Tóth VÉ, Nagy RN, Gergely TG, et al. Systematic transcriptomic and phenotypic characterization of human and murine cardiac myocyte cell lines and primary cardiomyocytes reveals serious limitations and low resemblances to adult cardiac phenotype. *Journal of Molecular and Cellular Cardiology*. 2022;165:19-30. doi: https://doi.org/10.1016/j.yjmcc.2021.12.007
253. Erttmann R, Erb N, Steinhoff A, Landbeck G. Pharmacokinetics of doxorubicin in man: dose and schedule dependence. *Journal of Cancer Research and Clinical Oncology*. 1988;114:509-513. doi: 10.1007/BF00391502
254. Lee BY, Han JA, Im JS, Morrone A, Johung K, Goodwin EC, Kleijer WJ, DiMaio D, Hwang ES. Senescence-associated β-galactosidase is lysosomal β-

galactosidase. *Aging Cell*. 2006;5:187-195. doi: https://doi.org/10.1111/j.1474-9726.2006.00199.x

255. Sarvazyan N. Visualization of doxorubicin-induced oxidative stress in isolated cardiac myocytes. *American Journal of Physiology-Heart and Circulatory Physiology*. 1996;271:H2079-H2085. doi: 10.1152/ajpheart.1996.271.5.H2079

256. Goormaghtigh E, Chatelain P, Caspers J, Ruysschaert JM. Evidence of a specific complex between adriamycin and negatively-charged phospholipids. *Biochimica et Biophysica Acta (BBA) - Biomembranes*. 1980;597:1-14. doi: https://doi.org/10.1016/0005-2736(80)90145-5

257. Barnes LM, Moy N, Dickson AJ. Phenotypic variation during cloning procedures: Analysis of the growth behavior of clonal cell lines. *Biotechnology and Bioengineering*. 2006;94:530-537. doi: https://doi.org/10.1002/bit.20856

258. Cappetta D, Rossi F, Piegari E, Quaini F, Berrino L, Urbanek K, De Angelis A. Doxorubicin targets multiple players: A new view of an old problem. *Pharmacological Research*. 2018;127:4-14. doi: https://doi.org/10.1016/j.phrs.2017.03.016

259. Nemoto H, Umemura M, Suzuki F, Nagasako A, Nagao K, Hidaka Y, Nakakaji R, Uchida K, Suzuki S, Masuda M, et al. Store-operated calcium entry via ORAI1 regulates doxorubicin-induced apoptosis and prevents cardiotoxicity in cardiac fibroblasts. *PLOS ONE*. 2022;17:e0278613. doi: 10.1371/journal.pone.0278613

260. Ivey MJ, Kuwabara JT, Pai JT, Moore RE, Sun Z, Tallquist MD. Resident fibroblast expansion during cardiac growth and remodeling. *Journal of Molecular and Cellular Cardiology*. 2018;114:161-174. doi: https://doi.org/10.1016/j.yjmcc.2017.11.012

261. Tallquist MD. Cardiac Fibroblast Diversity. *Annual Review of Physiology*. 2020;82:63-78. doi: 10.1146/annurev-physiol-021119-034527

262. Lovitt CJ, Shelper TB, Avery VM. Doxorubicin resistance in breast cancer cells is mediated by extracellular matrix proteins. *BMC Cancer*. 2018;18:41. doi: 10.1186/s12885-017-3953-6

263. Wen S-h, Su S-c, Liou B-h, Lin C-h, Lee K-r. Sulbactam-enhanced cytotoxicity of doxorubicin in breast cancer cells. *Cancer Cell International*. 2018;18:128. doi: 10.1186/s12935-018-0625-9

264. Faute MAd, Laurent L, Ploton D, Poupon M-F, Jardillier J-C, Bobichon H. Distinctive alterations of invasiveness, drug resistance and cell–cell

organization in 3D-cultures of MCF-7, a human breast cancer cell line, and its multidrug resistant variant. *Clinical & Experimental Metastasis*. 2002;19:161-167. doi: 10.1023/A:1014594825502

265. Chekhun VF, Kulik GI, Yurchenko OV, Tryndyak VP, Todor IN, Luniv LS, Tregubova NA, Pryzimirska TV, Montgomery B, Rusetskaya NV, et al. Role of DNA hypomethylation in the development of the resistance to doxorubicin in human MCF-7 breast adenocarcinoma cells. *Cancer Letters*. 2006;231:87-93. doi: https://doi.org/10.1016/j.canlet.2005.01.038
266. Doyle LA, Yang W, Abruzzo LV, Krogmann T, Gao Y, Rishi AK, Ross DD. A multidrug resistance transporter from human MCF-7 breast cancer cells. *Proceedings of the National Academy of Sciences*. 1998;95:15665-15670. doi: doi:10.1073/pnas.95.26.15665
267. Holliday DL, Speirs V. Choosing the right cell line for breast cancer research. *Breast Cancer Res*. 2011;13:215. doi: 10.1186/bcr2889
268. Cailleau R, Olivé M, Cruciger QVJ. Long-term human breast carcinoma cell lines of metastatic origin: Preliminary characterization. *In Vitro*. 1978;14:911-915. doi: 10.1007/BF02616120
269. Yu S, Kim T, Yoo KH, Kang K. The T47D cell line is an ideal experimental model to elucidate the progesterone-specific effects of a luminal A subtype of breast cancer. *Biochem Biophys Res Commun*. 2017;486:752-758. doi: 10.1016/j.bbrc.2017.03.114
270. Keepers YP, Pizao PE, Peters GJ, van Ark-Otte J, Winograd B, Pinedo HM. Comparison of the sulforhodamine B protein and tetrazolium (MTT) assays for in vitro chemosensitivity testing. *European Journal of Cancer and Clinical Oncology*. 1991;27:897-900. doi: https://doi.org/10.1016/0277-5379(91)90142-Z
271. Ghasemi M, Turnbull T, Sebastian S, Kempson I. The MTT Assay: Utility, Limitations, Pitfalls, and Interpretation in Bulk and Single-Cell Analysis. *Int J Mol Sci*. 2021;22. doi: 10.3390/ijms222312827
272. Louisse J, Wüst RCI, Pistollato F, Palosaari T, Barilari M, Macko P, Bremer S, Prieto P. Assessment of acute and chronic toxicity of doxorubicin in human induced pluripotent stem cell-derived cardiomyocytes. *Toxicology in Vitro*. 2017;42:182-190. doi: https://doi.org/10.1016/j.tiv.2017.04.023
273. Huang X, Shi Z, Wang W, Bai J, Chen Z, Xu J, Zhang D, Fu S. Identification and characterization of a novel protein ISOC2 that interacts with p16INK4a.

Biochemical and Biophysical Research Communications. 2007;361:287-293. doi: https://doi.org/10.1016/j.bbrc.2007.06.181

274. Stewart-Ornstein J, Lahav G. Dynamics of CDKN1A in Single Cells Defined by an Endogenous Fluorescent Tagging Toolkit. *Cell Reports*. 2016;14:1800-1811. doi: https://doi.org/10.1016/j.celrep.2016.01.045
275. Rochette L, Dogon G, Zeller M, Cottin Y, Vergely C. GDF15 and Cardiac Cells: Current Concepts and New Insights. *International Journal of Molecular Sciences*. 2021;22:8889.
276. Hescheler J, Meyer R, Plant S, Krautwurst D, Rosenthal W, Schultz G. Morphological, biochemical, and electrophysiological characterization of a clonal cell (H9c2) line from rat heart. *Circ Res*. 1991;69:1476-1486. doi: doi:10.1161/01.RES.69.6.1476
277. Meléndez GC, Vasu S, Lesnefsky EJ, Kaplan JR, Appt S, D'Agostino RB, Hundley WG, Jordan JH. Myocardial Extracellular and Cardiomyocyte Volume Expand After Doxorubicin Treatment Similar to Adjuvant Breast Cancer Therapy. *JACC: Cardiovascular Imaging*. 2020;13:1084-1085. doi: doi:10.1016/j.jcmg.2019.10.020
278. Peter AK, Bjerke MA, Leinwand LA. Biology of the cardiac myocyte in heart disease. *Mol Biol Cell*. 2016;27:2149-2160. doi: 10.1091/mbc.E16-01-0038
279. Boyle AJ, Shih H, Hwang J, Ye J, Lee B, Zhang Y, Kwon D, Jun K, Zheng D, Sievers R, et al. Cardiomyopathy of aging in the mammalian heart is characterized by myocardial hypertrophy, fibrosis and a predisposition towards cardiomyocyte apoptosis and autophagy. *Experimental Gerontology*. 2011;46:549-559. doi: https://doi.org/10.1016/j.exger.2011.02.010
280. Tamamori M, Ito H, Hiroe M, Terada Y, Marumo F, Ikeda M-A. Essential roles for G1cyclin-dependent kinase activity in development of cardiomyocyte hypertrophy. *American Journal of Physiology-Heart and Circulatory Physiology*. 1998;275:H2036-H2040. doi: 10.1152/ajpheart.1998.275.6.H2036
281. Redgrave RE, Dookun E, Booth LK, Camacho Encina M, Folaranmi O, Tual-Chalot S, Gill JH, Owens WA, Spyridopoulos I, Passos JF, et al. Senescent cardiomyocytes contribute to cardiac dysfunction following myocardial infarction. *npj Aging*. 2023;9:15. doi: 10.1038/s41514-023-00113-5
282. Dai D-F, Johnson SC, Villarin JJ, Chin MT, Nieves-Cintrón M, Chen T, Marcinek DJ, Dorn GW, Kang YJ, Prolla TA, et al. Mitochondrial Oxidative Stress Mediates Angiotensin II–Induced Cardiac Hypertrophy and Gαq

Overexpression–Induced Heart Failure. *Circ Res*. 2011;108:837-846. doi: doi:10.1161/CIRCRESAHA.110.232306

283. Doroshow JH, Locker GY, Myers CE. Enzymatic Defenses of the Mouse Heart Against Reactive Oxygen Metabolites: ALTERATIONS PRODUCED BY DOXORUBICIN. *J Clin Invest*. 1980;65:128-135. doi: 10.1172/JCI109642
284. Antonucci S, Di Sante M, Tonolo F, Pontarollo L, Scalcon V, Alanova P, Menabò R, Carpi A, Bindoli A, Rigobello MP, et al. The Determining Role of Mitochondrial Reactive Oxygen Species Generation and Monoamine Oxidase Activity in Doxorubicin-Induced Cardiotoxicity. *Antioxid Redox Signal*. 2021;34:531-550. doi: 10.1089/ars.2019.7929
285. Korolchuk VI, Miwa S, Carroll B, von Zglinicki T. Mitochondria in Cell Senescence: Is Mitophagy the Weakest Link? *EBioMedicine*. 2017;21:7-13. doi: https://doi.org/10.1016/j.ebiom.2017.03.020
286. Wang D, Liu Y, Zhang R, Zhang F, Sui W, Chen L, Zheng R, Chen X, Wen F, Ouyang HW, et al. Apoptotic transition of senescent cells accompanied with mitochondrial hyper-function. *Oncotarget*. 2016;7:28286-28300. doi: 10.18632/oncotarget.8536
287. Dalle Pezze P, Nelson G, Otten EG, Korolchuk VI, Kirkwood TBL, von Zglinicki T, Shanley DP. Dynamic Modelling of Pathways to Cellular Senescence Reveals Strategies for Targeted Interventions. *PLoS Comput Biol*. 2014;10:e1003728. doi: 10.1371/journal.pcbi.1003728
288. Yan B, Mei Z, Tang Y, Song H, Wu H, Jing Q, Zhang X, Yan C, Han Y. FGF21-FGFR1 controls mitochondrial homeostasis in cardiomyocytes by modulating the degradation of OPA1. *Cell Death Dis*. 2023;14:311. doi: 10.1038/s41419-023-05842-9
289. Takeda N, Manabe I, Uchino Y, Eguchi K, Matsumoto S, Nishimura S, Shindo T, Sano M, Otsu K, Snider P, et al. Cardiac fibroblasts are essential for the adaptive response of the murine heart to pressure overload. *J Clin Invest*. 2010;120:254-265. doi: 10.1172/JCI40295
290. Tang X, Li P-H, Chen H-Z. Cardiomyocyte Senescence and Cellular Communications Within Myocardial Microenvironments. *Frontiers in Endocrinology*. 2020;11. doi: 10.3389/fendo.2020.00280
291. St. Sauver JL, Weston SA, Atkinson EJ, Mc Gree ME, Mielke MM, White TA, Heeren AA, Olson JE, Rocca WA, Palmer AK, et al. Biomarkers of cellular

senescence and risk of death in humans. *Aging Cell*. 2023;22:e14006. doi: https://doi.org/10.1111/acel.14006

292. Sabbatinelli J, Matacchione G, Giuliani A, Ramini D, Rippo MR, Procopio AD, Bonafè M, Olivieri F. Circulating biomarkers of inflammaging as potential predictors of COVID-19 severe outcomes. *Mechanisms of Ageing and Development*. 2022;204:111667. doi: https://doi.org/10.1016/j.mad.2022.111667
293. Schafer MJ, Zhang X, Kumar A, Atkinson EJ, Zhu Y, Jachim S, Mazula DL, Brown AK, Berning M, Aversa Z, et al. The senescence-associated secretome as an indicator of age and medical risk. *JCI Insight*. 2020;5. doi: 10.1172/jci.insight.133668
294. Schindelin J, Arganda-Carreras I, Frise E, Kaynig V, Longair M, Pietzsch T, Preibisch S, Rueden C, Saalfeld S, Schmid B, et al. Fiji: an open-source platform for biological-image analysis. *Nature Methods*. 2012;9:676-682. doi: 10.1038/nmeth.2019
295. Valente AJ, Maddalena LA, Robb EL, Moradi F, Stuart JA. A simple ImageJ macro tool for analyzing mitochondrial network morphology in mammalian cell culture. *Acta Histochemica*. 2017;119:315-326. doi: https://doi.org/10.1016/j.acthis.2017.03.001
296. Grimshaw J. *James Grimshaw General Fiji Macros (Version 1.0.1);* 2024.
297. Otsu N. A Threshold Selection Method from Gray-Level Histograms. *IEEE Transactions on Systems, Man, and Cybernetics*. 1979;9:62-66. doi: 10.1109/TSMC.1979.4310076
298. Baker DJ, Childs BG, Durik M, Wijers ME, Sieben CJ, Zhong J, A. Saltness R, Jeganathan KB, Verzosa GC, Pezeshki A, et al. Naturally occurring p16Ink4a-positive cells shorten healthy lifespan. *Nature*. 2016;530:184-189. doi: 10.1038/nature16932
299. Jia K, Dai Y, Liu A, Li X, Wu L, Lu L, Bao Y, Jin Q. Senolytic Agent Navitoclax Inhibits Angiotensin II-Induced Heart Failure in Mice. *Journal of Cardiovascular Pharmacology*. 2020;76:452-460. doi: 10.1097/fjc.0000000000000878
300. Meyer JN, Leuthner TC, Luz AL. Mitochondrial fusion, fission, and mitochondrial toxicity. *Toxicology*. 2017;391:42-53. doi: https://doi.org/10.1016/j.tox.2017.07.019
301. Liu YJ, McIntyre RL, Janssens GE, Houtkooper RH. Mitochondrial fission and fusion: A dynamic role in aging and potential target for age-related disease.

Mechanisms of Ageing and Development. 2020;186:111212. doi: https://doi.org/10.1016/j.mad.2020.111212

302. Passos JF, Saretzki G, Ahmed S, Nelson G, Richter T, Peters H, Wappler I, Birket MJ, Harold G, Schaeuble K, et al. Mitochondrial Dysfunction Accounts for the Stochastic Heterogeneity in Telomere-Dependent Senescence. *PLOS Biology*. 2007;5:e110. doi: 10.1371/journal.pbio.0050110
303. Victorelli S, Salmonowicz H, Chapman J, Martini H, Vizioli MG, Riley JS, Cloix C, Hall-Younger E, Machado Espindola-Netto J, Jurk D, et al. Apoptotic stress causes mtDNA release during senescence and drives the SASP. *Nature*. 2023;622:627-636. doi: 10.1038/s41586-023-06621-4
304. Liu X, Hajnóczky G. Altered fusion dynamics underlie unique morphological changes in mitochondria during hypoxia–reoxygenation stress. *Cell Death & Differentiation*. 2011;18:1561-1572. doi: 10.1038/cdd.2011.13
305. Shimizu I, Minamino T. Physiological and pathological cardiac hypertrophy. *Journal of Molecular and Cellular Cardiology*. 2016;97:245-262. doi: https://doi.org/10.1016/j.yjmcc.2016.06.001
306. Tu VC, Bahl JJ, Chen QM. Signals of Oxidant-Induced Cardiomyocyte Hypertrophy: Key Activation of p70 S6 Kinase-1 and Phosphoinositide 3-Kinase. *Journal of Pharmacology and Experimental Therapeutics*. 2002;300:1101-1110. doi: 10.1124/jpet.300.3.1101
307. Métrich M, Lucas A, Gastineau M, Samuel J-L, Heymes C, Morel E, Lezoualc'h F. Epac Mediates β-Adrenergic Receptor–Induced Cardiomyocyte Hypertrophy. *Circ Res*. 2008;102:959-965. doi: doi:10.1161/CIRCRESAHA.107.164947
308. Huang Q, Huang J, Zeng Z, Luo J, Liu P, Chen S, Liu B, Pan X, Zang L, Zhou S. Effects of ERK1/2/PPARα/SCAD signal pathways on cardiomyocyte hypertrophy induced by insulin-like growth factor 1 and phenylephrine. *Life Sciences*. 2015;124:41-49. doi: https://doi.org/10.1016/j.lfs.2015.01.015
309. Sowah D, Brown BF, Quon A, Alvarez BV, Casey JR. Resistance to cardiomyocyte hypertrophy in ae3−/−mice, deficient in the AE3 Cl−/HCO3−exchanger. *BMC Cardiovascular Disorders*. 2014;14:89. doi: 10.1186/1471-2261-14-89
310. Wang J, Tang Y, Zhang J, Wang J, Xiao M, Lu G, Li J, Liu Q, Guo Y, Gu J. Cardiac SIRT1 ameliorates doxorubicin-induced cardiotoxicity by targeting sestrin 2. *Redox Biology*. 2022;52:102310. doi: https://doi.org/10.1016/j.redox.2022.102310

311. Martini H, Passos JF. Cellular senescence: all roads lead to mitochondria. *The FEBS Journal*. 2023;290:1186-1202. doi: https://doi.org/10.1111/febs.16361
312. Jenkins BC, Neikirk K, Katti P, Claypool SM, Kirabo A, McReynolds MR, Hinton A, Jr. Mitochondria in disease: changes in shapes and dynamics. *Trends in Biochemical Sciences*. 2024;49:346-360. doi: 10.1016/j.tibs.2024.01.011
313. Ahmad T, Aggarwal K, Pattnaik B, Mukherjee S, Sethi T, Tiwari BK, Kumar M, Micheal A, Mabalirajan U, Ghosh B, et al. Computational classification of mitochondrial shapes reflects stress and redox state. *Cell Death & Disease*. 2013;4:e461-e461. doi: 10.1038/cddis.2012.213
314. Glancy B, Kim Y, Katti P, Willingham TB. The Functional Impact of Mitochondrial Structure Across Subcellular Scales. *Frontiers in Physiology*. 2020;11. doi: 10.3389/fphys.2020.541040
315. Zhou Y, Long Q, Wu H, Li W, Qi J, Wu Y, Xiang G, Tang H, Yang L, Chen K, et al. Topology-dependent, bifurcated mitochondrial quality control under starvation. *Autophagy*. 2020;16:562-574. doi: 10.1080/15548627.2019.1634944
316. Long Q, Zhao D, Fan W, Yang L, Zhou Y, Qi J, Wang X, Liu X. Modeling of Mitochondrial Donut Formation. *Biophysical Journal*. 2015;109:892-899. doi: 10.1016/j.bpj.2015.07.039
317. Miyazono Y, Hirashima S, Ishihara N, Kusukawa J, Nakamura K-i, Ohta K. Uncoupled mitochondria quickly shorten along their long axis to form indented spheroids, instead of rings, in a fission-independent manner. *Scientific Reports*. 2018;8:350. doi: 10.1038/s41598-017-18582-6
318. Youle RJ, van der Bliek AM. Mitochondrial Fission, Fusion, and Stress. *Science*. 2012;337:1062-1065. doi: doi:10.1126/science.1219855
319. Ashley N, Poulton J. Anticancer DNA intercalators cause p53-dependent mitochondrial DNA nucleoid re-modelling. *Oncogene*. 2009;28:3880-3891. doi: 10.1038/onc.2009.242
320. Martínez MS, García A, Luzardo E, Chávez-Castillo M, Olivar LC, Salazar J, Velasco M, Rojas Quintero JJ, Bermúdez V. Energetic metabolism in cardiomyocytes: molecular basis of heart ischemia and arrhythmogenesis. *Vessel Plus*. 2017;1:130-141. doi: 10.20517/2574-1209.2017.34
321. Kelly G, Kataura T, Panek J, Ma G, Salmonowicz H, Davis A, Kendall H, Brookes C, Ayine-Tora DM, Banks P, et al. Suppressed basal mitophagy drives cellular

aging phenotypes that can be reversed by a p62-targeting small molecule. *Developmental Cell*. doi: 10.1016/j.devcel.2024.04.020

322. Harwig MC, Viana MP, Egner JM, Harwig JJ, Widlansky ME, Rafelski SM, Hill RB. Methods for imaging mammalian mitochondrial morphology: A prospective on MitoGraph. *Anal Biochem*. 2018;552:81-99. doi: 10.1016/j.ab.2018.02.022
323. Liu X, Yang L, Long Q, Weaver D, Hajnóczky G. Choosing proper fluorescent dyes, proteins, and imaging techniques to study mitochondrial dynamics in mammalian cells. *Biophys Rep*. 2017;3:64-72. doi: 10.1007/s41048-017-0037-8
324. Chandrakala AN, Sukul D, Selvarajan K, Sai-Sudhakar C, Sun B, Parthasarathy S. Induction of brain natriuretic peptide and monocyte chemotactic protein-1 gene expression by oxidized low-density lipoprotein: relevance to ischemic heart failure. *American Journal of Physiology-Cell Physiology*. 2012;302:C165-C177. doi: 10.1152/ajpcell.00116.2011
325. Jin HJ, Lee HJ, Heo J, Lim J, Kim M, Kim MK, Nam HY, Hong GH, Cho YS, Choi SJ, et al. Senescence-Associated MCP-1 Secretion Is Dependent on a Decline in BMI1 in Human Mesenchymal Stromal Cells. *Antioxid Redox Signal*. 2016;24:471-485. doi: 10.1089/ars.2015.6359
326. Liu H, Zhao D, Li H, Zhang W, Lin Q, Wang X, Zheng S, Zhang L, Li L, Hu S, et al. Blocking iASPP/Nrf2/M-CSF axis improves anti-cancer effect of chemotherapy-induced senescence by attenuating M2 polarization. *Cell Death & Disease*. 2022;13:166. doi: 10.1038/s41419-022-04611-4
327. Acosta JC, Banito A, Wuestefeld T, Georgilis A, Janich P, Morton JP, Athineos D, Kang T-W, Lasitschka F, Andrulis M, et al. A complex secretory program orchestrated by the inflammasome controls paracrine senescence. *Nature Cell Biology*. 2013;15:978-990. doi: 10.1038/ncb2784
328. Tarbit E, Singh I, Peart JN, Rose'Meyer RB. Biomarkers for the identification of cardiac fibroblast and myofibroblast cells. *Heart Failure Reviews*. 2019;24:1-15. doi: 10.1007/s10741-018-9720-1
329. Ling C, Nishimoto K, Rolfs Z, Smith LM, Frey BL, Welham NV. Differentiated fibrocytes assume a functional mesenchymal phenotype with regenerative potential. *Science Advances*. 2019;5:eaav7384. doi: doi:10.1126/sciadv.aav7384

330. Chalise U, Becirovic-Agic M, Lindsey ML. The cardiac wound healing response to myocardial infarction. *WIREs Mech Dis*. 2023;15:e1584. doi: 10.1002/wsbm.1584
331. Unverferth DV, Fetters JK, Unverferth BJ, Leier CV, Magorien RD, Arn AR, Baker PB. Human myocardial histologic characteristics in congestive heart failure. *Circulation*. 1983;68:1194-1200. doi: 10.1161/01.CIR.68.6.1194
332. Kang MJ, Kim J-S, Chae S-W, Koh KN, Koh GY. Cyclins and Cyclin Dependent Kinases during Cardiac Development. *Molecules and Cells*. 1997;7:360-366. doi: https://doi.org/10.1016/S1016-8478(23)13306-1
333. Ikenishi A, Okayama H, Iwamoto N, Yoshitome S, Tane S, Nakamura K, Obayashi T, Hayashi T, Takeuchi T. Cell cycle regulation in mouse heart during embryonic and postnatal stages. *Development, Growth & Differentiation*. 2012;54:731-738. doi: https://doi.org/10.1111/j.1440-169X.2012.01373.x
334. Nalobin D, Alipkina S, Gaidamaka A, Glukhov A, Khuchua Z. Telomeres and Telomerase in Heart Ontogenesis, Aging and Regeneration. *Cells*. 2020;9. doi: 10.3390/cells9020503
335. Alvarez R, Jr., Wang BJ, Quijada PJ, Avitabile D, Ho T, Shaitrit M, Chavarria M, Firouzi F, Ebeid D, Monsanto MM, et al. Cardiomyocyte cell cycle dynamics and proliferation revealed through cardiac-specific transgenesis of fluorescent ubiquitinated cell cycle indicator (FUCCI). *Journal of Molecular and Cellular Cardiology*. 2019;127:154-164. doi: 10.1016/j.yjmcc.2018.12.007
336. Kim H-S, Shin J-Y, Yun J-Y, Ahn D-K, Lee J-Y. Immortalization of human embryonic fibroblasts by overexpression of c-myc and simian virus 40 large T antigen. *Experimental & Molecular Medicine*. 2001;33:293-298. doi: 10.1038/emm.2001.47
337. Burridge PW, Matsa E, Shukla P, Lin ZC, Churko JM, Ebert AD, Lan F, Diecke S, Huber B, Mordwinkin NM, et al. Chemically defined generation of human cardiomyocytes. *Nature Methods*. 2014;11:855-860. doi: 10.1038/nmeth.2999
338. Burridge PW, Li YF, Matsa E, Wu H, Ong S-G, Sharma A, Holmström A, Chang AC, Coronado MJ, Ebert AD, et al. Human induced pluripotent stem cell–derived cardiomyocytes recapitulate the predilection of breast cancer patients to doxorubicin-induced cardiotoxicity. *Nature Medicine*. 2016;22:547-556. doi: 10.1038/nm.4087
339. Salameh A, Dhein S. Culture of neonatal cardiomyocytes. In: *Practical Methods in Cardiovascular Research*. Springer; 2005 568-576.

340. Guo G-r, Chen L, Rao M, Chen K, Song J-p, Hu S-s. A modified method for isolation of human cardiomyocytes to model cardiac diseases. *Journal of Translational Medicine*. 2018;16:288. doi: 10.1186/s12967-018-1649-6
341. Liu H, Bersell K, Kühn B. Isolation and Characterization of Intact Cardiomyocytes from Frozen and Fresh Human Myocardium and Mouse Hearts. In: Poss KD, Kühn B, eds. *Cardiac Regeneration: Methods and Protocols*. New York, NY: Springer US; 2021:199-210.
342. Willett M, Johnson P. An introduction to image analysis using ImageJ. In: University of Southampton.
343. Schneider VA, Graves-Lindsay T, Howe K, Bouk N, Chen H-C, Kitts PA, Murphy TD, Pruitt KD, Thibaud-Nissen F, Albracht D, et al. Evaluation of GRCh38 and de novo haploid genome assemblies demonstrates the enduring quality of the reference assembly. *Genome Research*. 2017;27:849-864. doi: 10.1101/gr.213611.116
344. Subramanian A, Tamayo P, Mootha VK, Mukherjee S, Ebert BL, Gillette MA, Paulovich A, Pomeroy SL, Golub TR, Lander ES, et al. Gene set enrichment analysis: A knowledge-based approach for interpreting genome-wide expression profiles. *Proceedings of the National Academy of Sciences*. 2005;102:15545-15550. doi: doi:10.1073/pnas.0506580102
345. Liberzon A, Birger C, Thorvaldsdóttir H, Ghandi M, Mesirov Jill P, Tamayo P. The Molecular Signatures Database Hallmark Gene Set Collection. *Cell Systems*. 2015;1:417-425. doi: 10.1016/j.cels.2015.12.004
346. Chen H, Li Y, Tollefsbol TO. Cell senescence culturing methods. *Methods Mol Biol*. 2013;1048:1-10. doi: 10.1007/978-1-62703-556-9_1
347. Freund A, Laberge RM, Demaria M, Campisi J. Lamin B1 loss is a senescence-associated biomarker. *Mol Biol Cell*. 2012;23:2066-2075. doi: 10.1091/mbc.E11-10-0884
348. Chaulin AM. Biology of Cardiac Troponins: Emphasis on Metabolism. *Biology*. 2022;11:429.
349. Yoshida Y, Nakanishi K, Daimon M, Ishiwata J, Sawada N, Hirokawa M, Kaneko H, Nakao T, Mizuno Y, Morita H, et al. Alteration of Cardiac Performance and Serum B-Type Natriuretic Peptide Level in Healthy Aging. *Journal of the American College of Cardiology*. 2019;74:1789-1800. doi: doi:10.1016/j.jacc.2019.07.080

350. Wang Z-D, Yao S, Shi G-P, Wang Y, Shi J-M, Guo J-H, Zhu Y-S, Jiang X-Y, Chu X-F, Wang X-F. Frailty index is associated with increased risk of elevated BNP in an elderly population: the Rugao Longevity and Ageing Study. *Aging Clinical and Experimental Research*. 2020;32:305-311. doi: 10.1007/s40520-019-01189-4

351. Kim EJ, Lee J, Jung YR, Park J-J, Park M-J, Lee J-S, Kim C-H, Lee Y-J, Lee M. Involvement of corin downregulation in ionizing radiation-induced senescence of myocardial cells. *Int J Mol Med*. 2015;35:731-738. doi: 10.3892/ijmm.2014.2048

352. Zamorano JL, Lancellotti P, Rodriguez Muñoz D, Aboyans V, Asteggiano R, Galderisi M, Habib G, Lenihan DJ, Lip GYH, Lyon AR, et al. 2016 ESC Position Paper on cancer treatments and cardiovascular toxicity developed under the auspices of the ESC Committee for Practice Guidelines. *European Journal of Heart Failure*. 2017;19:9-42. doi: https://doi.org/10.1002/ejhf.654

353. Chimenti C, Kajstura J, Torella D, Urbanek K, Heleniak H, Colussi C, Di Meglio F, Nadal-Ginard B, Frustaci A, Leri A, et al. Senescence and Death of Primitive Cells and Myocytes Lead to Premature Cardiac Aging and Heart Failure. *Circ Res*. 2003;93:604-613. doi: doi:10.1161/01.RES.0000093985.76901.AF

354. Ahuja P, Sdek P, MacLellan WR. Cardiac Myocyte Cell Cycle Control in Development, Disease, and Regeneration. *Physiological Reviews*. 2007;87:521-544. doi: 10.1152/physrev.00032.2006

355. Pasumarthi KBS, Field LJ. Cardiomyocyte Cell Cycle Regulation. *Circ Res*. 2002;90:1044-1054. doi: doi:10.1161/01.RES.0000020201.44772.67

356. Oubaha M, Miloudi K, Dejda A, Guber V, Mawambo G, Germain M-A, Bourdel G, Popovic N, Rezende FA, Kaufman RJ, et al. Senescence-associated secretory phenotype contributes to pathological angiogenesis in retinopathy. *Science Translational Medicine*. 2016;8:362ra144-362ra144. doi: doi:10.1126/scitranslmed.aaf9440

357. Benkafadar N, François F, Affortit C, Casas F, Ceccato J-C, Menardo J, Venail F, Malfroy-Camine B, Puel J-L, Wang J. ROS-Induced Activation of DNA Damage Responses Drives Senescence-Like State in Postmitotic Cochlear Cells: Implication for Hearing Preservation. *Molecular Neurobiology*. 2019;56:5950-5969. doi: 10.1007/s12035-019-1493-6

358. Safwan-Zaiter H, Wagner N, Wagner K-D. P16INK4A—More Than a Senescence Marker. *Life*. 2022;12:1332.

359. Belhadj J, Surina S, Hengstschläger M, Lomakin AJ. Form follows function: Nuclear morphology as a quantifiable predictor of cellular senescence. *Aging Cell*. 2023;22:e14012. doi: 10.1111/acel.14012

360. Heckenbach I, Mkrtchyan GV, Ezra MB, Bakula D, Madsen JS, Nielsen MH, Oró D, Osborne B, Covarrubias AJ, Idda ML, et al. Nuclear morphology is a deep learning biomarker of cellular senescence. *Nature Aging*. 2022;2:742-755. doi: 10.1038/s43587-022-00263-3

361. Sardão VA, Oliveira PJ, Holy J, Oliveira CR, Wallace KB. Morphological alterations induced by doxorubicin on H9c2 myoblasts: nuclear, mitochondrial, and cytoskeletal targets. *Cell Biology and Toxicology*. 2009;25:227-243. doi: 10.1007/s10565-008-9070-1

362. Rharass T, Gbankoto A, Canal C, Kurşunluoğlu G, Bijoux A, Panáková D, Ribou A-C. Oxidative stress does not play a primary role in the toxicity induced with clinical doses of doxorubicin in myocardial H9c2 cells. *Molecular and Cellular Biochemistry*. 2016;413:199-215. doi: 10.1007/s11010-016-2653-x

363. Bootcov MR, Bauskin AR, Valenzuela SM, Moore AG, Bansal M, He XY, Zhang HP, Donnellan M, Mahler S, Pryor K, et al. MIC-1, a novel macrophage inhibitory cytokine, is a divergent member of the TGF-β superfamily. *Proceedings of the National Academy of Sciences*. 1997;94:11514-11519. doi: doi:10.1073/pnas.94.21.11514

364. Hsiao EC, Koniaris LG, Zimmers-Koniaris T, Sebald SM, Huynh TV, Lee S-J. Characterization of Growth-Differentiation Factor 15, a Transforming Growth Factor β Superfamily Member Induced following Liver Injury. *Molecular and Cellular Biology*. 2000;20:3742-3751. doi: 10.1128/MCB.20.10.3742-3751.2000

365. Schober A, Böttner M, Strelau J, Kinscherf R, Bonaterra GA, Barth M, Schilling L, Fairlie WD, Breit SN, Unsicker K. Expression of growth differentiation factor-15/ macrophage inhibitory cytokine-1 (GDF-15/MIC-1) in the perinatal, adult, and injured rat brain. *Journal of Comparative Neurology*. 2001;439:32-45. doi: https://doi.org/10.1002/cne.1333

366. Koniaris LG. Induction of MIC-1/growth differentiation factor-15 following bile duct injury. *Journal of Gastrointestinal Surgery*. 2003;7:901-905. doi: 10.1007/s11605-003-0037-5

367. Schlittenhardt D, Schober A, Strelau J, Bonaterra GA, Schmiedt W, Unsicker K, Metz J, Kinscherf R. Involvement of growth differentiation factor-15/macrophage inhibitory cytokine-1 (GDF-15/MIC-1) in oxLDL-induced apoptosis of human

macrophages in vitro and in arteriosclerotic lesions. *Cell and Tissue Research*. 2004;318:325-333. doi: 10.1007/s00441-004-0986-3

368. Wollert KC, Kempf T, Wallentin L. Growth Differentiation Factor 15 as a Biomarker in Cardiovascular Disease. *Clinical Chemistry*. 2017;63:140-151. doi: 10.1373/clinchem.2016.255174
369. Conte M, Giuliani C, Chiariello A, Iannuzzi V, Franceschi C, Salvioli S. GDF15, an emerging key player in human aging. *Ageing Research Reviews*. 2022;75:101569. doi: https://doi.org/10.1016/j.arr.2022.101569
370. Auchampach J, Han L, Huang GN, Kühn B, Lough JW, O'Meara CC, Payumo AY, Rosenthal NA, Sucov HM, Yutzey KE, et al. Measuring cardiomyocyte cell-cycle activity and proliferation in the age of heart regeneration. *Am J Physiol Heart Circ Physiol*. 2022;322:H579-h596. doi: 10.1152/ajpheart.00666.2021
371. Bottomley MJ, Harden PN, Wood KJ. CD8+ Immunosenescence Predicts Post-Transplant Cutaneous Squamous Cell Carcinoma in High-Risk Patients. *J Am Soc Nephrol*. 2016;27:1505-1515. doi: 10.1681/asn.2015030250
372. Delgobo M, Heinrichs M, Hapke N, Ashour D, Appel M, Srivastava M, Heckel T, Spyridopoulos I, Hofmann U, Frantz S. Terminally differentiated CD4+ T cells promote myocardial inflammaging. *Frontiers in Immunology*. 2021;12:584538.
373. Liao L-E, Hu D-D, Zheng Y. A Four-Methylated lncRNAs-Based Prognostic Signature for Hepatocellular Carcinoma. *Genes*. 2020;11:908.
374. Kim Y-J, Lee H-E, Ryu J-C. Identification of marker genes related to cardiovascular toxicity of doxorubicin and daunorubicin in human umbilical vein endothelial cells (HUVECs). *Molecular & cellular toxicology*. 2007;3:246-253.
375. Murphy C, Jennings P, Wilmes A. Transcriptomic profile of human iPSC-derived podocyte-like cells exposed to a panel of xenobiotics. *Toxicology in Vitro*. 2024;97:105804. doi: https://doi.org/10.1016/j.tiv.2024.105804
376. Fridman AL, Tainsky MA. Critical pathways in cellular senescence and immortalization revealed by gene expression profiling. *Oncogene*. 2008;27:5975-5987. doi: 10.1038/onc.2008.213
377. Levine AJ. p53: 800 million years of evolution and 40 years of discovery. *Nature Reviews Cancer*. 2020;20:471-480. doi: 10.1038/s41568-020-0262-1
378. Rodier F, Muñoz DP, Teachenor R, Chu V, Le O, Bhaumik D, Coppé J-P, Campeau E, Beauséjour CM, Kim S-H, et al. DNA-SCARS: distinct nuclear structures that sustain damage-induced senescence growth arrest and

inflammatory cytokine secretion. *Journal of Cell Science*. 2011;124:68-81. doi: 10.1242/jcs.071340

379. Liu R, Jagannathan R, Sun L, Li F, Yang P, Lee J, Negi V, Perez-Garcia EM, Shiva S, Yechoor VK, et al. Tead1 is essential for mitochondrial function in cardiomyocytes. *Am J Physiol Heart Circ Physiol*. 2020;319:H89-h99. doi: 10.1152/ajpheart.00732.2019
380. Doenst T, Nguyen TD, Abel ED. Cardiac Metabolism in Heart Failure. *Circ Res*. 2013;113:709-724. doi: doi:10.1161/CIRCRESAHA.113.300376
381. Ma Y, Li J. Metabolic shifts during aging and pathology. *Compr Physiol*. 2015;5:667-686. doi: 10.1002/cphy.c140041
382. Serio S, Pagiatakis C, Musolino E, Felicetta A, Carullo P, Laura Frances J, Papa L, Rozzi G, Salvarani N, Miragoli M, et al. Cardiac Aging Is Promoted by Pseudohypoxia Increasing p300-Induced Glycolysis. *Circ Res*. 2023;133:687-703. doi: doi:10.1161/CIRCRESAHA.123.322676
383. Meredith A-M, Dass CR. Increasing role of the cancer chemotherapeutic doxorubicin in cellular metabolism. *Journal of Pharmacy and Pharmacology*. 2016;68:729-741. doi: 10.1111/jphp.12539
384. Quijano C, Cao L, Fergusson MM, Romero H, Liu J, Gutkind S, Rovira II, Mohney RP, Karoly ED, Finkel T. Oncogene-induced senescence results in marked metabolic and bioenergetic alterations. *Cell Cycle*. 2012;11:1383-1392. doi: 10.4161/cc.19800
385. Flor AC, Wolfgeher D, Wu D, Kron SJ. A signature of enhanced lipid metabolism, lipid peroxidation and aldehyde stress in therapy-induced senescence. *Cell Death Discovery*. 2017;3:17075. doi: 10.1038/cddiscovery.2017.75
386. Wiley CD, Campisi J. The metabolic roots of senescence: mechanisms and opportunities for intervention. *Nature Metabolism*. 2021;3:1290-1301. doi: 10.1038/s42255-021-00483-8
387. Wullschleger S, Loewith R, Hall MN. TOR Signaling in Growth and Metabolism. *Cell*. 2006;124:471-484. doi: https://doi.org/10.1016/j.cell.2006.01.016
388. Shackebaei D, Hesari M, Gorgani S, Vafaeipour Z, Salaramoli S, Yarmohammadi F. The Role of mTOR in the Doxorubicin-Induced Cardiotoxicity: A Systematic Review. *Cell Biochemistry and Biophysics*. 2024. doi: 10.1007/s12013-024-01475-7
389. Zhou B, Honor LB, He H, Ma Q, Oh J-H, Butterfield C, Lin R-Z, Melero-Martin JM, Dolmatova E, Duffy HS, et al. Adult mouse epicardium modulates

myocardial injury by secreting paracrine factors. *J Clin Invest*. 2011;121:1894-1904. doi: 10.1172/JCI45529

390. van Wijk B, Gunst QD, Moorman AFM, van den Hoff MJB. Cardiac Regeneration from Activated Epicardium. *PLOS ONE*. 2012;7:e44692. doi: 10.1371/journal.pone.0044692
391. Tsai T-H, Lin C-J, Hang C-L, Chen W-Y. Calcitriol Attenuates Doxorubicin-Induced Cardiac Dysfunction and Inhibits Endothelial-to-Mesenchymal Transition in Mice. *Cells*. 2019;8:865.
392. Pan JA, Zhang H, Lin H, Gao L, Zhang HL, Zhang JF, Wang CQ, Gu J. Irisin ameliorates doxorubicin-induced cardiac perivascular fibrosis through inhibiting endothelial-to-mesenchymal transition by regulating ROS accumulation and autophagy disorder in endothelial cells. *Redox Biol*. 2021;46:102120. doi: 10.1016/j.redox.2021.102120
393. Kovacic JC, Mercader N, Torres M, Boehm M, Fuster V. Epithelial-to-Mesenchymal and Endothelial-to-Mesenchymal Transition. *Circulation*. 2012;125:1795-1808. doi: doi:10.1161/CIRCULATIONAHA.111.040352
394. Akolkar G, da Silva Dias D, Ayyappan P, Bagchi AK, Jassal DS, Salemi VMC, Irigoyen MC, De Angelis K, Singal PK. Vitamin C mitigates oxidative/nitrosative stress and inflammation in doxorubicin-induced cardiomyopathy. *American Journal of Physiology-Heart and Circulatory Physiology*. 2017;313:H795-H809. doi: 10.1152/ajpheart.00253.2017
395. Urschel K, Cicha I. TNF-α in the cardiovascular system: from physiology to therapy. *International Journal of Interferon, Cytokine and Mediator Research*. 2015;7:9-25. doi: 10.2147/IJICMR.S64894
396. Xiao J, Gong Y, Chen Y, Yu D, Wang X, Zhang X, Dou Y, Liu D, Cheng G, Lu S, et al. IL-6 promotes epithelial-to-mesenchymal transition of human peritoneal mesothelial cells possibly through the JAK2/STAT3 signaling pathway. *Am J Physiol Renal Physiol*. 2017;313:F310-f318. doi: 10.1152/ajprenal.00428.2016
397. Sheng W, Yang F, Zhou Y, Yang H, Low PY, Kemeny DM, Tan P, Moh A, Kaplan MH, Zhang Y, et al. STAT5 programs a distinct subset of GM-CSF-producing T helper cells that is essential for autoimmune neuroinflammation. *Cell Res*. 2014;24:1387-1402. doi: 10.1038/cr.2014.154
398. Herr F, Lemoine R, Gouilleux F, Meley D, Kazma I, Heraud A, Velge-Roussel F, Baron C, Lebranchu Y. IL-2 phosphorylates STAT5 to drive IFN-γ production

and activation of human dendritic cells. *J Immunol*. 2014;192:5660-5670. doi: 10.4049/jimmunol.1300422

399. Socolovsky M, Fallon AEJ, Wang S, Brugnara C, Lodish HF. Fetal Anemia and Apoptosis of Red Cell Progenitors in Stat5a^{−/−}5b^{−/−} Mice: A Direct Role for Stat5 in Bcl-X_L Induction. *Cell*. 1999;98:181-191. doi: 10.1016/S0092-8674(00)81013-2
400. Mavrogonatou E, Papadopoulou A, Pratsinis H, Kletsas D. Senescence-associated alterations in the extracellular matrix: deciphering their role in the regulation of cellular function. *American Journal of Physiology-Cell Physiology*. 2023;325:C633-C647. doi: 10.1152/ajpcell.00178.2023
401. Sui S, Hou Y. Dual integrin αvβ3 and αvβ5 blockade attenuates cardiac dysfunction by reducing fibrosis in a rat model of doxorubicin-induced cardiomyopathy. *Scandinavian Cardiovascular Journal*. 2021;55:287-296. doi: 10.1080/14017431.2021.1955960
402. Kalluri R, LeBleu VS. The biology, function, and biomedical applications of exosomes. *Science*. 2020;367:eaau6977. doi: doi:10.1126/science.aau6977
403. Takasugi M, Okada R, Takahashi A, Virya Chen D, Watanabe S, Hara E. Small extracellular vesicles secreted from senescent cells promote cancer cell proliferation through EphA2. *Nature Communications*. 2017;8:15729. doi: 10.1038/ncomms15728
404. Rossi M. The Emergence of Senescent Surface Biomarkers as Senotherapeutic Targets. *Cells*. 2021;10:1740. doi: https://doi.org/10.3390/cells10071740
405. McGowan JV, Chung R, Maulik A, Piotrowska I, Walker JM, Yellon DM. Anthracycline Chemotherapy and Cardiotoxicity. *Cardiovasc Drugs Ther*. 2017;31:63-75. doi: 10.1007/s10557-016-6711-0
406. Peiyong Z, Junichi S. Cardiomyocyte senescence and the potential therapeutic role of senolytics in the heart. *The Journal of Cardiovascular Aging*. 2024;4:18.
407. Evangelou K, Vasileiou PVS, Papaspyropoulos A, Hazapis O, Petty R, Demaria M, Gorgoulis VG. Cellular senescence and cardiovascular diseases: moving to the “heart” of the problem. *Physiological Reviews*. 2023;103:609-647. doi: 10.1152/physrev.00007.2022
408. Kastury N, Hidalgo V, Pandi B, Li L, Lam MPY, Lau E. Senescence in human AC16 cardiac cells is associated with thymidine kinase induction and histone loss. *MicroPubl Biol*. 2023;2023. doi: 10.17912/micropub.biology.000865

409. Lu J, Zhang C, Wang W, Xu W, Chen W, Tao L, Li Z, Zhang Y, Cheng J. Exposure to environmental concentrations of glyphosate induces cardiotoxicity through cellular senescence and reduced cell proliferation capacity. *Ecotoxicology and Environmental Safety*. 2023;261:115112. doi: https://doi.org/10.1016/j.ecoenv.2023.115112

410. Hoppins S, Lackner LL, Lee JE, Mears JA. Chapter 20 - In vitro and in vivo assays for mitochondrial fission and fusion. In: Pon LA, Schon EA, eds. *Methods in Cell Biology*. Academic Press; 2020:491-518.

411. Wang S, Long H, Hou L, Feng B, Ma Z, Wu Y, Zeng Y, Cai J, Zhang D-w, Zhao G. The mitophagy pathway and its implications in human diseases. *Signal Transduct Target Ther*. 2023;8:304. doi: 10.1038/s41392-023-01503-7

412. Kelly G, Kataura T, Panek J, Ma G, Salmonowicz H, Davis A, Kendall H, Brookes C, Ayine-Tora DM, Banks P, et al. Suppressed basal mitophagy drives cellular aging phenotypes that can be reversed by a p62-targeting small molecule. *Developmental Cell*. 2024;59:1924-1939.e1927. doi: 10.1016/j.devcel.2024.04.020

413. Serrano J, Palmeira CM, Kuehl DW, Wallace KB. Cardioselective and cumulative oxidation of mitochondrial DNA following subchronic doxorubicin administration1Supported in part by NIH Grant HL58016. The manuscript was not subjected to internal Agency review and, thus, the opinions are those of the authors and are not officially endorsed by the U.S. Environmental Protection Agency. Mention of trade names or commercial products does not constitute endorsement nor is it intended to imply any form of judgment by the authors.1. *Biochimica et Biophysica Acta (BBA) - Bioenergetics*. 1999;1411:201-205. doi: https://doi.org/10.1016/S0005-2728(99)00011-0

414. Lebrecht D, Kokkori A, Ketelsen U-P, Setzer B, Walker UA. Tissue-specific mtDNA lesions and radical-associated mitochondrial dysfunction in human hearts exposed to doxorubicin. *The Journal of Pathology*. 2005;207:436-444. doi: https://doi.org/10.1002/path.1863

415. Šimůnek T, Štěrba M, Popelová O, Adamcová M, Hrdina R, Geršl V. Anthracycline-induced cardiotoxicity: overview of studies examining the roles of oxidative stress and free cellular iron. *Pharmacological reports*. 2009;61:154-171.

416. Hausenloy DJ, Yellon DM. Myocardial ischemia-reperfusion injury: a neglected therapeutic target. *J Clin Invest*. 2013;123:92-100. doi: 10.1172/JCI62874

417. Han Y, Xie H, Liu Y, Gao P, Yang X, Shen Z. Effect of metformin on all-cause and cardiovascular mortality in patients with coronary artery diseases: a systematic review and an updated meta-analysis. *Cardiovascular Diabetology*. 2019;18:96. doi: 10.1186/s12933-019-0900-7

418. Moiseeva O, Deschênes-Simard X, St-Germain E, Igelmann S, Huot G, Cadar AE, Bourdeau V, Pollak MN, Ferbeyre G. Metformin inhibits the senescence-associated secretory phenotype by interfering with IKK/NF-κ B activation. *Aging cell*. 2013;12:489-498.

419. Arunachalam G, Samuel SM, Marei I, Ding H, Triggle CR. Metformin modulates hyperglycaemia-induced endothelial senescence and apoptosis through SIRT1. *British journal of pharmacology*. 2014;171:523-535.

420. Tai S, Sun J, Zhou Y, Zhu Z, He Y, Chen M, Yang H, Xiao Y, Tu T, Tang L, et al. Metformin suppresses vascular smooth muscle cell senescence by promoting autophagic flux. *Journal of Advanced Research*. 2022;41:205-218. doi: https://doi.org/10.1016/j.jare.2021.12.009

421. Zilinyi R, Czompa A, Czegledi A, Gajtko A, Pituk D, Lekli I, Tosaki A. The cardioprotective effect of metformin in doxorubicin-induced cardiotoxicity: the role of autophagy. *Molecules*. 2018;23:1184.

422. Grosse L, Wagner N, Emelyanov A, Molina C, Lacas-Gervais S, Wagner K-D, Bulavin DV. Defined p16High senescent cell types are indispensable for mouse healthspan. *Cell Metabolism*. 2020;32:87-99. e86.

423. Meyer K, Hodwin B, Ramanujam D, Engelhardt S, Sarikas A. Essential Role for Premature Senescence of Myofibroblasts in Myocardial Fibrosis. *Journal of the American College of Cardiology*. 2016;67:2018-2028. doi: doi:10.1016/j.jacc.2016.02.047

Appendix A

Code for ImageJ/Fiji MiNA analysis to perform measurements of mitochondrial network morphology in VEH/DOX-treated AC16 cardiomyocytes

```
#@ File(label="Input Images Folder:", value = "", style="directory") InputFolder

#@ File(label="Roi Folder:", value = "", style="directory") RoiFolder

#@ File(label="Output Folder:", value ="", style="directory") OutputFolder


#@ String(label = "Thresholding Op:", value="otsu", choices={"huang", "ij1",
"intermodes", "isoData", "li", "maxEntropy", "maxLikelihood", "mean", "minError",
"minimum", "moments", "otsu", "percentile", "renyiEntropy", "rosin", "shanbhag",
"triangle", "yen"}) threshold_method


#@ OpService ops

#@ ScriptService scripts

#@ StatusService status

#@ UIService ui



import mina.statistics

import mina.tables

import mina.filters

from mina import mina_view


import warnings

import os

import traceback
```

```
from collections import OrderedDict

from ij import IJ
from ij import WindowManager
from ij.gui import Overlay
from ij.measure import Measurements
from ij.plugin import Duplicator
from ij.plugin.frame import RoiManager
from ij.io import FileSaver

from net.imglib2.img.display.imagej import ImageJFunctions

from sc.fiji.analyzeSkeleton import AnalyzeSkeleton_;

# Bioformats Imports
from loci.plugins import BF
from loci.plugins.in import ImporterOptions

def threshold_image(imp):
    # Create and ImgPlus copy of the ImagePlus for thresholding with ops...
    status.showStatus("Determining threshold level...")
    slices = imp.getNSlices()
    frames = imp.getNFrames()
    if imp.getRoi() != None:
```

```
        ROI_pos = (imp.getRoi().getBounds().x, imp.getRoi().getBounds().y)
    else:
        ROI_pos = (0, 0)

    imp_calibration = imp.getCalibration()
    imp_channel = Duplicator().run(imp, imp.getChannel(), imp.getChannel(), 1, slices,
1, frames)
    img = ImageJFunctions.wrap(imp_channel)

    # Determine the threshold value if not manual...
    binary_img = ops.run("threshold.%s"%threshold_method, img)
    binary = ImageJFunctions.wrap(binary_img, 'binary')
    binary.setCalibration(imp_calibration)
    binary.setDimensions(1, slices, 1)
    return binary

# The run function.....................................................................
def run(imp_original, threshold_method, roiname):
    imp = Duplicator().run(imp_original, imp_original.getChannel(),
imp_original.getChannel(), 1, imp_original.getNSlices(), 1,
imp_original.getNFrames())

    output_parameters = OrderedDict([("image title", ""),
                                     ("roi name", ""),
                                     ("thresholding op", float),
                                     ("mitochondrial footprint", float),
```

```
                        ("branch length mean", float),
                        ("branch length median", float),
                        ("branch length stdev", float),
                        ("summed branch lengths mean", float),
                        ("summed branch lengths median", float),
                        ("summed branch lengths stdev", float),
                        ("network branches mean", float),
                        ("network branches median", float),
                        ("network branches stdev", float),
                        ("donuts", int)])

# Perform any preprocessing steps...
status.showStatus("Preprocessing image...")

output_parameters["thresholding op"] = threshold_method

imp_title = imp.getTitle()
output_parameters["image title"] = imp_title
output_parameters["roi name"] = roiname

# Determine the threshold value if not manual...
binary = threshold_image(imp)

imp_calibration = imp.getCalibration()
# Get the total_area
```

```
    if binary.getNSlices() == 1:
        area = binary.getStatistics(Measurements.AREA).area
        area_fraction =
binary.getStatistics(Measurements.AREA_FRACTION).areaFraction
        output_parameters["mitochondrial footprint"] =  area * area_fraction / 100.0
    else:
        mito_footprint = 0.0
        for slice in range(1, binary.getNSlices()+1):
            binary.setSliceWithoutUpdate(slice)
            area = binary.getStatistics(Measurements.AREA).area
            area_fraction =
binary.getStatistics(Measurements.AREA_FRACTION).areaFraction
            mito_footprint += area * area_fraction / 100.0
        output_parameters["mitochondrial footprint"] = mito_footprint *
imp_calibration.pixelDepth


    # Generate skeleton from masked binary otherwise
    skeleton = Duplicator().run(binary)
    IJ.run(skeleton, "Skeletonize (2D/3D)", "")


    # Analyze the skeleton...
    status.showStatus("Setting up skeleton analysis...")
    skel = AnalyzeSkeleton_()
    skel.setup("", skeleton)
    status.showStatus("Analyzing skeleton...")
    skel_result = skel.run()
```

```
    status.showStatus("Computing graph based parameters...")
    branch_lengths = []
    summed_lengths = []
    graphs = skel_result.getGraph()

    num_donuts = 0
    for graph in graphs:
        summed_length = 0.0
        edges = graph.getEdges()
        vertices = {}
        for edge in edges:
            length = edge.getLength()
            branch_lengths.append(length)
            summed_length += length

            # keep track of the number of times a vertex appears in edges in a given
graph
            for vertex in [edge.getV1(), edge.getV2()]:
                if vertex in vertices:
                    vertices[vertex] += 1
                else:
                    vertices[vertex] = 1

        is_donut = True
```

```
        # donut_arms = 0
        for k in vertices:
            # if a vertex appeared less than twice
            if vertices[k] <= 1:
                # donut_arms += 1
                # if donut_arms > 1:
                is_donut = False
                break

        if is_donut and len(edges) >= 1:
            num_donuts += 1

        summed_lengths.append(summed_length)
    output_parameters["donuts"] = num_donuts

    output_parameters["branch length mean"] = mina.statistics.mean(branch_lengths)
    output_parameters["branch length median"] =
mina.statistics.median(branch_lengths)
    output_parameters["branch length stdev"] = mina.statistics.stdev(branch_lengths)

    output_parameters["summed branch lengths mean"] =
mina.statistics.mean(summed_lengths)
    output_parameters["summed branch lengths median"] =
mina.statistics.median(summed_lengths)
    output_parameters["summed branch lengths stdev"] =
mina.statistics.stdev(summed_lengths)
```

```
    branches = list(skel_result.getBranches())
    output_parameters["network branches mean"] = mina.statistics.mean(branches)
    output_parameters["network branches median"] =
mina.statistics.median(branches)
    output_parameters["network branches stdev"] = mina.statistics.stdev(branches)

    # Create/append results to a ResultsTable...
    morphology_tbl = mina.tables.SimpleSheet("Mito Morphology")
    morphology_tbl.writeRow(output_parameters)
    morphology_tbl.updateDisplay()

    status.showStatus("Done analysis!")
    return binary, skeleton

# Run the script...
if (__name__=="__main__") or (__name__=="__builtin__"):
    RM = RoiManager(True)
    for ImageFile in InputFolder.listFiles():
        try:
            Options = ImporterOptions()
            Options.setId(ImageFile.getPath())
            Options.setSplitChannels(True)
            Import = BF.openImagePlus(Options)
            ImageFilename = ImageFile.getName()
```

```
        RoiPath = os.path.join(RoiFolder.getPath(), ".".join(ImageFilename.split('.')[:-
1]) + ".zip")
        OutputImageFolder = os.path.join(OutputFolder.getPath(), "Cropped",
ImageFilename)
        if not os.path.exists(OutputImageFolder):
            os.makedirs(OutputImageFolder)
        OutputMaskFolder = os.path.join(OutputFolder.getPath(), "Mask",
ImageFilename)
        if not os.path.exists(OutputMaskFolder):
            os.makedirs(OutputMaskFolder)
        OutputSkeletonFolder = os.path.join(OutputFolder.getPath(), "Skeleton",
ImageFilename)
        if not os.path.exists(OutputSkeletonFolder):
            os.makedirs(OutputSkeletonFolder)
        RM.reset()
        RM.open(RoiPath)
        RoiList = RM.getRoisAsArray()
        for roi in RoiList:
            Import[0].setRoi(roi)
            IJ.run(Import[0], "Remove Overlay", "")
            IJ.run(Import[0], "Add Selection...", "")
            croppedImp = Import[0].crop("stack")
            croppedroi = croppedImp.getOverlay().toArray()[0]
            croppedImp.setRoi(croppedroi)
            IJ.run(croppedImp, "Clear Outside", "stack")
            IJ.run(croppedImp, "Remove Overlay", "")
```

```
            binaryout, skeletonout = run(croppedImp, threshold_method,
roi.getName())
            FileSaver(croppedImp).saveAsTiff(os.path.join(OutputImageFolder,
roi.getName() + ".tif"))
            FileSaver(binaryout).saveAsTiff(os.path.join(OutputMaskFolder,
roi.getName() + ".tif"))
            FileSaver(skeletonout).saveAsTiff(os.path.join(OutputSkeletonFolder,
roi.getName() + ".tif"))
        except Exception:
            print("Could not process:", ImageFile.getPath(), "\n Error:")
            traceback.print_exc()
```

Concentrations of cytokines in conditioned media from VEH/DOX-treated (non-senescent/senescent) AC16 cardiomyocytes

When individually analysing the cytokines detected in conditioned media from VEH/DOX-treated (non-senescent/senescent) AC16 cardiomyocytes, many cytokines appear to have significantly different concentrations between treatment groups. However, multiple testing such as this should be approached with caution, as this methodology increases the risk of false positive results (i.e. results being found to be significantly different, when in fact this is an artefact of repeated testing). The average concentration of each cytokine in the two treatment groups with their student's t test statistical significance values are included here for completeness, but more stringent analyses which includes corrections for multiple testing is detailed in the main body of this thesis (see **Figure 4.7**, section **4.3.4**).

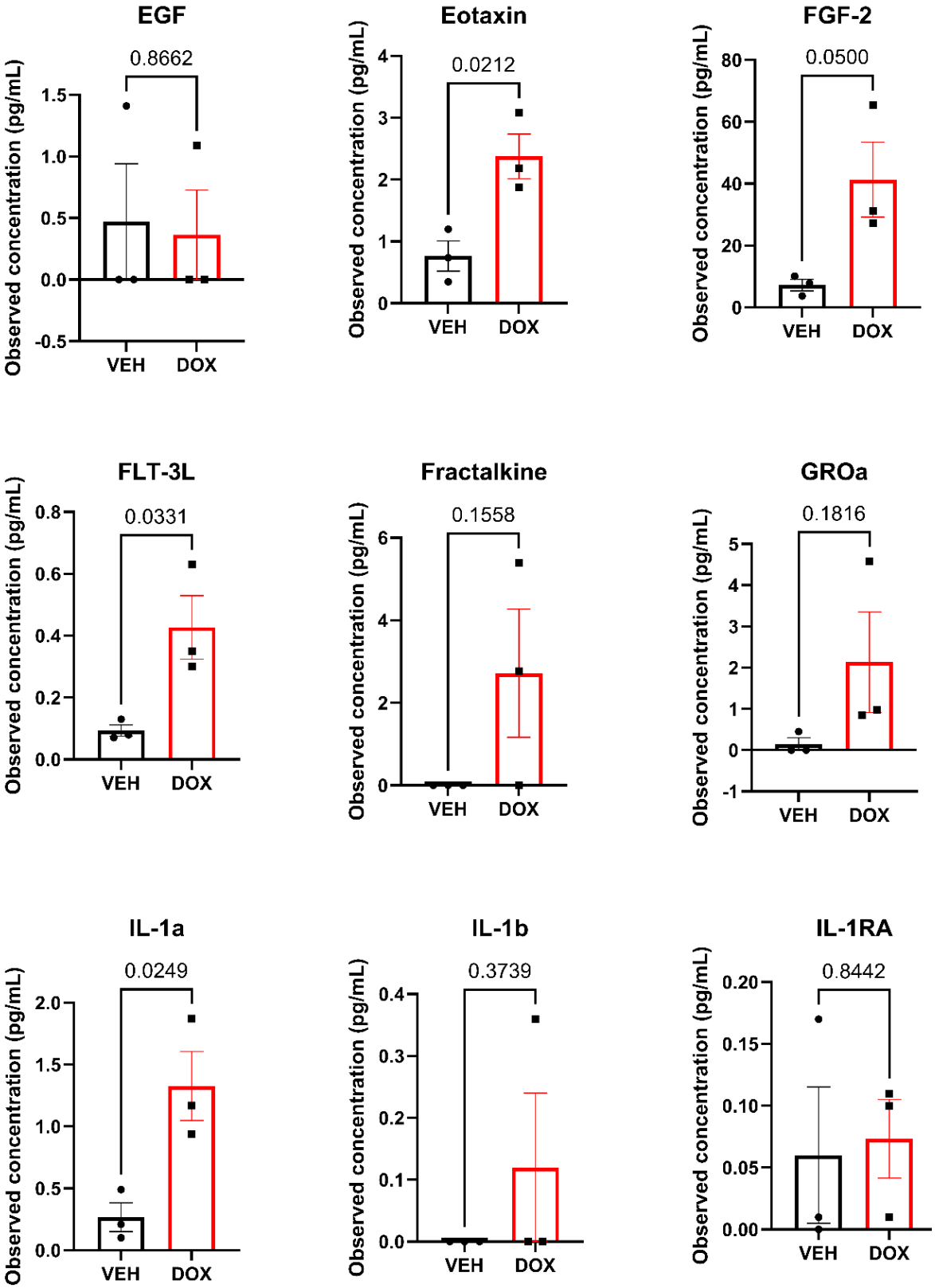
EGF
0.8662
Observed concentration (pg/mL)
1.5
1.0
0.5
0.0
-0.5
VEH
DOX
Eotaxin
0.0212
Observed concentration (pg/mL)
4
3
2
1
0
VEH
DOX
FGF-2
0.0500
Observed concentration (pg/mL)
80
60
40
20
0
VEH
DOX
FLT-3L
0.0331
Observed concentration (pg/mL)
0.8
0.6
0.4
0.2
0.0
VEH
DOX
Fractalkine
0.1558
Observed concentration (pg/mL)
6
4
2
0
VEH
DOX
GROa
0.1816
Observed concentration (pg/mL)
5
4
3
2
1
0
-1
VEH
DOX
IL-1a
0.0249
Observed concentration (pg/mL)
2.0
1.5
1.0
0.5
0.0
VEH
DOX
IL-1b
0.3739
Observed concentration (pg/mL)
0.4
0.3
0.2
0.1
0.0
VEH
DOX
IL-1RA
0.8442
Observed concentration (pg/mL)
0.20
0.15
0.10
0.05
0.00
VEH
DOX

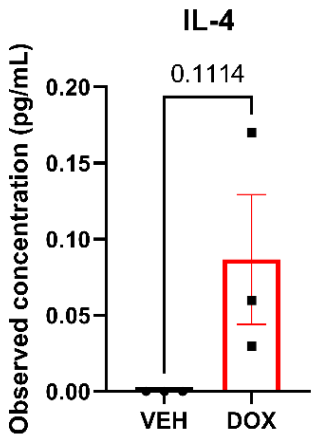
IL-4
0.1114
Observed concentration (pg/mL)
0.20
0.15
0.10
0.05
0.00
VEH
DOX

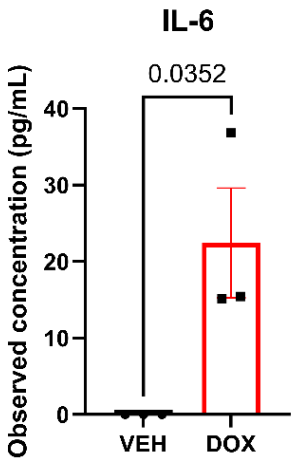
IL-6
0.0352
Observed concentration (pg/mL)
40
30
20
10
0
VEH
DOX

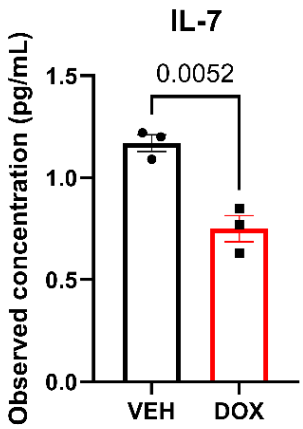
IL-7
0.0052
Observed concentration (pg/mL)
1.5
1.0
0.5
0.0
VEH
DOX

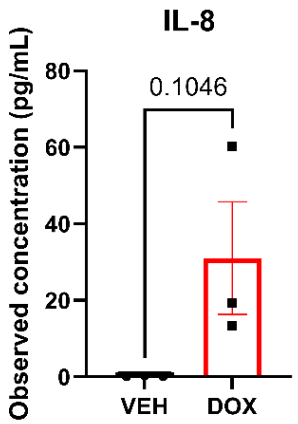
IL-8
0.1046
Observed concentration (pg/mL)
80
60
40
20
0
VEH
DOX

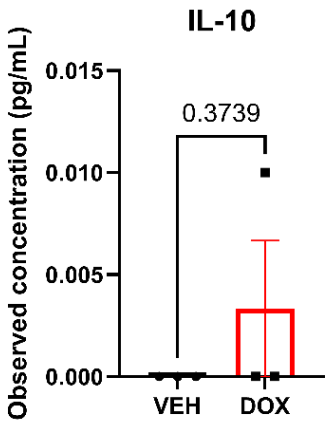
IL-10
0.3739
Observed concentration (pg/mL)
0.015
0.010
0.005
0.000
VEH
DOX

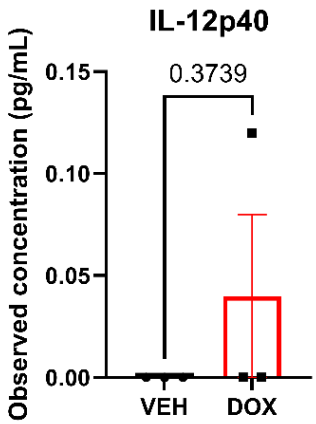
IL-12p40
0.3739
Observed concentration (pg/mL)
0.15
0.10
0.05
0.00
VEH
DOX

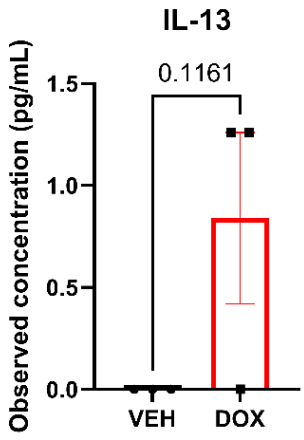
IL-13
0.1161
Observed concentration (pg/mL)
1.5
1.0
0.5
0.0
VEH
DOX

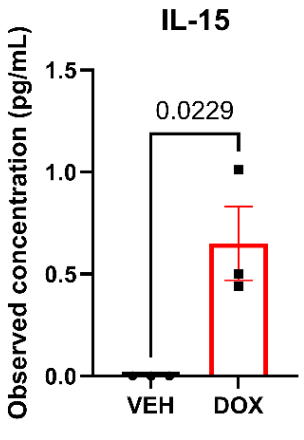
IL-15
0.0229
Observed concentration (pg/mL)
1.5
1.0
0.5
0.0
VEH
DOX

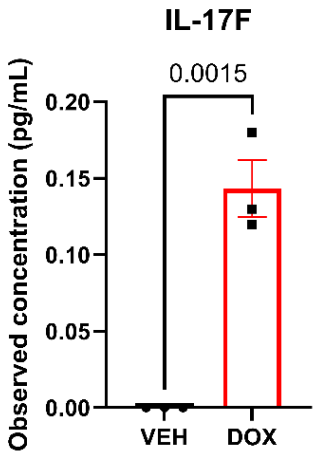
IL-17F
0.0015
Observed concentration (pg/mL)
0.20
0.15
0.10
0.05
0.00
VEH
DOX

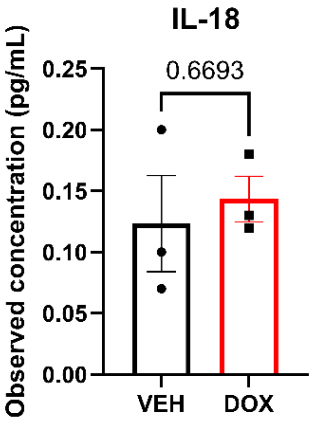
IL-18
0.6693
Observed concentration (pg/mL)
0.25
0.20
0.15
0.10
0.05
0.00
VEH
DOX

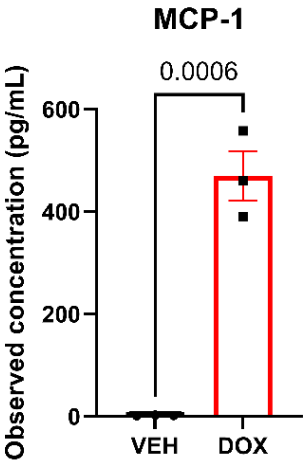
MCP-1
0.0006
Observed concentration (pg/mL)
600
400
200
0
VEH
DOX

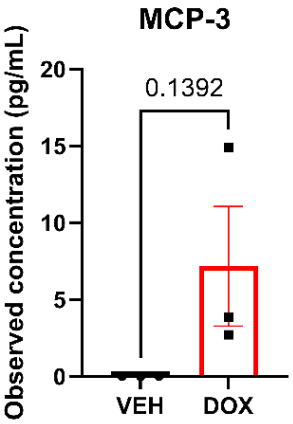
MCP-3
0.1392
Observed concentration (pg/mL)
20
15
10
5
0
VEH
DOX

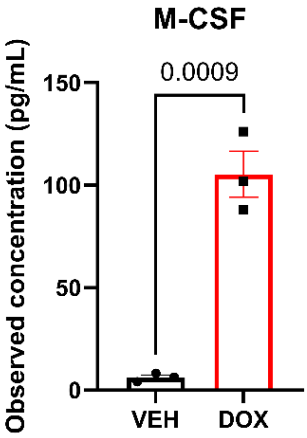
M-CSF
0.0009
Observed concentration (pg/mL)
150
100
50
0
VEH
DOX

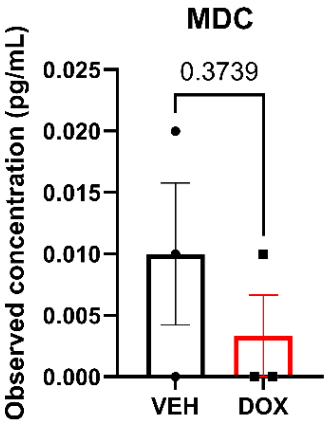
MDC
0.3739
Observed concentration (pg/mL)
0.025
0.020
0.015
0.010
0.005
0.000
VEH
DOX

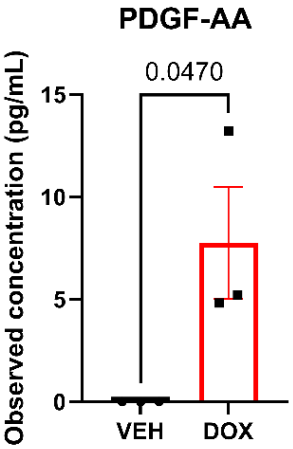
PDGF-AA
0.0470
Observed concentration (pg/mL)
15
10
5
0
VEH
DOX

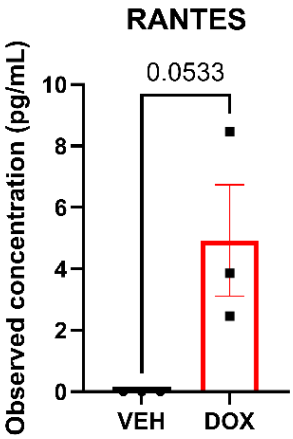
RANTES
0.0533
Observed concentration (pg/mL)
10
8
6
4
2
0
VEH
DOX

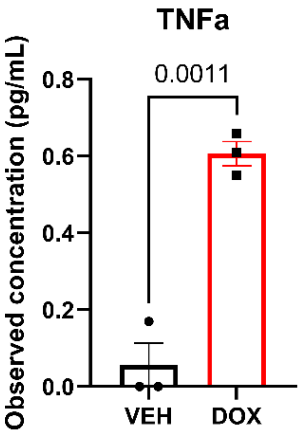
TNFa
0.0011
Observed concentration (pg/mL)
0.8
0.6
0.4
0.2
0.0
VEH
DOX

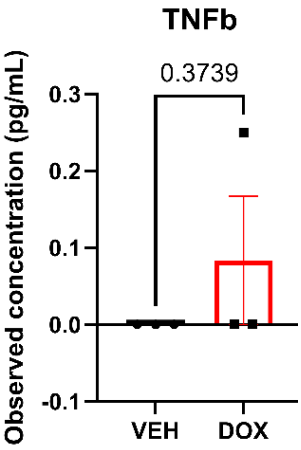
TNFb
0.3739
Observed concentration (pg/mL)
0.3
0.2
0.1
0.0
-0.1
VEH
DOX

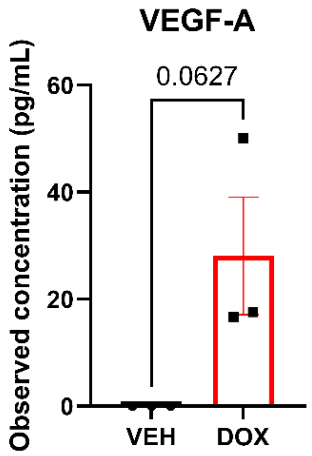
VEGF-A
0.0627
Observed concentration (pg/mL)
60
40
20
0
VEH
DOX

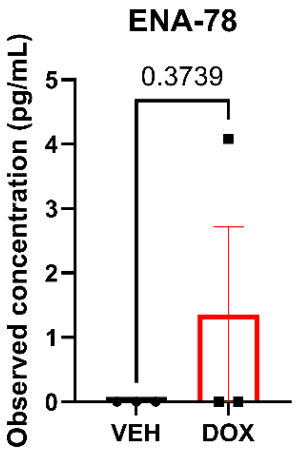
ENA-78
0.3739
Observed concentration (pg/mL)
5
4
3
2
1
0
VEH
DOX

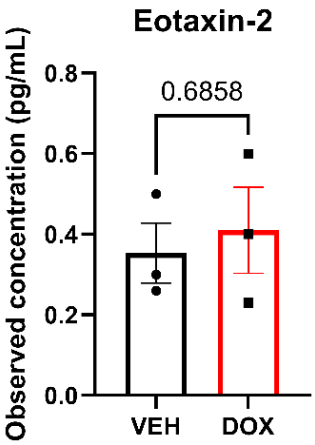
Eotaxin-2
0.6858
Observed concentration (pg/mL)
0.8
0.6
0.4
0.2
0.0
VEH
DOX

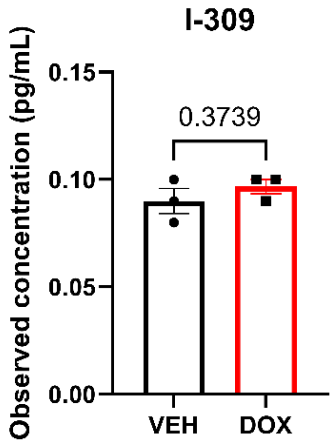
I-309
0.3739
Observed concentration (pg/mL)
0.15
0.10
0.05
0.00
VEH
DOX

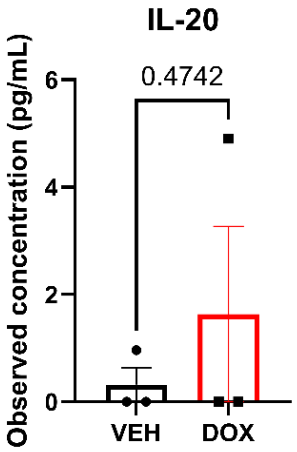
IL-20
0.4742
Observed concentration (pg/mL)
6
4
2
0
VEH
DOX

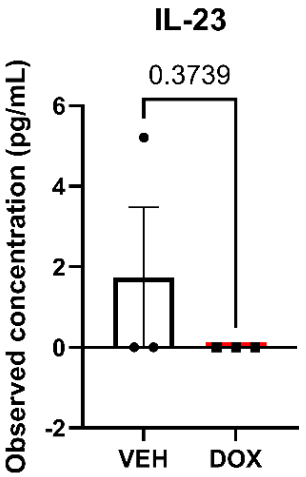
IL-23
0.3739
Observed concentration (pg/mL)
6
4
2
0
-2
VEH
DOX

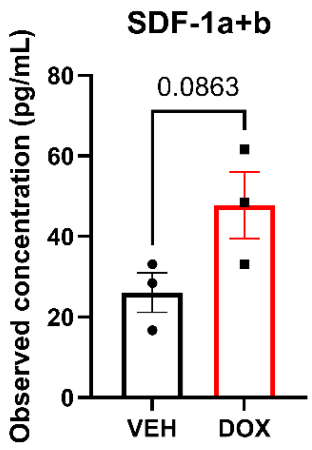
SDF-1a+b
0.0863
Observed concentration (pg/mL)
80
60
40
20
0
VEH
DOX

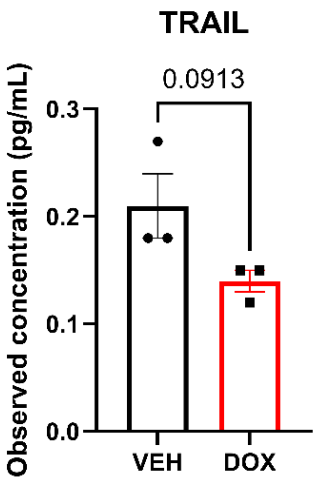
TRAIL
0.0913
Observed concentration (pg/mL)
0.3
0.2
0.1
0.0
VEH
DOX

Figure S1: Comparison of the concentrations of various cytokines in conditioned media collected from VEH/DOX-treated (non-senescent/senescent) AC16 cardiomyocytes. Data were analysed using an unpaired student's t test. Data is the mean of N = 3 independent experiments per treatment condition.

Code for ImageJ/Fiji macro to perform semi-automated measurement of nuclear p21 fluorescence intensity in VEH/DOX-treated iPSC-CMs

```
//Macro made by Emma Foster for Laura Booth August 2023

//Purpose: This macro uses the nuclear channel for segmentation and measure the values in the red channel



//Input folder - set location of folder with images to be processed (must already exist)

input_folder="O:/gdr/Laura/ipsc_macro/n1_p21.594/v/";



//Output folder - set location for output (must already exist)

output_folder="O:/gdr/Laura/ipsc_macro/n1_p21.594/v_output/";



//Makes a list of all the files in the folder

list = getFileList(input_folder);



//Counts the number of images in the list

image_number=list.length;



run("Set Measurements...", "area mean standard min centroid display redirect=None decimal=3");

roiManager("reset")

run("Clear Results");
```

```
//For loop to go through each image in the folder with all of our processing and analysis steps
for (i=0; i<image_number; i++) { //1 - for each image
	//Variables for file location and name
	file_location = input_folder + list[i];
	file_name=list[i];
	//Get the file name without the file extension extention
	split_file_name=split(file_name, ".");
	//Name of new save folder
	image_save_folder=output_folder+"/"+file_name+"/";
	//Create new save folder
	File.makeDirectory(image_save_folder);
	//Variable for making .csv files of results
	results_output=split_file_name[0] + "_results.csv";

	//Open file
	run("Bio-Formats Importer", "open=file_location");

	//Duplicate channel 3 for processing and segmentation
	run("Duplicate...", "duplicate channels=3");
	//background subtraction
	run("Subtract Background...", "rolling=100");
	//Apply blur for smooth cell shape
	run("Gaussian Blur...", "sigma=5");
	//Use Otsu auto threshold to pick out cell shapes
```

```
run("Auto Threshold", "method=Otsu white");
//Analyze particles to create regions of interest (ROI) and at them to ROI manager
run("Analyze Particles...", "size=10-Infinity add composite");

//Small for loop to convert individual ROI into and array
count = roiManager("count");
if (count>1){
	array = newArray(count);
	for (j=0; j<array.length; j++) {
	array[j] = j;
}
}
//Select the array
roiManager("select", array);
//Combine them
roiManager("Combine");
//Add them to ROI manager
roiManager("Add");
//Delete the array
roiManager("Delete");

roiManager("Select", 0);
//Rename the ROI to 'cells'
roiManager("Rename", "cells");
```

```
        //Save the ROI for validation later
        roiManager("Save", image_save_folder + "ROI"+ ".zip");
        //Close the processed version of channel 3
        run("Close");

        //Select the original image file
        selectWindow(file_location);
        //Split the channels into separate windows
        run("Split Channels");

        //Do measurements on channel 2
        selectWindow("C2-"+file_location);
        roiManager("Select", 0);
        run("Measure");
        //save the results
        saveAs("Results", image_save_folder+results_output);
        run("Clear Results");
        roiManager("reset")
        run("Close All");


}
```

Appendix B

Presented works & travel awards

Oral presentations

- BTS Annual Congress 2024 (Liverpool, UK)
    - Awarded £600 GBP BTS Student Bursary to attend
    - Best Oral Presentation prize
- International Pharmaceutical Federation Annual Congress 2023 (Brisbane, Australia)
- Gordon Research Conference: Cellular and Molecular Mechanisms of Toxicity 2023 (NH, USA)
    - Awarded €1200 EUR EUROTOX fellowship to attend
- Gordon Research Conference: Drug Safety 2022 (MA, USA)
    - Awarded $2180 USD to attend
- BTS Discovery Toxicology 2023 (Alderley Park, UK)
    - Best Oral Presentation prize
- BTS Annual Congress 2022 (Gateshead, UK)
    - Best Oral Presentation prize
- Northeast Postgraduate Conference 2021 (Online, UK)
- Newcastle University: School of Pharmacy, Toxicology MRes course, Centre for Cancer

Poster presentations

- BTS Annual Congress 2023 (Birmingham, UK)
    - Awarded £565 GBP BTS Student Bursary to attend
- BAS-BSCR Meeting at British Cardiovascular Society Annual Conference 2023 (Manchester, UK)
- Newcastle University Biosciences Institute 2023 (UK)
- Alliance for Healthy Aging Meeting 2022 (Minneapolis MN, USA)
    - Awarded $1234 USD Alliance for Healthy Aging travel award to attend
    - Excellent Abstract Submission prize
- Newcastle University Biosciences Institute 2022 (UK)

Personal prizes

- Newcastle University FMS Public Lecture Prize 2024

- Vitae 3 Minute Thesis (3MT) competition: winner of both Newcastle University competitions and Northeast region and **one of six UK national finalists** from approximately 1,500 competitors

Funding awarded

- Co-Investigator: “Characterising chemotherapy-induced cardiac cell senescence to ascertain its role in chemotherapy-induced heart failure” Project Grant PG/23/11571, British Heart Foundation: £279,661.
- Newcastle University Doctoral College Enhancement Fund: £1781
- Newcastle University Toxicity and Survivorship legacy fund: £1000

Publications

Booth LK, Redgrave RE, Tual-Chalot S, et al. Heart Disease and Ageing: The Roles of Senescence, Mitochondria, and Telomerase in Cardiovascular Disease. *Subcell Biochem* 2023;103:45-78

Booth LK, Redgrave RE, Folaranmi O, et al. Anthracycline-induced cardiotoxicity and senescence. *Frontiers in Aging* 2022;3

Camacho-Encina M, **Booth LK**, Redgrave RE, et al. Identifying optimal reference genes for qRT-PCR in human myocardial tissues. *Cardiovascular Research*. 2024 (in press)

Kelly, G, Kataura T, …, **Booth L**, et al. Suppressed basal mitophagy drives cellular aging phenotypes that can be reversed by a p62-targeting small molecule. *Developmental Cell*. 2024; 59(10.1016)

Camacho-Encina M, **Booth LK**, Redgrave RE, Folaranmi O, Spyridopoulos I, Richardson GD. Cellular Senescence, Mitochondrial Dysfunction, and Their Link to Cardiovascular Disease. *Cells*. 2024; 13(4):353.

Redgrave RE, Dookun E, **Booth LK**, et al. Senescent cardiomyocytes contribute to cardiac dysfunction following myocardial infarction. *npj Aging* 2023;9:15

Booth LK, Alsuhaibani R, Redgrave R, et al. Assessing the role of cardiomyocyte senescence and secreted factors in anthracycline-induced cardiotoxicity. FIP Brisbane 2023: Clinical Biology. *Pharmacy Education*, *23* (6) 2023., p. 52–60. - *Published conference proceedings*

Booth L, Redgrave R, Encina MC, et al. BS31 The senescence-associated secretory phenotype as a biomarker for age-related myocardial remodelling and cardiovascular disease. *Heart* 2023;109:A265-A6 - *Published conference proceedings*

Encina MC, Tyler A, Hardwick I, **Booth LK** et al. BS58 Identifying older donor hearts suitable for transplantation: the use of senescence as a marker of biological age. *Heart* 2023;109:A288-A9 - *Published conference proceedings*

Redgrave R, Dookun E, **Booth L**, et al. BS5 Senescent cardiomyocytes contribute to cardiac dysfunction following myocardial infarction. *Heart* 2023;109:A249 - *Published conference proceedings*

Abstract and poster presented at the British Toxicology Society Annual Congress 2023

Title: Exploring the role of senescence and associated secreted factors in anthracycline-induced cardiotoxicity

Anthracycline chemotherapies continue to underpin treatment strategies for countless cancer patients globally, but they have long been associated with delayed-onset cardiotoxicity, which is emerging as an unmet healthcare need in the ever-increasing cancer survivor population. The processes underpinning anthracycline-induced cardiotoxicity (AIC) remain unclear but cellular senescence has arisen as a possible contributory mechanism to the subclinical, structural changes which precede functional disturbances in the myocardium: AIC patients often display cardiac phenotypes associated with ageing, e.g. fibrosis, hypertrophy and maladaptive remodelling. We exposed human AC16 cardiomyocytes to 500 nM doxorubicin (DOX), a clinically-utilised anthracycline, for 3 hours only (representing a transient, sublethal and clinically-centred dose) or exposed cells to equivalent vehicle control. Cardiomyocytes were allowed to recover for 10 days before analyses were conducted. qPCR and immunocytochemistry analyses showed induction of classical and novel senescence markers 10 days post-DOX vs control (e.g. p21 transcript 4-fold increase, PURPL transcript 9-fold increase). In DOX-treated cardiomyocytes, morphological disturbances were observed in the treatment recovery phase, including hypertrophy. Conditioned media was collected from cardiomyocytes at days 8-10 post-treatment, and cytokine array analysis showed a classical senescence-associated secretory phenotype (SASP) in DOX-treated cardiomyocytes vs control, comprising immune-recruiting (MCP-1: 470 vs 2 pg/mL), pro-inflammatory (IL-6: 22 vs 0 pg/mL) and pro-remodelling (FGF-2: 41 vs 7 pg/mL) factors. The capacity of this SASP to both reinforce and spread the senescent phenotype through the cardiac microenvironment and beyond remains underappreciated in the cardiotoxicity of anthracyclines and will form the basis of future work.

Exploring the role of senescence and associated secreted factors in anthracycline-induced cardiotoxicity

Laura K. Booth[1], Rachael Redgrave[2], Simon Tual-Chalot[2], Ray Alsuhaibani[1], Gavin D. Richardson[2], Jason Gill[1]

1. Translational and Clinical Research Institute, Newcastle University
2. Biosciences Institute, Newcastle University

INTRODUCTION

- Anthracycline-induced cardiotoxicity (AIC) is a poorly characterised side effect of anticancer treatment – **delayed symptomatic disease** which can result in heart failure (HF).
- Maladaptive myocardial remodelling drives early-stage toxicity. Many remodelling processes resemble those seen in the ageing myocardium, where cellular senescence is prevalent.
- Anthracyclines induce senescence & the senescence-associated secretory phenotype (SASP) in cardiomyocytes (CMs) both *in vitro* and *in vivo*.

Problem:

The capacity of senescence to drive myocardial remodelling in AIC is poorly understood.

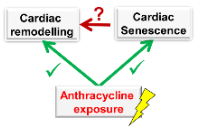

Aims:

1. Establish a clinically-relevant *in vitro* model
2. Building on previous work [1], characterise the SASP in this model

METHODS

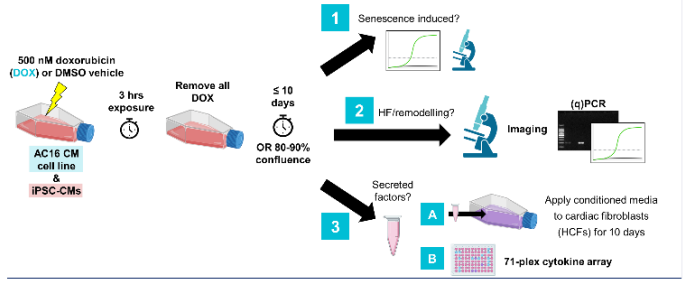

RESULTS

1 Sublethal DOX exposure induces classical and novel markers of senescence in AC16 CMs, 10 days post-insult

AC16 CMs treated with 500 nM DOX (< estimated C_{max} of 1.1 µM) expressed classical senescence markers **p16** (Fig. 1A, 1B) and **p21** (Fig. 1C, 1D) at the transcript and protein level, alongside elevated expression of senescence-associated transcripts **Bcl-2** (Fig. 1E) and lncRNA **PURPL** (Fig. 1F)

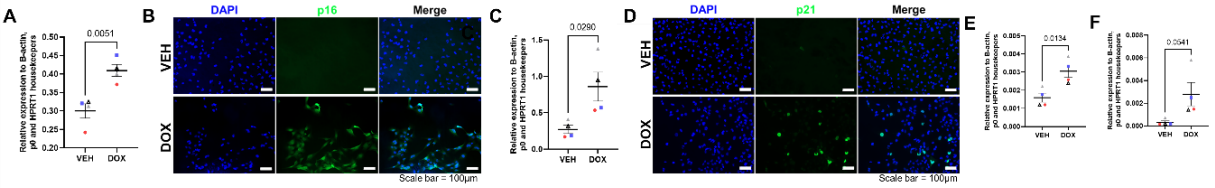

2 In AC16 CMs, DOX exposure associates with upregulated remodelling and HF-related transcripts, and disturbed *in vitro* morphology

500 nM DOX-dosed AC16 CMs showed upregulated expression of several genes associated with myocardial **remodelling** & clinical HF (Fig. 2A). **GDF15** is elevated (Fig. 2B) – this is a biomarker of HF, is associated with age-related CM senescence and has demonstrated pro-fibrotic properties [1]. DOX-insulted CMs displayed **disturbed morphology** & a significant increase in surface area 72 hrs post-exposure, indicating cellular **hypertrophy** (Fig. 2C, 2D).

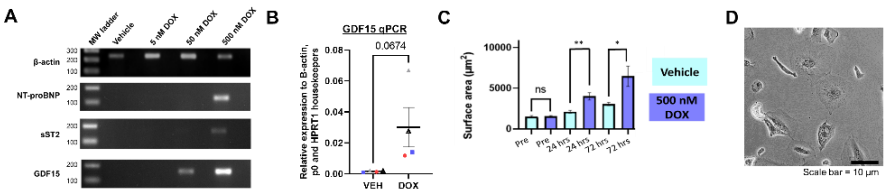

Findings from AC16 CMs were validated in iPSC-CMs

Commercial iPSC-CMs were characterised by assessing contractility and morphology in culture via **live cell imaging** (Fig. A) In pilot studies, 10 days post-DOX exposure (500 nM, 3 hr), transcript markers of **p21, PURPL, GDF15** and **BNP** (a clinical biomarker of cardiomyocyte stress) were **elevated** compared to vehicle controls (Fig. B, C, D, E). p16 and p21 protein expression was elevated in DOX-treated iPSCs (Fig. F)

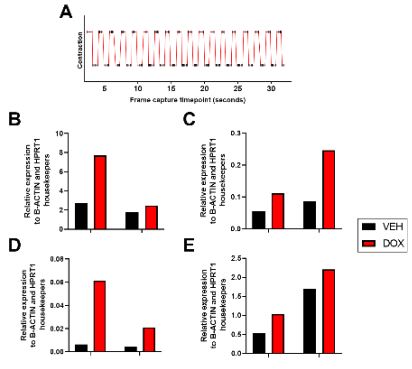

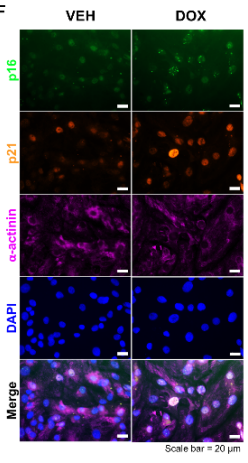

3 Senescent AC16 CMs SASP promotes phenotype change in HCFs through pro-remodelling cytokines

After **HCFs** were exposed to conditioned media collected from senescent AC16s for 10 days ("DOX cmed"), HCFs had a higher proportion of **αSMA stress fibre-positive** cells compared to vehicle conditioned media control ("VEH cmed") (Fig 3A, 3B). HCFs exposed to DOX cmed expressed elevated transcripts of myofibroblast markers **interleukin-8** (Fig. 3C) and **periostin** (Fig. 3D) when compared to control. Conditioned media was analysed using a 71-plex discovery **cytokine array** (Eve Technologies) and DOX cmed was found to comprise a classical **SASP** (Fig. 3E), containing higher concentrations of **pro-remodelling factors** than VEH cmed (e.g., M-CSF, IL-6, VEGF-A).

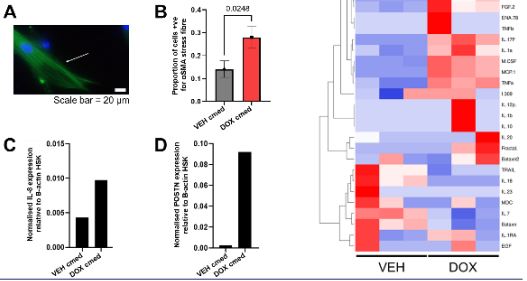

CONCLUSIONS

1. ***IN VITRO*, A CLINICALLY-INFORMED & SUBLETHAL DOSE OF DOXORUBICIN CAN INDUCE CARDIOMYOCYTE SENESCENCE, WHICH IS ASSOCITED WITH THE EXPRESSION OF GENES LINKED TO CARDIAC REMODELLING AND HEART FAILURE.**

2. **SENESCENT CARDIOMYOCYTES EXPRESS A SASP: THESE SECRETED FACTORS MAY BE KEY PLAYERS IN ANTHRACYCLINE-INDUCED MYOCARDIAL REMODELLING, LEADING TO HEART FAILURE IN A DELAYED FORM AFTER ANTICANCER TREATMENT**

Laura K. Booth
MRC ITTP candidate
laurakbooth
@laurakbooth